CHARACTERIZING THE PERFORMANCE OF FULL-SCALE ENHANCED HONEYCOMB SANDWICH COMPOSITE CROSS-ARM IN TRANSMISSION TOWER

By

AMIR BIN ABD LATIF

Thesis Submitted to the School of Graduate Studies, Universiti Putra Malaysia, in Fulfilment of the Requirements for the Degree of Doctor of Philosophy

June 2024

FK 2024 14

DEDICATION

To Al-Quran, the source of knowledge that is beyond doubt

"Proclaim! (or read!) in the name of thy Lord and Cherisher, Who created – Created man, out of a (mere) clot of congealed blood: Proclaim! And thy Lord is Most Bountiful, He Who taught (the use of) the pen, Taught man that which he knew not"

[Al-Alaq:1-5].

&

To my beloved father, Abd Latif Md Rasoll and my beloved mother, Mahaboobah Syed Mohamed for their invaluable sacrifices, encouragements, motivation and financial support throughout my study

&

To my beloved wife, Shahilah Salleh for her love, patience, sacrifices and understanding

&

To my beloved kids, Akma Safiyyah Amir, Ahmad Suhaib Amir and Asma Siddiqah Amir

Abstract of thesis presented to the Senate of Universiti Putra Malaysia in fulfilment of the requirement for the degree of Doctor of Philosophy

CHARACTERIZING THE PERFORMANCE OF FULL-SCALE ENHANCED HONEYCOMB SANDWICH COMPOSITE CROSS-ARM IN TRANSMISSION TOWER

By

AMIR BIN ABD LATIF

June 2024

Chairman : Mohamad Ridzwan Bin Ishak, PhD
Faculty : Engineering

This research addresses the critical challenges faced by transmission tower cross-arms, which endure significant bending and creep stresses over their operational lifespan, exacerbated by environmental factors that can lead to sudden failures. It is apparent that any material used in such applications is susceptible to attack from environmental factors. To mitigate these challenges a commercially available pultruded composite material, known as pultruded glass fiber reinforced polymer composite (PGFRPC) was further enhance by using a honeycomb sandwich composite structure due to its excellent structural attributes and lightweight nature. The objective of this research is to develop an enhanced pultruded glass fiber reinforced polymer composite (PGFRPC) cross-arm incorporating a honeycomb sandwich structure to improve performance and durability. A comprehensive methodology was employed, involving rigorous testing through three-point flexural deflection and creep assessments of both the existing and enhanced cross-arms, under individual and assembly conditions. The research revealed that the optimal 0° orientation angle for the facesheet made from woven glass fiber prepreg significantly improved bending properties. Utilizing the Theory of Inventive Problem Solving (TRIZ), morphological charts, and the Analytical Network Process (ANP), an optimal design for the honeycomb sandwich PGFRPC cross-arm was developed, with Concept Design 2 emerging as the top choice. The integration of the honeycomb structure on the existing cross-arm resulted in a 36.7% reduction in deflection and a 33.7% reduction in creep strain. Besides that, this research demonstrating a linear elastic behavior superior to traditional Balau wood cross-arms compared to composite cross-arm. The research also highlighted that the enhanced cross-arm's improved resistance to bending forces, creep resistance, and long-term stability could significantly extend its lifespan and reduce maintenance costs. Future research should focus on dynamic performance, flexibility reactions, failure modes, and creep analysis under normal and broken wire conditions, varying safety factors to better understand the effects of greater loads on the composite structure. Overall, this research establishes the superior creep properties of the enhanced PGFRPC cross-arm, providing valuable insights for future advancements in transmission tower technology.

Keywords: Elastic Modulus, Flexural Properties, Honeycomb Sandwich, PGFRPC cross-arm, Transmission Tower.

SDG: GOAL 9: Industry, Innovation and Infrastructure

Abstrak tesis yang dikemukakan kepada Senat Universiti Putra Malaysia sebagai memenuhi keperluan untuk ijazah Doktor Falsafah

MENCIRIKAN PRESTASI LENGAN SILANG KOMPOSIT SANDWIC SARANG LEBAH YANG DIPERTINGKATKAN BERSKALA PENUH BAGI MENARA TRANSMISI

Oleh

AMIR BIN ABD LATIF

Jun 2024

Pengurusi : Mohamad Ridzwan Bin Ishak, PhD
Fakulti : Kejuruteraan

Penelitian ini menangani cabaran kritikal yang dihadapi oleh lengan silang menara penghantaran, yang menanggung tekanan lenturan dan rayapan yang signifikan sepanjang hayat operasinya. Ia disebabkan oleh faktor persekitaran yang boleh menyebabkan kegagalan secara tiba-tiba. Adalah jelas bahawa sebarang bahan yang digunakan dalam aplikasi sedemikian terdedah kepada serangan daripada faktor persekitaran. Untuk mengatasi cabaran ini, bahan komposit pultrusi yang tersedia secara komersial, dikenali sebagai komposit polimer bertetulang gentian kaca (PGFRPC) telah dipertingkatkan lagi dengan menggunakan struktur komposit sarang lebah kerana sifat strukturnya yang sangat baik dan sifat ringan. Objektif penyelidikan ini adalah untuk membangunkan lengan silang PGFRPC yang dipertingkatkan dengan menggabungkan struktur sarang lebah untuk meningkatkan prestasi dan ketahanan. Metodologi menyeluruh digunakan, melibatkan ujian mendalam melalui lenturan tiga titik dan penilaian rayapan pada kedua-dua lengan silang sedia ada dan yang dipertingkatkan, dalam keadaan individu dan pemasangan. Penyelidikan ini mendedahkan bahawa sudut orientasi 0° yang optimum untuk lapisan muka yang dibuat daripada tenunan gentian kaca secara signifikan meningkatkan sifat lenturan. Menggunakan Teori Penyelesaian Masalah Inventif (TRIZ), carta morfologi, dan Proses Rangkaian Analitik (ANP), reka bentuk optimum untuk lengan silang PGFRPC sarang lebah telah dibangunkan, dengan Reka Bentuk Konsep 2 muncul sebagai pilihan terbaik. Integrasi struktur sarang lebah pada lengan silang sedia ada menghasilkan pengurangan 36.7% dalam pesongan dan pengurangan 33.7% dalam regangan rayapan. Selain itu, penyelidikan ini menunjukkan tingkah laku elastik linear yang lebih baik berbanding lengan silang kayu Balau tradisional berbanding lengan silang komposit. Penyelidikan ini juga menekankan bahawa lengan silang yang dipertingkatkan menunjukkan peningkatan rintangan terhadap daya lenturan, rintangan rayapan, dan kestabilan jangka panjang yang boleh memanjangkan jangka hayatnya dan mengurangkan kos penyelenggaraan. Penyelidikan masa depan harus memberi tumpuan kepada prestasi dinamik, tindak balas fleksibiliti, mod kegagalan, dan analisis rayapan di bawah keadaan dawai normal dan patah, dengan memvariasikan faktor keselamatan untuk memahami kesan beban yang lebih besar pada struktur komposit. Secara keseluruhan, penyelidikan ini membuktikan sifat rayapan unggul lengan silang PGFRPC yang dipertingkatkan, memberikan pandangan berharga untuk kemajuan masa depan dalam teknologi menara penghantaran.

Kata Kunci: Modulus Keanjalan, Sifat Lenturan, Sarang Lebah Sandwic, Lengan Silang PGFRPC, Menara Transmisi

SDG: MATLAMAT 9: Industri, Inovasi dan Infrastruktur

ACKNOWLEDGMENT

"IN THE NAME OF ALLAH, THE MOST GRACIOUS, THE MOST MERCIFUL"

In the name of the creator (Al-Khalid), The Most merciful (AR – Rahman) , most Beneficent (Ar- Rahim), ALLAH S.W.T. I seek His mercy and His noble prophet PBUTH Muhammad S.A.W in gave me strength, knowledge and guidance to complete my PhD Degree.

I would like to express my gratitude and thanks to my supervisor, Assoc. Prof. Dr. Mohamad Ridzwan Ishak, and co-supervisor, Assoc. Prof. Dr. Noorfaizal Yidris and Dr. Mohd Zuhri Mohamed Yusoff. Thank you for the support, patience, guidance, encouragement with advice and ideas throughout the completion of my study.

The biggest gratitude I would like to express to my beloved father (Abd Latif Md Rasoll) and my beloved mother (Mahaboobah Syed Mohamed) for their love and support in every aspect including motivation, spiritual and financing for achieve successful for this thesis completion. It is a great pleasure to have you as my parents. I owe a special thanks to my dearest wife, Shahilah Salleh for her continuous support and sacrifice to handles all my children (Akma Safiyyah Amir, Ahmad Suhaib Amir and Asma Siddiqah Amir) throughout my study. Moreover, I would like to give special thanks to both my father in-law (Salleh Ismail) and my mother in-low (Zariah Othman). Without their loves and supports, I would not be able to accomplish this research.

I would like to convey my great appreciation to Kementerian Pendidikan Tinggi Malaysia (Ministry of Higher Education Malaysia) for the financial support through fundamental

research grant scheme (FRGS). I would like to thank to all my peers and friends especially Muhammad Asyraf Muhammad Rizal, Hussein Khadim Sharaf and Waqas Ashraf, who were supporting and helpful during my doctorate degree journey. Last but not least, I would like to thank also to the staffs of Faculty of Engineering of their assistance during the experimental phase of this research.

This thesis was submitted to Senate of Universiti Putra Malaysia and has been accepted as fulfilment of the requirement for the Doctor of Philosophy. The members of the Supervisory Committee were as follows:

Mohamad Ridzwan Ishak, PhD
Associate Professor
Faculty of Engineering
Universiti Putra Malaysia
(Chairman)

Mohd Zuhri Mohamed Yusoff, PhD
Senior Lecturer
Faculty of Engineering
Universiti Putra Malaysia
(Member)

Noorfaizal Yidris, PhD
Associate Professor
Faculty of Engineering
Universiti Putra Malaysia
(Member)

____

ZALILAH MOHD SHARIFF, PhD
Professor and Dean
School of Graduate Studies
Universiti Putra Malaysia

Date: 12 Sept. 2024

TABLE OF CONTENTS

LIST OF TABLES

LIST OF FIGURES

LIST OF ABBREVIATIONS

ANP	Analytic Network Process
ASTM	American Society for Testing and Materials
AVG	Average value
CAD	Computer aided drawing
CB	Core buckling
CS	Core shear
DBD	Debonding
DLM	Delamination
FEA	Finite element analysis
FF	Facesheet failure
GFRP	Glass fibre reinforced polymer
IND	Indention
PGFRP	Pultruded glass fibre reinforced polymer
PGFRPC	Pultruded glass fibre reinforced polymer composite
SD	Standard deviation
SIS	Sandwich inner side
SOS	Sandwich outer side
TNB	Tenaga Nasional Berhad
TRIZ	Theory of The Resolution of Invention-Related Tasks
UPE	Unsaturated polyester
3-PB	Three point bending

LIST OF SYMBOLS

F_S	Core shear ultimate stress
F_X	Working load in longitudinal direction
F_Y	Working load in vertical direction
F_Z	Working load in transverse direction
F_{RN}	Resultant force for normal wire condition
F_{RB}	Resultant force for vertical, transverse and longitudinal force
F_{RXZ}	Resultant force for transverse and longitudinal force
P	Acting force
P_{max}	Maximum force prior to the first failure
h	Sandwich thickness
h_e	Cross-arm thickness
c	Core thickness
b	Sandwich width
b_e	Cross-arm width
S	Span length
t	Facesheet thickness
σ	Facesheet bending stress
σ_e	Cross-arm bending stress
σ_n	Specific cross-arm bending stress
L	Effective length
L_{SB}	Load span length (for sandwich honeycomb beam)
L_S	Span length (for individual cross-arm member)
L_C	Total length of the cross-arm member
U	Transverse shear rigidity
y	Mid-span deflection
D	Flexural stiffness

E	Elastic modulus
E_c	Effective elastic modulus for the individual cross-arm member
E_a	Apparent elastic modulus for the individual cross-arm member
E_e	Elastic modulus for the assembly cross-arm member
E_0	Initial elastic modulus for the cross-arm member
E_t	Elastic modulus for the cross-arm member at selected time
k	Elastic coefficient
G	Shear modulus
G_c	Shear modulus for cross-arm member
A	Cross-sectional area
w	Priority vector
n	Number of criteria
a_{ij}	Important scale
S_A	Stiffness
I	Moment of inertia
δ	Deflection
δ_{max}	Maximum deflection
$f_{1,2}(y)$	Load deflection function
r	Radius of gyration
ε_t	Strain across the cross-arm member
t	time
χ	Reduction factor

CHAPTER 1

INTRODUCTION

1.1 Background of study

At the beginning of line development for power transmission in Malaysia, timber cross-arms were utilized on transmission towers (Rawi et al., 2017). In 1929, Chengal wood (Neobalanocarpus) was specifically employed for the wooden cross-arms on 66kV towers, and by 1963, it was extended to 132 kV suspension towers (The National Electricity Board, 1988). Over time, it became evident that the wooden cross-arms were prone to failure due to aging, and by the late 1990s, high-quality Chengal wood had become scarce. Additionally, natural defects in the wood led to failures in wooden cross-arms after only 14 years of service, which was below the expected lifespan (Grzybowski et al., 2012). These issues prompted the study and research to replace wooden cross-arms as an alternative solution. Consequently, Glass Fiber Reinforced Polymer (GFRP) composite cross-arms were equipped on the middle, top and bottom phases of a selected tower in Malaysia as part of a pilot project (Engineering Department of TNB Transmission Division, 2013). The pultruded manufacturing process for GFRP composites was chosen due to its suitability for mass production and superior properties compared to wooden cross-arms (Turvey & Zhang, 2018a; Vieira et al., 2018).

The cross-arm's failure has become appear as a serious concern due to the limited solution can be found. Currently, efforts to enhance the sustainability of pultruded glass fibre reinforced polymer composites (PGFRPC) cross-arms involve temporary strengthening with additional structural elements. Research by Mohamad et al. explored the numerical deformation behavior of improved cross-arms using sleeve installations on both arms

(Mohamad et al., 2019). In the construction field, sleeve installations are widely employed for joining and strengthening beam-column connections due to their effectiveness (Cao et al., 2020; Y. Liu et al., 2020). Another enhancement method involves installing bracing on cross-arm members, with numerical simulations showing that bracing support can bear loads applied to one end of the cross-arm (Mohamad et al., 2019). Sharaf et al. proposed a different bracing design suitable for three types of cross-arm members (Sharaf et al., 2020). However, the use of bracing in cross-arm towers can lead to slip potential due to high stress on the beams.

Numerous studies have recommended modifications in the structural design of cross-arm systems to mitigate or prevent failures. Despite these efforts, fundamental research on new material designs for these components remains limited. This study will investigate the potential of honeycomb sandwich structures for cross-arms. A sandwich composite structure is a type of multi-layered structure with outer facings and an inner core. Various core designs, such as balsa wood, foam, honeycomb, tetrahedral truss, and corrugated cores, have been utilized (R. Bai et al., 2020; Ferdous et al., 2017; X. Li et al., 2019; Önder & Robinson, 2020; Qi et al., 2017; Thiruganasambanthan et al., 2022). The facings are typically thinner than the core, providing strength and stiffness while maintaining a lightweight profile. Glass or carbon fibre is often used for the facings due to their cost-performance benefits and resistance to environmental damage. Facings can also be made from single metallic layers or laminated or woven composite materials to enhance the sandwich structure's strength (Ilyas et al., 2022; Singh et al., 2022). The choice of sandwich structure materials depends on the structure's function and application, such as lifetime loading, availability, and cost considerations, especially in aerospace, marine, automotive, and other lightweight structural applications (Alsubari et al., 2021; Birman & Kardomateas, 2018; Önder & Robinson, 2020).

Many researchers are increasingly focusing on incorporating composite structures into hollow beams or tubes, an idea that can also be utilized to enhance cross-arm structures. Commonly, these structures are filled with materials such as honeycomb core, polymeric foam cores, or wood cores, which have been validated as effective fillers for hollow beams and tubes. (Güden & Kavi, 2006; Niknejad et al., 2012). In various fields like aerospace, automotive, construction and marine industries, sandwich structures are being used successfully in areas where there are limitations on weight while the strength requirements are high (Xin et al., 2016). Among the sandwich structures, the cellular core materials are the most efficient ones, especially in reducing the weight of a product and achieving enhanced strength (Bakis et al., 2003). Honeycomb core are the examples of the cellular core materials that are widely used in present study. The honeycomb cores are usually made of either aluminum or polymeric materials. In sandwich structures application, the honeycomb core is adhesively bonded with the face sheets with co-curing and secondary bonding (Z. Wang & Liu, 2019). The capabilities of sandwich structure are mostly refer to the core materials which need to be adequately characterized before using in applications.

Hussein et al., investigated failure mode of hollow and honeycomb core filled square carbon fibre reinforced polymer (CFRP) tubes during compressive test (Hussein et al., 2016). In addition, other researcher has used the honeycomb filled othogrid core sandwich to improve the stiffness of the structure (Shi et al., 2014). The use of honeycomb filled structure also can improve stiffness in some application as mention by Corradi et al. (Corradi et al., 2018). Besides that, a tandem honeycomb structure has showed improvement in mechanical behaviour such as energy absorption in multi-cell tubes application (Z. Wang et al., 2017). Moreover, the honeycomb filled tube has showed an excellent energy absorption compare to hollow tube (Yin et al., 2011). Additionally, studies comparing analytical and numerical results have demonstrated consistent findings regarding the load-carrying capacity of sandwich structures (Qin & Wang, 2013). Moreover, filled structures are favored in composite applications, particularly for energy absorption and load-bearing capacities, due to their straightforward design and ease of manufacturing (Z. Wang, 2019).

To enhance the strength of honeycomb structures in construction applications, Fu et al. have examined the flexural properties and shear stiffness of honeycomb sandwich panels with both hollow and foam-filled cells. (Y. Fu & Sadeghian, 2020). The flexural characteristics properties of sandwich panels with shape memory alloy wires embedded in between the facesheets have been studied by another researcher and showed that energy absorption during flexural characteristics test is greater in case of the specimen with pre-strained wires (Khalili et al., 2020). Several researchers have used this techniques especially to prepare test specimens and evaluate their mechanical properties such as the flexural characteristics (Jaafar et al., 2018). Other researcher has study the failure mood and creep properties of the honeycomb foam-filled aluminium tube during quasi-static compressive test (Hussein et al., 2017). It was found that, the best specimens in this study was the square aluminium tube filled with both polyurethane foam and aluminium honeycomb.

The creep behavior of composite sandwich beams with GFRP face sheets demonstrates linear viscoelastic properties at load levels below 40%, while creep failure occurs at load levels above 60% (X. Li et al., 2019). Additionally, researchers have proposed models that align with experimental creep curves, using sandwich panels in building floor applications (Garrido et al., 2016). Creep is a mechanical phenomenon that occurs when a material is subjected to prolonged steady stress, beginning with instantaneous deformation and progressing through primary (transient), secondary (steady-state), and tertiary (accelerated) stages until structural failure (Hunt et al., 2015; Lala et al., 2018). In the primary stage, the creep rate decreases linearly over time due to strain hardening or movable dislocations. During the secondary stage, a balance between dislocation production and recovery results in a nearly constant creep rate. The tertiary stage sees a rapid increase in creep rate leading to material rupture due to accumulated strain over time (Beddu et al., 2018; Sá et al., 2011a). Creep shear yielding causes void chain slippage, growth development, and fiber breakage, leading to material fracture. The current composite cross-arms, made from pultruded E-glass fiber-reinforced unsaturated polyester composites, are considered anisotropic structures (Syamsir et al., 2023). However, due to induced creep rupture, these composite materials sometimes exhibit interfacial strength instability, reducing the mechanical strength of the material.

However, literature indicates a scarcity of research focused on enhancing high transmission tower cross-arms using honeycomb sandwich structures. Therefore, this study aims to introduce an innovative honeycomb sandwich composite structure for these cross-arms. Such methods can produce continuous beams ideal for structural applications. Conducting a thorough investigation into the durability of these materials is crucial. These studies will provide insights into the current material failures and suggest alternative materials expected to sustain higher loads and extend service life.

1.2 Problem statements

While previous studies have highlighted the potential benefits of Pultruded Glass Fiber Reinforced Polymer Composite (PGFRPC) cross-arms, a significant gap remains in understanding their performance under actual working load conditions. There is a notable lack of comprehensive studies evaluating their load-deflection behavior in real-world assembly conditions compared to traditional Balau wood cross-arms (Asyraf et al., 2021c; Sharaf et al., 2020). It is crucial to bridge this gap by thoroughly analyzing and comparing the load-deflection behavior of PGFRPC cross-arms under both normal and broken wire scenarios to validate their structural enhancements and higher bending stress resilience. Besides that, several failure cases have been reported by TNB which created an urgency for finding alternatives solution for enhanced the cross-arm in transmission tower (Rawi et al., 2017). Based on these reports, this study was conducted and serves as a catalyst for producing solutions that can assist TNB while also establishing it as the national leader in electricity

Moreover, the aerospace and structural industries have recognized the exceptional bending performance of honeycomb sandwich composites, which depend on the characteristics of their facesheet and core materials. The facesheet enhances bending strength and surface stiffness, while the core provides rigidity and distributes applied loads over a larger area. Different fiber angle in the facesheets can result in varied mechanical properties, making these structures suitable for diverse applications (Adekomaya & Adama, 2017; Kharratzadeh et al., 2018; Pai et al., 2021). To fully harness the benefits of honeycomb sandwich composites, it is essential to investigate the influence of woven glass-fiber prepreg angle on their behavior. This study aims to fill this knowledge gap by examining the flexural behavior, ultimate strength, and failure mechanisms of honeycomb sandwich panels with different prepreg angle, ultimately enhancing the properties of PGFRPC cross-arms.

Sustainability considerations for existing PGFRPC cross-arm members extend beyond temporary strengthening measures such as install bracing system, applied sleeve and change laminate properties of the cross-arm members (Asyraf et al., 2023; Bulut et al., 2017; Mohamad et al., 2020; Mohamad et al., 2019). Enhancing pultruded GFRP composites with a honeycomb sandwich structure could provide a viable alternative for sustaining cross-arms due to their superior mechanical performance. Although, pultruded composites are typically strong in tension and compression but might lack sufficient in flexural rigidity. A honeycomb sandwich structure can significantly improve the flexural stiffness and strength of the composite, making it more suitable for load-bearing applications. Therefore, design optimization of the honeycomb sandwich configuration for PGFRPC cross-arms, focusing on performance, cost-effectiveness, and manufacturability, is necessary. The new design is expected to reduce deformation at critical points and increase the service life of cross-arms.

Existing literature has predominantly focused on coupon-scale studies or simulations, which may exaggerate factors due to the neglect of full-scale geometry and profile, leading to a lack of comprehensive knowledge about the full-scale and real-world environmental assessments of the PGFRPC cross-arms either for individual and assembly conditions (Alhayek et al., 2023; Asyraf et al., 2023; Syamsir et al., 2022, 2023). To address this issue, it is imperative to develop methods for evaluating the properties of full-scale PGFRPC cross-arms under real environmental conditions particularly when integrated with honeycomb sandwich structures. This will provide more reliable data on deflection behavior, elastic properties, flexural performance, and predictions of property reductions, advancing transmission tower technology and ensuring the resilience of power transmission infrastructure. By addressing these gaps, this study will significantly contribute to the advancement of PGFRPC cross-arm technology and the overall resilience of transmission tower infrastructure.

1.3 Research objectives

The objective of this study is to evaluate the performance and durability of PGFRPC cross-arms used in transmission towers with presence of honeycomb sandwich composite structure using experimental and numerical approaches.
The specific objectives of this study are summarized as follows:

1. To analyze and compare the deformation behavior of full-scale PGFRPC and wood cross-arm under actual working load conditions.
2. To synthesize and characterize the fiber angle orientation on the flexural properties of honeycomb sandwich structure.
3. To optimize the design of honeycomb sandwich composite structure configuration on the PGFRPC cross-arm using concurrent engineering concept.
4. To investigate the influence of honeycomb sandwich PGFRPC cross-arm on load deflection and creep performance including their flexural properties of individual and assembly cross-arm member.

1.4 Significance of study

The significant contribution of this study are listed below:
1. The comprehensive knowledge of the assembly PGFRPC cross-arm performance under actual and working load condition compare to traditional Balau wood can validate the cross-arm potential in structural enhancement.
2. The development and enhancement of honeycomb sandwich structure with appropriate fiber orientation used for cross-arm will improve the current cross arm structure performance in high transmission tower.

3. The finding from the study are expected to enrich the knowledge of flexural properties, deflection behavior and creep performance in enhancing the current PGFRPC cross-arm towards longer service life and better durable structure in transmission tower application.
4. The successful of this study assist to produce the state of art new material structure that can be used in cross arm for high transmission tower and other beam application which can reduce maintenance cost, safety risk to workers and also any casualties which may occur.

1.5 Scope and limitation of the research

The primary focus of this study is on the development and characterization of a new material structure for cross arms in high transmission towers using a honeycomb sandwich structure to enhance the mechanical properties of existing PGFRPC cross arms. The study analyzes the performance of these cross arms under flexural deformation and creep response. Two configurations of cross arms, individual and assembly members, were tested using two flexural tests: three-point bending and cantilever beam tests, following ASTM standards. The tests were conducted in an outdoor environment to simulate actual conditions experienced by cross arms in transmission towers. The creep test was conducted over 1000 hours, as the minimum required time to observe trends from instantaneous strain through primary and secondary creep stages. Other limitations of this study include:

1. Scope of Mechanical Properties Only: This study focuses exclusively on the mechanical properties, characterization, and performance of composite materials for high transmission cross arms. It does not consider the material's electrical conductivity and insulating properties.

2. Specific Tower Types and Voltage Levels: Although transmission towers come in various types such as tension towers, suspension towers, terminal towers, and transposition towers, this study is limited to the cross arms of suspension towers only. Additionally, the study targets the 13L cross arm design specifically for 132 kV towers. Other voltage levels like 500 kV and 275 kV were not considered. The 132 kV cross arms are widely used due to high demand from small industries and residential areas.
3. Creep Test Methodology: The creep test implemented in this study is a load-based creep test, chosen to reflect the actual bending deformation experienced by cross arms due to shear stress during operation. Dial gauges with magnetic holders were used for measuring deformation and creep strain in both the cantilever beam test and three-point bending test. Strain gauges with data loggers were not used due to the requirement for special tools, high costs, and complications associated with conducting the tests outdoors under uncontrolled climate conditions.
4. Limited Sample Availability: As Tenaga Nasional Berhad (TNB) monopolizes the electricity supply sector in Malaysia and owns all transmission towers, they control and restrict the supply of cross arms for these towers. Consequently, only a limited number of full-scale PGFRPC cross arm members were available for experimental testing. This limitation affected the study by allowing the testing of only one sample at a time for the assembly cantilever beam test and several samples concurrently for individual three-point bending tests.

1.6 Structure of thesis

This thesis consists of up of five parts. Chapter 1 is the introduction, and Chapter 5 is the conclusion and suggestions. In the first chapter, it covers the overall introduction to this study, which is mostly made up of study background, problem statement, study goals, study scopes, importance of study, and overall thesis structure. Chapter 2 shows the literature review that was done for the study. It focuses on recent studies and issues related to cross arms, product developments, current creep tests, and numerical analyses. In this chapter also, the overview on sandwich composite product and their enhancement in structural application have been done. For Chapter 3, it describes the general study method and the specific methods used to do this study. This covers the process for developing the product, the materials used, and the steps involved in fabrication, deflection, and creep characterization when it comes to the cross arm for high transmission tower construction. The findings of the tests, their analysis, and their significance are covered in Chapter 4. Chapter 5 gives the overall and specific conclusions of this study, as well as suggestions for future work.

CHAPTER 2

LITERATURE REVIEW

2.1 Introduction

This chapter aims to give comprehensive knowledge for the latest information on the application of honeycomb sandwich structure and pultruded glass fibre-reinforced polymer composite (PGFRPC) cross-arms for high transmission towers. The flexural and creep criteria are used to understand and analyse the enhancement of the existing PGFRPC cross-arm under actual scale for individual and assembled arrangement. Various articles have been reviewed and discussed on the enhancement of pultruded glass fibre and honeycomb sandwich structure for coupon and actual scale testing, such as tensile, flexural, and compression properties. The consolidation between honeycomb structure and pultruded glass fibre is given particular attention in this literature, specifically for the composite cross-arm for high transmission towers. Potential issues can eventually be resolved more satisfactorily in the future.

2.2 High transmission towers

Over the past few decades, numerous design concepts for overhead power line transmission towers have been developed, primarily driven by increasing environmental constraints alongside rising power demands. Typically, the design of transmission towers must support the weight of the transmission conductor at a specified height from the ground and facilitate the connection between power generators and substations. (Alhassan et al., 2020). In recent years, Malaysia has been growing steadily, especially in several leading sectors, and the country also indirectly requires sufficient power supply capability. In Malaysia, Tenaga Nasional Berhad (TNB) is a government-linked company that is responsible to generate, supply, distribute, and maintain the electricity needed by consumers via their transmission division lines. The range of the supply voltage is approximately 66–500 kV, in which the transmission network in circuit joined together almost 12,200 km across the Peninsular Malaysia with approximately 420 power substations as shown in Figure 2.1 (Bakar et al., 2018).

Energy is commonly produced by traditional power plants that burn fossil and nuclear fuels, and these plants are probably situated far from the load centres due to environmental restrictions. Other sources for energy production are coal, hydropower, oil, natural gas, renewable resources, and solar thermal energy. Coal is the main energy source used to generate electricity in Malaysia. Transmission lines are used as the most practical way to move electrical energy from generating units to load centres (Kishore & Singal, 2014). The transmission system forms the backbone of the integrated power system and operates at the highest possible system voltage. Usually, power transmission is done using the AC system at high voltage to minimise transmission losses; therefore, the power transfer capability of the line will increase (Dunlop et al., 1978).

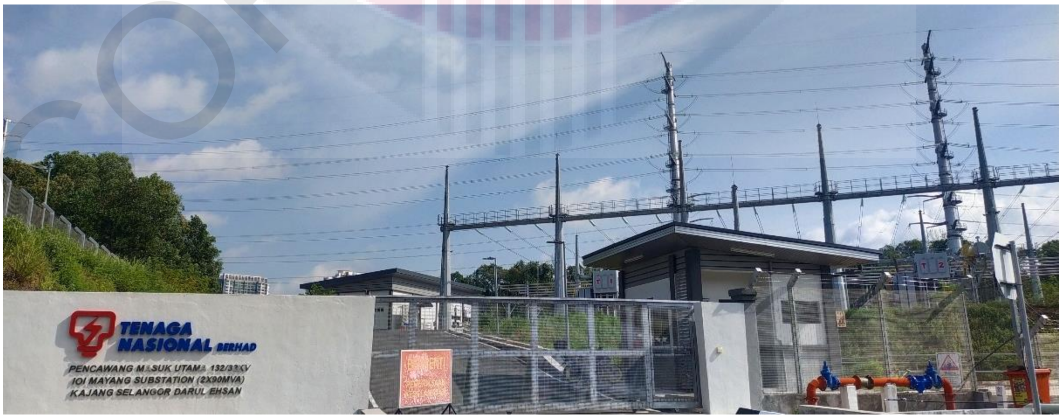

Figure 2.1: 132/33 kV IOI Mayang TNB substation in Kajang, Selangor.

2.2.1 Transmission towers and design

Transmission towers are essential components in the electrical grid, facilitating the transmission of electricity between power plants, load centers, and various transmission systems. These towers are categorized into tension, terminal, transposition, and suspension types, each serving a specific function in the grid (Kang et al., 2007; Li et al., 2015). The choice between overhead and underground transmission line systems is influenced by factors such as aesthetics, public safety, and urbanization (Robert & Lemelin, 2002). In overhead systems, lattice steel towers and steel tubular monopoles are commonly utilized as shown in Figure 2.2, with lattice steel towers being suitable for open spaces and steel tubular monopoles for urban areas with limited space (Albermani & Kitipornchai, 2003). The construction of transmission lines is a complex process that necessitates meticulous planning due to technical, geographical, and regulatory considerations (Kang et al., 2007).

The design of a transmission tower is critical for its structural integrity and operational efficiency. A transmission tower comprises components such as a peak, cage, tower body, beam, and cross-arm, with the cross-arm playing a crucial role in supporting the transmission conductor and maintaining safe wire distances above the ground (Bhowmik & Chakraborti, 2019). Designing transmission towers requires a profound understanding of structural engineering principles, modern design codes, and practical experience to ensure their stability and strength (Kamarudin et al., 2018). Additionally, considerations such as wind load, ice load, and seismic factors are vital in the design process to meet both electrical and structural requirements (Albayrak & Morshid, 2020; H. Liang et al., 2023; Y. Liu et al., 2022). Optimization techniques, including mode-pursuing sampling and machine learning classification, are employed to enhance the design of transmission towers, focusing on aspects like weight reduction and structural efficiency (An et al., 2010;

Z. Liang et al., 2023). By integrating advanced modeling methods and dynamic analysis, engineers can guarantee the reliability and safety of transmission towers under various operating conditions.

Transmission towers are crucial for the reliability and safety of the power grid, with their structural behavior being of utmost importance (He et al., 2021). Failures in these structures can result in significant economic and social consequences, leading to interruptions in power supply (G. Liu & Li, 2009). Optimizing tower designs plays a key role in enhancing structural efficiency and reducing construction costs (F. Y. Wang et al., 2017). Advanced modeling techniques, including multi-scale modeling and machine learning, are applied to improve performance and reliability (F. Wang et al., 2019). By integrating optimization algorithms and structural analysis strategies, engineers can create designs that meet electrical requirements while considering topographical factors and costs (X. Zhang et al., 2018). Research on dynamic responses under various conditions offers valuable insights for designing towers capable of withstanding environmental challenges (Huang et al., 2018). Continuous progress in design and analysis methodologies is essential for guaranteeing the resilience and efficiency of power transmission infrastructure.

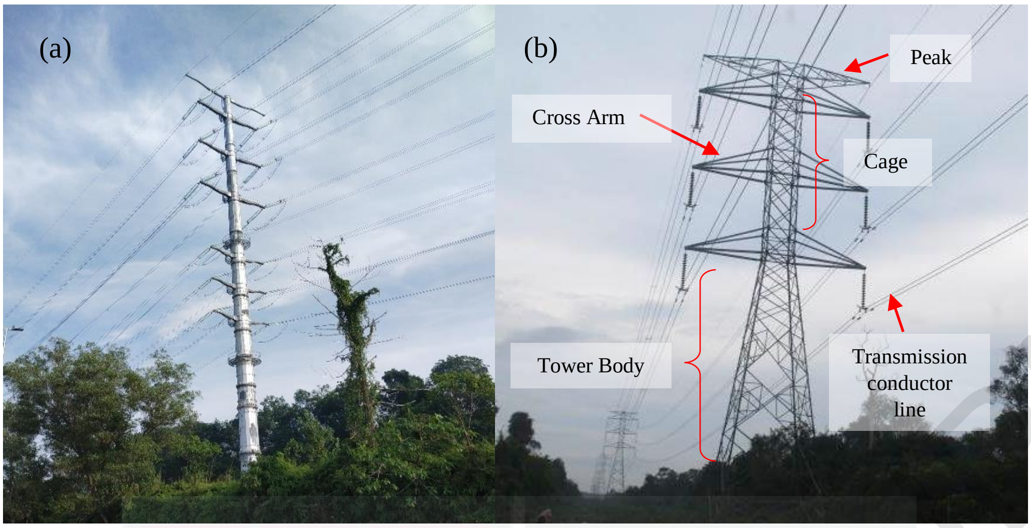

Figure 2.2: Transmission towers in Malaysia (a) steel tubular monopoles (b) lattice steel towers.

2.2.2 Cross-arm fabrication materials

Generally, suspension towers are also made of non-conductive material to avoid unexpected accidents on humans and properties due to electrical current and electromagnetic radiation from high-voltage lines (Sarah Sulaiman et al., 2018). In some cases, the cross-arm failure in transmission towers would cause disruption towards electrical supply to end users, resulting in additional maintenance costs to the electrical corporation (Nadhirah et al., 2017; Rao et al., 2005). Therefore, the materials used for cross-arm fabrication also need to have high mechanical strength as the main objective of the cross-arm is to sustain cables during load application. Besides, the ability to quench the electric arc during lightning strikes has also become one of the priorities in choosing the material for cross-arm fabrication.

Since 1929, the 132 kV cross-arm assembly has been commissioned in the Malaysian electrical grid using Chengal and Balau wood as the structural material. This is due to their better mechanical efficiency and excellent quenching of the electric arc (Bakar et al., 2018), and about 22 different types of wood were selected as the wooden cross-arm and mounted on high transmission towers (Sharaf et al., 2020). Moreover, wood has long been a versatile material for various structural applications. Wood-based materials are easily accessible and can be processed inexpensively in large quantities. However, wooden timber cross-arms generally require frequent inspections over time due to their vulnerability to natural biodegradation such as rotting and damage from natural pests like woodpeckers and termites (Ilyas et al., 2021). This has highlighted several issues with wooden cross-arms, particularly the structural failures that tend to occur after 20 years of service on transmission towers. In addition to natural wood defects (Asyraf et al., 2021), these structural deficiencies are often caused by creep deformation over prolonged use. In some cases, the failure of a cross-arm on a transmission tower can disrupt the electrical supply to end users and lead to increased maintenance costs for the electrical company (Nadhirah et al., 2017). Additionally, a failed cross-arm structure may increase the risk of injury to nearby pedestrians (Rao et al., 2005).

Aside from using wood, several types of steel insulator material have also been used for cross-arm fabrication for high-voltage transmission towers in the last 50 years. The cross-arm application is constantly evolving in response to new challenges, such as the interference of high-voltage lines in densely populated regions, conductor overheating due to overrating, mechanical withstand capacity constraint, and others (Ahsan et al., 2022). With the increasing load demand, the governments and utility companies need to increase the capacity of existing transmission lines to fulfil the demands (Daconti & Lawry, 2003; Ntuli et al., 2016). It can be done by increasing voltage, upgrading, or refurbishing. However, most of the lattice transmission towers with steel cross-arm face the problems of rust and short life span due to capacitance issues, which deal with heavy conductors (Rao et al., 2005). Several studies have found that the failure of the steel cross-arm is also due to its low flexibility and construction of support tie-bars (Papailiou, 1999; Prasad Rao et al., 2012). Researchers have introduced some insulator cross-arms and composite cross-arms to counter the steel cross-arm issues (Albizu et al., 2005; B. Burkhardt et al., 2003).

Recently, composites have been widely chosen in the development of structural applications, including cross-arms for high transmission towers, especially in China, India, United Kingdom, and Malaysia (Nadhirah et al., 2017; Peesapati et al., 2012; Selvaraj et al., 2013; X. Yang et al., 2014). Their advantages include high strength, corrosion resistance, chemical stability, and good performance as insulators in lightning impulse strength for cross-arms in high transmission towers (Selvaraj et al., 2013). Researchers have been urged by this troubling situation to replace the cross-arms with new materials, such as polymeric composites. Therefore, PGFRPC cross-arms have been implemented on transmission towers to replace the previous wooden cross-arms (Beddu et al., 2018) to fulfil the criteria of cross-arm alternatives. Among the benefits of using PGFRPC are light weight, non-biodegradable, and versatile in nature (T. Liu et al., 2020). The good combination between the type of material used (GFRP) composite and the fabrication method (pultruded) enhances the mechanical properties of cross-arms compared to the previous cross-arms, which have been proved by several studies, as shown in Table 2.1.

Table 2.1: Mechanical properties of PGFRPC and wood cross-arm in coupon scale.

Properties	Cengal-wood	Balau-wood	Pultruded GFRP composite
Density	915-980 kg/m3	850-1155 kg/m3	2580 kg/m3 – E-glass 1350 kg/m3 – Unsaturated polyester
Texture	Fine and even with deeply interlocked grain	Fine and even with deeply interlocked grain	Fine, homogenously and unidirectional fibre along the matrix
Shrinkage	High	High	Low
Natural Durability	Very High	High	Low
Modulus of Elasticity	19.6 GPa	20.1 GPa	29.8 GPa
Modulus of Rupture	149.0 MPa	142.0 MPa	858.0 MPa

(Source: Arnandha et al., 2017; Chengal Wood Technical Informations, 2019)

2.2.3 PGFRPC cross-arm

The use of PGFRPC cross-arms in transmission towers is increasing due to their potential to replace previous wooden cross-arms, offering enhanced mechanical performance and durability (Cardoso & Harries, 2019). While PGFRPC materials have been extensively studied for their long-term behavior under various environmental conditions, including exposure to water, moisture, and temperature fluctuations (T. Q. Liu et al., 2020), there is a research gap focusing on the full-scale mechanical efficiency and structural stability of PGFRPC cross-arms to withstand prolonged duty loads (Asyraf et al., 2020). Most existing studies have concentrated on computer simulations, small-scale experiments, and beam analyses, lacking a comprehensive characterization of the assembly as a whole.

The cross-arm assembly is crucial for supporting electrical conductor cables and insulators in transmission towers, ensuring continuous electrical energy supply from power generators to substations and end users (Asyraf et al., 2021a). In the Malaysian power grid system, cross-arms are essential components for transmitting electricity through cables at different voltage levels, such as 132, 275, and 500 kV, with the largest transmission structures being at 500 kV, followed by 275 kV and 132 kV systems (Syamsir et al., 2022). However, further research is needed to evaluate the performance of PGFRPC cross-arms comprehensively, considering factors like mechanical efficiency, structural stability, and long-term integrity under operational loads to ensure the reliability of the power transmission infrastructure.

In general, the assembly of cross-arm members are directly fitted in the galvanised socket and fittings at the cage component of the transmission tower (Bakar et al., 2018). Figure 2.3 displays the schematic diagram of the cross-arm assembly in a transmission tower. This would ensure that the electrical energy can be supplied continuously via these cables that hang on the cross-arms from the power generator to substations before it gets to end users. In conclusion, the adoption of PGFRPC cross-arms in transmission towers offers a promising alternative to conventional materials, providing improved mechanical properties and durability. Future research should focus on conducting full-scale mechanical assessments and structural analyses to ensure the long-term performance and reliability of PGFRPC cross-arms under operational conditions, addressing the current research gap in the field and contributing to the advancement of power transmission infrastructure.

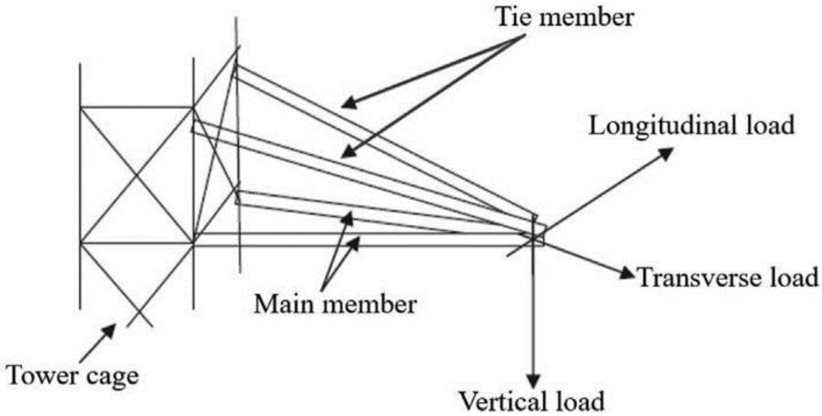

Figure 2.3: Schematic diagram of the cross-arm attached to the tower body.
(Source: Munusamy Selvaraj et al., 2013)

2.3 Mechanical properties and performance of PGFRPC cross-arm

The PGFRPC cross-arms demonstrate significant mechanical properties that position them as a preferred choice in transmission tower applications. Research has been conducted to assess the load-carrying capacity, deformation behavior, and structural integrity of PGFRPC cross-arms under various conditions. For instance, Huang et al. (2023) investigated the mechanical properties of the cross arm-insulator system under horizontal wind loads, offering insights into the behavior of PGFRPC materials when exposed to external forces. Additionally, Asyraf et al. (2021) conducted creep experimental and numerical analyses to explore how additional bracing arms can strengthen PGFRPC cross-arms, emphasizing the importance of considering long-term mechanical performance.

The reliability and durability of transmission tower structures heavily rely on the performance of PGFRPC cross-arms. Recent advancements have concentrated on evaluating the performance of full assembly Glass Fiber-Reinforced Polymer (GFRP) composite cross-arm tubes in high voltage transmission towers using Finite Element (FE) analysis. Syamsir et al. (2022) have contributed to this field by assessing the performance of GFRP composite cross-arms, shedding light on the structural efficiency and reliability of these components. Furthermore, the potential utilization of honeycomb-filled composite structures in composite cross-arm components has been explored to enhance mechanical properties and structural integrity, showcasing the ongoing enhancements in PGFRPC cross-arm technology.

Despite the benefits of PGFRPC cross-arms, there are still challenges that require attention to optimize their performance. Studies have emphasized the necessity for comprehensive evaluations of PGFRPC cross-arms to tackle issues related to mechanical efficiency, structural stability, and long-term integrity under operational loads. By considering factors such as material properties, load-carrying capacity, and deformation behavior, researchers aim to address challenges associated with PGFRPC cross-arms and improve their overall performance in transmission tower applications.

2.4 Recent issues of PGFRPC cross-arm

The utilization of Pultruded Glass Fiber-Reinforced Polymer Composite (PGFRPC) cross-arms in high transmission towers presents several critical issues that researchers have identified (Andreotti et al., 2020). One significant concern is the lightning performance of these cross-arms, as lightning strikes can have detrimental effects on transmission line structures. While PGFRPC cross-arms exhibit higher dielectric strength compared to traditional wooden cross-arms, they are still susceptible to lightning impulse over-voltage, which can lead to structural damage. As technology advances, the development of cross-arms evolves accordingly. Experimental and simulation studies by Rawi et al. (2017) demonstrated that PGFRPC cross-arms exhibit greater dielectric strength than wooden cross-arms, particularly in performance against lightning strikes (see Figure 2.4). Other researchers have worked on enhancing the lightning performance of transmission lines by developing grounding systems for transmission towers (Koehler & Swingler, 2018; Shariatinasab et al., 2016). Researchers have highlighted the importance of developing proper insulation methods, such as using higher-rated insulators or additional insulation components, to mitigate the impact of lightning strikes on PGFRPC cross-arms (Grzybowski et al., 2012).

Another pressing issue for PGFRPC cross-arms is the impact of environmental degradation on their properties. The aging of composite components due to climate change, fluctuating temperatures, and exposure to moisture and heat can significantly affect the structural integrity of GFRP materials as shown in Figure 2.4. Despite the advantages of PGFRPC cross-arms over wooden counterparts, the environmental conditions to which these cross-arms are exposed in transmission line assemblies can lead to substantial structural defects and degradation over time (Hu et al., 2016; Syamsir et al., 2019; Zainuddin et al., 2010). It is inevitable that the GFRPC cross-arms in transmission towers will be exposed to ecological factors. Numerous studies in this area have shown that the mechanical properties of the structure will decline as a result of the simultaneous activity of mechanical loadings and natural effects like increased temperature, humidity, and others, which act as vicious agents that accelerate the degradation of composite material structures (François-Heude et al., 2014; Lu et al., 2016). Additionally, the considerable degradation effect in GFRP applications in this analysis raises questions about durability and structures before considering cost and design methods.

Figure 2.4: Lightning and environmental degradation issues on cross-arm lead to structural damage.
(Source: Rawi et al. (2017))

Moreover, researchers have highlighted the challenge of sudden failure in PGFRPC cross-arms within high transmission towers as a critical issue. Sudden failures pose significant risks, including shortening the cross-arm's lifespan, causing disruptions in electrical transmission, and incurring additional maintenance costs for electrical providers (Asyraf, Rafidah, et al., 2023). Factors contributing to sudden failures include low fiber bonding, stacking sequence issues, compression and tension failures, and material creep (Abu Bakar et al., 2020; Alhayek et al., 2022; Betts et al., 2021; Segovia et al., 2013). Addressing these issues requires comprehensive assessments and enhancements in cross-arm designs and materials to ensure the long-term reliability and safety of transmission tower structures (G. Li et al., 2020).

In conclusion, the issues surrounding PGFRPC cross-arms in high transmission towers, such as lightning performance, environmental degradation, and sudden failure risks, underscore the importance of ongoing research and development efforts to enhance the durability, reliability, and structural integrity of these critical components in power transmission infrastructure.

2.5 Overview of honeycomb sandwich composite structure

A sandwich composite structure is a type of multi-layered construction consisting of outer facings and an inner core. A variety of core designs have been employed, such as balsa wood, foam, honeycomb, tetrahedral truss, corrugated cores, and various bio-inspired cores. (R. Bai et al., 2020; Ferdous et al., 2017; X. Li et al., 2019; Önder & Robinson, 2020; Qi et al., 2017; Thiruganasambanthan et al., 2022). The facings, or facesheets, are typically thinner than the core, providing strength and stiffness while maintaining a lightweight property. Glass or carbon fiber is commonly used for the facesheets of sandwich composites due to their cost-performance benefits and superior resistance to environmental damage. Additionally, the facings can be made from a single metallic layer or laminated or woven composite materials, which are widely used to reinforce the sandwich structure (Ilyas et al., 2022; Singh et al., 2022).

The choice of sandwich structure materials typically depends on the structure's functions and applications, including factors like lifetime loading, availability, cost, and weight considerations, particularly in fields such as aerospace, marine, automotive, and other lightweight structural applications (Birman & Kardomateas, 2018; Cantwell et al., 1999; Composite Materials Handbook, Volume 6. Structural Sandwich Composites, 2013). A standard sandwich structure resembles an I-beam, where the flanges bear most of the bending and in-plane loads, while the web handles transverse shear, redistributes concentrated normal forces to the surface, and maintains the structure's overall integrity.

2.5.1 Mechanical performance of honeycomb sandwich composite

The mechanical performance of honeycomb sandwich composites is a subject of extensive research and interest within the materials science and engineering community.

Honeycomb sandwich composites are well-known for their mechanical performance in various applications. To meet the demands of lightweight design, high specific strength, good energy absorption, impact resistance, bending properties, compression characteristics, low-velocity impact behavior, and shear performance, researchers have explored different methods to enhance the mechanical properties of these composites (Luo et al., 2019; Wu et al., 2019; W. Zhao et al., 2021).

Research has indicated that the incorporation of nanotechnology, such as Multi-Walled Carbon Nanotubes (MWCNTs), can help reduce damages during impacts, thus enhancing the mechanical properties of fiber-reinforced honeycomb sandwich composites (Demirci, 2020). Moreover, the out-of-plane mechanical properties of composite honeycomb sandwich structures are crucial for improving energy absorption characteristics, making them suitable for impact scenarios (Chang et al., 2024). Besides that, defects in aluminum honeycomb cores can significantly impact the mechanical properties of sandwich structures, underscoring the importance of core quality in maintaining overall performance. Impact damage has been identified as a factor that can decrease the shear strength of honeycomb sandwich panels, emphasizing the need to address impact-related issues for optimal performance (A. Chen et al., 2023).

Additionally, the compression characteristics of honeycomb sandwich structures, particularly those reinforced with carbon fibers, offer benefits in terms of lightweight design, high specific strength, and good energy absorption capabilities (Xue et al., 2022). Studies on low-velocity impact responses have highlighted the potential of all-composite Kagome honeycomb sandwich structures for lightweight engineering applications (Song et al., 2024). Furthermore, extensive research has been conducted on the energy absorption and impact resistance properties of honeycomb sandwich panels, demonstrating their effectiveness in applications requiring high specific strength and good energy absorption capabilities (Yaakob et al., 2020). The dynamic cushioning energy absorption of paper composite sandwich structures with corrugation and honeycomb cores has also been investigated, revealing excellent mechanical properties (Ji et al., 2022).

In conclusion, the mechanical performance of honeycomb sandwich composites is influenced by various factors such as core quality, impact resistance, compression characteristics, and shear strength. Researchers are continuously exploring innovative approaches, including nanotechnology and composite reinforcements, to enhance the mechanical properties of these composites for diverse applications. With their good quality of mechanical performance also, the honeycomb sandwich composite structure has been proposed in this study as the enhancement structure on the PGFRPC cross-arm.

2.5.2 Influence of core and facesheet materials

The influence of core and facesheet materials on sandwich structures is crucial for determining the overall performance and characteristics of these composite systems. The core materials, such as honeycomb, balsa wood, foam, corrugated and tetrahedral truss, and bio-inspired cores, play a significant role in providing strength, stiffness, and lightweight properties to the sandwich structures (R. Bai et al., 2020; Ferdous et al., 2017; X. Li et al., 2019; Önder & Robinson, 2020; Qi et al., 2017). For instance, honeycomb-filled structures are widely used due to their simplicity, manufacturability, and energy absorption capabilities (Shi et al., 2014; Z. Wang et al., 2017; J. Xiang & Du, 2017). Studies have shown that the mechanical behavior of sandwich structures with honeycomb cores can be enhanced by innovative designs like tandem honeycomb structures and embedding honeycomb cells with foam or tubes as shown in Figure 2.5 (M. Li et al., 2013).

These designs have demonstrated improved energy absorption and mechanical properties compared to traditional structures (Joseph et al., 2023).

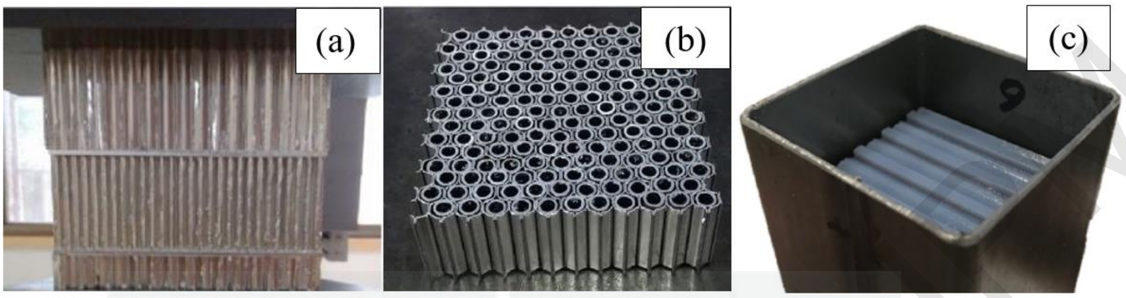

Figure 2.5: Innovations in honeycomb structures, (a) tandem honeycomb structures, (b) embedded honeycomb structures, and (c) honeycomb-filled structures.
(Source: Shi et al., 2014; Z. Wang et al., 2017; Xiang & Du, 2017).

Honeycomb core-based structures have gained significant popularity among researchers and industries for the production of sandwich structure products in various applications. Compared to other core or base structures, honeycomb cores offer unique advantages and properties. The honeycomb structure consists of a series of hexagonal cells, providing excellent strength-to-weight ratio, stiffness, and energy absorption capabilities (Q. Liu et al., 2017; Niknejad et al., 2012; J. Xiang & Du, 2017; Zarei Mahmoudabadi & Sadighi, 2011). These characteristics make honeycomb cores ideal for applications that require lightweight and strong materials, such as aerospace, automotive, and marine industries. Additionally, honeycomb cores offer enhanced thermal and acoustic insulation properties, making them suitable for applications where temperature control and sound dampening are crucial (R. Bai et al., 2020; D'Alessandro et al., 2013; Roy et al., 2014). The versatility and superior performance of honeycomb core-based structures have made them a preferred choice, driving ongoing study and innovation in this field.

The properties of sandwich constructions are heavily influenced by the selection of appropriate material for the facesheets (Fagerberg & Zenkert, 2005). The role of the facesheets in sandwich structures is to withstand the bending forces applied to the structure. During bending, one facesheet undergoes compression while the other experiences tensile pressure. This compression can cause local instability in the thin facesheets, potentially leading to buckling or debonding failure (Ley et al., 1999). Various studies have investigated facesheet materials, including synthetic composites, reinforced petroleum-based composites, bio-based composites, and hybrid composites (Azwa et al., 2013; Du et al., 2012; Mak et al., 2015; Petrone et al., 2013; Plevris & Triantafillou, 1995; Santulli et al., 2013). Continued study and innovation in core and facesheet materials will drive advancements in sandwich structure technology for diverse industrial applications, specifically for structural applications.

On the other hand, facesheet materials, particularly fibre-reinforced polymer composites, contribute to the exceptional mechanical properties, lightweight characteristics, and design flexibility of sandwich structures (Grove et al., 2006). Fibre reinforcement, such as glass or carbon fibres, provides high strength and stiffness to the facesheets, enabling them to withstand bending forces effectively. The use of fibre-reinforced polymer composites in sandwich structures ensures a favourable strength-to-weight ratio, contributing to weight reduction and improved performance in industries like aerospace, automotive, and construction (Deogonda & Chalwa, 2013; Genedy et al., 2015; Mohd Nurazzi et al., 2017). The polymer matrix surrounding the fibres enhances durability and impact resistance, leading to a favourable strength-to-weight ratio in the sandwich structures (Joseph et al., 2023). Research and development efforts continue to advance the capabilities of fibre-reinforced polymer composites, expanding their utilization in sandwich structures and driving innovation in lightweight, high-performance materials.

Lastly, the selection and design of core and facesheet materials are paramount in determining the structural integrity, mechanical performance, and lightweight characteristics of sandwich structures. The strength of the interfacial bonding between these components significantly influences the mechanical properties, controlling energy absorption, force transfer, and overall structural response under various loading conditions (Hegde & Hojjati, 2019; G. Sun et al., 2020). Ongoing research focusing on innovative used of honeycomb sandwich designs are driving the development of more efficient and high-performance sandwich structures for diverse applications. Optimizing the configuration and material selection of both core and facesheet components is essential for enhancing the mechanical properties, load-carrying capabilities, and overall efficiency of these structures.

2.5.3 Effect of fibre angle orientation

Several experimental studies have investigated the behavior and characterization of different fiber lay-up orientations of facesheets. Kharratzadeh et al. examined the delamination behavior of sandwich structures made from plain woven glass/epoxy resin composites, focusing on the impact of the interface fiber angle (Kharratzadeh et al., 2018). Their findings indicated that for a sandwich structure produced by the hand lay-up method with a 0°/0° interface, changes in the delamination interface angles had minimal effect on the initiation and propagation fracture toughness, as well as the length of the fracture process zone. Another study by Adekomaya and Adama (2017) explored the tensile and impact strength of composite sandwich materials with three fiber orientations (0°, 30°, and 60°), demonstrating enhanced strength for high fiber composites with a 0° orientation (Adekomaya & Adama, 2017).

Table 2.2 summarizes previous studies on fiber lay-up orientation; however, there is a notable gap in research on the flexural behavior of woven prepreg glass fiber orientations. Therefore, this study aims to investigate the effect of woven prepreg glass fiber orientation on the flexural behavior of honeycomb sandwich composite panels using a three-point bending test. Consistent with previous research, the results of this study could be applied to reinforce PGFRPC cross-arms in high transmission towers. To the best of my knowledge, limited research has been conducted on woven prepreg glass fiber composites with different fiber orientation facesheets, particularly concerning flexural behavior. This study is expected to provide valuable insights into the impact of various fiber orientations on the structural performance of glass fiber honeycomb composite structures.

Table 2.2: Previous studies on fibre orientation layup.

Research	Facesheet Orientation	Finding	Ref.
Multiscale deformation and failure mechanisms of various fiber orientation angles analyzed through digital image correlation	Woven GFRP composite (0°, 45°, 90°)	Significant local deformation is observed in 45° off-axis specimens, while fiber pull-out is the primary failure mode for facesheets with 0° and 90° fiber orientations.	(Koohbor et al., 2015)
Theoretical and experimental methods for assessing flexural and compression properties	Twill weave carbon/epoxy prepreg (0°, 90°)	Sandwich composites with a single core exhibit higher flexural stiffness and greater average critical collapse load values compared to those with multilayer cores.	(Naresh et al., 2021)
Theoretical and experimental methods for evaluating warpage properties of honeycomb sandwich structures	Unidirectional carbon-fibre prepreg (0°, 45°, 90°)	The symmetric [45/−45/core/−45/45] configuration reduces warpage by 76%, highlighting the significant impact of fiber orientation on warpage in panel configurations.	(Burnley & Correia, 2019)
Failure behavior and energy absorption performance of aluminum honeycomb sandwich beams	Unidirectional E-glass fibre prepreg and adhesive film (0°, 45°, 90°)	Changes in fiber-laying angles show no significant differences in peak force, load-carrying capacity, or energy absorption capacity.	(J. Zhang et al., 2022)
Full-field strain measurements of textile deformation at different scales and the deformation behavior of woven textiles	Uniaxial and yarn glass woven fabrics weave (0°, 45°, 90°)	Full-field strain measurements are essential for routine use during shear and tension tests of textile reinforcements.	(Lomov et al., 2008)

Some reported advantages and disadvantages of different glass fibres are listed in Table 2.3. The used of E-glass fiber was convenient with the cross-arm application in high transmission tower. Recent researchers used the YPH-42T prepreg epoxy resin for the woven prepreg fibre because it is a solvent-free epoxy resin (Jiang et al., 2022, 2023; Z. Sun et al., 2018; J. Zhang et al., 2020). It is specifically designed to manufacture high-strength carbon fibre, fibreglass, and aramid fibreglass. Furthermore, it has high thermal deformation, impact resistance, and excellent operational properties, and it is suitable for manufacturing fishing rods, tennis rackets, and other equipment requiring a low content of resin-moulding products.

Table 2.3: Glass-fibre classification and application.

Type	Composition	Characteristics	Application
A-glass	Alkali-lime with little or no boron oxide	Not very resistant to alkali	When alkali resistance is not a requirement
C-glass (T-glass)	Alkali-lime with high boron oxide content	Resistant to chemical attack and most acids that dissolve E-glass	When higher chemical resistance to acid is required, for example, glass staple fibres
D-glass	Borosilicate	High dielectric constant	When high dielectric constant is preferred
E-glass	Alumino-borosilicate with less than 1 wt% alkali oxides	Not chloride-ion resistant; E-glass surface is soluble	Mainly for glass-reinforced plastics; originally for electrical applications
E-CR-glass	Alumino-lime silicate with less than 1 wt% alkali oxides	High acid resistance	When high acid resistance is required
R-glass	Alumino-silicate without MgO or CaO	Good mechanical properties	With high mechanical requirements
S-glass	Alumino-silicate without CaO but with high MgO content	Highest tensile strength among all types of fibre	Aircraft components and missile casings, when high tensile strength is required

(Source: P.K. Mallick, 2007; M. Zhang & Matinlinna, 2012).

2.6 Enhancing PGFRPC cross-arm

Numerous studies have dedicated their efforts to enhancing the cross-arm for high transmission towers by employing various approaches. A significant portion of these studies focused on improving the existing cross-arm design by implementing innovative modifications. Researchers have explored ways to enhance structural integrity, increase load-bearing capacity, and optimise performance. Additionally, some studies investigated the potential of changing the material composition of the cross-arm, aiming to utilise advanced materials with superior mechanical properties, such as high-strength alloys or composite materials. Alongside material enhancements, studies have also explored novel cross-arm designs to improve functionality and reliability. These combined efforts contribute to the continuous improvement and optimisation of cross-arms for high transmission towers, ensuring the robustness and efficiency of the overall tower structure.

2.6.1 Adopting new materials and innovative designs

Since the primary goal of cross-arm design is to support the weight of the transmission conductor at a specified height, many studies have focused on improving cross-arm designs (Marzuki & Jaafar, 2016; Selvaraj, 2012; Yeh & Yang, 1997). For example, Selvaraj et al. investigated the mechanical properties of composite cross-arms constructed from pultruded rods with crimped metal end clamps. Their research highlights the potential for using composite cross-arms with an FRP tower body to decrease the horizontal phase distance, thereby facilitating the creation of more compact transmission lines . (Selvaraj et al., 2013).

In the form of insulator cross-arm types, Kunikazu et al. presented their improvement on the cross-arm design made by polymer composite insulators and has a truss structure with two horizontal units and one suspension unit (Izumi et al., 2000). In this full-scale test, the performance of the new insulation arm design was greater compared to the long rod-type insulator cross-arm in terms of mechanical performance. Another improvement has done by other researchers (Jannat Alipour et al., 2007; Selvaraj, 2015) using a polymer insulation arm with an insulator line post for a high transmission tower, which increased the power transfer capability from 206 to 454 MW with minimal changes required to the upper part of the tower. The potential consequences of failures are highly hazardous, leading to severe accidents and, tragically, loss of life. Consequently, it is crucial to conduct an in-depth examination for enhancing the cross-arm structure. Table 2.4 summarizes various identified issues with cross-arms along with proposed solutions, which have been thoroughly explored in multiple studies.

Table 2.4: Challenges related to cross-arms and the recommendations provided by different studies.

Cross-arm Issue	Recommendations	Ref.
Steel and wood cross-arms suffer from deterioration and corrosion due to environmental and weather conditions.	Glass fiber composites are used as alternatives to steel and wood cross-arms.	(Yeh & Yang, 1997; Yeh & Yeh, 2001)
The materials used for cross-arms are heavy, complicating their handling during assembly.	Develop composite cross-arm materials with various fiber orientations.	(Marzuki & Jaafar, 2016; Mohamad et al., 2019)
High deformation and stress occur in composite cross-arm beams; adding sleeve spans at critical points can help mitigate this.	Adding sleeve spans at critical points can help mitigate this.	(Cao et al., 2020; Y. Liu et al., 2020; Mohamad et al., 2019; Q. Yan et al., 2018; Z. Zhang et al., 2016)
The mechanical performance of composite cross-arms declines over time.	Bracing supports can be installed on cross-arms to enhance their performance.	(Mohamad et al., 2019; Mohammadi et al., 2016; Sharaf et al. 2020)

Table 2.4: Continued

The horizontal phase distance of the cross-arm can cause slack in the transmission line.	Composite cross-arms can be used with either steel or FRP tower bodies.	(Selvaraj et al., 2013)
Environmental factors and load requirements can restrict the mechanical properties of composite cross-arms.	Natural fiber reinforced polymers or filled-honeycomb sandwich structures can be used to replace existing cross-arms.	(Alsubari et al., 2021)

2.6.2 Optimisation of existing cross-arms

Another method of improvement is by installing bracing on the cross-arm members. By using numerical simulation, some studies have installed bracing support at the cross-arm members and then subjected them to a load at one end of the cross-arm. The results showed that by using bracing, the total deformation of the cross-arm was reduced compared to the cross-arm without bracing (Mohamad et al., 2019). Hussein et al. introduced a conceptual design for transmission tower cross-arms by applying bracing to the main and tie cross-arm members to find the best solution (Sharaf et al., 2020). Asyraf et al. found that adding braced arms to the existing actual cross-arm structure decreased the total creep strain of the main cross-arm members by 8–20% compared to the existing cross-arm design (without bracing installation) and improved both elastic and viscous moduli (Asyraf et al., 2021d).

Selvaraj et al. (Selvaraj et al., 2012) discussed the experimental studies on linear-elastic responses, including buckling considerations for X-braced panel design of transmission line towers made of FRP pultruded sections as replacements. Furthermore, by using finite element method analysis, several studies were conducted for bracing applications on various beam types, depending on the bracing stiffness and restraint required. Thus, numerical equations were proposed in designing convenient bracing systems (Mohammadi et al., 2016, 2018; Mohebkhah & Showkati, 2005; Park et al., 2004). However, the bracing system can also contribute to slip potential due to the large beam stress of the beams (Klasson et al., 2018).

At present, the issues pertaining to the sustainability of existing PGFRPC cross-arm members are being addressed by temporarily strengthening materials with additional structural members. Mohamad et al. conducted a numerical study of cross-arm improvement with sleeve installation. A 1-m sleeve span was installed on both arms, and the results between previous and improved methods were recorded. The total deformation was reduced from 127.49 mm to 95.367 mm by introducing the sleeve (Mohamad et al., 2019). The use of sleeve has become one of the viable solutions to reduce the deformation level of cross-arms, thus extending its life span and reducing maintenance costs. In addition, for construction field, sleeve installation is widely employed for joining and strengthening the connection between beam columns or other connections due to its ability of influencing energy dissipation and ductility of the joint, as well as exhibiting good seismic performance (Cao et al., 2020; Y. Liu et al., 2020; Q. Yan et al., 2018). Zhujing Zhang et al. carried out a numerical analysis with experimental validation for an innovative bonded sleeve connection for joining tubular GFRP beams and steel members (Z. Zhang et al., 2016).

Recent published studies have focused on the improvement of PGFRPC cross-arm members for high transmission towers by manipulating and altering the fibre stacking sequences. Researchers recognised that the arrangement of fibres in composite materials plays a crucial role in determining their mechanical properties (Ashraf et al., 2017; Bhudolia et al., 2018; Patel & Chokshi, 2018). By strategically changing the fibre stacking sequence, they were able to enhance the performance and strength of the GFRP cross-arm member. This optimisation improved the mechanical properties and performance of the composite beam, including load-bearing capacity, increased stiffness, and enhanced resistance to external forces and environmental conditions (Karahan, 2008).

While other researcher investigated the flexural creep performance of PGFRPC laminates with different stacking sequence arrangements and found that the stacking sequence of alternating fibres between 0°/45° contributed to the strength of the structure (Kharratzadeh et al., 2018; Supian et al., 2023; Y. Zhang et al., 2013). In general, the stacking sequence of fibres has been identified as a critical factor in enhancing the long-term mechanical properties of composite structures. Previous research has highlighted the effectiveness of woven textiles as reinforcing structures to facilitate physical interactions within the fibre-matrix systems (Ma et al., 2019; Mohamad et al., 2019).

Besides, the lamination characteristics can be modified to improve the PGFRPC cross-arm members for high transmission towers, as done by several studies (Xin et al., 2017). The modification involves altering the properties of the laminate, such as fibre type, fibre volume fraction, resin matrix composition, and interfacial bonding. By carefully selecting and adjusting these laminate properties, the cross-arm members or other structural applications can exhibit improved strength, stiffness, and durability (Antonucci et al., 2016; Riezzo et al., 2019; Xin, Liu, Mosallam, & Zhang, 2016). Additionally, modifications to the laminate properties can enhance resistance to environmental factors, such as ultraviolet radiation, temperature fluctuations, and moisture. By using a three-dimensional finite element model integrated with Hashin's failure subroutine, Mohamad et al. investigated the inter-laminar damage and mechanical behaviour of the composite cross-arm. The investigation determined that varying the laminate properties led to different levels of structural deflection and laminate damage. Johari et al. (Johari et al., 2020b) indicated that the presence of $CaCO_3$ slightly improved the overall performance of PGFRPC cross-arm through a conventional bending method and the time-temperature superposition principle.

In conclusion, previous studies has proposed various methods to improve the PGFRPC cross-arm members for high transmission towers. These methods include installing bracing on the cross-arm members, altering the fibre stacking sequences, and modifying the laminate properties. The studies conducted through numerical analysis and experimental validation have provided valuable insights into the performance and behaviour of the composite cross-arm members under different conditions. However, from the literature, there is still lack of study that is focusing on overcoming the cross-arm failure by applying honeycomb sandwich components to the GFRPC cross-arm, where the ideas can also be used to improve the cross-arm structure. These findings contribute to the ongoing efforts in optimising the design and performance of GFRPC cross-arm members for sustainable and reliable transmission tower applications.

2.7 Experimental and numerical approaches

The PGFRPC have become increasingly popular in various engineering applications due to their unique mechanical properties. The load-deflection characteristics of these materials are critical, as PGFRPC beams tend to exhibit significant deflection under typical service conditions, influencing their maximum span length and load-bearing capacity. Extensive studies have examined the flexural behavior of PGFRPC beams, revealing that excessive deflection often limits their structural performance. Additionally, the creep properties of PGFRPC are of paramount importance for long-term applications, as these materials can undergo significant deformation under sustained loads, affecting their structural integrity. Empirical models, such as Findley's power law, have been employed to predict and analyze the creep behavior of these composites, providing valuable insights for their use in practical applications. This study aims to investigate the load-deflection and creep properties of full-scale PGFRPC cross-arms, focusing on enhancing their performance through innovative designs like honeycomb sandwich structures.

2.7.1 Load-deflection property of PGFRPC

In recent years, PGFRPC structural products have gained significant traction in various fields, including civil engineering, mechanical engineering, and aerospace. Numerous studies have been conducted to assess their performance, with typical applications encompassing main and secondary beams and columns in structures like cooling towers, pedestrian bridges, and various frame structures (X. Zou et al., 2018, 2020; X. X. Zou et al., 2016). PGFRPC beams, with their relatively low modulus of elasticity and significant material anisotropy, behave differently from traditional materials such as concrete and steel (W. Liu et al., 2017; J. Q. Yang & Feng, 2020). Although recent research has concentrated on theoretical models of viscoelastic composite structures (Barretta et al., 2015; Barretta & Luciano, 2014), there is still a lack of comprehensive information on the use of full-scale PGFRPC cross-arm members and assemblies for high transmission tower applications, particularly due to strict deformability requirements.

Firstly, GFRP beams can experience excessive deflection under typical service conditions, severely limiting their maximum span length. Several studies have sought to evaluate the flexural behavior of PGFRPC beams. Bank (Bank, 1989b, 1989a), for instance, conducted pioneering tests on GFRP I-beams and introduced a testing method to determine flexural and shear moduli. Likewise, several researchers conducted bending tests on GFRP I- and box-beams, assessing flexural and shear stiffness (Estep et al., 2016; Roberts & Al-Ubaidi, 2002). While others, delved into both major and minor-axis flexural behavior of GFRP I-beams, providing design equations for deflection and flexural modulus calculations (Turvey, 2016; Turvey & Zhang, 2018b). These studies collectively revealed that pultruded GFRP beams tend to fail due to excessive deflection rather than reaching the material's strength limit.

Moreover, extensive research has been conducted on the deflection behavior of PGFRPC structural components, particularly focusing on initially straight cantilever beams under various loads. This analysis covers a range of applications, such as folder and window locking mechanisms, pole vaulting, board jumps, and fishing rods. Singhal & Narayanamurthy (2019) proposed a theoretical approach for analyzing both large and small deflections in cantilever beams, with the small deflection theory suggesting linear transverse or vertical deflection at the beam's tip. Conversely, the large deflection analysis predicts realistic, nonlinear transverse, and longitudinal deflections. However, within the linear elastic working range, both small and large deflection approaches yield identical results, making the simpler small deflection approach suitable for engineering design (Bisshopp & Drucker, 1945; Zeng et al., 2021).

Furthermore, small deflection behavior analysis establishes the fundamental requirements for structural design and identifies the range of structural applicability. The bending behavior of beams is commonly analyzed using the Bernoulli-Euler theory and Hooke's law (Beléndez et al., 2003; Tari, 2013; T. M. Wang, 1968). According to Bernoulli-Euler theory, the bending moment at any point along a beam is proportional to its curvature. Meanwhile, Hooke's law states that the applied load is proportional to the extension of the beam, provided the deflection is minimal and the material does not yield. Secondly, several studies have honed in on the behavior of pultruded GFRP beams, revealing that premature failures can substantially diminish the ultimate load-bearing capacities of these beams (E. J. Barbero et al., 1991; Mittelstedt, 2020; Mosallam & Bank, 1992).

In addition, researchers have paid critical attention to potential failure modes, including excessive deflection and complex buckling behaviors of PGFRPC beams (Correia et al., 2007). These deflection and buckling behaviors can lead to sudden catastrophic failures of entire structures, a concern emphasized in virtually all existing design guidelines (ACMA, 2012; Wg, 2018). Consequently, this research prioritizes the study of deflection behaviors in PGFRPC beams. Given these critical issues, the objective is to enhance PGFRPC cross-arms with a honeycomb sandwich structure capable of mitigating adverse deformations and preventing premature failures. To achieve this objective, comprehensive investigations into the load deflection of both individual and assembled PGFRPC cross-arm components are warranted.

2.7.2 Creep property of PGFRPC

Creep is a mechanical behavior observed in materials exposed to long-term and steady stress. This phenomenon progresses through multiple stages primary, secondary, and tertiary deformations each exhibiting unique characteristics (Hunt et al., 2015; Lala et al., 2018). During the primary creep stage, the rate of deformation decreases linearly due to factors like strain hardening. The secondary creep stage features a nearly constant deformation rate as a balance between dislocation production and recovery is reached. In the tertiary creep stage, there's a rapid increase in deformation until the material eventually fails, often due to phenomena like shear yielding, void chain slippage, growth development, and fiber breakage (Beddu et al., 2018; Sá et al., 2011a).

Composite cross-arms, particularly those made from E-glass fiber-reinforced unsaturated polyester composite, exhibit anisotropic characteristics and can experience interfacial strength instability due to creep rupture (Johari et al., 2020b; Syamsir et al., 2023). Previous study by Bank and Mosallam assessed the long-term creep behavior of a full-scale frame constructed from wide-flange pultruded sections, finding significant deflection over time and reductions in stiffness properties over a 10-year period (Bank & Mosallam, 1992). The frame underwent four-point bending until it reached 25% of its maximum static load capacity for about 10,000-hour of testing period. Notably, there was a more pronounced creep behavior observed during the initial 2,000 hours of testing, after which the creep rate stabilized and remained relatively constant. To forecast the frame's long-term deflections using a theory that considers shear deformations, the researchers utilized Findley's linear model to ascertain properties related to stiffness that change over time.

Similarly, Sa et al. examined the flexural creep response of a PGFRPC I-section beam, observing increased deflection predictions over time (Sá et al., 2011b). The beam, with a span of 1.80 meters, underwent four-point bending until it reached 1/3 of its maximum static load capacity, and this testing continued for 1600 hours. A power law model was effectively employed to match the mid-span deflections caused by creep over time. The predictions indicated that there would be creep deflection increases ranging from 35% to 100% after 1 to 50 years of continuous loading. Additionally, the authors conducted creep flexural tests on small-scale laminates taken from the I-section walls, and these tests displayed creep rates that closely resembled those observed in the full-size beam.

Shao and Shanmugam explored the shear creep contribution to deformation in PGFRPC sheet piles, with predictions of reduced moduli after 30 years (Shao & Shanmugam, 2004). Two PGFRPC (E-glass/polyester) sheet piles, each spanning 6.1 meters, underwent testing in three-point bending. They were loaded to 25-50% of their maximum static load capacity for a duration of 9000 hours. Monitoring the axial tensile and shear strains during the test allowed the derivation of equations to describe the viscoelastic moduli over time, using a simplified version of Findley's model. The studies projected that, after 30 years, the time-dependent tensile and shear moduli would decrease by 68% and 36%, respectively, compared to their initial values. These moduli were then employed to calculate long-term deflections using Timoshenko's beam equation, resembling Findley's power law, based on averaged creep parameters.

Several studies have also explored coupon-scale PGFRPC cross-arms, focusing on factors such as stacking sequences, creep behavior under various stress conditions, and the application of mathematical models like Findley's power law and Burger's model (Alhayek et al., 2022; Supian et al., 2023; Syamsir et al., 2023). Additionally, Allhayek investigated PGFRPC cross-arm specimens exposed to high temperatures and different stress levels, observing brittle failure during static four-point bending tests and confirming the accuracy of the mathematical models used (Alhayek et al., 2023). The specimens were observed for a period of 720 hours, equivalent to 30 days. The study observed that these specimens experienced brittle failure in static four-point bending tests, with an average ultimate strength measuring 242.6 MPa. Notably, both mathematical models, namely Findley's power law model and Burger's model, effectively replicated the creep behavior observed in GFRP laminates, closely mirroring the experimental findings.

Agusril et al. have study the performance of PGFRPC cross-arm tubes in full-scale within 275 kV transmission towers using experimental and FEA analysis (Syamsir et al., 2022). The analysis replicates real-world conditions, including both normal and broken wire scenarios, with loads five and three times higher than the working load. Additionally, the mechanical properties of the GFRP composite were incorporated based on prior experimental study conducted on coupon samples of GFRP tubes. While others have study creep behavior of full-scale PGFRPC cross-arm for 1000 h of test period and compared with wooden cross-arm (Asyraf et al., 2023). However, previous study on the flexural creep behavior of full-scale PGFRPC cross-arms in practical applications has been limited.

To address these research gaps, this study examines the flexural creep behavior of full-scale PGFRPC cross-arm members, both individually and in assembly. Conducting creep tests is essential for documenting, analyzing, and forecasting long-term creep performance. Evaluating the mechanical performance of PGFRPC cross-arms with and without a honeycomb sandwich structure under actual loads and tropical environmental conditions will yield important insights into the long-term durability of these cross-arm applications. This approach aims to offer a comprehensive understanding of the entire system's behavior and contribute practical insights for academics and engineers regarding the long-term mechanical performance and life prediction of PGFRPC cross-arms.

2.7.3 Empirical Findley's Power Law model

The Findley model, also known as the Findley's power law model, is an empirical approach that describes creep properties using the power-rule method. It proves valuable in predicting creep strain-time curves through transient creep, aided by material stress exponent and stress-dependent coefficient (D'Antino & Pisani, 2019). However, the model has limitations, mainly in its application due to the straightforward numerical formula, neglecting dimensional changes in creep testing (Findley et al., 1977; Z. Yang et al., 2018). Additionally, it lacks the capability to analyse creep properties under the influence of external factors, such as moisture content, humidity, and temperature, which can affect material structure and deformation during the creep process.

Despite its limitations, the Findley model has found application in various studies for analysing the creep behaviour of different materials, including layered silicate/starch-polycaprolactone blend nanocomposites, wood floor high-density polyethylene/laminated veneer lumber coextruded composites, and polyamide 66 nanocomposites (H. Fu et al., 2020; Pérez et al., 2008). These investigations have demonstrated the effectiveness of the model in characterising the viscoelastic properties of polymer composites, particularly for anisotropic materials such as plastics. The Findley model offers good accuracy over a wide time scale and is less sensitive to stress, making it suitable for forecasting long-term creep properties with satisfactory applicability and a simple expression (Scott & Zureick, 1998). Although the model has its limitations, it remains a valuable tool in the study and prediction of creep behaviour in various materials and composite systems.

To further investigate the creep characteristics of PGFRPC cross-arms, this study employed a well-established empirical creep model validated by prior research (Alhayek et al., 2023). The non-linear Findley's power law model was utilized to analyze and explain transient creep in relation to stress components and material constants. While this model is broadly applicable across different systems, its use is limited by its relatively simple and direct numerical computations (Findley, 1944; Y. Fu & Sadeghian, 2020).

Besides that, most of researchers have proved the numerical analysis revealed that the Findley model, exhibiting the smallest deviations from the experimental findings, stands out as the most suitable creep model for predicting the creep behavior in pultruded composite materials. Furthermore, when it comes to evaluating the creep properties of anisotropic materials, the Findley model proves to be the most accurate. In addition, the PGFRPC cross-arm was regarded as an isotropic substance. Thus, the Findley model was used to simulate the creep pattern and was represented in this study.

2.8 Development of honeycomb sandwich PGFRPC cross-arm using hybrid concurrent engineering

Besides having advantages over its predecessor (wooden cross-arm), it has been found that after several times, the PGFRPC cross-arm will lose its mechanical integrity and experience some failure, depending on the intensity of environmental exposure (Syamsir et al., 2022). Therefore, the use of concurrent engineering is a very important part of making composite structures in order to reduce costly modifications during the end stage in product development. Engineers and scientists use the systematic approach of the theory of inventive problem solving (TRIZ) to place any concession between product design gaps and develop better outcomes for future technologies and products with lower risk (Fiorineschi et al., 2018; Jama-Rodzeńska et al., 2021).

Currently, the use of TRIZ to solve engineering problems has seen a lot of success and improvement. Also, it is widely used by designers and researchers. This is demonstrated by the fact that many designers and researchers have conducted and published studies on the design selection for various applications in order to build a product systematically using the TRIZ principle. Cascini et al. (Cascini et al., 2011) implemented the TRIZ method to visualise the idea of new sheet metal snips, which were visualised by a computer-aided drawing model based on the TRIZ contradiction matrix. The morphological chart, TRIZ, and analytic network process (ANP) were used by Mansor et al. (Mansor et al., 2014) to generate ideas for a novel kenaf fibre polymer composite parking brake lever. The study proposed different design concepts based on the existing parking brake lever mechanism and its application.

In advance of conceptual design, previous researchers used the integration of TRIZ-morphological chart-ANP method to develop the conceptual design of a multi-operation outdoor flexural creep test rig. Through the ANP method, the concept design with the addition of Chevron bracing was selected as the best product design because it has the highest normalised value compared to other design options (Labuda, 2015; Sharaf et al., 2020). The study used the TRIZ contradiction matrix to develop four design concepts, and the best design concept was chosen using the ANP method based on the importance of the requirements. The researcher also applied the same method to create a conceptual design for a full-scale cross-arm creep testing rig. In the study, the best design was selected using the ANP principle through the pairwise comparison technique, and they deduced that the best concept design was the creep test rig with a hybrid bracing design, which ranked first and scored the highest values. Their study then focused on the development of an FRPC portable fire extinguisher based on the concept design of a portable fire extinguisher made of a hybrid carbon/flax polymer reinforced composite.

Up to the latest knowledge, no design and study have been found regarding honeycomb sandwich composite in the previous literature for the cross-arm in high transmission tower applications. Thus, the optimization of new proposed honeycomb sandwich composite structure configuration for the PGFRPC cross-arm suitable for a 132 kV transmission tower in Malaysia is essential. Due to concurrent engineering design, which makes use of a synthesis of TRIZ, a morphological chart, and the ANP, this study could construct and investigate the conceptual design of a honeycomb structure. Using this approach, four stages of design development were executed: idea generation, idea refinement, concept development, and design selection. At the end of the study, seven new design concepts were created, and the best concept design was selected according to product design specification.

2.8.1 Theory of Inventive Problem Solving (TRIZ)

G. Altshuller was a founder of the TRIZ method in 1946, which used concurrent engineering principles to produce the most suitable solutions to the problems arising from a design. The TRIZ term stands for "Theory of Inventive Problem Solving" (Kremer et al., 2012), which offers numerous benefits in the concurrent engineering process and product development, including assisting designers and researchers in diagnosing issues and problems related to the freedom of using any technique while modernising traditional issues towards inventive product development (G. Navas, 2013; Sheu & Lee, 2011). In most cases, the TRIZ approach to problem solving involves identifying and addressing the fundamental root causes of the issue at hand. The method is extremely useful for generating excellent engineering and science concepts from the ground up. Its goal is to resolve any disagreements over the modification that may arise in any problem by focusing on the identified issue. A study uses the TRIZ contradiction matrix to determine the solution to its product that does not bargain any important parameters during the process of designing.

The TRIZ method's solution can be implemented by using four main approaches to generate solutions that are able to solve problems. Commonly, the Prediction of Technology Trends, 76 Standard Inventive Solutions, 40 Inventive Principle Solutions, and the Algorithm of Inventive Problem Solving are used for generating solutions (G. Navas, 2013; Ghani et al., 2016; San YT, 2011). In this study, the approach of 40 Inventive Principle Solutions was used to find a solution for the product without compromising any important parameters along the designing process. Generally, 39 engineering parameters are linked together between the improving and worsening attributes to find the solution principle based on 40 inventive principles (Rosli et al., 2013). The improving and worsening parameters are determined using the IF-THEN-BUT technique (Mazani et al., 2019). IF is the statement where changes are made and THEN defines the benefits gain in the future when changes are made. This will act as the improving parameters, while BUT explains the effect of the changes made, also known as the worsening parameter (Mazani et al., 2019). Determining the improving and worsening parameters allows the construction of the contradiction matrix. Using the matrix, several solutions can be produced when referring to the 40 inventive principle solutions. The best solution recommended is chosen to create a design strategy for the problem.

2.8.2 Morphological Chart

The refinement of design solutions by the morphological chart can help to improve the selected TRIZ inventive solutions into design specifications and characteristics. The morphological chart is used in idea generation to represent concepts in the form of qualities. As the TRIZ solution is inherently abstract, it is not possible to describe it comprehensively in the design specification; hence, this technique is utilised instead. Therefore, adhering to the criteria, the generic solution description must be converted into specific design characteristics (M. C. Yang, 2009). This makes it possible for designers to come up with concept designs based on the TRIZ innovative way of solving problems by eliminating contradictions between improving and worsening features. As the proposed solutions rely greatly on the designer's ability to visualise the image and construct the particular features in accordance with the TRIZ technique, the designer's skill and expertise are crucial to the method's success. Therefore, designers may utilise the improved idea from the morphological chart stage to narrow down and generate unique design concepts.

2.8.3 Analytic Network Process

The ANP takes place after the solutions are generated to select the best conceptual design to develop a new product design. The objective of used this approach is to find the final conceptual design to be develop and fabricate. In the decision-making process, this method is important because it allows multiple suggested criteria and design alternatives to be analysed simultaneously. These techniques can be used in a combination selection process for targeted design specifications (Azammi et al., 2018). This mathematical theory was developed by Thomas L. Saaty to determine the priority of multiple attributions in the decision-making process. The ANP is an enhanced approach of the analytical hierarchical process (AHP), where the former includes all the connections among the attribution levels that form a network structure. It basically depends on the overall decision structure's feedback. This method is very helpful as it helps the users to prioritise the requirement to select the best design alternative. The AHP is divided into several clusters, also known as the multi-level hierarchical structure, whereas the ANP is portrayed by a network. The level is broken up into goals, criteria, and alternatives. Further elaboration on the cross-arm engineering parameters, matrix contradiction, and selection of relevant principle solutions will be discussed in the following subtopics.

2.9 Summary

The literature reviewed highlights various methods to enhance the performance of pultruded glass fiber-reinforced polymer composite (PGFRPC) cross-arm members in high transmission towers. These methods include installing bracing on the cross-arm members, altering fiber stacking sequences, and modifying laminate properties. Both numerical analyses and experimental validations offer valuable insights into the behavior and performance of these composite cross-arm members. However, there remains a gap in the literature regarding the use of honeycomb sandwich components to address cross-arm failures in GFRPC cross-arms, a concept with potential for structural improvement.

PGFRPC cross-arms are crucial in transmission towers, supporting electrical conductor cables and insulators for continuous energy supply. Research reveals their significant load-carrying capacity, deformation behavior, and structural integrity under various conditions. Recent advancements highlight the performance of full-assembly GFRP composite cross-arm tubes, showcasing their structural efficiency and reliability. Despite these advancements, environmental degradation and sudden failure risks pose ongoing challenges, necessitating further research and development to enhance the durability and reliability of PGFRPC cross-arms. Besides that, addressing these issues requires comprehensive assessments and enhancements in cross-arm designs and materials for long-term reliability and safety.

The adoption of honeycomb sandwich composite structures is proposed as a promising enhancement for PGFRPC cross-arms. These structures, comprising outer facings with a core between them, offer strength, stiffness, and lightweight properties. Honeycomb cores provide advantages such as simplicity, manufacturability, and energy absorption capabilities. Studies show that innovative designs like tandem honeycomb structures and embedding honeycomb cells with foam or tubes improve energy absorption and mechanical properties.

In conclusion, the literature underscores the potential of various methods to improve PGFRPC cross-arm members' performance. While significant advancements have been made in understanding these materials' mechanical properties and performance, further research is needed to address environmental degradation and sudden failure challenges.

Integrating honeycomb sandwich composite structures presents a promising avenue for enhancing PGFRPC cross-arms' durability, reliability, and structural integrity. Future research should focus on full-scale mechanical assessments and structural analyses to ensure the long-term performance and reliability of these components, thereby advancing power transmission infrastructure.

CHAPTER 3

METHODOLOGY

3.1 Introduction

This chapter outlines the flow of this study, which begins with the literature review and the background study to gain a comprehensive understanding of the study area. The behaviour of a pultruded glass fibre-reinforced polymer composite (PGFRPC) cross-arm was analysed and characterised during load application for both normal and broken wire conditions, and the results were compared with the wood cross-arm's deflection properties. The subsequent step involves characterising and fabricating a honeycomb sandwich composite structure, including investigating the orientation of woven glass fibre prepreg used for the facesheet at $\alpha = 0°$, 45°, and 90°. Using concurrent engineering, a conceptual design of the honeycomb sandwich PGFRPC cross-arm was developed, and seven conceptual designs were evaluated based on weight, cost, and performance. The best design was chosen for fabrication with the maximum deformation obtained should less than the existing cross-arm (without any enhancement) which is 4.60 mm. Finally, the enhanced PGFRPC cross-arm was tested for load-deflection and creep properties in full-scale assemble and individual cross-arm tests using the cantilever beam and three-point bending tests, respectively. The creep life of the existing PGFRPC and the enhanced honeycomb sandwich PGFRPC cross-arm structure was achieved and evaluated during creep test. The study flow for the experimental study according to the objectives is displayed in Figure 3.1, while the detail and elaboration are presented in the following section.

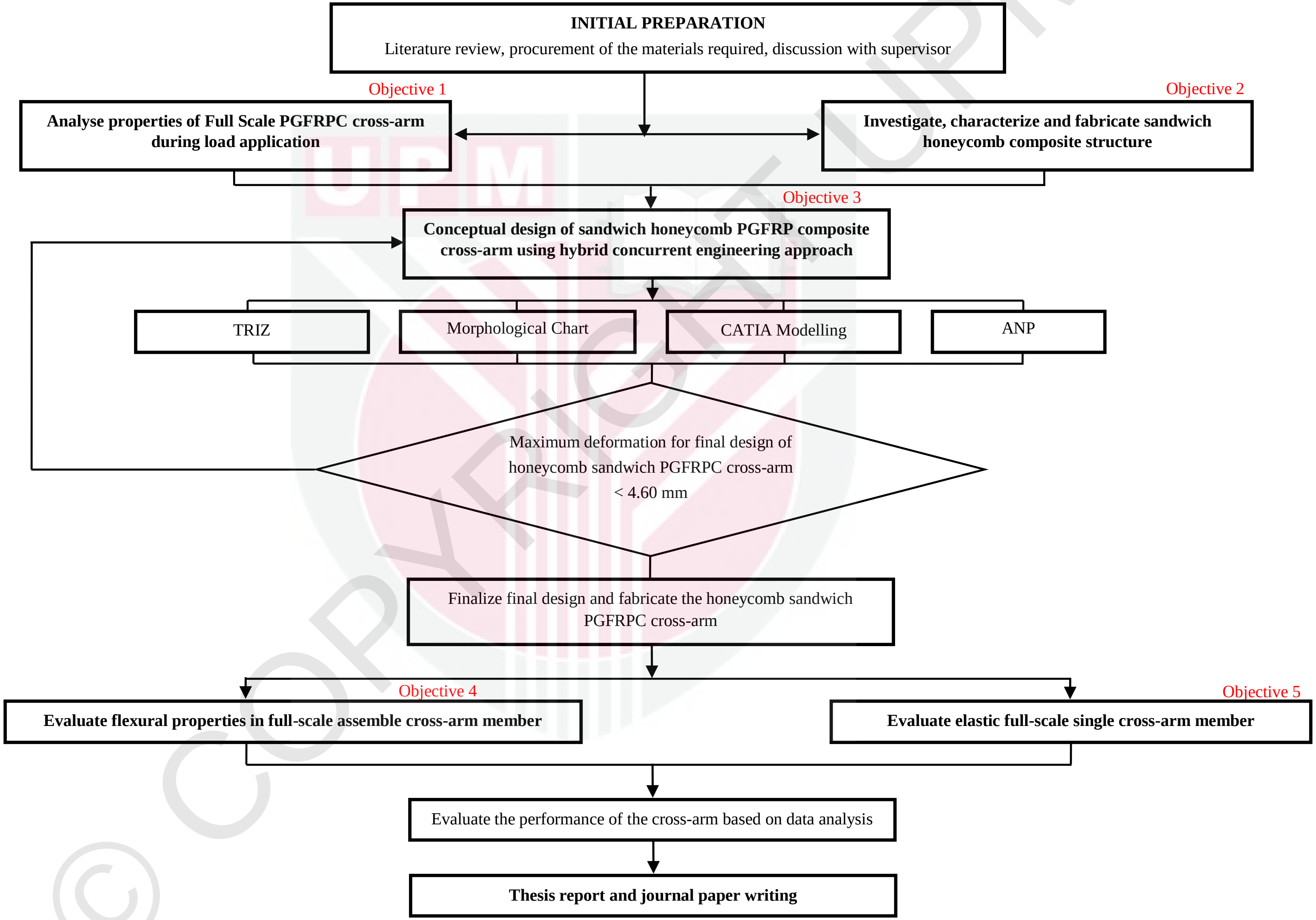

Figure 3.3: The experimental flow and the progression of this study.

3.2 Specimen materials

The three main materials involved in this study are as follows: (a) the PGFRPC supplied by Electrius Sendirian Berhad, Klang, Selangor; (b) woven E-glass fibre prepreg supplied by CA Composites Limited, Shanghai, China; and (c) the aluminium honeycomb core supplied by Phoenix Environmental Protection Materials, Jiangsu, China. The complete specification of the materials is discussed in the following section.

3.2.1 PGFRPC cross-arm

This study primarily focuses on the PGFRPC cross-arm designed for a 13 L type, 132 kV suspension tower in Malaysia. The cross-arm was obtained from Electrius Sendirian Berhad, a local manufacturer in Klang, Selangor. The cross-arm assembly includes one tie and two main components, all produced through pultrusion using unsaturated polyester resin as the matrix and E-glass fibers for reinforcement. The PGFRPC cross-arm that is ready to be used on the high transmission tower is shown in Figure 3.2.

Figure 3.2: Complete mass manufactured PGFRPC cross-arm.

3.2.2 E-Glass woven fibre prepreg

The facesheets of the honeycomb sandwich composite structure were made of woven prepreg E-glass fibre (plain weave) with a surface density of 200 g/m^2 and a thickness of 0.2 mm, provided from CA Composites Limited, Shanghai, China. The prepreg adhesive of YPH-42T type with 18–25 kg/m·s viscosity and 1.21–1.25 g/m^2 density was used. For this study, the E-glass fibre was used due to its higher strength and electrical resistivity (Sathishkumar et al., 2014). This woven prepreg has axial stiffness, shear stiffness, and bending strength of 18.5 GPa, 2.47 GPa, and 100–110 MPa, respectively. Figure 3.3 shows the ply of woven E-glass fibre prepreg used for facesheet fabrication.

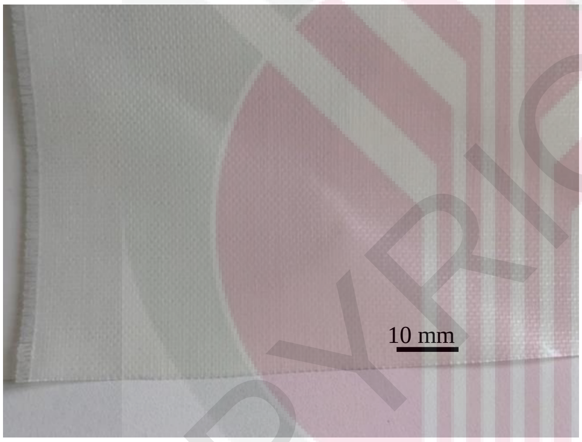

Figure 3.3: Woven E-glass fibre prepreg ply for facesheet fabrication.

3.2.3 Aluminium honeycomb core

For this study, an aluminum honeycomb core was utilized in the fabrication of the sandwich structure. The core was supplied by Phoenix Environmental Protection Materials in Jiangsu, China. It measured 300 mm in length and 85 mm in width. Constructed from A5052 aluminum grade, the honeycomb core had a cell size of 3.4 mm and a cell thickness of 25 mm. Figure 3.4 shows the aluminium honeycomb core used for sandwich structure fabrication in this study.

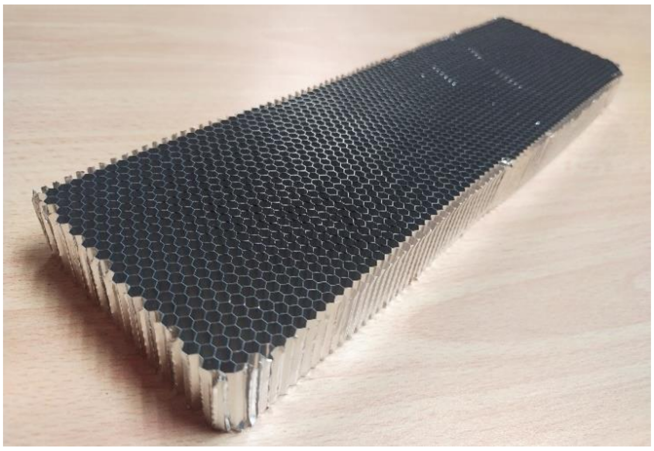

Figure 3.4: Aluminium honeycomb core used for honeycomb sandwich composite fabrication.

3.3 Fabrication of specimen materials

This section discusses the fabrication of the PGFRPC cross-arm member and honeycomb sandwich composite structure involving the actual scale size. Furthermore, details on the tools and machine used for the fabrication process are also mentioned in this section.

3.3.1 Cross-arm member

The estimated percentages of E-glass fibre and unsaturated polyester resin in the PGFRPC cross-arm were 37% and 63%, respectively The pultruded composites are made up of ten layers of different stacking sequences, which are 45°/-45°/0°/0°/0°/0°/0°/0°/-45°/45° (Mohamad et al., 2019). The properties of the PGFRPC cross-arm in the coupon sample are described in Table 2.1. The cross-arm had a square cross-sectional dimension of 102 × 102 mm², featuring a smooth, uniform, and unidirectional fiber alignment in the direction of the polymer matrix composites, adhering to the specifications outlined by Tenaga Nasional Berhad (TNB) (Rawi et al., 2017; Rawi & Ab Kadir, 2015). The total length of the main cross-arm members was 3,651 mm while the tie member was 3,472 mm. Bolts and nuts were used with fastening brackets to attach each cross-arm member to the test rig for the assembled condition (refer Appendix 1). Meanwhile, for the three-point bending test, a simple jig for the test was set up to evaluate the individual cross-arm member.

3.3.2 Honeycomb sandwich composite structure

The preparation of honeycomb sandwich composite structure specimens can be categorised into two major parts. The first part is to fabricate the facesheets and the second part is to fabricate the sandwich panel. The facesheets were made of woven prepreg E-glass fibre (plain weave) with the surface density of 200 g/m^2 and the thickness of 0.2 mm, provided by CA Composites Limited, Shanghai, China. This woven prepreg has axial stiffness, shear stiffness, and bending strength of 18.5 GPa, 2.47 GPa, and 100–110 MPa, respectively. In this study, each facesheet was manufactured using the hand lay-up method with four layers of woven prepreg glass fibre stacked together at different fibre orientation angles of α = 0°, 45°, and 90°. A schematic view of the orientation of the test specimens is illustrated in Figure 3.5.

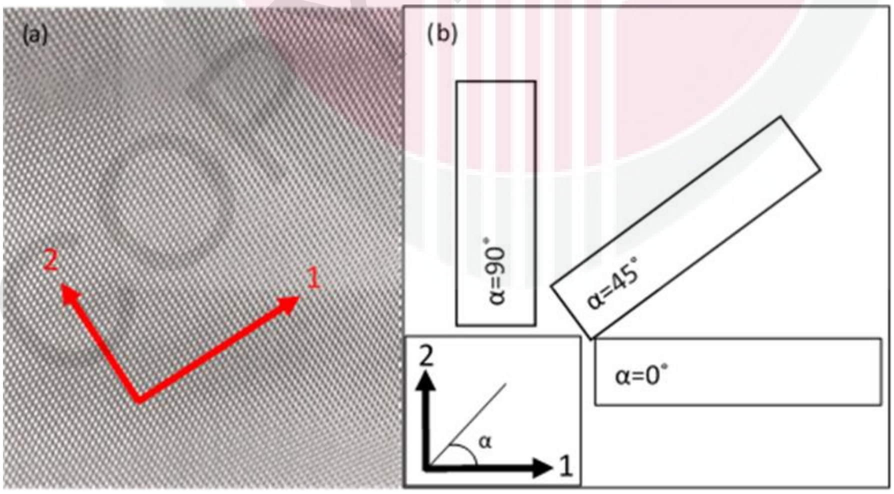

Figure 3.5: Schematic illustration of the woven prepreg glass fiber utilized in this study: (a) The woven glass-fiber structure with primary directions labeled as 1 and 2. (b) The orientation of the facesheet fiber fabric as taken from the original sheet.

The facesheet dimensions matched those of the honeycomb core, which were 300 mm × 85 mm. After layering four sheets of woven prepreg glass fiber, epoxy prepreg film was applied to both sides of the core to bond the facesheets and the honeycomb core together. According to Ashraf et al. (2019), the four-layer prepreg sample demonstrated greater ultimate force and pressure compared to non-prepreg glass laminates. The facesheets and honeycomb core were then joined using a hot press machine, which was set to 130 °C for 3 hours (Farooq et al., 2017). The temperature increased at a rate of approximately 3 °C/min, with a constant pressure of 5 bar applied via a hydraulic pump (Ashraf et al., 2019). After the 3-hour period, the press machine was turned off, and the temperature was allowed to decrease to 40 °C while maintaining the pressure on the specimens. Figure 3.6 illustrates the materials used for the honeycomb sandwich panel and the hot press machine employed in this study.

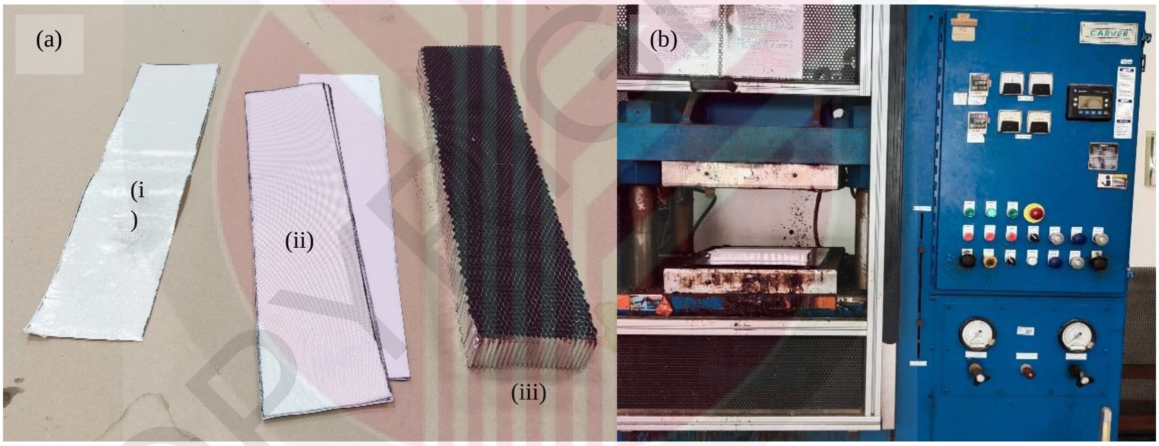

Figure 3.6: (a) Honeycomb sandwich panel fabrication material: (i) epoxy prepreg film; (ii) four layers of woven prepreg glass-fibre facesheet; and (iii) aluminium honeycomb core. (b) Hot press machine for the curing process.

3.4 Honeycomb sandwich quasi-static three-point flexural test

Consistent with existing research, the flexural test specimens were prepared following ASTM C 393 standards (ASTM C393/C393M, 2020). All specimens were cut into rectangular sections with dimensions of 200 mm in length and 75 mm in width, adhering to the standard testing sample size (Farooq et al., 2017). Each honeycomb sandwich structure featured four plies of woven glass fiber prepreg for the top and bottom facesheets.

The cured thickness of the honeycomb sandwich panel, processed in a hot press system under constant temperature and pressure, was approximately 28 mm. The specimens were categorized into three groups based on the orientation angles of the woven glass fiber facesheets—α = 0°, 45°, and 90°. Seven samples from each group were tested to obtain average values for the flexural properties of the honeycomb sandwich structure. Three-point flexural quasi-static tests were conducted using an INSTRON 3382 electronic universal testing machine at a constant rate of 6 mm/min. The support and loading steel cylinders used had a diameter of 25 mm, with a support span length of 150 mm, as illustrated in Figure 3.7. The laboratory conditions during testing were recorded using a digital temperature and humidity meter, showing a room temperature of 24 °C and a relative humidity of 53%.

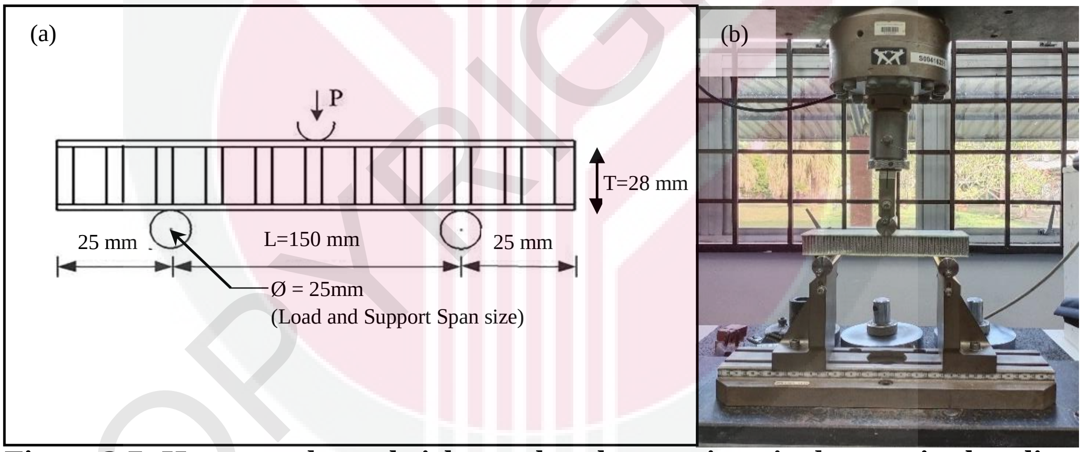

Figure 3.7: Honeycomb sandwich panel under quasi static three-point bending test (a) Schematic diagram, (b) actual condition during testing.

3.4.1 Characterisation of sandwich structure flexural properties

In this study, the load-mid-span deflection curve described the relationship between the mechanical response and the structural flexural properties under the three-point bending (3-PB) test. The values for the flexural properties obtained from the average of seven repetitions in a quasi-static 3-PB test using the INSTRON universal testing machine were recorded, such as the maximum load, stress, and flexural modulus. Three typical results for different angular orientations of the woven glass fibre facesheet included $\alpha = 0°, 45°$, and 90°. Figure 3.8 illustrates the honeycomb sandwich panel dimension used in this study, and the average values were used in the calculation.

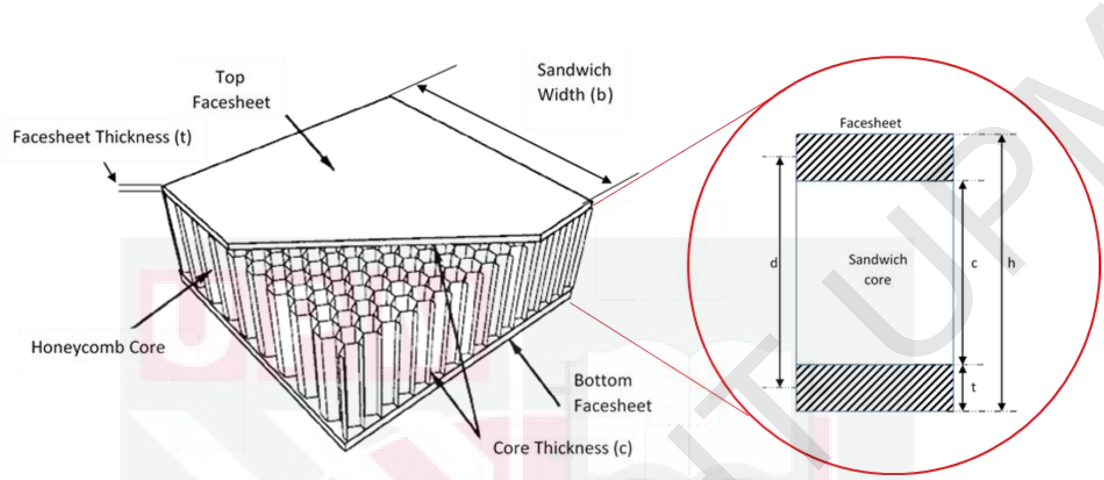

Figure 3.8: The honeycomb sandwich panel's dimensions are described as follows: 'd' represents the distance between the central lines of the upper and lower facesheets, and 'h' denotes the overall thickness of the panel.

Subsequently, the flexural characteristics of the honeycomb sandwich panels such as facesheet bending stress, core shear ultimate stress, transverse shear rigidity, and core shear modulus were determined from the load-deflection curve, as indicated in Equation (3.1). This calculation followed the guidelines set by ASTM C393/C393M and ASTM D7250/D7250M standards (ASTM C393/C393M, 2020; ASTM International, 2009):

$$F_s = \frac{P_{max}}{(h + c)b} \quad \text{Equation (3.1)}$$

Here, F_s represents the core shear ultimate stress (MPa), Pmax is the peak force before the initial failure (N), h denotes the total thickness of the sandwich panel (mm), c is the thickness of the core (mm), and b is the width of the sandwich panel (mm). The stress in the facesheets was determined as follows:

$$\sigma = \frac{P_{max}\,S}{2t\,(h + c)b} \qquad \text{Equation (3.2)}$$

Here, σ represents the bending stress in the facesheet (MPa), t is the thickness of the facesheet (mm), and S denotes the span length (mm). The transverse shear rigidity was computed using:

$$U = \frac{P_{max}(S - L_{SB})}{4\left[y - \frac{P_{max}(2S^3 - 3SL_{SB}{}^2 + L_{SB}{}^3)}{96D}\right]} \qquad \text{Equation (3.3)}$$

In this context, U represents the transverse shear rigidity (N), L_{SB} stands for the load span length (mm), y is the deflection at mid-span (mm), and D denotes the flexural stiffness (N-mm²). For the 3-point bending (3-PB) tests in this study, L_{SB} was set to zero because the load span was applied at the center of the specimens. Due to the complexity introduced by two variables in Equation (3.3), solving it was challenging. Therefore, the elastic modulus E, determined from the quasi-static tests, was used to calculate the flexural stiffness with the following Equation (3.4):

$$D = \frac{E(h^3 - c^3)b}{12} \qquad \text{Equation (3.4)}$$

The change in load (P) and the change in mid-span deflection (y) were measured at the maximum force just before the initial failure. These results were then used in Equation (3.5) to determine the transverse shear rigidity for different woven angle orientations. Subsequently, the core shear modulus (G) was calculated as:

$$G = \frac{U(d - 2t)}{(d - t)^2 b} \qquad \text{Equation (3.5)}$$

3.4.2 Analytical prediction of sandwich beam deflection

The total deflection (δ) at the midpoint of a honeycomb sandwich beam during a three-point bending test (3-PB) is composed of the deflections resulting from the bending of the facesheets and the shear of the honeycomb core, based on Allen's theory (Allen, 2013). The straightforward analytical model for the total deflection of a simply supported sandwich beam is expressed as:

$$\delta = \delta_f + \delta_c = \frac{PS^3}{48D} + \frac{PS}{4(AG)_{eq}} \qquad \text{Equation (3.6)}$$

In this equation, P represents the force applied at the beam's center, S is the support span length, A is the cross-sectional area of the sandwich beam, D is the beam's flexural stiffness, and G is the core's effective shear modulus. The term (AG)eq stands for the equivalent shear rigidity of the honeycomb core (Wei et al., 2020; Xiong et al., 2014). For long beams with substantial shear stiffness, shear deformation is typically minor. However, in short beams or those with weak shear characteristics, shear deformation can be significant or even dominant. It should be noted that the bending response expression assumes small elastic deformation due to the minor failure of the glass fiber material. Additionally, within the small deflection range, the effects of geometrical non-linearity on the load-deflection response are negligible (Fam et al., 2016; Yuan et al., 2016).

3.5 Modelling and Finite Element Analysis

Finite element analysis (FEA) was performed to simulate the deflection behaviour of the PGFRPC cross-arm under loading conditions. First, the cross-arm parts (i.e., fitting, main cross-arm, tie cross-arm, screws, and nuts) were modelled using CATIA V5R18. Later, the CATIA model was exported to ANSYS using the FEA software package for analysis, in which the software implemented equations governing the behaviour of these elements and solved them, producing a comprehensive explanation of how the system acts as a whole (S. & S., 2011). To validate the FEA results, it was assumed that the results converged to a solution and that they were independent of the mesh size. A mesh convergence study was performed by varying the number of elements along the length of the cross-arm model. Then, the graph of maximum deflection versus the number of elements in the model was plotted. The point at which the response of the system converged to the number of elements was used as the verified numerical result and was later compared with the experimental results.

For the FEA analysis of the load-deflection behaviour of the cross-arm, the material properties used based on the findings reported by Agusril (2022). The Young's modulus, E_y used for the PGFRPC was 10,200 MPa, the Poisson's ratio was 0.28 and the density was 2.03 g/cm^3. The geometry of the cross-arm was identical to that of the actual cross-arm, where the dimension of the square section of the cross-arm was 102 × 102 mm^2 and 8.5 mm thick. In this study, the thickness of the PGFRPC cross-arm was assumed to be relatively constant through the cross-arm members. In addition, the fiber content and densities were also relatively constant on all sides and even in the corners coherent with previous study (Alhayek et al., 2022; Syamsir et al., 2022).

To obtain good analysis results, the medium mesh type and tetrahedron meshing method were selected. Subsequently, a mesh convergence study was done to evaluate the validity of the results. The element size was set to 30 mm, which resulted in 19,775 elements for the whole assembly parts, including fittings body, main members, and tie member. Static structure tool was used in this FEA analysis since it is one part of ANSYS software that can predict deflection due to applied loads. For the simulation process in assemble condition, the normal wire condition was considered and the load applied defined as Y component. In addition, the simulation process for individual cross-arm used only in conceptual design was considered also only on Y component for load applied. In this study the cross-arm was define as solid material since the main objective is only focused on the deformation behaviour of the PGFRPC cross-arm during load deflection and the design.

The boundary condition for assembly cross-arm was set as fixed support at the end of main and tie cross-arm members. While loads in form of force was applied at the other end of assembly cross-arm at Y-component. For the nuts and bolts used on fitting during assemble the cross-arm used constrain condition. Furthermore, during individual FEA analysis study, the frictional contacts was used between the lower surface of load span and the upper surface of the cross-arm while the frictionless contact were used between the lower surface of the cross-arm and the upper surface of the support spans. Then the force was applied on the load span with free remote displacement setting on Y-component. The load applied was increased by the steps of 1,000 N during the FEA analysis. By doing so, the assembled cross-arm member would be allowed to deflect similar to a cantilever beam. The deflection results from the FEA analysis were recorded and used to compare and validate the experimental results.

3.6 Conceptual design of honeycomb sandwich PGFRPC cross-arm

Engineers and scientists use the systematic approach in the Theory of Inventive Problem Solving (TRIZ) to place any concession between product design gaps and develop better outcomes for future technologies and products with lower risk. Currently, the use of TRIZ to solve engineering problems has seen a lot of success and improvement. Also, it is widely used by designers and researchers. This is demonstrated by the fact that many designers and researchers have conducted and published studies on design selection for various applications in order to build a product systematically using the TRIZ principle. Cascini et al. (Cascini et al., 2011) implemented the TRIZ method to visualise the idea of new sheet metal snips, which were visualised by a computer-aided drawing model based on the TRIZ contradiction. The morphological chart, TRIZ, and analytic network process (ANP) were used by Mansor et al. (Mansor et al., 2014) to generate ideas for a novel kenaf fibre polymer composite parking brake lever. The study proposed different design concepts based on the existing parking brake lever mechanism and its application.

This study developed an innovative honeycomb sandwich PGFRPC cross-arm design using a hybrid approach that drew inspiration from TRIZ, morphological chart, and ANP. The technique was used to investigate potential solutions to the issue, especially during the conceptual design phase. The main objective of this design is to improve the existing product of PGFRPC cross-arm, specifically to strengthen the centre of the beam that deals with structural failure over long-time services. A morphological chart based on TRIZ recommended solutions was subsequently built for use in the selection of submitted designs. Finally, the ANP principle was applied during design selection to decide which design concepts to pursue based on the product design specification. The overall concurrent engineering concept to develop a honeycomb sandwich PGFRPC cross-arm for high transmission towers is depicted in Figure 3.9 and discussed in the next subsection.

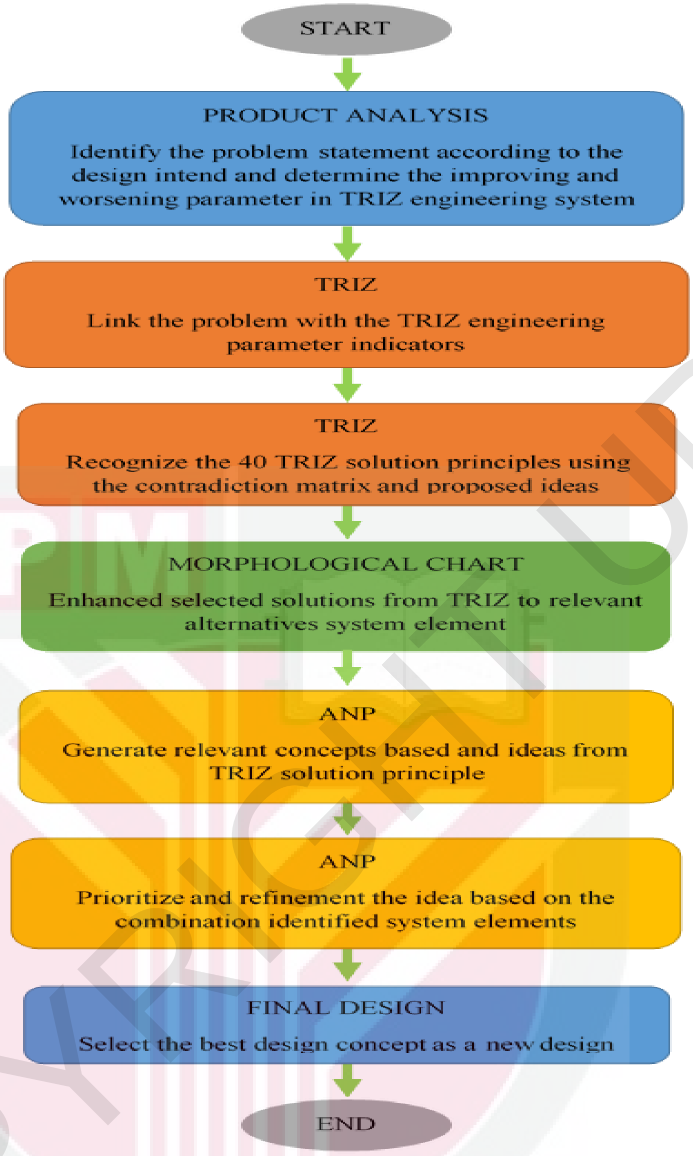

Figure 3.9: Overall process of TRIZ-Morphological Chart-ANP method.

3.6.1 Determining engineering parameters for cross-arm

The identified issue was addressed through engineering utilising the TRIZ technique. First, the limits of the deterioration and enhancement in engineering were established. There are 39 indicators that a technical system should formulate as sources of contradiction to identify improving and worsening features in the TRIZ system (Labuda, 2015). The target is to fix the design intent and failure issue of the PGFRPC cross-arm during application on transmission towers. In this project, the main failure issue of the cross-arm is the occurrence of complete failure, which lowers the service life than expected. This is due to the stacking sequence and proportion layers of the GFRPC with different fibre directions during fabrication. Additionally, the country's tropical climate (constantly hot and wet weather) exacerbated the cross-arm failure in Malaysia. The critical point of failure was at the centre of main cross-arm members, as mentioned by Asyraf et al. (Asyraf et al., 2021a).

The focal design of the composite cross-arm structure is that it should be stronger without disregarding its weight, structural integrity, functionality, and performance. The improving parameters involved were the durability of non-moving object, the strength, and ease to manufacture of the cross-arm. These parameters should fix the failure issue, especially at the centre of the PGFRPC main cross-arm members. The TRIZ 'IF-THEN-BUT' technique was used to identify the technical contradiction for the development of a new concept for the cross-arm structure using the TRIZ approach (as shown in Table 3.1). Subsequently, the engineering parameters, both improving and worsening, were matched with the 39 engineering parameters found in the TRIZ solution approach.

Table 3.1: TRIZ (IF-THEN-BUT) technique term's detail.

Terms	Worsening Feature
IF	Potential for change of parameter/subject
THEN	Improving parameter
BUT	Worsening parameter

Note: **If** the honeycomb sandwich panel is used to enhance the PGFRPC cross-arm, **then** the strength of the composite cross-arm would increase, **but** the manufacturing of the structure would be more complex and costly.

3.6.2 Performing Analytic Network process for design selection using Pairwise Comparison

On the basis of the TRIZ solution principle and morphological chart, seven honeycomb sandwich panel conceptual designs for composite cross-arm were proposed. The ANP is one of the most exhaustive and dependable methods for selecting a design because it enables designers to provide a comprehensive and systematic multi-criteria decision-making process through the use of a pairwise comparison technique (Ho, 2008; Rosli et al., 2013). A decision-making procedure addresses the generalisation of the analytical hierarchical process implementation method, which highlights the customer's requirements. To accomplish the concept design selection objective, three key components were selected, namely performance, weight, and cost. In addition, as shown in Table 3.2, each enumerated initial sub-element was converted into an equivalent design indicator.

Table 3.2: Honeycomb sandwich Product Design Specification elements and indicators.

PDS main element	PDS sub-elements	Equivalent Design Indicator
Performance	Stiffness	Deformation (mm)
	Strength	Von Mises stress (N/m^2)
Weight	Density	Mass (kg)
Cost	Raw material cost	Process complexity
	Manufacturing cost	Cost of raw material (RM)

The Product Design Specification (PDS) elements were further interpreted into the main criteria and sub-criteria, where the details are depicted in Figure 3.10 in the form of four-level hierarchy. At the first level, the goal of the project was determined, and the design was selected in accordance with the appropriate Level 2 and 3 criteria and sub-criteria from the ANP network framework. After that, all seven design concepts produced for the honeycomb sandwich PGFRPC cross-arm were listed as alternatives at Level 4.

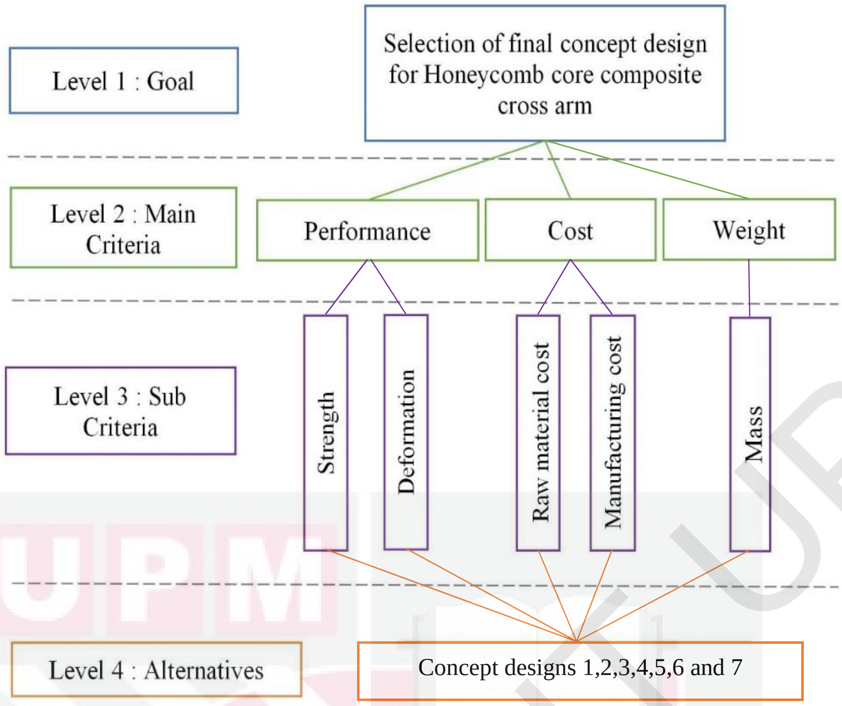

Figure 3.10: Honeycomb sandwich composite cross-arm ANP Framework design selection.

The designs were created using CATIA V5 modelling software and evaluated with the finite element structural analysis in ANSYS Workbench to predict their structural performance, including deflection and stress. In addition, the cross-arm member's structural design incorporated a square hollow section with the cross-section dimensions of 0.102 m × 0.102 m × 3,651 m, whereas the dimensions of a honeycomb sandwich were 0.300 m × 0.085 m × 0.030 m. The enhanced honeycomb sandwich PGFRPC cross-arm was subjected to the 3-PB test, and the results were recorded. Based on each created model, the mass value and geometry complexity were determined. However, the prices of primary materials for the honeycomb sandwich panels and PGFRPC cross-arms were estimated based on the average market value price, and external costs such as delivery and handling costs were not considered.

This study employed the Super Decision 2.10 software to establish four levels of ANP hierarchy, allowing for the evaluation and ranking of the proposed designs based on the predetermined main criteria and sub-criteria. The conceptual designs incorporated honeycomb sandwich panels in various configurations: on the top and bottom of the cross-arm surface for SOS1 and SOS2, on the top-bottom and left-right sides for SOS3 and SOS4, and on each cross-arm surface for SOS5. Furthermore, for design concepts SIS1 and SIS2, the hollow cross-arm was filled with honeycomb sandwich panels using tandem and infill concepts in both vertical and horizontal directions. These approaches represent valuable advancements in enhancing the cross-arm structure and contribute to the overall understanding of improved design possibilities for future implementation.

Using the numerical values for each concept design, the pairwise comparison technique was implemented in accordance with the ANP concurrent engineering approach, as shown in Figure 3.11. The numerical value was assign to indicate the scale of pairwise comparison by follow the number range 1 to 9 as listed in Table 3.3. The degree of importance among all conceptual design in the deformation behaviour of honeycomb sandwich PGFRPC cross-arm was illustrated numerically based on the design results. The primary and secondary criteria were compared to the concept design alternatives based on the relative importance of the criteria. The primary objective of the design selection process is the performance of the honeycomb sandwich PGFRPC cross-arm because the enhanced cross-arm must accommodate greater load capacity during services. By enhancing the strength of the cross-arm member, the service life can be extended and failure occurrence can be reduced. However, the weight criterion and cost attribute are deemed to be of equal importance under the condition that the weight criterion influences the design's cost.

Figure 3.11: Pairwise comparison among alternative in design selection process.

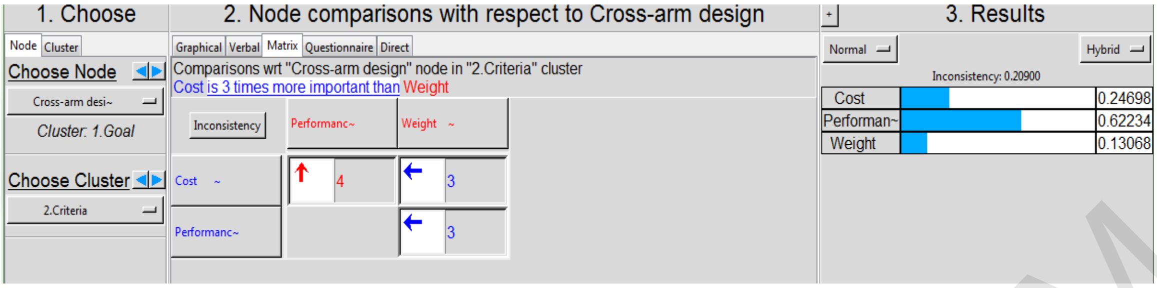

Table 3.3: Scale for pairwise comparison.

Relative intensity / score	Definition	Explanation
1	Equal value	Those two requirement are same value
3	Slightly more value	Different slightly favour one requirement over another
5	Essential or strong value	Different strongly favour one requirement over another
7	Very strong value	A requirement is strongly favoured and its dominance is demonstrate in practice
9	Extreme value	The evidence favouring one over another of the highest possible order affirmation
2, 4, 6, 8	Intermediate value between two adjacent judgement	When compromise is needed
Reciprocal	Reciprocal for inverse comparison	-

(Source: Ishak et al., 2012)

The matrix representation of the pairwise comparison was used to derive the priority vector value, denoted as w, as given by Equation (3.7):

$$w = \frac{1}{n}\sum_{j=1}^{n}\frac{a_{ij}}{\sum_{i=1}^{a} a}, \qquad i, j = 1,2,\ldots,n \qquad \text{Equation (3.7)}$$

In this equation, w represents the priority vector, a_{ij} corresponds to the importance scale, and n represents the number of criteria. The ANP method utilised the overall priority values obtained from the pairwise comparison (priority vector) method to determine the overall ranks of the alternative concept designs.

3.7 Cross-arm configuration for testing activity

In this research, testing was conducted on a full-scale cross-arm in two conditions: assembled and individual. Since the cross-arm functions similarly to a cantilever beam in its fully assembled state, a two-point bending test was used to analyze the properties of the PGFRPC cross-arm. The testing methods were based on the layout used by Sharaf et al., 2020. Mitutoyo MTY2046S analogue dial gauges were employed to measure the deflection of the cross-arm, placed at various points using magnetic base holders. The test was performed outdoors at the aircraft hangar, Faculty of Engineering, Universiti Putra Malaysia.

It is worth mentioning that dial gauges were chosen over strain gauges for this study due to the latter's unsuitability for the experimental setup. Strain gauges may detach over time, potentially affecting the results, making dial gauges more appropriate for the load deflection and creep tests. The deflection measurement was restricted to the main cross-arm members in the Y-axis direction, as this was a critical issue for the cross-arm. Deflection in the tie members and other axes were not considered. The distance between the gauges was 0.61 m at the main members, with point 1 (Y1) being the closest to the free end of the cross-arm. Additionally, five dial gauges were set on each main member, as illustrated in Figure 3.12.

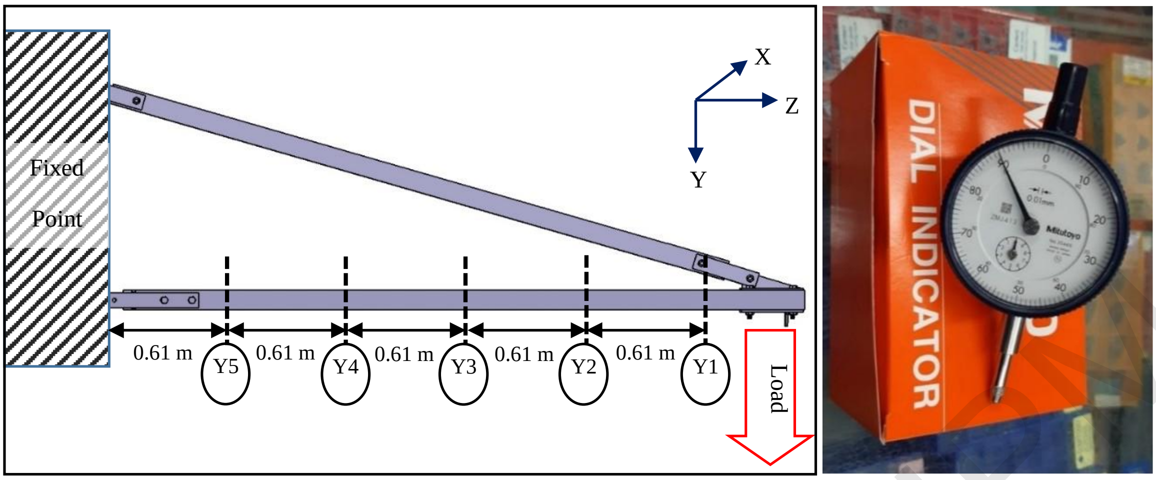

Figure 3.12: The placement interval of dial gauges on the cross-arm member during the testing condition and the specific analogue dial gauge utilized in this study.

In addition, for individual condition, a 3-PB test was performed to study the properties of the individual PGFRPC cross-arm. A universal three-point bending jig was fabricated to suit the actual cross-arm scale. The test was done in an open area with outdoor environment located at the aircraft hangar, Faculty of Engineering, Universiti Putra Malaysia. The jig setup includes essential components, such as a steel loading frame, a load cage, steel span support, steel jig support and a dial gauge support frame, as shown in Figure 3.13. This arrangement allows for accurate testing and evaluation of the panels' behaviour under various service conditions. A Mituttoyo MTY2046S analogue dial gauges was set on the centre of the cross-arm so that the vertical mid-span deflection can be recorded easily. The size of the load and support span steel cylinder used was 60 mm in diameter, connected by a rectangle hollow steel beam as a support (Sá et al., 2016). In this study, the deflection value for individual cross-arm also was limited at the main cross-arm members on Y-axis direction only while the tie members and other axis deflection were not considered same as in assemble condition.

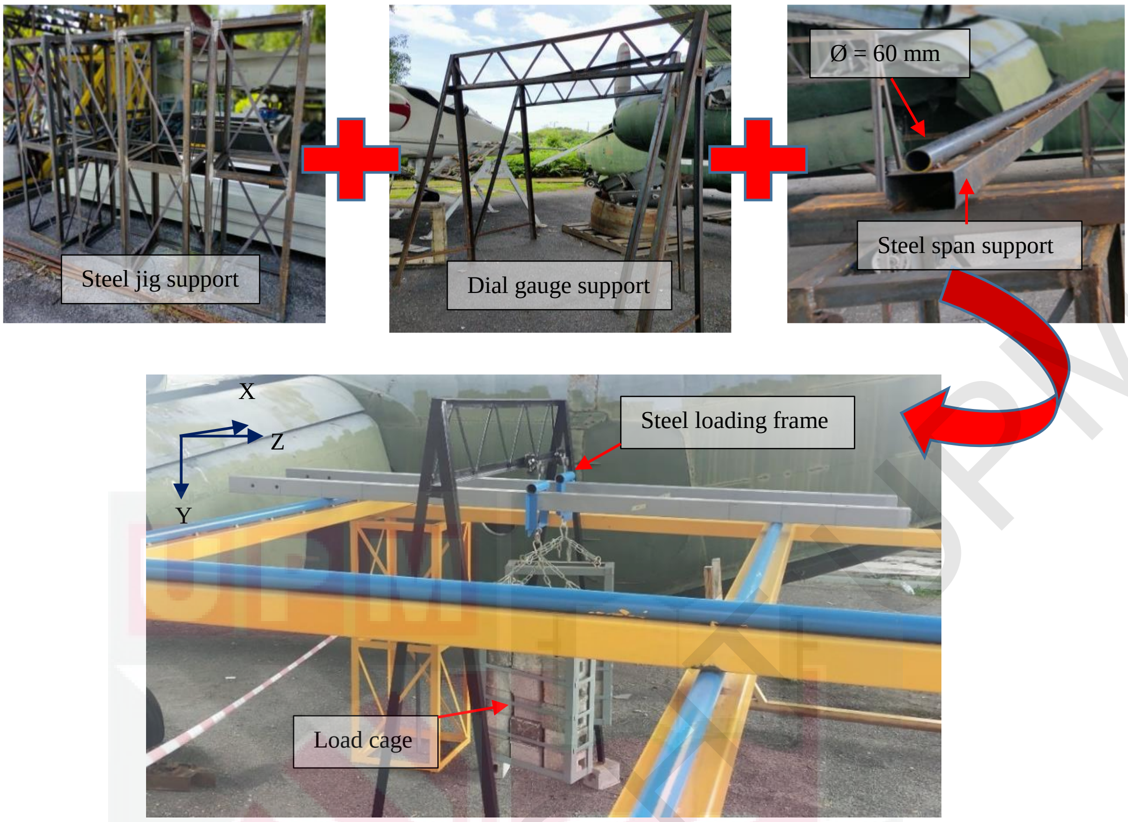

Figure 3.13: Three-point bending test jig set-up for individual full-scale cross-arm.

3.7.1 Assembled cross-arm installation for load-deflection test

A fully assembled cross-arm includes one tie member and two main members. After assembling the cross-arms, they were matched with the necessary setup and fittings, then transported to the required height using a forklift. The cross-arms were lifted and stabilized while the end fittings were securely bolted to the test rig fittings. To ensure precise positioning, the forklift was used to make final adjustments, aligning the cross-arms with the transmission tower's location. Figure 3.14 shows the assembly of the cross-arms on the test rig. A concrete block weighing nearly 1.6 tons was used as the applied load during the load deflection test. A 3-ton crane scale measured the gradually increased load at the free end of the cross-arm until the actual working load, in line with TNB standards, was reached. The dial gauge setup was the same as depicted in Figure 3.12.

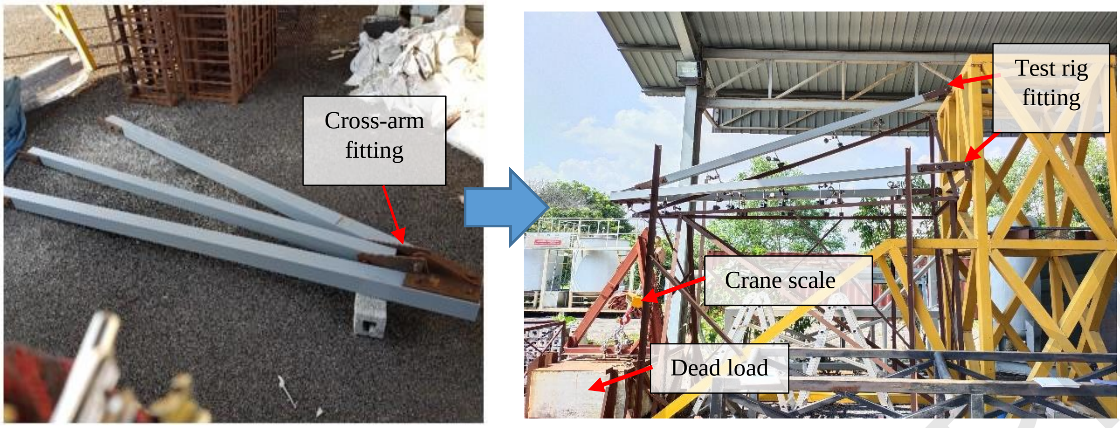

Figure 3.14: Assemble and mounting the cross-arm onto the test rig.

3.7.2 Assembled cross-arm installation for flexural creep test

For the full-scale assembled creep test, the cross-arm positioning and dial gauge setup were consistent with Figure 3.12. A load was suspended at the free end of the cross-arm, as illustrated in Figure 3.15. The creep test was conducted for 1,000 hours in an outdoor setting at the Aircraft Hangar, Faculty of Engineering, Universiti Putra Malaysia, following ASTM D2990 standards. Dial gauge readings were recorded at intervals of 0, 0.1, 0.2, 0.5, 1, 2, 5, 20, 50, 100, 200, 500, 700, and 1,000 hours. The initial strain, or "immediate strain," was measured 15 seconds after applying the working tension. As the test was performed outdoors, the cross-arms were subjected to tropical weather and environmental conditions. The test results included creep strain values, modulus comparisons, and quantitative creep analysis of both current and improved cross-arm designs. The dial gauge setup was identical to that shown in Figure 3.12 for all cross-arm members.

Figure 3.15: Assemble cross-arm layout during creep test.

3.7.3 Individual cross-arm installation for load deflection and creep test

To evaluate the deformability and determine the full-scale elastic constants (apparent and effective moduli) of an individual PGFRPC cross-arm member, a three-point bending (3-PB) test was used, aligned longitudinally with the pultrusion direction. The experimental method for obtaining the elastic moduli followed the ASTM D790 standard using a 3-PB flexural test. The study included three cross-arm members, labeled S1, S2, and S3, tested at four span lengths of 1.50, 2.00, 2.50, and 3.00 meters for each set. The cross-arm member was manually loaded and measured using a 3-ton crane scale, with deflection recorded manually using a Mitutoyo analogue dial gauge positioned at the center of the cross-arm member, as shown in Figure 3.16. During the creep test, the load was applied at the same point and setup as the load deflection test.

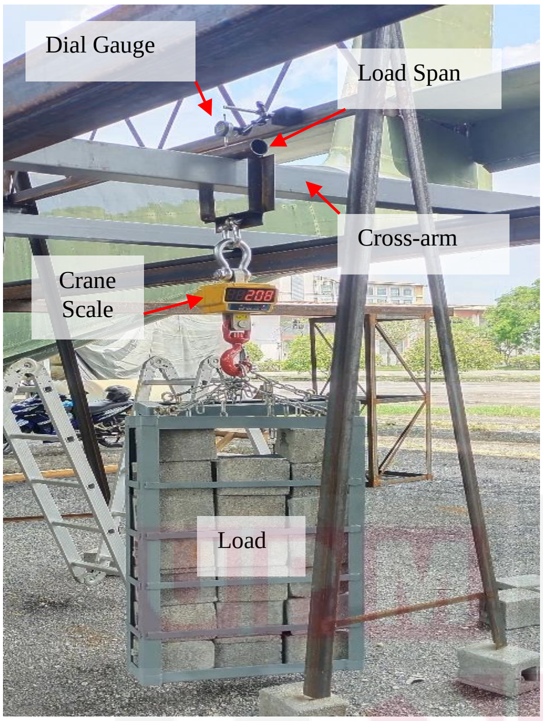

Figure 3.16: Individual beam three-point bending load deflection layout.

3.8 Deflection performance of the composite cross-arm

The flexural behaviour of cross-arm and sandwich structures is a crucial aspect of engineering and material study, particularly in the field of construction and composite materials. Cross-arms are essential components in high transmission towers in Malaysia and most of the developed countries. Cross-arms are subjected to significant bending loads during their service life. Understanding the flexural behaviour of cross-arm structures is vital to ensure their structural integrity and safety under different loading conditions.

3.8.1 Load deflection for normal wire conditions on assembly cross-arm

Two wire conditions were considered to be evaluated in this study, namely normal wire conditions and broken wire conditions. Normal wire conditions mimic the conductor wire on the cross-arm in normal condition during service, while broken wire conditions mimic the conductor wire in detached or broken condition from the cross-arm. A 3-ton crane scale was used to measure the applied load at the free end of the cross-arm that was increased gradually until the actual working load was achieved, which was in accordance with the TNB standard (refer Appendix 2). In TNB specification, the standard normal wire condition refers to the force acting in vertical and transverse directions for the transmission conductor wire connected to the cross-arm properly (Sharaf et al., 2020). The working load is a resultant force of 132 kV 13 L PGFRPC cross-arm in transverse and vertical directions, which are 4.67 and 6.47 kN, respectively, as shown in Figure 3.17.

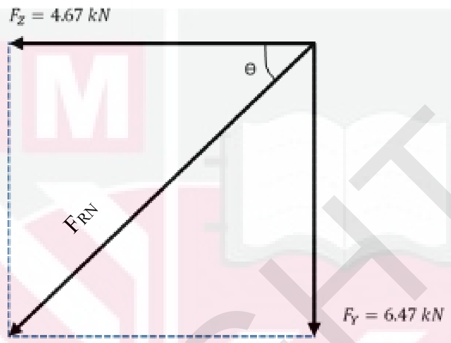

Figure 3.17: Force projection of working load in normal wire condition.

By applying Pythagoras' theorem, the resultant force (F_{RN}) and the angle in horizontal direction (θ_{RN}) for normal wire conditions, obtained from both transverse and vertical force, was calculated using Equation (3.8) and (3.9), respectively:

$$F_{RN} = \sqrt{F_Y{}^2 + F_Z{}^2} \quad \text{Equation (3.8)}$$

$$\theta_{RN} = \tan^{-1}\left(\frac{F_Y}{F_Z}\right) \quad \text{Equation (3.9)}$$

The schematic diagram and actual layout of the complete assemble PGFRPC cross-arm during the load-deflection test for normal wire conditions are shown in Figure 3.18 and 3.19.

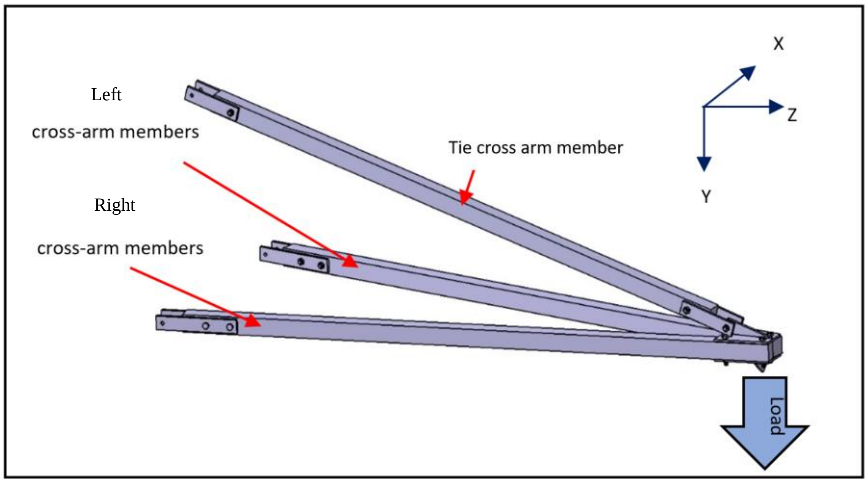

Figure 3.18: Isometric view of complete cross-arm assembly.

Figure 3.19: Actual PGFRPC cross-arm condition during normal wire condition test.

3.8.2 Load deflection for broken wire conditions on assembly cross-arm

The broken wire condition in the TNB specification refers to the force acting in vertical, transverse, and longitudinal directions for the broken transmission conductor wire (Sharaf et al., 2020). The working load is a resultant force of 132 kV 13 L PGFRPC cross-arm in vertical, transverse, and longitudinal directions, where the values are 3.43, 4.97, and 15.35 kN respectively, as shown in Figure 3.20.

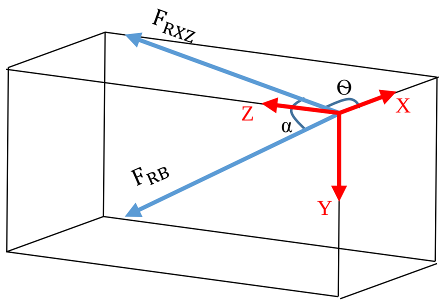

Figure 3.20: Force projection of working load in broken wire condition.

By applying Pythagoras' theorem, the resultant force (F_{RB}) obtained from vertical, transverse, and longitudinal forces was calculated using Equation (3.10):

$$F_{RB} = \sqrt{{F_X}^2 + {F_Y}^2 + {F_Z}^2} \qquad \text{Equation (3.10)}$$

Meanwhile, the resultant force between X-axis and Z-axis (F_{RXZ}) was calculated using Equation (3.11):

$$F_{RXZ} = \sqrt{{F_X}^2 + {F_Z}^2} \qquad \text{Equation (3.11)}$$

Afterwards, the angle for the horizontal (θ) and vertical (α) directions from the resultant force of (F_{RB}) and (F_{RXZ}) can be defined as Equation (3.12) and (3.13), respectively:

$$\theta = \tan^{-1}\left(\frac{F_Z}{F_X}\right) \qquad \text{Equation (3.12)}$$

$$\alpha = \cos^{-1}\left(\frac{F_{RXZ}}{F_{RB}}\right) \qquad \text{Equation (3.13)}$$

3.8.3 Load deflection and elastic properties for individual full-scale cross-arm

From the previous literature, there were limited studies on the deflection behaviour of a full-scale PGFRPC cross-arm for the 3-PB test, specifically on the maximum deflection and applied load. However, the maximum deflection behaviour of the cross-arm was known during the assembled cross-arm load-deflection test for normal wire conditions in this study. Therefore, the mid-span deflection test of an individual PGFRPC cross-arm member for actual scale was conducted by using the stiffness obtained in the assemble load deflection condition. The stiffness of the cross-arm member in the cantilever beam set-up can be defined as:

$$S_A = \frac{P}{\delta} = \frac{3EI}{L_C{}^3} \qquad \text{Equation (3.14)}$$

Where S_A is the stiffness (N/m) of the PGFRPC cross-arm during assembled condition, P is the force (N) exerted on the cross-arm member, δ is the deflection (m), E is the elastic modulus (N/m^2), I is the moment of inertia (m^4), and L_C is the total length of the cross-arm (m). In order to estimate the applied load required on the individual cross-arm in the 3-PB setup, the static elastic modulus and moment of inertia were calculated with the total cantilever beam length to gain the stiffness value of the cross-arm in assembly condition. With the stiffness value and the working load of the cross-arm, the deflection value of the cross-arm in individual condition was determined. Subsequently, the experiment of an individual cross-arm was conducted by applying load until the calculated deflection value for each span length type was achieved. The knowledge yield from this experiment was used for the flexural creep 3-PB test.

The PGFRPC cross-arm was treated as an anisotropic material, so the deflection equations for beams considering shear deformation, as studied by Bank, 2006, for pultruded fiber-reinforced members, were applied in this research. According to the shear deformation beam theory, two variables describe the beam's deformation under transverse loading: the total deflection and the slope from bending deformation. For isotropic materials, the deflection equation is given by Equation (3.15):

$$\delta(y) = \frac{f_1(y)}{EI} + \frac{f_2(y)}{kAG} \qquad \text{Equation (3.15)}$$

Here, δ(y) is the beam deflection function, f1(y) and f2(y) are functions dependent on the loading and boundary conditions, E is the isotropic elastic modulus, I is the second moment of area, k is the shear coefficient, A is the cross-sectional area, and G is the isotropic shear modulus.

The PGFRPC cross-arm in this study was analysed as a thin-walled beam composed of anisotropic composite material, as discussed by Bank (Bank, 1989b). Therefore, a beam section shear modulus was proposed and identified as G, designated as G_c, where the subscript stands for "cross-arm member". G_c replaces the term kG in the isotropic formulation and function based on the material properties and the geometrical properties of the cross-arm member. Similar to the isotropic elastic modulus of the material, E was replaced with E_c as the beam section flexural modulus. Under these conditions, the shear modulus and flexural modulus were different from the longitudinal modulus of the coupon scale due to the difference that exists in the laminated structure of the pultruded composite material and the variation in the properties in the parts of the cross-arm member cross-section. Thus, Equation (3.8) becomes Equation (3.16):

$$\delta(y) = \frac{f_1(y)}{E_c I} + \frac{f_2(y)}{G_c A} \qquad \text{Equation (3.16)}$$

By using Equation (3.16), the significance of shear deflection in the PGFRPC cross-arm member can be investigated analytically by considering the response of the simply supported centre-loaded beam of span length (L_s). For this case, the maximum deflection (δ_{max}) under the applied load (P) can be written as:

$$\delta_{max} = \frac{P{L_s}^3}{48 E_c I} + \frac{P L_s}{4 G_c A} \qquad \text{Equation (3.17)}$$

Disregarding shear deflection, the deflection can be expressed using an apparent beam section flexural modulus (Ea) as follows:

$$\delta_{max} = \frac{PL_s^{\ 3}}{48E_aI} \qquad \text{Equation (3.18)}$$

To relate both Equations (3.17) and (3.18), the apparent cross-arm member section flexural modulus in terms of the section anisotropy ratio (E_c/G_c) and the slenderness ratio(L/r), and r is the radius of gyration, as shown in Equation (3.19), where L is the effective length of the cross-arm member:

$$E_a = \frac{E_c}{1 + 12[(E_c/G_c)/(L/r)^2]} \qquad \text{Equation (3.19)}$$

From his graph (refer to Figure 3.21), Bank proved that a plot of the ratio for E_a/E_c against the slenderness ratio for values of E_c/G_c is suitable for a pGFRP structure. As the impact of shear deflection becomes more significant, the E_a/E_c ratio gradually decreases from its maximum value of 1.0. Shear deflection effects become more significant when the anisotropy ratio of the section increases and the slenderness ratio decreases. For L/r ratios below 60, shear deflection effects are most outstanding. Therefore, it is highly recommended to include the contribution of shear deflection in deflection calculations when L/r is less than 60.

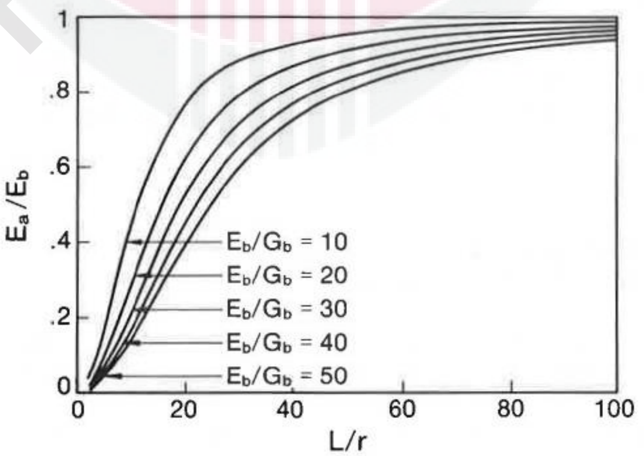

Figure 3.21: The apparent flexural modulus as influenced by anisotropy and slenderness ratio.
(Source: Bank, 1989b)

The study involves applying a load to a supported beam at its midpoint and measuring the resulting deflection. The relationship between the midpoint deflection (δ), the applied load (P), and the elastic moduli of the section, as shown in Equation (3.17), can be expressed in terms of the cross-sectional area (A) as follows:

$$\frac{4A\delta}{PL_s} = \frac{(L_s)^2}{12E_c} + \frac{1}{G_c} \qquad \text{Equation (3.20)}$$

Equation (3.20) represents a straight line in the $\frac{4A\delta}{PL_s}$ versus $(L_s)^2$ plane, with a slope of $\frac{1}{12E_c}$ and an intercept of $\frac{1}{G_c}$. Experimental data points are obtained by measuring the midpoint deflection (δ) for a constant applied load (P) at various $(L_s)^2$ values. Linear regression is then performed on these data points to determine the slope and intercept, allowing the calculation of the section moduli. This equation was used in this study as Method 1. Alternatively, Equation (3.20) can be rewritten in terms of the moment of inertia (I) as:

$$\frac{4I\delta}{PL_s{}^3} = \frac{1}{(L_s)^2 G_c} + \frac{1}{12E_c} \qquad \text{Equation (3.21)}$$

In this form, Gc is derived from the slope, while Ec is obtained from the intercept in the $\frac{4I\delta}{PL_s{}^3}$ versus $\frac{1}{(L_s)^2}$ plane. This equation was used in the study as Method 2. Both methods were employed to determine the section moduli during the investigation.

3.9 Flexural creep behaviour of composite cross-arm

In this study, the cross-arm structure was treated as a cantilever beam extending horizontally from a fixed support. Mechanical properties of the cross-arm were evaluated using cantilever beam equations and their derivations. As expected, the cross-arm showed deflection, with the top section under tension and the bottom section under compression. To examine long-term performance, flexural creep tests were conducted in both assembled and individual member conditions. Studying individual beams provided valuable insights into each cross-arm member's properties, while testing the assembled cross-arm offered practical insights for real-world applications.

3.9.1 Flexural creep properties of assembled cross-arm

The force-deflection relationship of the cantilever beam was assumed to be linear for small deflections and when the material does not yield (Rosato & Rosato, 2003). Since the cross-arm material, PGFRPC, has uniform density along its length, Hooke's law implies that the applied force is proportional to the extension. According to Figure 3.22, the stress-strain relationship of the cross-arm is given by:

$$P = k\delta \qquad \text{Equation (3.22)}$$

Where P represents the force on the beam (N), k is the elastic coefficient (N/m), and δ is the deflection (m). The elastic coefficient can be calculated using:

$$k = \frac{3E_e I}{L^3} \qquad \text{Equation (3.23)}$$

Here, Ee is the elastic modulus (N/m²) for the assembled cross-arm member, I is the moment of inertia (m^4), and L is the cantilever beam length (m). Substituting Equation (3.22) into Equation (3.23) yields:

$$P = \left(\frac{3E_e I}{L^3}\right) \times \delta \qquad \text{Equation (3.24)}$$

For a square cross-arm profile, the elastic modulus Ee can be expressed as:

$$E_e = \frac{4PL^3}{\delta b_e {h_e}^3} \qquad \text{Equation (3.25)}$$

Where b_e and h_e are the width and thickness of the cross-beam arm, respectively. Using this equation, the maximum bending stress can be predicted (Cowin, 2001). Typically, the highest stress occurs at the fixed end (x=0) and the lowest at the load end (x=L). Maximum and minimum stresses σ_e can be calculated using:(Hunt et al., 2015):

$$\sigma_e = \frac{P(L-x)\frac{h_e}{2}}{I} = \frac{6P(L-x)}{b_e {h_e}^2} \qquad \text{Equation (3.26)}$$

Strain across the beam at any time and location can be determined from Hooke's law:

$$\varepsilon_t = \frac{\sigma_n}{E_e} \qquad \text{Equation (3.27)}$$

Where ε_t is the strain at a specific point and time, σ_n is the stress, and E_e is the elastic modulus at that location.

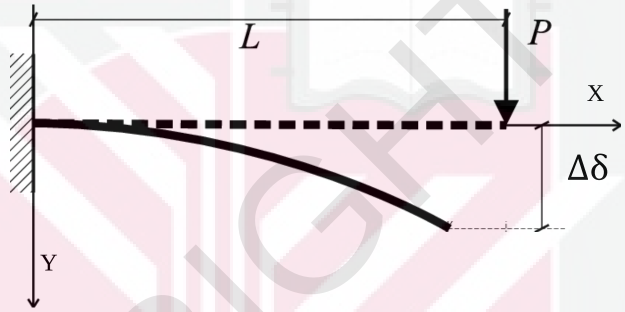

Figure 3.22: Schematic diagram of a cross-arm structure modeled as a cantilever beam.

3.9.2 Flexural creep and elastic properties for individual full-scale cross-arm

Flexural creep tests were conducted on full-scale panels to meet the study's objectives. Three cross-arm members were tested using a three-point bending setup with a 2.5 m span length, as determined from previous load deflection studies. The load was set as previously determined for this span length, and the creep test was performed for 1,000 hours under Malaysia's outdoor conditions. The test setup involved placing a dead load on the loading cage, as shown in Figure 3.16. Load application was done manually to ensure a smooth load increase and minimize dynamic effects. The load and support span used were 60 mm in diameter, consistent with those in the load deflection tests. Mid-span deflection was measured with a Mitutoyo analogue dial gauge, with a range of 5 to 20 mm and precision of 0.01 mm. Temperature and humidity were monitored with a digital meter.

Due to the large experimental setup (approximately 43 m²), the test could not be conducted in a controlled environment. Consequently, recorded temperature and humidity data were assessed. The deflection measurements for the three panels were analyzed in the time domain, and effective elastic and shear moduli were evaluated using Bank's methodology. The methodology followed Bank's approach (Bank, 1989b; Sá et al., 2016); with the addition of time *t* for the creep test. Equations (3.20) and (3.21) were modified to account for time:

$$\frac{4A}{PL_s}\delta(t) = \frac{1}{12E_c(t)} \cdot (L_s/r)^2 + \frac{1}{G_c(t)} \qquad \text{Equation (3.28)}$$

$$\frac{4I}{PL_s{}^3}\delta(t) = \frac{1}{G_c(t)} \cdot \frac{1}{\left(\frac{L_s}{r}\right)^2} + \frac{1}{12E_c(t)} \qquad \text{Equation (3.29)}$$

Here, L_s , A, and I retain their previous definitions from the load deflection tests. These equations represent straight lines at a given time t, with slope and intercept directly related to the flexural and shear moduli. Regression analysis of experimental data provides the initial effective moduli, which are compared to those from the 3-PB test. The time-dependent reduction factor, χ(t), for the elastic moduli was calculated using Findley's power law model:

$$\chi(t) = \left(1 + \frac{E_0}{E_t} * t^n\right)^{-1} \qquad \text{Equation (3.30)}$$

Where E_0 is the initial elastic modulus, E_t is the creep modulus at time t, E_a is the apparent elastic modulus for creep, and n is a material constant. The apparent modulus at time t is:

$$E_a(t) = E_0 * \chi(t) \qquad \text{Equation (3.31)}$$

Combining these equations yields the general apparent elastic modulus:

$$E_a(t) = E_0 \times \left[\frac{1}{1 + \left[\frac{E_0}{E_t} * t^n\right]}\right] \quad \text{Equation (3.32)}$$

This allows predictions of the time-dependent behavior of the full-scale cross-arm for up to 50 years.

3.9.3 Empirical creep model

The investigation into the creep properties of the PGFRPC cross-arm was extended using an established empirical creep model validated by previous research (Asyraf et al., 2020). The non-linear Findley's power law model was employed to analyze transient creep based on stress components and material constants. Despite its generic applicability, the model requires straightforward numerical calculations. Given that the PGFRPC cross-arm is considered anisotropic, the Findley model was used to simulate the creep behavior, represented by:

$$\varepsilon(t) = \varepsilon_0 + mt^n \quad \text{Equation (3.33)}$$

Where ε_0 is the instantaneous strain after applying the load, and mmm and n are load constants and material exponents derived from experimental data. Substituting stress σ\sigmaσ for elastic strain and dividing by the modulus E_0, the equation becomes:

$$\varepsilon(t) = \frac{\sigma_e}{E_0} + mt^n \quad \text{Equation (3.34)}$$

This power law equation models the creep characteristics of the PGFRPC cross-arm, predicting strain at specific times and stress levels based on material parameters m and n. The Findley model effectively represents both primary and secondary creep stages and is straightforward to apply.

3.10 Conclusions

This chapter provides a summary of the experimental study and numerical analysis conducted, which focused on characterising and fabricating materials for the cross-arm and honeycomb sandwich structure used in this study. This chapter also explores the numerical methods employed to study the deflection behaviour and creep properties of the cross-arm structure. To achieve the research objectives, the following activities were carried out:

1. Analysing the deflection behaviour of the PGFRPC cross-arm and comparing it with the previous wooden cross-arm.
2. Characterising and fabricating the honeycomb sandwich composite structure.
3. Studying the conceptual design of the honeycomb sandwich PGFRPC cross-arm to be used in the 132kV transmission tower.
4. Investigating the deflection behaviour of both assembled and individual cross-arm members.
5. Evaluating the flexural creep characteristics of both PGFRPC cross-arms, with and without the honeycomb sandwich structure, followed by further assessment using numerical analysis.

Detailed findings and discussion on this methodology are presented in Chapter 4 of this thesis.

CHAPTER 4

RESULTS AND DISCUSSION

4.1 Introduction

This chapter elaborates the results of all design simulations and experiments conducted during the study. A study on the deformation behaviour of the assembled full-scale pultruded glass fibre-reinforced polymer composite (PGFRPC) cross-arm has become the initial study on this research. The results of load-deflection behaviour and the bending properties of the composite cross-arm were compared with the conventional one (Balau wood cross-arm). Then, the next subsection discusses the characterisation and fabrication of honeycomb sandwich composite structure that can suit the PGFRPC cross-arm enhancement. After that, the subsequent subsection defines the conceptual design of the honeycomb sandwich PGFRPC cross-arm in actual scale. In order to describe the properties of existing and improved cross-arm, a three-point bending (3-PB) test involving the load deflection and flexural creep test was conducted. Furthermore, in this subsection, the life estimation of the composite cross-arm due to reduction factors was determined. The full-scale assemble behaviour for flexural deformation and creep properties was studied in the last subsection for a better understanding on the potential of the advancement of the existing PGFRPC cross-arm with high demand composite structure, honeycomb sandwich panel for 132 kV transmission towers.

4.2 Properties of PGFRPC cross-arm during load application

This section investigates the load-deflection behaviour of PGFRPC cross-arms in high transmission towers and compares them to traditional wooden cross-arms. The study considers normal and broken wire conditions using experimental and finite element analysis (FEA) approaches.

4.2.1 Working load for normal wire conditions

For normal wire conditions, the working load was calculated using Equations (3.8) and (3.9). The resultant force obtained by the PGFRPC cross-arm was:

$$F_{RN} = \sqrt{{F_Y}^2 + {F_Z}^2}$$

$$F_{RN} = \sqrt{4.67^2 + 6.47^2}$$

$$\underline{F_{RN} = 7.98\ kN}$$

Afterwards, the angle of the resultant force is defined as:

$$\theta = tan^{-1}\left(\frac{F_Y}{F_Z}\right)$$

$$\theta = tan^{-1}\left(\frac{6.47}{4.67}\right)$$

$$\underline{\theta = 54.2°}$$

Using a safety factor of 1.0, the cross-arm was tested at an applied load of 7.98 kN and an angle of 54.2° from the horizontal plane.

4.2.2 Working load for broken wire conditions

In order to find the working load for broken wire conditions, Equations (3.10) and (3.11) were used. The resultant force obtained by the PGFRPC cross-arm was:

$$F_{RB} = \sqrt{{F_x}^2 + {F_Y}^2 + {F_Z}^2}$$

$$F_R = \sqrt{15.35^2 + 4.97^2 + 3.43^2}$$

$$\underline{F_R = 16.5\ kN}$$

Meanwhile, the resultant force between X-axis and Z-axis (F_{RXZ}) was obtained as follows:

$$F_{RXZ} = \sqrt{{F_x}^2 + {F_Z}^2}$$

$F_{RXZ} = \sqrt{15.35^2 + 3.43^2}$

$F_{RXZ} = 15.73\ kN$

Afterwards, the angle of the resultant force for F_R (θ) and F_{RXZ} (α) was determined using Equations (3.12) and (3.13):

$$\theta = tan^{-1}\left(\frac{F_Z}{F_X}\right)$$

$$\theta = tan^{-1}\left(\frac{3.43}{15.35}\right)$$

$\underline{\theta = 12.6°}$

$$\alpha = cos^{-1}\left(\frac{F_{RXZ}}{F_R}\right)$$

$$\alpha = cos^{-1}\left(\frac{15.73}{16.5}\right)$$

$\underline{\alpha = 17.57°}$

By using a safety factor of 1.0, the cross-arm was tested at an applied load of 16.5 kN with the angles of 12.6° from the horizontal plane and 17.57° from the vertical plane. A summary of the working load and angle required under normal and broken wire conditions for the cross-arm based on the TNB Sdn. Bhd. specification is shown in Table 4.1(Sharaf et al., 2020).

Table 4.4: Working-load and angle specification for PGFRPC cross-arm.

Wire Condition	Working Load (kN)	Angle (˚)	
		From Horizontal	From Vertical
Normal	7.98	54.2	-
Broken	16.5	12.6	17.57

4.2.3 Load-deflection under normal wire conditions

Figure 4.1 illustrates the load-deflection characteristics of the left and right PGFRPC cross-arm main members under standard wire conditions along the Y-axis. The data reveals a linear relationship between the applied load and the resulting deflection, provided that the deflection remains small and the material does not undergo yielding (Beléndez et al., 2002). Consequently, the PGFRPC is treated as a linear elastic material, following Hooke's law. Additionally, the greatest deflection consistently occurred at the free end, while the least deflection was observed at the fixed end of the cross-arm member. This deflection analysis parallels studies of cantilever beams and addresses a three-dimensional problem. The impact of Poisson's ratio is negligible, given that the beam's length is significantly greater than its cross-sectional thickness and less than the curvature radius of the beam (Feynman, 1964).

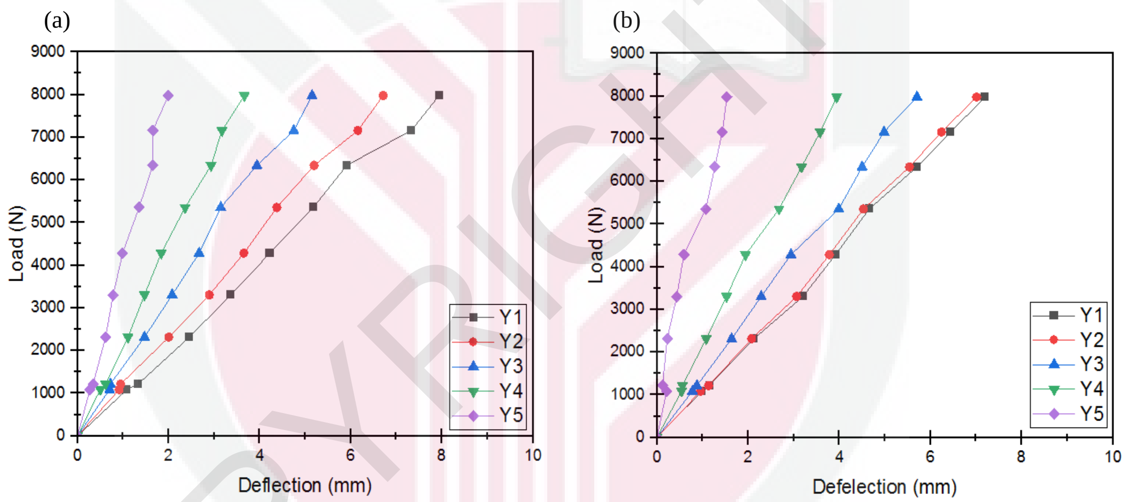

Figure 4.1: Load-deflection of PGFRPC cross-arm members in Y-axis for normal wire condition; (a) Left cross-arm members, (b) Right cross-arm members.

Figure 4.1 also shows that the maximum value of deflection for both left and right cross-arm member was less than 8 mm which are 7.94 mm and 7.19 respectively. Furthermore, the deflection of the left cross-arm member increased uniformly along its length. However, the deflection of the right cross-arm member increased unevenly due to the applied angle from the horizontal plane of the cross-arm structures. The deflection value at point Y2 was slightly higher than that at point Y1, which was suspected to be due to the applied angle that caused the force acting on the right member to be higher than the force acting on left member. Furthermore, the compression and tension on the right cross-arm member caused it to be twisted, especially at point Y2. It also resulted in an increase in the graph slope for the right cross-arm member in comparison to the left cross-arm member. Nevertheless, both left and right cross-arm members exhibited the same linear relationship between the applied load and the deflection.

Several researchers have used the same methodology used in this study to study the deflection behaviour of cantilever beams in various loading conditions using numerical and mathematical modelling (Ang et al., 2002; L. Chen, 2010; De Bona & Zelenika, 1997). C. M. Wang et al. (C. M. Wang et al., 1997) proved that the magnitude of deflection behaviour of a beam is dependent on the load position on the beam. The deflection increases as the distance between the applied load and the fixed point increases, reaching its maximum value when the load is applied at the free end of the beam. The classical beam theory was used by H. J. Barten et al. and T. Balendez et al. (Barten, 1944; Beléndez et al., 2002) in computing a mathematical model for the deflection of a cantilever beam of varied stiffness. The results proved the linear relationship between the load and the deflection. Besides, the study on non-linear applied load angle of the cantilever beam is required to understand their behaviour, as determined by several researchers (Nallathambi et al., 2010; Y. G. Wang et al., 2012). However, this study only focuses on the deflection behaviour and not on the applied load angle as the specification was given by the supplier.

The deflection values of the PGFRPC cross-arm obtained at points Y1 and Y5 for a minimum load (min) of 1,000 N and a maximum load (max) of 7,980 N were compared to those of Balau wood cross-arm, which was evaluated by Sharaf et al., 2020. The difference in the deflection values of both cross-arm members at Y1 and Y5 is shown in Figure 4.2.

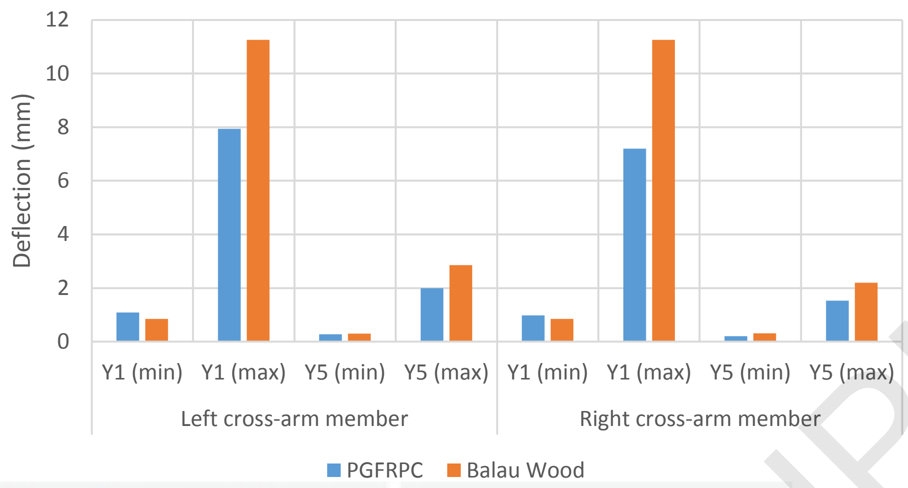

Figure 4.2: Difference of deflection value of PGFRPC and Balau wood cross-arm in normal wire condition.

It was observed that the deflection values were slightly higher for both left and right PGFRPC cross-arm members when the minimum load was applied at point Y1 as compared to those of the Balau wood cross-arm member. However, the difference in deflection values was small at point Y5 for both cross-arm types, which was approximately 0.12 mm. On the other hand, in the working load conditions, the deflection value of the Balau wood cross-arm member was significantly higher compared to that of the PGFRPC cross-arm members, where the difference of the deflection value between these two types of cross-arms was almost 3.7 mm. Although the deflection gap between Balau wood and PGFRPC cross-arm are relatively high, however these value are acceptable and coherent with previous study (Asyraf et al., 2021b; Sharaf et al., 2020) on Balau wood for coupon scale and actual scale. Since there are limited study done on the deflection behaviour of PGFRPC cross-arm, therefore the result obtained in this study was compared with the simulation study as discuss in section 4.2.5. A study of deflection behaviour in working load conditions is crucial for high transmission towers to determine the durability of the cross-arm member.

Figure 4.2 demonstrates that the PGFRPC cross-arm could sustain greater bending stress than the Balau wood cross-arm. In this point of view, the pultruded composite cross-arm was fabricated using the pultrusion of ten layers of ±45° and 0° glass fibre reinforced unsaturated polyester (UPE) matrix. The employment of alternating stacking sequence between +45° and -45° at the outermost and innermost layers would result in resisting the shear strain due to torsional loading by the cable, as determined by Syamsir et al. (Mohamad et al., 2020; Syamsir et al., 2022). As the lamination sequence changed between 0° and 45°, the higher content of continuous roving in the fabrication of the profiles led to these outcomes (Kelkar et al., 2006; L. Yan et al., 2014). Additionally, both sides of the 0° outer layers of pultruded composite allowed principal loading direction, which was aligned with the ply orientation, according to Hashim et al. (Hashim et al., 2021). Hence, this situation would aid the PGFRPC cross-arm to be exposed in an orthogonal manner in order to elevate the bending strength of the structure (Y. Bai et al., 2021). The alternation between 0° and ±45° of the ply orientation resulted in varied stiffness along the thickness of the laminates (Bandaru et al., 2015; Fotouhi et al., 2017; Kasiviswanathan et al., 2015). This would result in the delay in the breakage of glass fibre upon applied force, which protected the composite laminate. Additionally, due to the macromolecular chain of UPE matrix that slid and stretched at a greater elasticity rate (Nurazzi et al., 2019; Pandita et al., 2014), the glass fibre rupture was delayed. Using UPE as a matrix in the composite laminate enhanced its toughness and rigidity. Moreover, E-glass fibre is compatible with UPE resin.

Although the deformation values of Balau wood and PGFRPC cross-arms were different, both materials exhibited almost the same quality in resisting elastic deformation. The difference in the deflection values between left and right cross-arm members was probably due to the alignment angle after the load was applied. The deflection on right main member was slightly higher than left main member of the PGFRPC cross-arm during load application in normal wire condition test. It should be noted that the load was applied manually and was dependent on inconsistent manpower energy. Thus, it is suggested to use an automated system during load application to improve the angle of cross-arm from the horizontal plane and to reduce the difference in the deflection value between left and right cross-arm members. Figure 4.2 also shows that wood possesses lower mechanical properties compared to PGFRPC due to the composition of natural fibre that consists of cellulose, hemicellulose, lignin, and pectin (Pandita et al., 2014). This composition leads to weak interaction among the fibres, which promotes internal defects and cracks. Subsequently, it induces early crack development growth.

4.2.4 Load-deflection under broken wire conditions

The load-deflection behaviour of cross-arm in broken wire conditions was studied using the same method used in normal wire conditions but with different angles from the horizontal and vertical planes. The results obtained for left and right cross-arm members in this condition were compared with the previous results obtained by Sharaf et al. on the Balau Wood cross-arm structure, which had similar profiles and dimensions. By using a safety factor of 1.0, an actual working load of 16,500 N was applied on the cross-arm at an angle of 12.6° from the horizontal plane and 17.57° from the vertical plane.

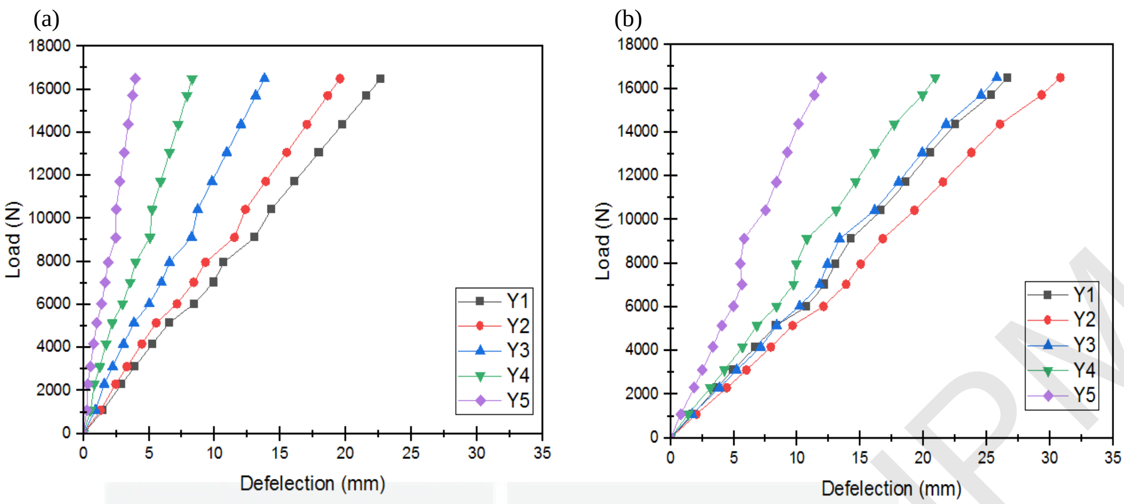

Figure 4.3: Load-deflection of PGFRPC cross-arm members in Y-axis for broken wire condition; (a) Left cross-arm members, (b) Right cross-arm members.

Figure 4.3 shows the load-deflection behaviour of the left and right PGFRPC cross-arm members subjected to actual working load in broken wire conditions. The deflection value and the applied load for the existing PGFRPC cross-arm were in a linear relationship, similar to the normal wire conditions. All considerations and properties discussed in Subsection 4.2.3 were used in obtaining the results in this condition. The broken wire conditions mimic the actual position of the cross-arm with broken wires. Thus, the working load applied was 48% higher than the load in normal wire conditions, which was 16,500 N. In this study, the load was increased gradually from 0 to 16,500 N by steps of 1,000 N.

The maximum deflection value obtained for the Left cross-arm member was approximately 21.59 mm, while for the right cross-arm member, the deflection value was about 25.37 mm. The deflection of the left cross-arm member increased uniformly along its length. However, the deflection increment of the right cross-arm member was uneven, which was suspected to be due to the tested angle of the cross-arm structures. On the other hand, the deflection value of the right cross-arm member at point Y2 was higher than the deflection value at point Y1 for all applied loads. The unpredictable results were obtained even though the specification given by the supplier on the applied angle from the horizontal and vertical planes for broken wire conditions had been followed. The results also indicated that the applied angle caused the force acting on the right cross-arm member to become higher than the force acting on the left cross-arm member. In addition, the compression and tension on the right cross-arm member caused it to be more twisted, especially at point Y2. It also resulted in the reduction of the graph slope for the right cross-arm member as compared to the left cross-arm member. Nevertheless, both left and right cross-arm members exhibited the same linear relationship between the applied load and the deflection.

Generally, the broken wire conditions mimic the sudden breakage of wires in a transmission line, which resulted in sudden unbalanced forces in the system. The resulting loads acting on the system can be very large and can lead to failure of either the cross-arm or the whole support structures. Several studies have performed static analysis of the broken wire conditions to determine the residual wire tensions and support structure loads (Campbell, 1970; Lindsey, 1978; POSKITT, 1964; Richardson Jr, 1977). Mozer et al. presented the analysis results of broken wire conditions and provided static and dynamic data on the longitudinal loading and structure response using prototype line systems (Mozer et al., 1981). The corresponding static displacement and member forces acting on the cross-arm were measured and analysed using the static analysis computer programme. By using the equilibrium equations, researchers derived an equation for insulator cable displacement by substituting the stiffness formulation into the force equilibrium relationships at each wire attachment (Fleming & Pohlman, 1977). The various angles during load application due to broken wires played a role in determining the displacement of the cross-arm structures.

The maximum and minimum deflection of the PGFRPC cross-arm obtained at points Y1 and Y5 were compared with the results obtained by Sharaf et al., 2020. The difference in the deflection values for both cross-arm member types in broken wire conditions at Y1 and Y5 is shown in Figure 4.4.

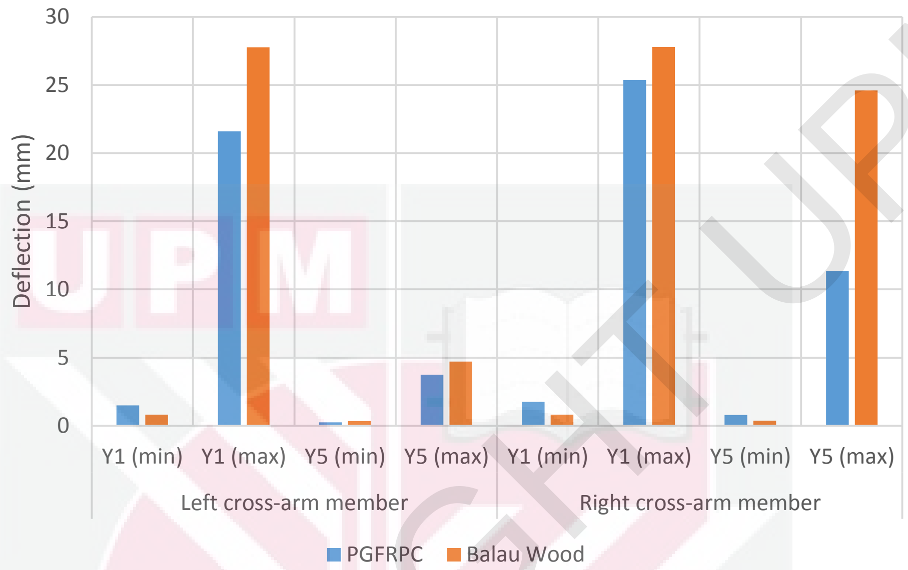

Figure 4.4: Difference of deflection value of PGFRPC and Balau wood cross-arm in broken wire condition.

It can be noted that the deflection values were slightly higher for both left and right PGFRPC cross-arm members during the application of the first load of 1,000 N at point Y1 as compared to the Balau wood cross-arm member. However, the deflection value difference was considered small at point Y5 for both types of cross-arm members, which was around 0.43 mm. The PGFRPC cross-arm responded immediately once the first load was applied, and the deflection became stable after the working load was applied, where the deflection value was slightly higher at the beginning of the load application.

In the working load conditions, the deflection value increased drastically for the Balau wood cross-arm compared to the PGFRPC cross-arm, specifically for the Left cross-arm member. For the Right cross-arm member, the deflection values at points Y5 became higher than those of the Left cross-arm member due to the applied load angle from the horizontal and vertical planes (refer Table 4.1), which caused the cross-arm to be twisted in the direction of the angle. This results also coherent with study of made by Sharaf et al. (2020). Thus, in assembly condition, during broken load application, the cross-arm was estimated to be twisted either more on the right cross-arm member or left cross-arm member according to the situation it is heavy on which side during broken condition. In this study, the given angle of applied load was only considered for the cross-arm twisted more on the right cross-arm member. Although that, this study focuses only on obtaining the deflection behaviour of the existing PGFRPC cross-arm and compared them to that of Balau wood cross-arm. Thus, the twisting moment and torsional buckling were not discussed.

The difference between these two types of cross-arms was caused by Balau wood's higher elastic modulus and flexibility when compared to the PGFRPC material. The PGFRPC cross-arm, on the other hand, could sustain more bending stress than the Balau wood cross-arm, and the pultruded technique provided value in terms of reinforcing the composite structure. Although the deformation values of the Balau wood and PGFRPC cross-arms varied, both materials demonstrated about the same resistance to elastic deformation. Under both normal and broken wire conditions, the linear relationship between load and deflection was the same. This understanding will serve as the foundation for future advancements in the cross-arm application for high transmission towers.

4.2.5 FEA model accuracy and validation

A mesh convergence study was performed to verify the accuracy of the FEA model, namely to ensure that the FEA model captures the system behaviour and gives the most accurate data. By using an iterative method, the number of elements in the mesh was increased from 7,000 to 32,600 along the model length and was solved. The complexity of the model and the response was recorded. The deflection at point Y1 of the model subjected to the working load of 7,980 N was chosen as the response, while the number of elements in the mesh became the complexity of the model (Patil & Jeyakarthikeyan, 2018; I. T. Wang, 2014).

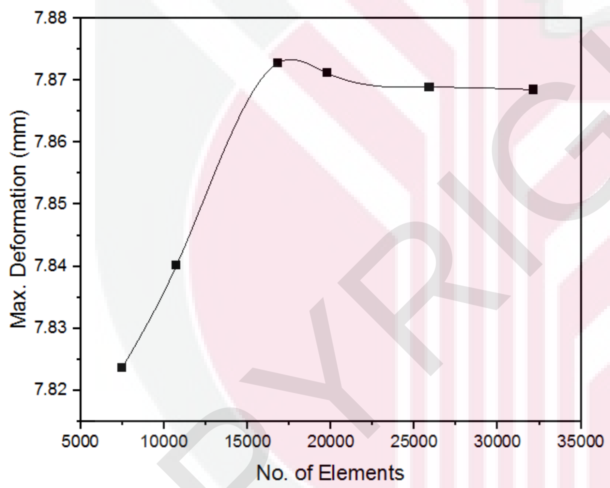

Figure 4.5: Mesh convergence study for FEA model.

Using the tetrahedron meshing method on the cross-arms and the auto-meshing method on the fitting body, the FEA model was meshed and their maximum deflection results were observed. Figure 4.5 presents the mesh convergence study of the FEA model. In the beginning, the maximum deflection increased linearly with the number of mesh elements. However, the graph started to converge and remained constant after reaching 25,000 elements. Furthermore, it was observed that no further variation in the deflection value occurred after 32,600 elements, and this number of elements exhibited stable conditions as compared to other number of elements. Thus, 32,172 elements were chosen as a criterion for the mesh convergence result for the FEA deformation analysis as shown in Figure 4.6.

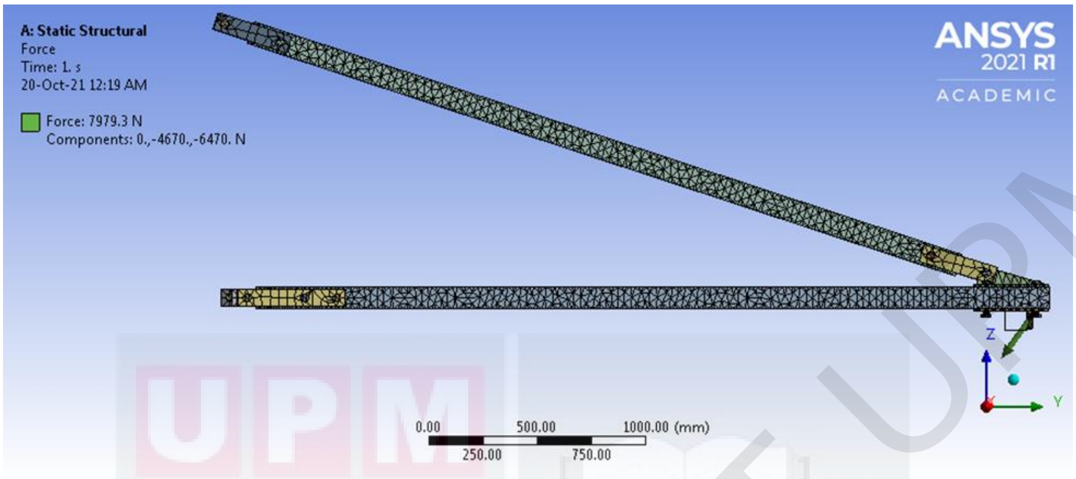

Figure 4.6: Meshes of PGFRPC Cross-arm assembly.

By implementing the cantilever beam concept, the experimental results of the PGFRPC cross-arm were verified against the FEA results on the deflection behaviour, where one end of the beam was fixed and the load was applied to the free end, which was gradually increased until the working load condition was achieved. The force applied in the FEA model was the same as in the experiment. It is noted that, only the normal wire condition was chosen for comparing purpose between experimental results and simulation results, and focus only on the maximum deflection occurring at point Y1.

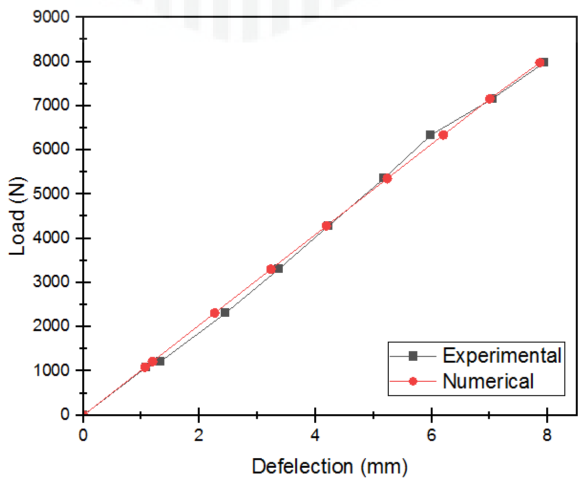

Figure 4.7: Result comparison between Experimental and Numerical analysis (FEA simulation).

Figure 4.7 shows that the deflection behaviour obtained from the experiment and FEA simulation had a linear relationship with the applied load. The FEA results were stiffer than the experimental results due to the assumption that the FEA model possessed perfect material bonding and the load was applied uniformly (Paul & Sahu, 2020). The maximum deflection under working load obtained from the experiment and FEA simulation was 7.939 and 7.866 mm, respectively. The relative error between them was less than 1%, which was acceptable and complied with the cantilever beam concept. The result of experiment and FEA simulation was almost near at each point due to accurate model presentation of materials properties and load application. Besides that, close agreement on the displacement and failure point metrics lead the results difference become smaller. In addition, the manufacturing process for the experimental sample which is PGFRPC cross-arm, ensures consistency and uniformity in the composite material and represent the theoretical model used in FEA simulation. Figure 4.8 shows the FEA results for the total deflection of the PGFRPC cross-arm in normal conditions. From the images of the deflected and non-deflected cross-arms, it could be seen that the maximum deflection occurred at the free end, while the minimum deflection occurred at the fixed point.

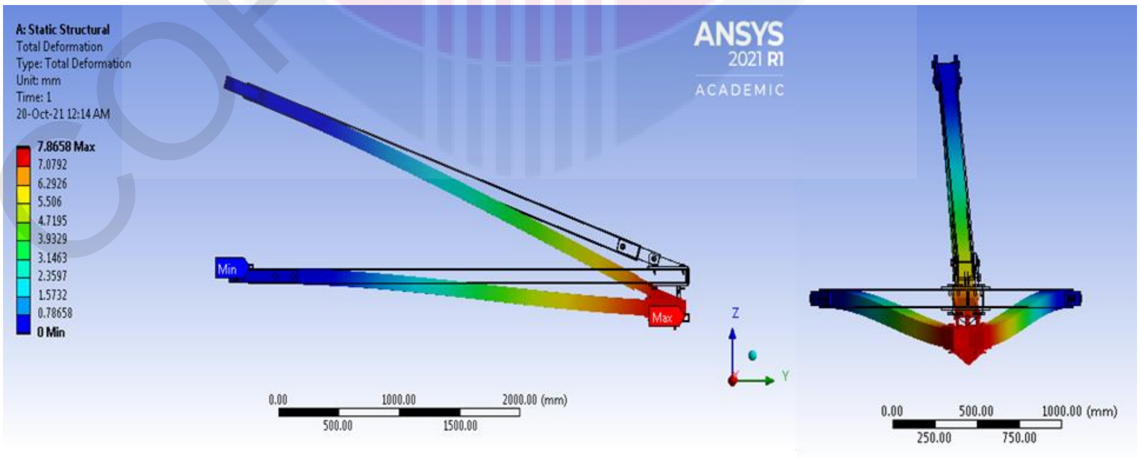

Figure 4.8: Deflection behaviour of Cross-arm's FEA model.

4.2.6 Cross-arm load deflection behaviour

The study presented the load-deflection behavior of left and right main members of PGFRPC cross-arm members under normal and broken wire conditions by using actual scale cross-arm, simulating the real-world scenario of wire condition in transmission lines. The load-deflection relationship for the existing PGFRPC cross-arm in broken wire conditions was linear, similar to normal wire conditions, despite a 52% increase in working load compared to normal wire conditions. In general, the maximum deflection observed was at the free end of the cross-arm structure while the minimum deflection always occur at the fix point of the cross-arm structure. The data also indicates that in the case of a broken wire condition, the primary structural components of the composite cross-arm exhibited the highest critical value at the outer ply as proved by Alhayek et al. (2019) in numerical simulation study as shown in Figure 4.9. This led to deflection in the cross-arm, with some lateral torsional buckling occurring due to the broken wire condition same as results obtained in this study. The research findings suggest that delamination could potentially lead to the failure of a composite cross-arm in the event of broken wires.

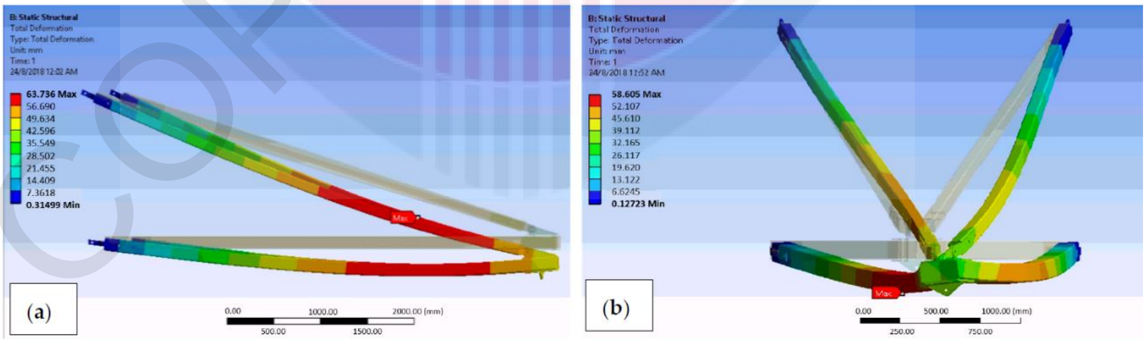

Figure 4.9: Deflection movement for (a) normal and (b) broken wire conditions.
(Source: Alhayek et al., 2019)

In general, the deflection value should be almost the same and symmetry between right and left main members. However, during load-deflection test in normal wire condition, it was found that, the left cross-arm member exhibited uniform deflection along its length, while the right cross-arm member showed uneven deflection, likely due to the tested angle of the cross-arm structures and the fitting condition. Besides that, the applied angle from the horizontal and vertical planes in broken wire conditions resulted in higher forces and twisting of the right cross-arm member as shown in Table 4.2 during maximum working load application specifically at point Y1. In addition, the arrangement of the composite layers also give minor impacts to the performance of a PGFRPC cross-arm structure when subjected to multiaxial loading coherent with previous study (Mohamad et al., 2019) as shown in Figure 4.10. Other researchers investigated the influence of composite stacking sequence on the performance of a composite cross-arm subjected to multiaxial quasi-static loading on coupon scale PGFRPC cross-arm structure and found that, the percentage of layers with separate fibre orientations had a significant impact on the structure's static-arm displacement (Mohamad et al., 2019). Nevertheless, it was observed that the failure of the cross-arm laminate was influenced by the stacking order and the proportion of layers with unique fiber orientations.

Table 4.2: Deflection value at Point Y1 during maximum working load applied for both PGFRPC and Balau wood cross-arm.

Loading Condition	Left-cross-arm member (mm)		Right-cross-arm member (mm)	
	PGFRPC	Balau	PGFRPC	Balau
Normal	7.94	11.26	7.19	11.27
Broken	21.59	27.78	25.37	27.81

Table 4.2 shows that, in normal wire condition, the PGFRPC cross-arm deflection value was about 30% less than Balau wood cross-arm, while in broken wire condition, the PGFRPC cross-arm deflection value was about 22% less than Balau wood cross-arm. In this point of view, the cross-arm with the higher Young modulus and ultimate bending loads only has one mode of failure (i.e., fibre buckling). Nonetheless, the laminate designs

and characteristics did not prevent the cross-arm from failing when subjected to multiaxial loading. It could be seen in the previous sections that the PGFRPC cross-arm had a quick response towards the applied load in the early stage as compared to the Balau wood cross-arm in normal wire conditions, and it stabilised as the applied load reached the working load. Since the PGFRPC cross-arm was made up of different stacking sequences as mention in subsection 3.3.1, the PGFRPC cross-arm was able to withstand higher stress as the application of 0° at both outermost layers would provide load distributors, which distributed the force uniformly within the polymer matrix (Cordin et al., 2018; Shibata et al., 2005). The middle alternating orientation between ±45°/0° sequences aided as an energy absorber (Bandaru et al., 2015; Q. Liu & Hughes, 2008; Riccio et al., 2014). Amaro et al. (Amaro et al., 2012) and Reis et al. (Reis et al., 2018) established that the stacking sequences with variation of thickness of ply layers significantly contributed to the enhancement of energy absorbing properties for polymer composites. This would result in the prolonging the time of the glass fibre to be fractured as the force was applied. The presence of UPE as a matrix in the composite laminate provided higher toughness and stiffness, apart from the compatibility of E-glass fibre with UPE resin (Sapuan et al., 2013; Sousa et al., 2018). However, the Balau wood cross-arm exhibited critical deflection behaviour during the application of the working load due to its lower mechanical properties and weak interaction among the fibres (refer Table 4.2). This proves that the PGFRPC cross-arm has overcome its predecessor cross-arm due to its good material strength and fabrication process. The PGFRPC cross-arm results obtained experimentally in this study were compared with the finite element analysis (FEA) and discussed in the next section.

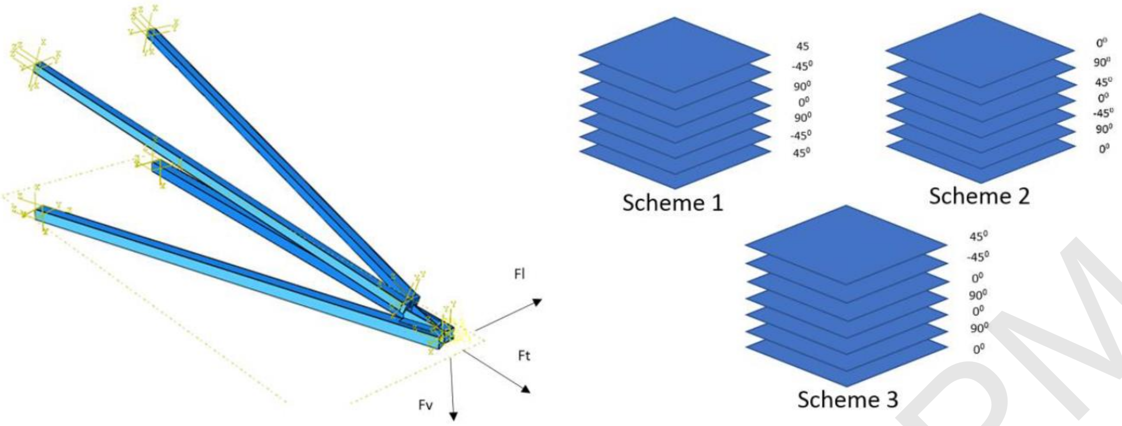

Figure 4.10: Schematic sequence of fabric layers of composite cross arms.
(Source: Mohamad et al., 2019)

4.3 Honeycomb sandwich composite characterisation and fabrication

This section investigates the flexural behaviour of honeycomb sandwich composite structures, which are relevant to aerospace and structural industries. It examines the impact of woven glass fibre prepreg orientation on the sandwich panel's properties using the 3-PB test. The results indicated several failure modes occurring among orientations, but 0° orientation demonstrated higher load capacity due to increased flexibility. The 0° orientation also exhibited the maximum stress and flexural modulus, aligning with the highest load. The experimental and analytical deflection results correlated well. The study concludes that the 0° orientation is suitable for improved bending applications, suggesting enhancement potential for glass fibre-reinforced polymer composite components, like transmission tower cross-arms.

4.3.1 Failure modes of honeycomb sandwich composite structure

During testing, various failure and damage modes were observed in the honeycomb sandwich composite structure, affecting both the facesheet and the core. These included indentation, core shear, core buckling, delamination, debonding, and fibre breakage or facesheet failure, as illustrated in Figure 4.11. Table 4.3 summarizes the failure modes for specimens with different facesheet orientation angles. It was found that each group of specimens exhibited multiple failure modes, with seven identical specimens tested. The loads leading to these failures were similar, with transitions between failure modes often occurring due to minor variations in geometry and honeycomb cell placement.

Table 4.3 reveals that for the 0° and 90° orientations, failures predominantly occurred in the laminated facesheet rather than the core, unlike the 45° orientation. Additionally, the average peak load was highest for the 0° orientation, followed by the 90° and 45° orientations. The 3-PB test indicated that local indentation, associated with core crushing under the indenter, was most common in the 90° orientation. This suggests that the compressive stress for woven glass fibre at the 90° orientation exceeds the compressive strength of the aluminum honeycomb core at peak load. Conversely, the bending stiffness affects the distribution of load at the point of application. The flexural test results indicated that indentation failure in the sandwich panel is largely dependent on the core (S. M. Lee & Tsotsis, 2000). Core buckling was predicted and observed as the initial damage mode, particularly for the 45° orientation. Core shear failure can occur when the facesheet is significantly stiffer than the core, owing to the anisotropic nature of the honeycomb structure. The core's shear strength also varies with the loading direction (Petras & Sutcliffe, 1999).

Table 4.3: Summary of failure modes for the three-point bending test.

Orientation Angle (°)	Peak Load (N)		* Failure Modes					
α	**AVG**	**SD**	**DLM**	**IND**	**DBD**	**CS**	**CB**	**FF**
0°	2747.79	206.64	5	3	2	2	2	5
90°	2475.80	490.38	2	5	2	1	3	5
45°	1352.50	1023.07	1	3	5	4	6	3

Note: AVG = average, SD = standard deviation, DLM = delamination, IND = indentation, DBD = debonding, CS = core shear and CB = core buckling, FF = facesheet failure. * Numbers of specimens out of seven identical specimens with identical failure mode for each orientation angle group.

Given that the core has sufficient stiffness, the overall deflection of the sandwich structure tends to be significant, leading to high in-plane tensile forces that can cause tensile cracking (Wen et al., 1998; Zhou et al., 2006). The 0° orientation exhibited the highest tensile strength and elongation at break compared to the 45° and 90° orientations, due to the presence of long, continuous glass fibres. In contrast, the other orientations had shorter, broken, and discontinuous fibres due to the specimen cutting direction (Tungjitpornkull & Sombatsompop, 2009). When examining the effect of fibre orientation on the composite structure, the angle between the fibre axis and the loading direction must be taken into account. Furthermore, delamination, a common damage mode in laminated composites, increased with higher peak loads. Delamination occurs when the interlaminar shear strength is exceeded and is influenced by the peak load. Debonding between the facesheets and core, due to weak bonding, also significantly reduces stiffness and strength, as shown by Zhou et al., 2007 and Zhu & Chai, 2011. Notably, in the 45° orientation, debonding caused most specimens to fail in the core rather than the facesheet.

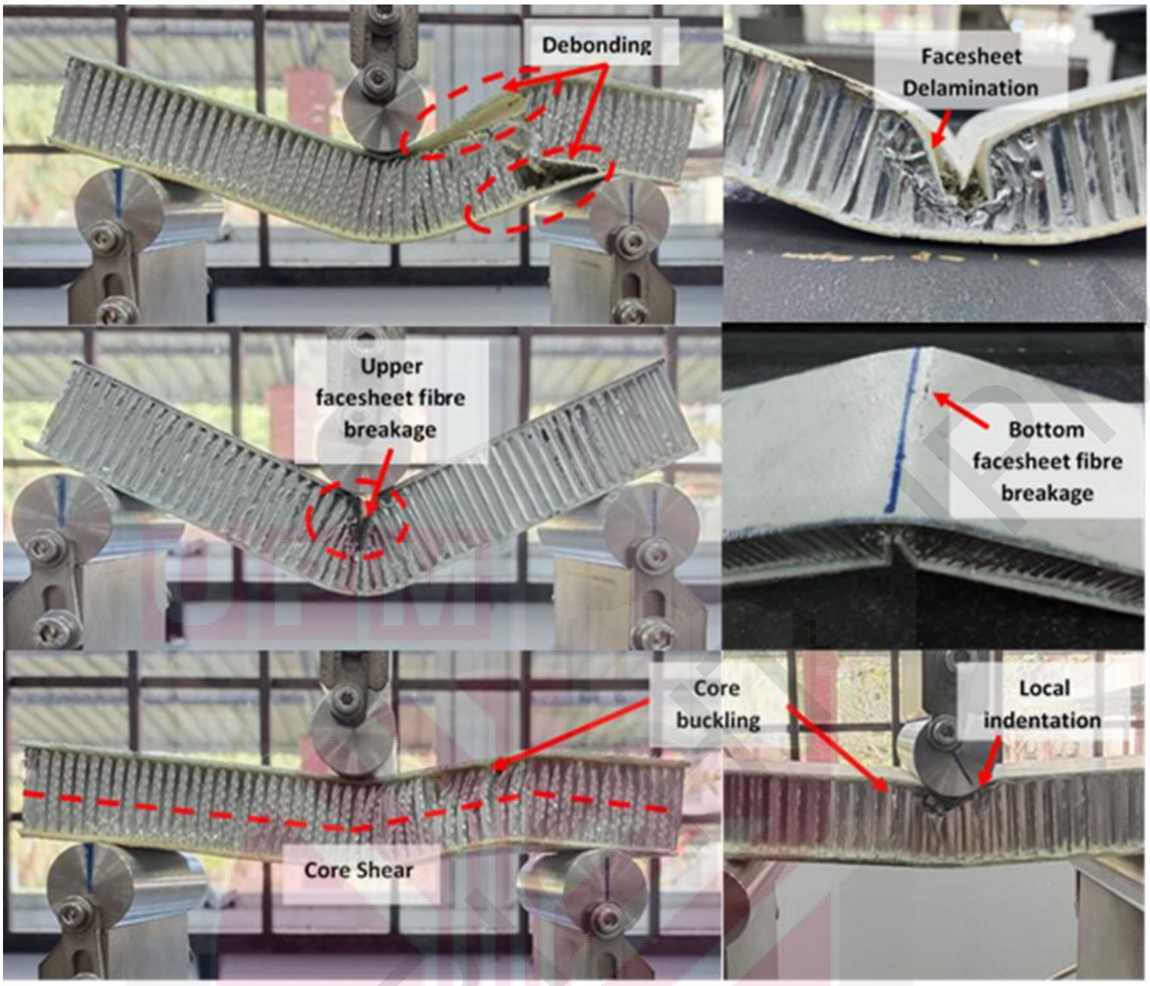

Figure 4.11: Failure modes observed in an aluminum honeycomb sandwich panel after conducting a quasi-static three-point bending flexural test.

From a microscopic point of view, the reinforcing fibres prevent crack propagation by chemically bonding to the polymer matrix with covalent bonds (Rudo & Karbhari, 1999). The E-glass fiber composite utilized in this study is a continuous/aligned fiber-reinforced type, which can exhibit various degrees of anisotropy depending on the number of fiber orientations and directions (P.K. Mallick, 2007). E-glass, composed of aluminoborosilicate with less than 1 wt.% alkali oxides, was chosen for its superior electrical properties, relevant for enhancing cross-arms in high transmission towers. Recent research has also highlighted the use of YPH-42T prepreg epoxy resin in woven prepreg fibers due to its distinctive features. As noted by Jiang et al. (2022, 2023), Sun et al. (2018), and J. Zhang et al. (2020), this solvent-free epoxy resin is specifically designed for high-strength applications such as carbon fiber, fiberglass, and aramid fiberglass, providing excellent resistance to thermal deformation and impact, making it ideal for producing items like fishing rods and tennis rackets with minimal resin content.

4.3.2 Properties of honeycomb sandwich composite structure during load application

This section examines the mid-span deflection curves under load, revealing how different woven glass fiber orientations affect mechanical responses and structural failure during 3-PB tests. The deflection at mid-span was averaged from measurements taken at two locations: the mid-span and the bottom skin of each specimen. Figure 4.12 illustrates three representative mid-span load-deflection curves for glass fiber orientations of α = 0°, 45°, and 90°. These curves were selected because they closely represent the average energy absorption values for each group, demonstrating typical performance for each sandwich panel type. The load-deflection relationship across all specimens exhibited non-linearity, attributed to the thermoplastic component.

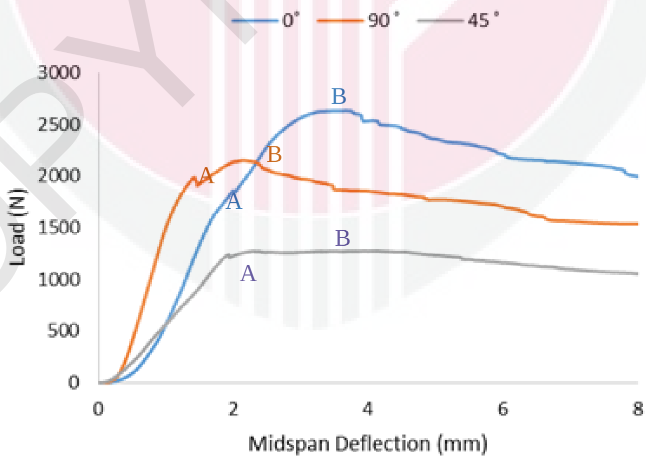

Figure 4.12: Load–deflection characteristics for different woven-fiber orientations in the honeycomb sandwich structure, where point A indicates the end of linear elastic behavior, and point B represents the maximum load leading to panel failure.

Figure 4.12 highlights two specific points on the mid-span deflection curves to illustrate deflection behavior for each facesheet orientation group. Up to point A, the aluminum honeycomb sandwich panel behaved in a linear elastic manner. For α = 45°, linear elastic deformation was approximately 1.6 times less compared to α = 0° and 90°, due to multiple fiber/matrix failures. During loading, the applied force is shared between the flexible matrix and the stiffer fiber bundles. In woven composites, fibers tend to align with the loading direction, which contrasts with the α = 0° and 90° orientations (Koohbor et al., 2015). Although linear elastic behavior for α = 90° was higher than for α = 0°, the critical load was lower for α = 90°. These findings indicate that a sandwich panel with α = 0° orientation has lower stiffness but greater flexibility compared to one with α = 90° orientation.

The rigidity of the sandwich panels generally decreases from point A to point B, where point B represents the critical load that leads to panel failure. At this stage, localized indentations and core buckling begin to occur. The sandwich panels support increasing loads until reaching point B, beyond which load support diminishes, and significant plastic deformation becomes evident. Ideally, a biaxial symmetry response is expected for orthotropic materials, suggesting similar mechanical responses for fibers oriented at 0° and 90°. However, practical differences in the amount of reinforcing fibers in these orientations result in varying mechanical and fracture properties (Koohbor et al., 2014; Shifa et al., 2017). The highest critical load recorded was 2,620 N for α = 0°, 2,151 N for α = 90°, and 1,275 N for α = 45°.

4.3.3 Experimental and analytical properties for sandwich structure

This section compares the experimental and analytical results for honeycomb sandwich beams with different woven glass fiber facesheet orientations under a 3-PB load. The experimental data on total deflection and bending stiffness are compared with analytical predictions in Table 4.4. Total deflection was computed using Equation (3.6), and bending deflection errors were calculated. The average values from seven samples for each fiber orientation were used for these calculations.

Table 4.4: Comparison of three-point bending deflection with predicted and measured values for honeycomb sandwich panels.

Orientation Angle (°) α	Experimental, δ (mm)	Analytical, δ (mm)	Error % (δ)	Experimental, P/δ (N/mm)	Analytical, P/δ (N/mm)	Error % (P/δ)
0°	3.72	3.34	12.22	826.48	919.22	1.19
90°	1.83	1.95	26.80	1517.22	1368.17	2.12
45°	2.90	2.30	58.58	486.27	738.54	5.99

When shear stiffness remains constant, the slope of the load vs. mid-span deflection curve is steeper, and shear deformation becomes a more significant part of total deformation as the glass fiber orientation changes to α = 0°. When shear stiffness is reduced, shear deformation becomes more pronounced. Table 4.4 shows that the experimental values of P/δ align well with the predicted values. The discrepancies between analytical and experimental results mainly arise from shear deflection restrictions and the consideration of total shear deformation, including both facesheet and core. The sandwich panel with α = 0° exhibits higher strength due to its high critical load, which is crucial for enhancing PGFRPC cross-arm members.

4.3.4 Flexural bending behaviour for sandwich structure

Table 4.5 summarizes the flexural performance obtained from the quasi-static 3-PB test for various facesheet orientations. The maximum load before initial failure was 2,747.78 N for α = 0°, 2,478.25 N for α = 90°, and 1,454.91 N for α = 45°. The highest load occurred for α = 0°, followed by α = 90°, with the lowest for α = 45°. Ideally, biaxial symmetry is expected for orthotropic materials, suggesting similar mechanical responses for fibers oriented at 0° and 90°. However, differences in fiber quantities result in varying mechanical and fracture properties (Mallon et al., 2015). Consequently, breaking the fiber bonding in α = 0° orientation requires a higher load compared to α = 90°. Additionally, significant shear deformation, particularly at 45°, can lead to void nucleation and coalescence at the fiber/matrix interface, causing earlier failure under lower loads (Godara & Raabe, 2007).

Table 4.5: Flexural behavior of honeycomb sandwich panels from the quasi-static 3PB test.

Orientation Angle (°) α	Max. Load (N) *P*	Max. Stress (MPa) *σ*	Flex. Moduli (MPa) *E*
0°	2747.78	10.60	1148.26
90°	2478.25	9.81	1440.20
45°	1454.91	5.56	706.16

Changes in the facesheet orientation angle affect bending strength, as shown using Equation (3.2): 27.22 MPa for α = 0°, 23.75 MPa for α = 90°, and 12.95 MPa for α = 45° (Figure 4.13(a)). During the 3-PB test, fibers with higher stiffness and lower ductility bear most of the load until their failure strain is reached, after which the matrix bears the load. Core shear ultimate strength also decreases with changing facesheet orientation: 0.70 MPa for α = 0°, 0.65 MPa for α = 90°, and 0.34 MPa for α = 45° (Figure 4.13(b)). The core shear ultimate strength for α = 0° and α = 90° is slightly higher than for α = 45°, likely due to enhanced fiber/matrix bonding and energy absorption.

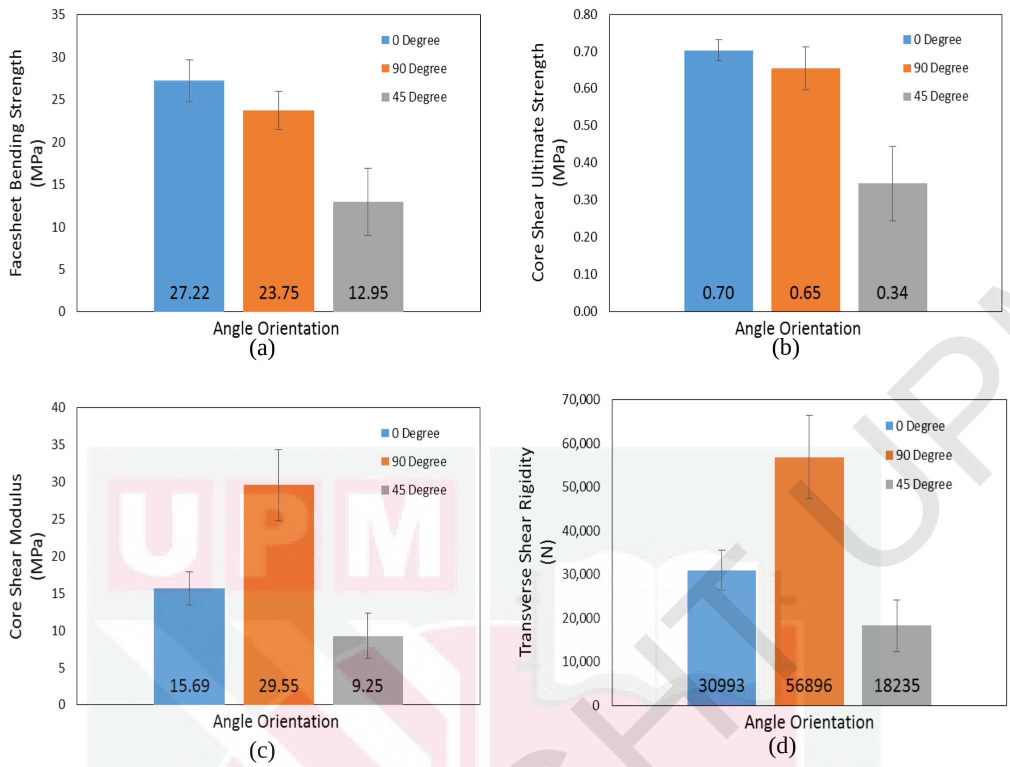

Figure 4.13: Properties of honeycomb sandwich panels for α = 0°, 90°, and 45° orientations: (a) facesheet bending strength; (b) core shear ultimate strength; (c) core shear modulus; (d) transverse shear rigidity.

The core shear modulus and transverse shear rigidity exhibit irregular variations compared to bending strength and core shear ultimate strength. Core shear modulus values are 15.69 MPa for α = 0°, 29.55 MPa for α = 90°, and 9.25 MPa for α = 45° (Figure 4.13(c)). Transverse shear rigidity values are 30,993 N for α = 0°, 56,896 N for α = 90°, and 18,235 N for α = 45° (Figure 4.13(d)). The core shear modulus and transverse shear rigidity first increase from α = 0° to α = 90°, then decrease for α = 45°. This trend may result from the combined effects of core geometry and adhesive bonding (Abedzade Atar et al., 2020). Variations in transverse shear rigidity could also be influenced by core shear modulus dependency on peak load and cross-head displacement. The transverse shear rigidity is notably higher for α = 90° compared to α = 0° and 45°.

4.4 Conceptual design development and fabrication of honeycomb sandwich PGFRPC cross-Arm

This study project introduced a honeycomb sandwich structure for enhancing the design of PGFRPC cross-arms. This innovative approach combined elements from TRIZ, morphological charts, and ANP for inspiration. The purpose of this technique was to explore potential solutions, primarily during the conceptual design stage, with the primary goal of optimizing the PGFRPC cross-arm. The specific focus was on reinforcing the central part of the beam, which is prone to structural failure over extended periods of service. Further details will be elaborated upon in the following subsections.

4.4.1 Implementing and redefining selected solution of TRIZ contradiction matrix

In the context of the TRIZ contradiction matrix principle, a pair of broad engineering attributes (parameters for enhancement and degradation) was established and interconnected during the analysis of outcomes to achieve design objectives. The distinct set of 39 engineering parameters, utilising the TRIZ contradiction matrix approach, assisted in recognising conflicts between the factors that enhance and those that hinder during the initial phases of design evolution. Ultimately, the TRIZ 40 inventive principles technique was employed to identify a suitable solution principle for addressing the complexity.

Based on the contradiction, in relation to the honeycomb sandwich cross-arm structure, the improving parameters are #16 durability of non-moving object and #14 strength (G. Navas, 2013). As the transmission conductor wire has a specific weight, the cross-arm needs to be able to support that weight at a certain height above ground. Besides, a honeycomb core structure has high bending strength and stiffness, which allow it to be one of the expected enhancements related to high durability and longer service for cross-arm structure (Sezgin et al., 2010). Meanwhile, the worsening parameter is #32 ease of manufacture. The manufacturing, fabrication, and assembly of a honeycomb can be complicated as several methods are used. Table 4.6 displays the contradiction matrix produced based on the design goal for this study. There are five recommended solutions that can be used to encounter the contradiction that occurred. However, solution principle #35 was chosen to further produce a specific solution idea as it is the most applicable solution in this study.

Table 4.6: The contradiction of TRIZ principle for cross-arm design.

Improving Feature	Worsening Feature	TRIZ inventive principle
#14 Strength #16 Durability of non-moving object	#32 Ease of manufacture	#3 Local quality #10 Preliminary action #11 Beforehand cushioning #32 Colour changes #35 Parameter changes

Due to the transformation of a hollow cross-arm into a honeycomb sandwich cross-arm, the convenient solution principle #35 was selected based on the results of the TRIZ contradiction matrix. Besides that, this principle also fitting with this study due to changing the degree of flexibility and durability of the existing cross-arm related to the flexural behaviour. The inventive principle was selected to improve dependability and prevent the loss of strength in the cross-arm, as well as to increase the durability of a stationary object while facilitating its fabrication. Based on the TRIZ solution principle, Table 4.7 summarises the design strategies used to produce the honeycomb sandwich PGFRPC cross-arm.

Table 4.7: Design strategy based on identified TRIZ solution principles.

TRIZ solution principle	Solution Description	Design strategy description
#35 Parameter change	- Change the concentration or consistency - Make each part of an object function in conditions most suitable for its operation	- Apply a glass fibre composite as a face-sheet of the honeycomb sandwich panel for the cross-arm member to improve its mechanical and physical performances - Vary the location and the arrangement of the enhance component according to the stress concentration value. - Minimize structure modification to avoid delamination and high costing on the composite cross arm. - Using epoxy as an adhesive in order to ensure the panel is strongly bonded to the cross arm surface.

4.4.2 Developing honeycomb sandwich composite cross-arm concept generation from Morphological Chart

As an example, according to the parameter change (#35) solution principle, there is a description on how the existing parameter of the cross-arm will change, either the whole cross-arm member or a part of the cross-arm member. The general solution suggested has a very broad scope and requires further clarification before it can be implemented in the design. Thus, the combination of TRIZ and morphological chart enables designers to rapidly convert a general solution into a systematic and organised procedure. Figure 4.14 depicts the morphological chart for TRIZ and the design features of the honeycomb sandwich PGFRPC cross-arm. Two main concept designs were chosen (i.e., sandwich inner side (SIS) and sandwich outer side (SOS)), as shown in Figure 4.15.

TRIZ Solution Principle	Design Features	Solutions		
		1	2	3
#35 Parameter change Apply a glass fibre composite as a face-sheet of the honeycomb sandwich panel for the honeycomb sandwich composite for cross-arm member to improve its mechanical and physical performances	Type of honeycomb sandwich face-sheet	Synthetic	Natural	
	Material	D-Glass Fibre	E-Glass Fibre	R-Glass Fibre
	Type of Material	Woven Prepreg Fibre	Woven Fibre + Raisin	Staple Fibre + Raisin
Place honeycomb sandwich composite panel at the middle of the cross arm member to minimize the use of honeycomb and the cost of manufacture	Core shape	Square core	Hexagonal core	Flex core
	Material	Aluminum	Nomex	Composite
	Position in cross-arm member	Whole cross-arm	Front and end	Middle
Fix the honeycomb sandwich composite panel on the cross arm member by using epoxy as an adhesive in order to ensure the panel is strongly bonded to the surface	Type of adhesive	Polyurethane	Epoxy	Acrylic

Figure 4.14: Morphological chart of TRIZ solution principle and honeycomb design features.

Based on Figure 4.14, the overall proposed design concepts are summarised as follows:

1. Synthetic fibre was used due to its higher strength, lightweight, and better mechanical properties, especially when exposed to direct sunlight and ageing compared to natural fibre. Besides, synthetic fibre also has high resistance to biological decay and is not easily attacked by living organisms, such as fungi, which can lead to rot and mildew (T. Q. Liu et al., 2020; Omrani et al., 2016).

2. Glass fibre is a synthetic fibre that is commonly used in composite material structures because it is the most affordable option, ensuring high availability and allowing the sandwich structure to gain strength and energy absorbing characteristics. Although both D- and R-glass fibres have good mechanical properties, E-glass fibre was chosen in this conceptual design due to the capability and high strength when incorporated with fibre-reinforced polymer (material for the cross-arm member). Besides, E-glass fibre, made of aluminoborosilicate with less than 1 wt.% alkali oxides, was used in this concept design compared to other types of glass fibres due to their great properties for electrical applications, as the final result of this study will be used to enhance the cross-arm in high transmission towers (Davalos et al., 2001; P.K. Mallick, 2007; M. Zhang & Matinlinna, 2012). Aside from that, glass fibre is commonly used as the facesheet of sandwich composite structures because it offers a cost-performance advantage and is more resistant to environmental attack (Birman & Kardomateas, 2018; Cantwell et al., 1999; *Composite Materials Handbook, Volume 6. Structural Sandwich Composites*, 2013).

3. The woven prepreg glass fibre was chosen due to ease of manufacture and its good strength compared to others. Various composite qualities can be achieved by weaving the fibres in various patterns due to its distinctive architectural characteristics, simplicity of handling, low manufacturing cost, and exceptional mechanical qualities (Shindo et al., 2009). Several factors influence the compressive and tensile behaviour of woven glass fibre-reinforced polymer composite materials, such as the type of material, weaving pattern, fabric geometry, fibre volume fraction, laminate configuration (Asi, 2009), void content, and woven linear density.

4. The core shape chosen is hexagonal core. Hexagonal honeycomb structures offer an outstanding mechanical performance due to the efficient hexagonal configuration, where the walls support each other; moreover, the compression strength of honeycomb cores is typically higher.

5. An aluminium honeycomb core was chosen due to its strength, light weight, good lifetime loading capability, availability, and affordable costing compared to Nomex and composite core.

6. The composite cross-arm experiences buckling at the middle of the beam. To increase the structural strength and minimise the cost, a honeycomb core is incorporated into the cross-arm structure only at the middle part.

7. Epoxy is commonly known to joint surfaces together. Epoxy has great bond strength and is able to adhere to a variety of substrates. It is also highly resistant to chemicals, which help to minimise corrosion and any chemical reaction when exposed to acid or basic substances.

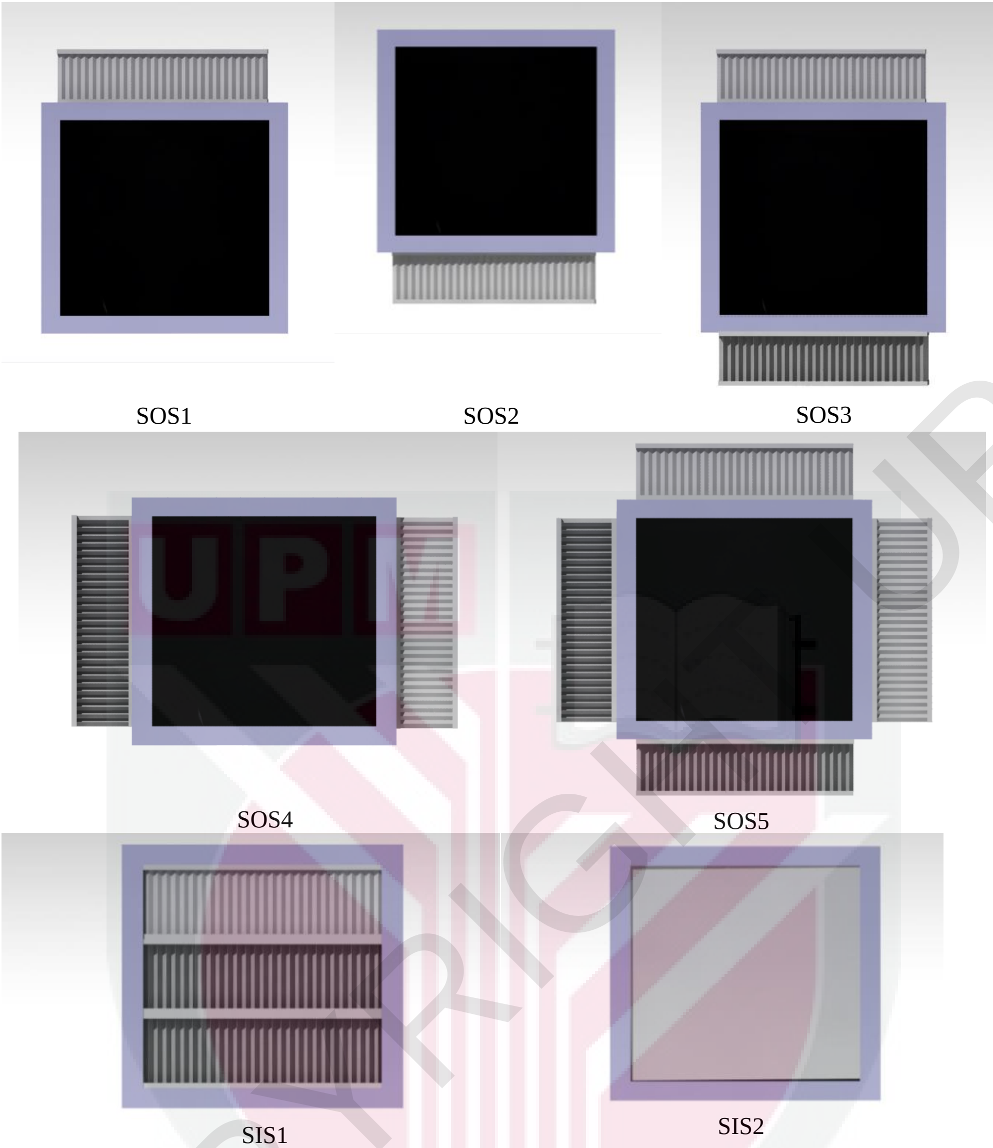

Figure 4.15: Honeycomb sandwich composite cross-arm design concepts.

The primary distinction between all proposed concept designs is the location of the honeycomb sandwich panel on the composite cross-arm, as depicted in Figure 4.15, either the honeycomb sandwich is on the outer side (SOS) or the inner side (SIS) of the cross-arm member. There are five different locations for the honeycomb sandwich panel design at the outer side of the cross-arm, which are at the top (SOS1), bottom (SOS2), top and bottom (SOS3), side (SOS4), and each side (SOS5). Meanwhile, there are two designs for the honeycomb sandwich panel at the inner side of the cross-arm, which are the honeycomb sandwich panel in vertical direction (SIS1) and horizontal direction (SIS2) to the cross-arm. The concept of tandem honeycomb sandwich panel was used in the SIS design concept in order to fill the cross-arm hollow. Based on the design concept suggested by the morphological chart solution, the honeycomb sandwich panel was installed at the middle of the cross-arm, as shown in Figure 4.16.

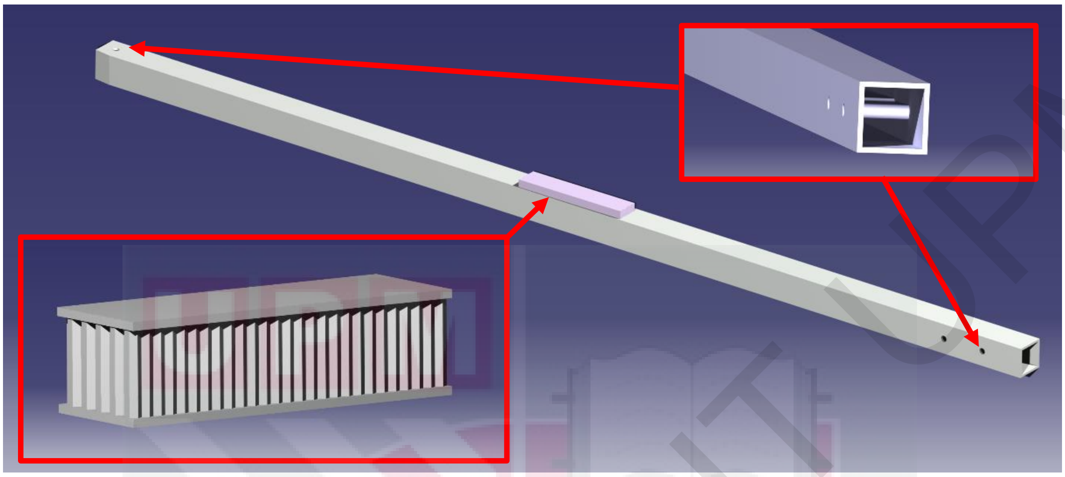

Figure 4.16: Position of honeycomb sandwich panel design and fitting hole on PGFRPC cross-arm member.

4.4.3 Analytic Network Process in conceptual design selection

Using the numerical values for each concept design, the pairwise comparison technique was implemented in accordance with the analytic network process (ANP) concurrent engineering approach. The primary and secondary criteria were compared to the concept design alternatives based on the relative importance of the criteria. The primary objective of the design selection process is the performance of the honeycomb sandwich PGFRPC cross-arm because the enhanced cross-arm must accommodate a greater load capacity during services. By enhancing the strength of the cross-arm member, the service life could be extended, and the failure occurrence could be reduced. In addition, the weight criterion and cost attribute are deemed to be of equal importance under the condition that the weight criterion influences the design's cost. Table 4.8 summarises the honeycomb sandwich composite cross-arm concept design description by considering the performance, weight, and cost.

In accordance with the primary objective established earlier for the development of design concepts, design concept SOS2 received the highest score in all seven simulated conditions. Table 4.9 shows the overall synthesised alternatives that depict the design's ranking. The von Mises stress at the structure's critical point is lowest for Design Concept 2, which is also the most efficient design. When subjected to a 3-PB simulation test, the honeycomb sandwich panel position showed the lowest value of deformation, suggesting that it is the best design to withstand the given force. Besides that, the deformation value obtained also become the optimum parameters required for the best honeycomb sandwich PGFRPC cross-arm with the maximum deformation obtained was less than the existing cross-arm (without any enhancement) which is 4.60 mm. The ANP selection approach effectively rates due to the performance for all the proposed idea designs shown in Figure 4.17(a). In addition, the SOS2 concept design's improved cross-arm evolved with less material, making the whole structure lighter.

Table 4.8: Summary of honeycomb sandwich PGFRPC cross-arm concept design description.

Design selection attributes		**Concept designs**						
		SOS1	SOS2	SOS3	SOS4	SOS5	SIS1	SIS2
					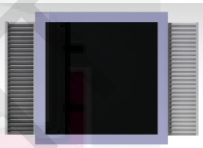			
Performance	Max. stress (Von-Mises stress),(N/m^2)	40.125	40.114	42.075	42.081	40.210	41.032	41.041
	Max deformation (mm)	5.1812	4.5807	5.0811	5.0324	5.0915	4.9812	5.1002
Weight	Mass (kg)	98.95	98.93	110.01	110.05	110.35	110.15	110.30
	Volume (m^3)	0.0124	0.0124	0.0131	0.0131	0.0147	0.0139	0.0134
Cost	Raw material cost (RM)	732	732	782	782	882	832	810
	Shape complexity	Low	Low	Medium	Medium	High	Very High	Very High

Note: For comparison purposes, assumed sandwich honeycomb panel density 235.29 kg/m^3, PGFRPC density 3932 kg/m^3 as given by supplier. Raw material cost used in this study was given by the selected supplier as discusses in section 3.2, for cross-arm RM 672 per member, sandwich honeycomb panel RM 60 per panel (the size of panel 300 mm x 85 mm x 30 mm). The price might be differ for other supplier.

The simplest structural design is possible with the SOS2 concept, which may reduce manufacturing time and consequently decrease production costs. Generally, affixing the honeycomb sandwich panel on the cross-arm surface by using epoxy raisin is not difficult (referring to concept designs SOS 1, 2, 3, 4, and 5). However, the rating used in Table 4.8 for shape complexity is due to the number of honeycomb sandwich used, as increasing the honeycomb sandwich panels will increase the complexity of the shape of cross-arm design. Nonetheless, the design of the filled cross-arm with the honeycomb sandwich will become more complicated due to the fabrication of tandem honeycomb sandwich and cutting it in the form of vertical and horizontal positions (referring to concept designs SIS 6 and 7). In addition, the honeycomb sandwich panel cannot be filled directly due to the border on the fitting hole; otherwise, the cross-arm is cut on the required part, as shown in Figure 4.16. This activity requires more precaution so that the properties of the cross-arm will not be affected. Hence, concept designs SIS 6 and 7 become very high due to shape complexity, in addition to high manufacturing and production costs. From Figure 4.17(b) and (c), the concept design SOS2 was selected because it has a high sensitivity rating of the lowest weight among other designs that use fewer raw materials with less cost to produce.

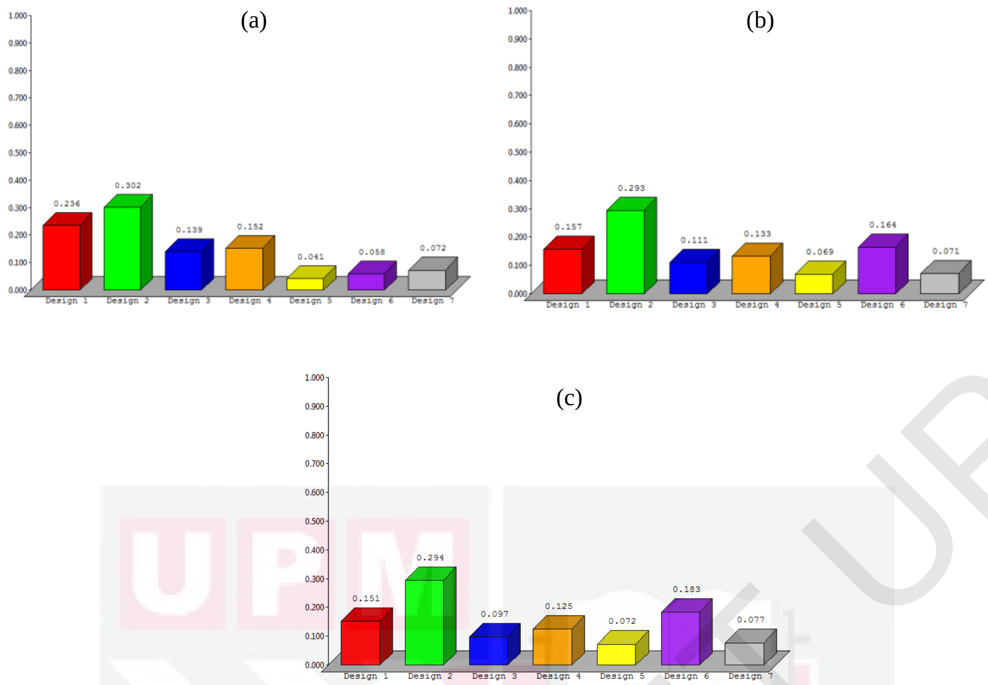

Figure 4.17: Sensitivity graph of main criteria in respect to (a) performance, (b) weight and (c) cost criteria.

Table 4.9: Overall synthesized for the design alternatives.

Conceptual Design	Normal	Ideal	Graphic bar	Rangking
SOS 1	0.5545	0.1647		2
SOS 2	1.0000	0.2970		1
SOS 3	0.3793	0.1127		5
SOS 4	0.4532	0.1346		4
SOS 5	0.2172	0.0645		7
SIS 6	0.5174	0.1537		3
SIS 7	0.2451	0.0728		6

In this case, the material properties of the PGFRPC cross-arm used during computational simulation were 29.8 GPa for the modulus of elasticity and 2,580 kg/m^3 for the density. Furthermore, the density and modulus of elasticity of the honeycomb sandwich panel used were 1.25 kg/m^3 and 110 MPa, respectively (Y. Fu & Sadeghian, 2020; Shi et al., 2014). Figure 4.18 shows the enhanced honeycomb sandwich cross-arm in the 3-PB simulation test with full capacity for the final design verification using ANSYS Workbench. By applying the honeycomb sandwich panel at the bottom surface of the critical part of the cross-arm surface as Concept Design 2, the mechanical properties and performance of the PGFRPC cross-arm also increased.

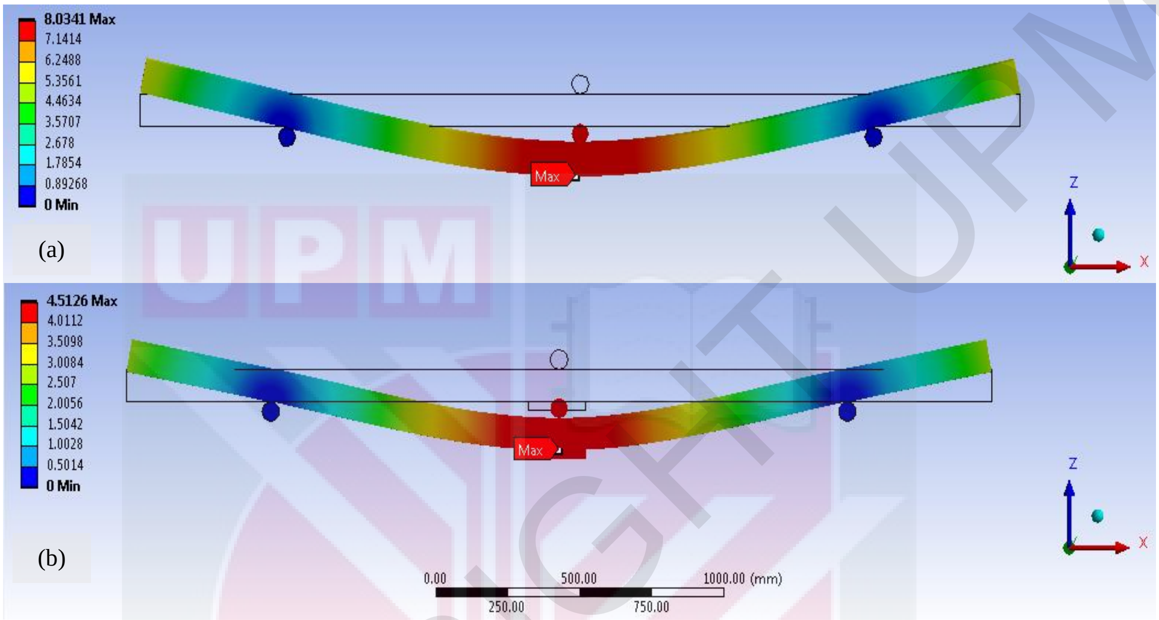

Figure 4.18: Three-point bending deformation across the PGFRPC cross-arm in maximum load capacity (a) Cross-arm without any enhancement (b) Cross-arm with honeycomb sandwich panel at bottom surface.

4.4.4 Fabrication of selected conceptual design for honeycomb sandwich composite cross-arm

According to Figure 4.19, Concept Design SOS 2, which was selected using the ANP technique, was fabricated. The best quality of woven glass fibre prepreg honeycomb sandwich composite structure as discussed in Section 4.3 was used in this fabrication process. The honeycomb sandwich composite panel was attached to the center of the PGFRPC cross-arm member using epoxy adhesive to ensure a robust bond. This epoxy resin, mixed with a fast-setting hardener at a 40:1 weight ratio, was chosen for its strength and superior stress resistance (Betts et al., 2017; Wroblewski et al., 2016). Prior to epoxy application, the cross-arm surface was prepared by sanding and wiping with a smooth cloth to remove any dust and rust. The epoxy was applied using the hand lay-up method, and the honeycomb panel was positioned on the PGFRPC cross-arm and weighted down for about 72 hours (3 days) to allow the epoxy to cure fully (Y. Fu & Sadeghian, 2020). After curing, the honeycomb sandwich composite cross-arm was completed and subjected to characterization tests for its performance and properties. Subsequently, tests for flexural deflection and long-term durability were conducted and analyzed.

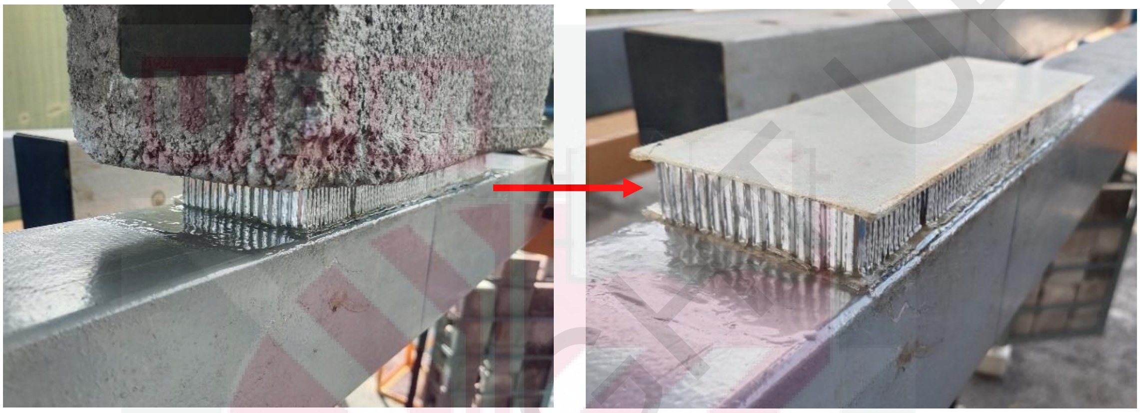

Figure 4.19: Final fabrication of selected conceptual design of influence honeycomb sandwich PGFRPC cross-arm.

4.5 Elastic properties of full-scale PGFRPC cross-arm

4.5.1 Elastic full-scale cross-arm in load deflection properties

To determine the load necessary for the beam to exhibit deflection comparable to the operational load on the assembled cross-arm, the stiffness was computed using Equation (3.14). The cross-arm's dimensions and geometric details are provided in Table 4.10.

Table 4.10: Dimensions and geometric details of PGFRPC cross-arm.

Height, H (mm)	Width, B (mm)	Wall-thickness, t (mm)	Length, L (mm)	Length @Y3, L (mm)	Moment of inertia, I (mm^4)	Working Load, P (kN)
102	102	8.50	3651	1830	4.6702 x 10^6	7.980

The stiffness of the assembled cross-arm under a working load was found to be 1,470.56 kN/m. Using this stiffness value and the working load for the normal wire condition, the maximum deflection for an individual cross-arm member under the same load was 5.426 mm. For the study, loads were applied to different span lengths of an individual cross-arm member during the 3-PB test until the mid-span deflection reached approximately 6 mm. Figure 4.20 depicts the load versus mid-span deflection curves for various span lengths of the full-scale cross-arm. All specimens displayed linear elastic behavior across the five span lengths tested. The apparent elastic modulus (E_a) varied from 2.15 GPa for shorter spans to 17.7 GPa for longer spans, with a correlation coefficient above 0.992 in all tests, indicating reliable data.

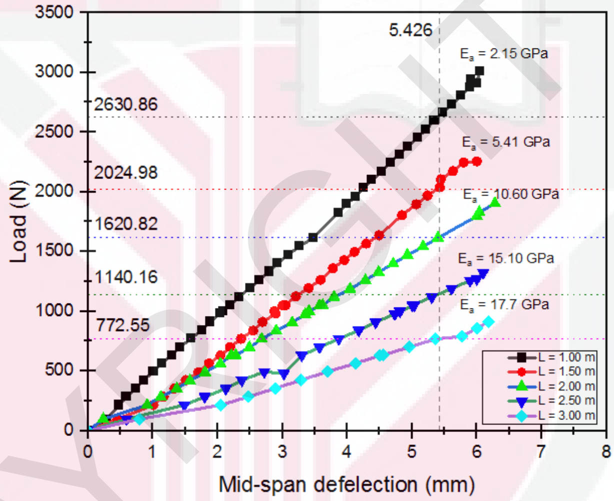

Figure 4.20: Load vs mid-span deflection curves for PGFRPC cross-arm at different span lengths.

The graph indicates that the required load decreases with increasing span length: 2,630.86 N for 1.00 m, 2,024.98 N for 1.50 m, 1,620.82 N for 2.00 m, 1,140.16 N for 2.50 m, and 772.55 N for 3.00 m. This suggests an inverse relationship between load requirement and span length. With the cross-arm end condition assumed fixed, the slenderness ratio was 95.25, exceeding 60 (refer to Figure 3.20). Consequently, shear deflection effects were minimal, as noted by Bank. For consistent values of apparent and effective cross-arm section flexural modulus, tests required loading a simply supported beam at mid-span and measuring deflection. Average deflection values for three different spans (2.00, 2.50, and 3.00 m) were used to plot graphs for Method 1 and Method 2, as shown in Figure 4.21.

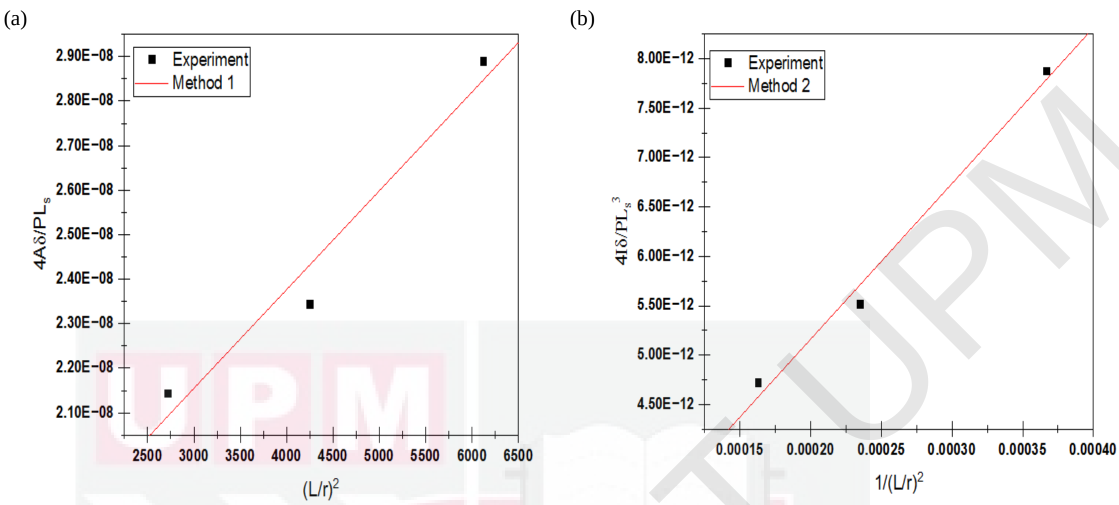

Figure 4.21: Predicted flexural modulus for PGFRPC cross-arm member: (a) Method 1, (b) Method 2.

The effective cross-arm member section flexural modulus (E_c & G_c) was derived from the line equations of Methods 1 and 2. For Method 1, the slope of the line equals $\frac{1}{12E_c}$ and the intercept is $\frac{1}{G_c}$; for Method 2, the slope is $\frac{1}{G_c}$ and the intercept is $\frac{1}{12E_c}$. Experimental data were collected by measuring deflection (δ) under a constant load (P) across different span lengths (L). The apparent elastic modulus (E_a) was averaged from three span lengths. The results for apparent and effective flexural moduli, including the coefficient of determination (R^2) are presented in Table 4.11.

Table 4.11: Elastic and shear modulus of individual PGFRPC cross-arm.

	Slope	Intercept	E_a(GPa)	E_c(GPa)	G_c (GPa)	R^2
Method 1	2.2191 x 10^{-12}	1.4892 x 10^{-8}	-	37.55	0.00672	0.95935
Method 2	1.5754 x 10^{-8}	2.0106 x 10^{-12}	-	41.45	0.00635	0.98787
Apparent	-	-	10.20	-	-	0.99341

The data in Table 4.11 reveal that the flexural stiffness values obtained via Methods 1 and 2 are higher than those derived from numerical values. The table also shows that flexural stiffness is directly proportional to panel slenderness, while shear stiffness is inversely proportional. The G-modulus is relatively low compared to the E-modulus, consistent with Bank's ratio graph (Bank, 1989b, 2007) of E_a/E_c versus the slenderness ratio E_c/G_c, fitting the PGFRPC cross-arm structure. The R^2 value for Method 2 is closer to 1 compared to Method 1, though both methods align well with the regression model. This suggests that the variation in the full-scale range of anisotropic structure is generally low. Additional span lengths and different geometric samples should be considered, as supported by prior studies (Sá et al., 2016). This study proposes a new method for determining the flexural modulus of full-scale PGFRPC cross-arms, focusing on the creep deflection behavior of spans of 2.00, 2.50, and 3.00 m.

4.5.2 Flexural creep test for full-scale cross-arm

To achieve one of the study's objectives, flexural creep tests were conducted on the full-scale cross-arm member, focusing on the flexural properties of a full-scale PGFRPC cross-arm using the 3-PB test. Three beams, each with different span lengths (2.00, 2.50, and 3.00 m), were stacked to collect average data. These span lengths were selected to simulate real-world conditions, allowing significant deformation under the applied load. A static load of 1,324 N was applied at the beam's center, which is 1.7 times the load required to deflect a single cross-arm member similarly to the assembled cross-arm under working conditions. The test was conducted over approximately 1,000 hours in an open area with a surrounding temperature of 29.3 °C and relative humidity of 75.79%, as illustrated in Figure 4.22.

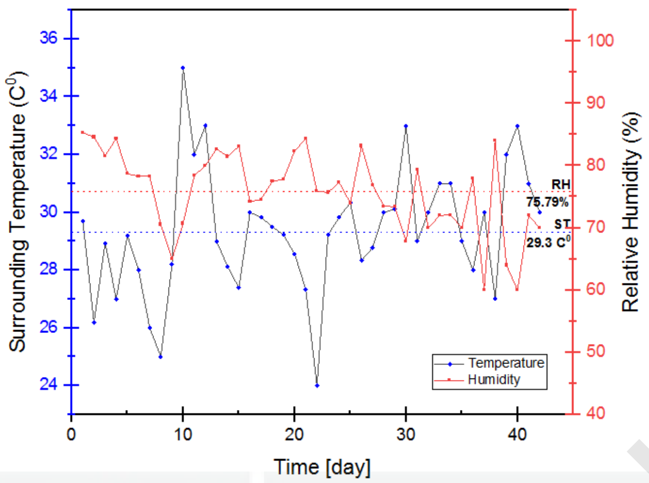

Figure 4.22: Records of the surrounding temperature and relative humidity during the creep test period.

Figure 4.23 presents the mid-span deflection results for the average of three samples with varying span lengths over time. The graph indicates a direct proportionality between initial creep deflection and span length at the same load, with initial deflections of 4.567 mm, 6.147 mm, and 9.047 mm for 2.00 m, 2.50 m, and 3.00 m spans, respectively. The viscoelastic behavior of the cross-arm member remained consistent. The creep deflection rate showed a rapid initial deformation that slowed over time (primary stage) and then maintained a relatively steady rate (secondary stage). The deformation rate difference between the 2.50 m and 3.00 m spans was smaller than that between the 2.50 m and 2.00 m spans, possibly due to the geometric configuration and reduced properties of the PGFRPC cross-arm, especially near the fixing hole at the 3.00 m span length.

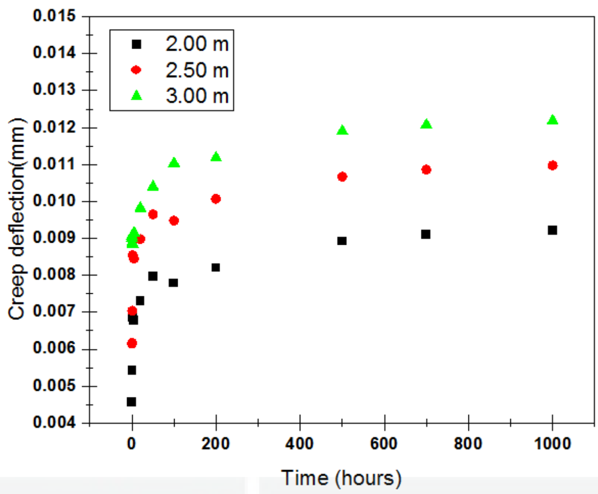

Figure 4.23: Creep deflection curves at mid-span section of the cross-arm.

The strain-time graph for different span lengths is shown in Figure 4.24. It demonstrates an inverse relationship between span length and creep strain: as span length increased, creep strain decreased, consistent with previous studies (Sá et al., 2016). The creep strain observed in this study was comparable to previous research (Hunt et al., 2015). with variations possibly due to environmental conditions and the scale of the tested specimens. The data in Figure 4.24 highlight two phases over the 1,000-hour creep test: an initial elastic phase and a subsequent viscoelastic phase. This transition is marked by an arrow in Figure 4.24, in line with findings by Sanyang et al. (2016), where materials with anisotropic properties, such as polymeric composites, show initial elasticity followed by viscoelastic behavior before reaching plastic deformation.

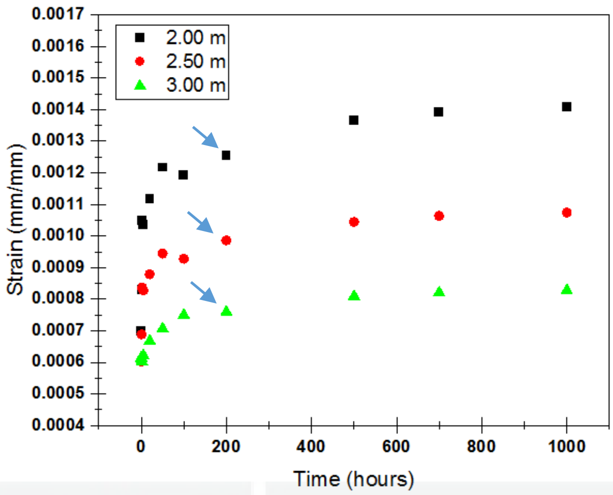

Figure 4.24: Creep-strain comparison for different span lengths.

4.5.3 Time-dependent full-scale apparent modulus of cross-arm properties

This section details the prediction of the time-dependent properties of the full-scale PGFRPC cross-arm member. Initially, the creep behavior of the cross-arm was modeled assuming a linear regime. Subsequently, methods to predict the viscoelastic apparent and effective moduli of the panels were presented. The full-section apparent flexural modulus over time, $E_a(t)$, was predicted using the derived equation from Findley's general equation (Equation (3.34)). Figure 4.25 displays the curve fitting for each span length to determine the parameters mmm and nnn for Findley's power law model. The parameters obtained from the experimental data fitting are summarized in Table 4.12.

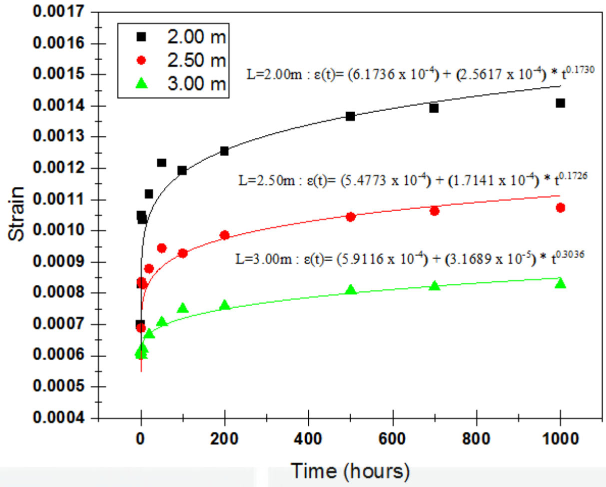

Figure 4.25: Evaluation of Findley's power law parameters for different span lengths.

Table 4.12: Summary of flexural creep experimental results using Findley's power law fitting.

Span length, (L_s)	Stress, σ (MPa)	ε_0, (10^{-4})	m, (10^{-4})	n	$E_0 = \sigma/\varepsilon_0$, (GPa)	$E_t = \sigma/m$ (GPa)	E_t/E_0	R^2
2.00 m	7.230	6.1736	2.5617	0.1730	11.71	28.22	2.41	0.9032
2.50 m	9.037	5.4773	1.7141	0.1726	16.50	52.72	3.20	0.9041
3.00 m	10.844	5.9116	0.3169	0.3036	18.34	342.21	18.66	0.9606
Average			0.7624	0.2164	15.52	141.05	8.09	0.9226

Figure 4.25 demonstrates the application of Findley's power law model to replicate the creep characteristics of the PGFRPC cross-arm, estimating strain over time using material-specific parameters *m* and *n* obtained through curve fitting. The equation closely matches the observed data, confirming Findley's model's effectiveness in representing the creep behavior of the PGFRPC cross-arm. The R2 values indicate a good fit to Findley's model. However, under higher stress conditions, discrepancies between experimental data and predictions suggest that the generalized Findley's equation may struggle to accurately represent strain. The average value from Table 4.12 was used to calculate the predicted full-scale apparent elastic modulus of the PGFRPC cross-arm, as shown in Equation (3.35):

$$E_a(t) = 15.3938 \times \left[\frac{1}{1+\left(\frac{t^{0.2164}}{8.09}\right)}\right]$$ Equation (3.35)

4.5.4 Time-dependent full-scale effective modulus of cross-arm properties

The deformation data used to predict the time-dependent apparent modulus of the full-scale cross-arm member was also employed to determine the corresponding effective moduli through empirical modeling over extended periods. The experimental procedure previously applied to characterize the initial full-scale effective elastic constants of the cross-arm members was modified for the linear viscoelastic regime. An average creep deflection value for three beams tested at different span lengths (2.00, 2.50, and 3.00 m) was recorded. Graphs of $\frac{4A\delta}{PL_s}$ versus $(L/r)^2$ were plotted for Method 1, and graphs of $\frac{4I\delta}{PL_s{}^3}$ versus $\frac{1}{(L/r)^2}$ were plotted for Method 2. As an example, Figure 4.26 shows the linear curve fitted at t=0.5 hours of the creep test period. In this case, the flexural and shear moduli at the instant ttt were determined from the intercept and slope of the linear equation, respectively, for Methods 1 and 2. The number of estimated flexural and shear moduli values matched the number of linear regressions fitted at each instant.

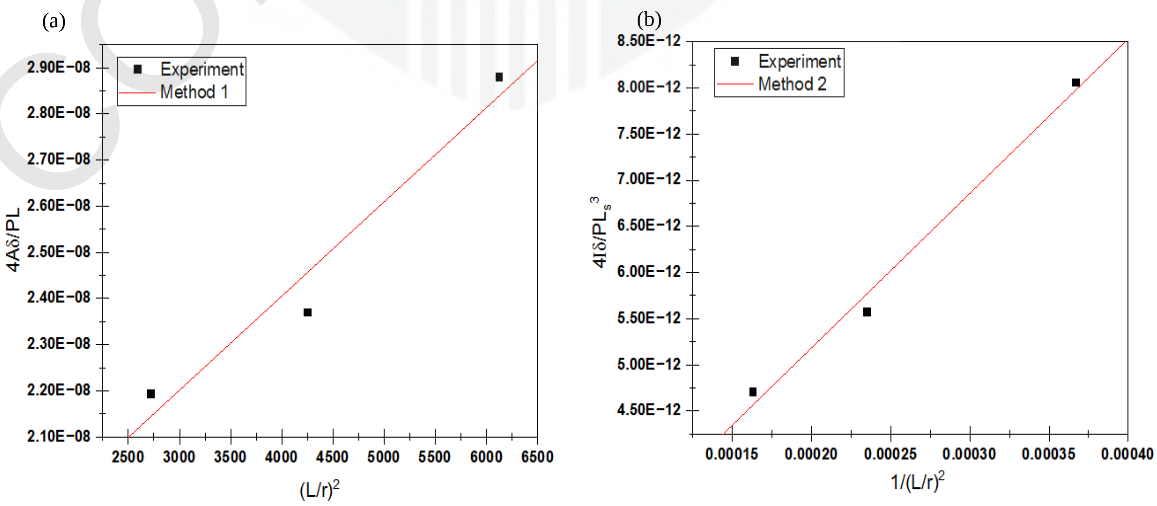

Figure 4.26: Predicted creep flexural modulus for PGFRPC cross-arm member using (a) Method 1, and (b) Method 2.

The effective cross-arm member section creep flexural modulus $E_c(t)$ and shear modulus $G_c(t)$ were measured from the linear equation for Methods 1 and 2. For Method 1, the slope of the line is $\frac{1}{12E_c}$ and the intercept is $\frac{1}{G_c}$. For Method 2, the slope is $\frac{1}{G_c}$ and the intercept is $\frac{1}{12E_c}$. The experimental data points were obtained by measuring the deflection δ for a constant load P at different span lengths L. The apparent elastic modulus E_a was calculated from the average value obtained from the three span lengths. The obtained data for apparent and effective flexural moduli along with the R^2 values are shown in Table 4.13.

Table 4.13: Results of creep elastic and shear modulus of individual PGFRPC cross-arm.

	Slope	Intercept	E_a(GPa)	E_c(GPa)	G_c (GPa)	R^2
Method 1	2.0421 x 10^{-12}	1.5885 x 10^{-8}	-	40.81	0.00629	0.9539
Method 2	1.6732 x 10^{-8}	1.8373 x 10^{-12}	-	45.36	0.00598	0.9896
Apparent	-	-	13.91	-	-	0.9226

The results in Table 4.13 show that the estimated value of the flexural stiffness obtained using Methods 1 and 2 is higher than the flexural stiffness obtained numerically. The table also shows that the estimated flexural and shear stiffness are directly and inversely proportional to the panel's slenderness, respectively. The G-modulus obtained is relatively low compared to the E-modulus, similar to Bank's ratio graph (Bank, 1989b, 2007) of E_a/E_c against the slenderness ratio E_c/G_c, which fits the PGFRPC cross-arm structure as discussed earlier. Additionally, the R^2 value for Method 2 was close to 1 compared to Method 1; however, both methods fit the regression model well. This shows that the scatter obtained when considering the full-scale range of anisotropic structures for three spans is generally lower, and more span length ranges with different geometrical samples need to be considered, as proven by previous literature (Sá et al., 2016). This new method can be used to determine the flexural modulus of the full-scale PGFRPC cross-arm for future studies.

Using the estimated flexural and shear moduli method, it is notable that the initial effective moduli obtained from the creep test, $E_{c1,0}$ = 39.77 GPa and $G_{c1,0}$ = 0.00637 GPa for Method 1 are quite close to those obtained from the 3-PB test using the same standard procedures of the tested spans, with E_{c1} = 37.55 GPa and G_{c1} = 0.00672 GPa. The same trend was also observed using Method 2, where the initial effective moduli obtained from the creep test, $E_{c2,0}$ = 44.64 GPa and $G_{c2,0}$ = 0.00601 GPa are close to those obtained from the 3-PB test, with E_{c2} = 41.5 GPa and G_{c2} = 0.00635 GPa. Considering the shear effects on the overall elastic deformation, the results indicate that the shear contribution of the PGFRPC cross-arm derived from the creep tests is only slightly higher than that derived from the static one.

4.5.5 Prediction of time-dependent full-scale flexural modulus of cross-arm

To predict future creep modulus and strength reduction over 50 years, reduction factors for the apparent and effective elastic moduli were determined. The full-scale cross-arm's estimated apparent elastic moduli were defined using Findley's power law model (Equation (3.32)), while the effective elastic moduli were measured using the method proposed by Bank, incorporating a variable time method. Due to the relatively low shear modulus obtained from the 3-PB deflection test, the shear modulus was not considered in this prediction, although shear activity may occur during the test period; therefore, only the elastic modulus was considered in this study. In the first step of this degradation model and prediction, the reduction factor of apparent and effective moduli, $\chi_a(t)$ and $\chi_c(t)$, was evaluated, with the highest stiffness reduction during the test period corresponding to the elastic modulus. This engineering technique is widely used to predict the structure's long-term performance under various loading scenarios and environmental conditions, leading to revised material selection, improved design mechanisms, and enhanced safety performance.

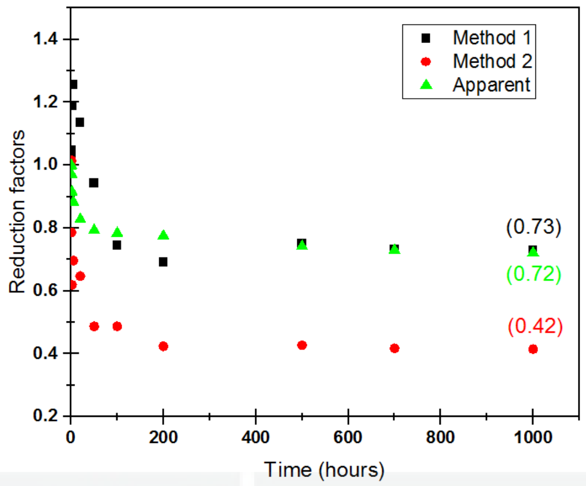

Figure 4.27: Effective reduction factors for composite cross-arm using Method 1 and Method 2.

Figure 4.27 shows that the highest stiffness reduction occurred in the early stage, around 24 hours of the initial test period. However, the creep rate reduction decreased slightly at a lower rate due to bending after the early stage period. Additionally, the curve shows that the apparent reduction factor decreased almost consistently compared to both Methods 1 and 2. At the end of the test period (1,000 hours), the effective elastic modulus of 28.98 GPa was obtained using Method 1, representing a reduction of approximately 27% from the initial effective modulus, with an effective reduction factor of 0.73. For Method 2, the effective elastic modulus at 1,000 hours was 18.53 GPa, representing a reduction of approximately 58% from the initial effective modulus, with an effective reduction factor of 0.42. In terms of bending, both Methods 1 and 2 agree with the apparent creep reduction factors. However, the creep reduction factor for Method 1 was almost close to the apparent creep reduction factor until the end of the test period. The apparent elastic modulus derived from Findley's power law model at the end of the test period was 9.92 GPa, representing a reduction of about 35% from the initial effective modulus, with an effective reduction factor of 0.64. Given the similar pattern of the reduction factor curve for both apparent and effective elastic moduli, the prediction of the time-dependent full-scale PGFRPC cross-arm for up to 50 years was performed.

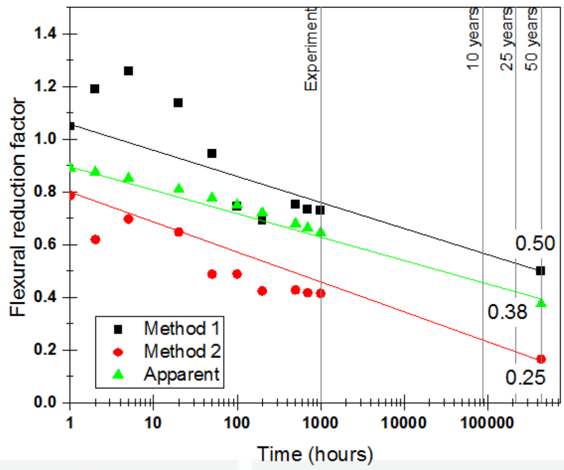

Figure 4.28: Predicted curves of the effective reduction factors over time.

To find the best fit linear functions for the reduction factor trends, the bi-linear scale diagram (as illustrated in Figure 4.27) was replotted in a bi-log format, as seen in Figure 4.28. Using this figure, the linear model of Findley's law was utilized to forecast the time-dependent effective moduli of the full-scale PGFRPC cross-arm for up to 50 years, along with the apparent moduli as estimated from Equation (3.30). The initial day showed better agreement between the predicted moduli reduction factors and experimental results, particularly for bending. The experimental values exhibited a near-linear fit when compared to both predicted methods, with Method 2 showing a lower predicted value and Method 1 a higher one. As previously mentioned, additional samples with varying span lengths and geometric properties are necessary for more accurate flexural modulus values. According to previous researchers (Engineering Department of TNB Transmission Division, 2013; Johari et al., 2020a; Rawi et al., 2017), their coupon scale tests suggested that the PGFRPC cross-arm could last up to 24 years. Table 4.14 provides the predicted elastic moduli and reduction factors for an individual full-scale PGFRPC cross-arm after 50 years of service.

Table 4.14: Predicted life-span of full-scale PGFRPC cross-arm.

	E_0(GPa)	$E_{t,50y}$(GPa)	Reduction factor $_{t,50y}$	% reduce	R^2
Method 1	39.77	19.83	0.50	50.14	0.77327
Method 2	44.64	7.40	0.25	83.42	0.87531
Apparent	15.39	5.77	0.38	62.50	0.98035

The estimates showed reductions in the effective flexural modulus over 50 years: 50.14% for Method 1, 83.42% for Method 2, and approximately 62.50% for the apparent flexural modulus. These values assume the cross-arm was in service at an average ST and RH of 29 °C and 75%, respectively. This study only examined creep performance up to the secondary creep phase, excluding the tertiary creep stage. During the tertiary creep stage, significant increases in creep strains and elastic moduli occur before rupture, but these factors were not considered in this study. According to Loni et al. (2013), once the tertiary stage is reached, the remaining service life is minimal and of limited design relevance (Loni et al., 2013). Thus, ignoring the tertiary stage is reasonable. Additionally, because the ultimate strength of the PGFRPC is unknown, the maximum achievable elastic moduli for the cross-arm member cannot be precisely defined. Future studies are needed to accurately predict the lifespan of this beam.

4.5.6 Influence of honeycomb sandwich structure on the PGFRPC cross-arm in load-deflection behaviour

To address the sudden failure in existing cross-arms, an enhanced PGFRPC cross-arm with a honeycomb sandwich structure was developed, as discussed earlier. This study focused on analyzing the deformation behavior and long-term mechanical performance of both the existing full-scale PGFRPC cross-arm and the enhanced version designed for 132 kV transmission towers. A 3-PB test with a 2.50 m span length and a load of 1,400 N was conducted to measure mid-span deflection for both versions. Additionally, a load of 1,324

N, representing 1.7 times the operational load deflection, was applied to assess long-term mechanical performance. The study also examined long-term creep reduction using apparent elastic moduli obtained from the tests. The findings provide insights into the long-term durability and benefits of integrating the honeycomb sandwich structure into the PGFRPC cross-arm.

In the 3-PB test with a 2.50 m span length and a load of 1,400 N, the deflection behavior of both the existing and enhanced cross-arms was measured. Three samples of each type were tested to obtain average values. Equation (3.18) was used to calculate the elastic moduli from the deflection values.

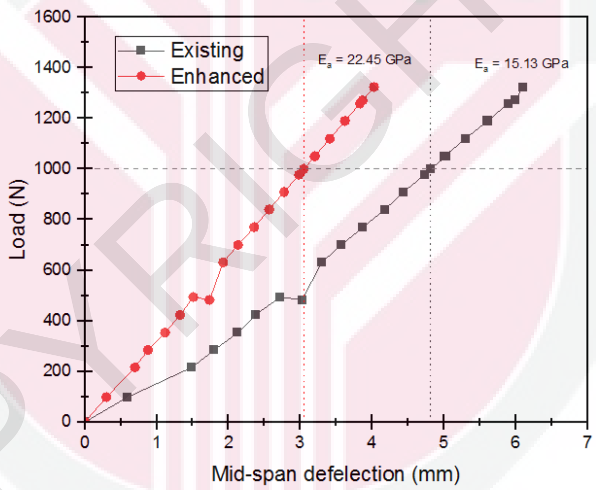

Figure 4.29: Deflection behaviour for both existing and enhance PGFRPC cross-arm.

Figure 4.29 shows that the existing cross-arm exhibited higher deformation under the same load compared to the enhanced PGFRPC cross-arm. This is attributed to the superior bending properties of the honeycomb sandwich composite structure added to the existing cross-arm. The pultruded composite cross-arm was manufactured using pultruded glass fiber reinforced UPE matrix. The outer layers of the pultruded composite allowed alignment of the principal loading direction with the ply orientation, as noted by Hashim et al. (2021). This alignment improves the bending strength of the structure (Y. Bai et al.,

2021) and delays the breakage of glass fibers under applied force, thus protecting the composite laminate.

The honeycomb sandwich composite structure, characterized by lower stiffness and higher flexibility, further delays glass fiber rupture in the enhanced cross-arm, increasing its toughness and rigidity. For instance, under a 1,000 N force, the existing cross-arm deflected about 4.82 mm, while the enhanced cross-arm deflected about 3.05 mm, showing a deflection reduction of approximately 36.7%. The apparent elastic modulus of the existing cross-arm was lower than that of the enhanced cross-arm (15.13 GPa and 22.45 GPa, respectively), indicating lower flexural strength for the existing cross-arm, consistent with the literature (Asyraf et al., 2023; Sá et al., 2016). However, both cross-arms displayed the same linear relationship between applied load and mid-span deflection. Studying deflection behavior under load is crucial for high transmission towers to determine the future durability of the cross-arm member.

4.5.7 Influence of honeycomb sandwich structure on the PGFRPC cross-arm in creep behaviour

The beams underwent testing for 1,000 hours in an open area, exposed to tropical weather and environmental conditions. The average values of surface temperature (ST) and relative humidity (RH) during this period were 29 °C and 75%, respectively. Deformation values were recorded at intervals of 0, 0.1, 0.2, 0.5, 1, 2, 5, 20, 50, 100, 200, 500, 700, and 1,000 hours. The test results included creep deflection, strain, modulus comparisons, and a quantitative analysis of creep for both the current and enhanced cross-arm designs.

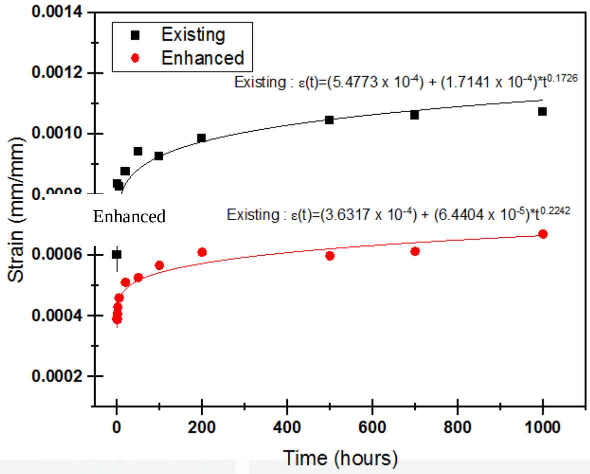

Figure 4.30: Creep strain behaviour for both existing and enhanced PGFRPC cross-arm.

Figure 4.30 shows the average strain values for three samples of existing and enhanced cross-arms with a 2.50 m span length over time. The figure also demonstrates the use of Findley's power law model to simulate the creep characteristics of the PGFRPC cross-arm and estimate strain at specific times by deriving material-specific parameters (m and n) through curve fitting. The close alignment between the equation and observed data confirms Findley's power law's effectiveness in modeling the creep behavior of the PGFRPC cross-arm. Additionally, the R2 values for the graphs fit well with Findley's model. The initial elastic moduli over time were calculated by dividing the stress (9.037 MPa) of the cross-arm by the initial strain obtained from the equation. A summary of the flexural moduli is provided in Table 4.15.

Table 4.15: Summary of apparent flexural moduli for existing and enhanced cross-arm using Findley's power law fitting.

Cross arm	**ε_0, (10^{-4})**	**m, (10^{-4})**	**n**	$E_0 = \sigma/\varepsilon_0$ **(GPa)**	$E_t = \sigma/m$ **(GPa)**	E_t/E_0	**R^2**
Existing	5.4773	1.7141	0.1726	16.50	52.72	3.20	0.9041
Enhanced	3.6317	0.6440	0.2242	24.88	140.33	5.64	0.9507

The initial creep strain (ε_0) for the enhanced cross-arm was lower than for the existing cross-arm, with values of 3.6317 × 10-4 mm/mm and 5.4773 × 10-4 mm/mm, respectively, due to lower initial creep deflection. The initial elastic moduli derived from Findley's power law model at the end of the test period were 16.50 GPa for the existing cross-arm and 24.88 GPa for the enhanced cross-arm. The differences in values from the load-deflection test are likely due to varying real weather conditions like temperature and humidity. The honeycomb sandwich structure increases the bending strength of the beam as the load is shared between the compliant matrix and stiffer fiber bundles within the beam and honeycomb sandwich structure (Koohbor et al., 2015). The woven E-glass fiber used in the facesheet of the honeycomb sandwich composite is classified as a continuous fiber-reinforced composite with solvent-free epoxy resin designed for high-strength glass fiber materials.

The viscoelastic response of the cross-arm member remained consistent. The primary stage of creep shows rapid deformation that slows over time, while the secondary stage exhibits a relatively uniform deflection rate. The study demonstrates that incorporating the honeycomb sandwich structure reduces creep strain by approximately 33.7%, potentially extending the cross-arm's lifespan. Findley's graph fitting confirms the model's ability to simulate the creep behavior of the composite cross-arms, with R^2 values of 0.9041 and 0.9507 for the existing and enhanced cross-arms, respectively.

To predict the full-section apparent flexural modulus over time $E_{a,exist}(t)$ and $E_{a,enhanced}(t)$ for the composite cross-arm, Findley's equation from the fitting curve was used, as shown in Table 4.16. The apparent elastic moduli reduction factors were determined to predict future creep modulus and strength reduction for 50 years. Due to the low shear modulus from the 3-PB deflection test, shear modulus was not considered in this prediction. Only elastic modulus was considered. The reduction factors over time of apparent modulus ($\chi_{a,existing}(t)$ and $\chi_{a,enhanced}(t)$), for existing and enhanced PGFRPC cross-arms were evaluated, showing the highest stiffness reduction during the test period corresponded with the elastic modulus.

Table 4.16: Equation to predict apparent elastic moduli over time.

Cross arm	Equation to predict Apparent elastic moduli at given time
Existing	$E_{a,existing}(t) = 16.50 \times \left[\frac{1}{1 + \left(\frac{t^{0.1726}}{3.20} \right)} \right]$
Enhanced	$E_{a,enhance}(t) = 24.88 \times \left[\frac{1}{1 + \left(\frac{t^{0.2242}}{5.64} \right)} \right]$

Table 4.16 shows that the initial apparent flexural modulus over time for the existing, $E_{a,exist}(t)$, cross-arm was lower than for the enhanced, $E_{a,enhanced}(t)$, cross-arm (16.50 GPa and 24.88 GPa, respectively). Adding the honeycomb sandwich structure improved the elastic properties of the PGFRPC cross-arm, aligning with other literature (Dawood et al., 2010; L. Zhang et al., 2019; D. Zhao et al., 2022) Referring to Figure 4.31, the highest stiffness reduction occurred in the early stage, approximately 24 hours into the initial test period. However, the creep rate reduction decreased slightly after the early stage. The curve shows that the apparent reduction factor decreased consistently for both existing and enhanced cross-arms. The linear fitted line closely matched the experimental values throughout the testing period, enabling predictions of the reduction factor and effective moduli up to 50 years.

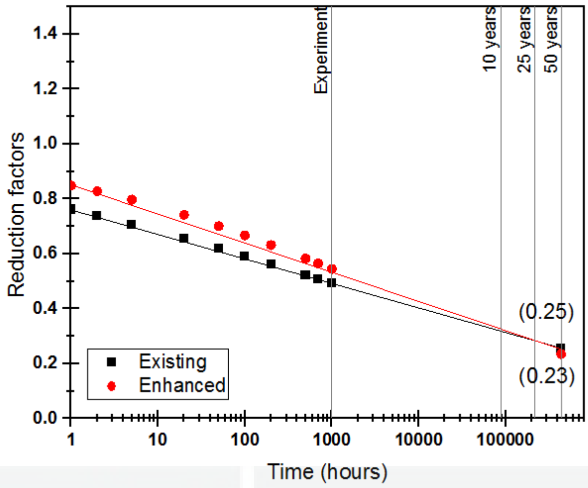

Figure 4.31: Comparison of flexural moduli reductions over five decades.

At the end of the 1,000-hour testing period, the elastic modulus for the existing cross-arm was 8.13 GPa, a decrease of approximately 50% from the initial effective modulus. The elastic modulus for the enhanced cross-arm decreased by about 45%, with an effective value of 13.56 GPa at that point. Predictions for the individual cross-arms at 50 years show a reduction of approximately 75% for the existing cross-arm and 70% for the enhanced cross-arm from the initial modulus. The honeycomb sandwich structure enhanced the existing PGFRPC cross-arm by nearly 5%.

Compared to the initial values, estimates indicated that the flexural moduli reductions for the enhanced cross-arm began to slowly decrease over the five-decade prediction period, compared to the existing cross-arm. Generally, materials maintain their initial stiffness when the reduction factor is close to 1, but a reduction factor nearing 0 indicates significant stiffness loss. The predicted elastic moduli for the enhanced cross-arm with the honeycomb sandwich structure at 10, 25, and 50 years were higher than those for the existing cross-arm, as shown in Table 4.17. Regression analysis for both existing and enhanced cross-arms showed a best fit with experimental and predicted data points, consistent with other literature, with values ranging from 0.98 to 0.99 (E. Barbero et al., 2000; Bhattacharya et al., 2021).

Table 4.17: Summary of predicted life-span individual PGFRPC existing and enhanced cross-arm.

Cross arm	$E_{a@10\ years}$ (GPa)	$E_{a@25\ years}$ (GPa)	$E_{a@50\ years}$ (GPa)	Reduction factor $_{@\ 50\ years}$	R^2
Existing	5.11	4.57	4.19	0.25	0.9976
Enhanced	7.60	6.56	5.84	0.23	0.9883

This study confirms that using a honeycomb sandwich composite structure to enhance the existing PGFRPC cross-arm increases its strength and extends its lifespan. Applying this knowledge to full-scale individual cross-arm members can reduce maintenance costs, as only an individual beam cross-arm would need replacement. Previous studies primarily focused on the lifespan of PGFRPC cross-arm members for high transmission towers under small-scale conditions.

4.6 Flexural properties of full-scale assembly cross-arm

This section discusses the results of load deflection and creep tests for both the existing and the honeycomb sandwich-enhanced PGFRPC cross-arm (enhanced cross-arm) in a fully assembled condition on a 132 kV 13L transmission tower. It covers creep-strain values and the creep model for both cross-arms. Additionally, the elastic modulus of the cross-arms at different points was determined using the load and deflection data from the tests, and these values were compared with the elastic modulus obtained from the 3PB test on full-scale individual cross-arm members. The coefficient of determination (R^2) values of Findley's model for both existing and enhanced cross-arms were also calculated and compared. This section concludes with a summary of the load deflection and creep benefits for the full-scale 132 kV 13L cross-arm, demonstrating the effectiveness of incorporating honeycomb sandwich composites into the existing cross-arm.

4.6.1 Load deflection behavior of full-scale assembly cross-arm

The load-deflection values were measured using dial gauges at various points along the main cross-arm members in the Y-axis direction, as depicted in Figure 3.12. The cross-arms included those without and with honeycomb sandwich enhancement. Each measurement was repeated three times to obtain an average load deflection value. The load-deflection values were then plotted against the marked points: Y1 being the closest to the cross-arm's free end and Y5 the closest to the fixed point of the PGFRPC cross-arm. Load was applied up to 9705 N, 1.5 times the normal load acting in the transverse direction as mentioned in subsection 3.5.1.

Figure 4.32 illustrates that the deflection behavior of the PGFRPC cross-arm is directly proportional to the applied load, consistent with previous studies. This proportionality holds as long as the deflection is small and the beam material does not yield (Beléndez et al., 2002; Mohamad et al., 2020). Therefore, PGFRPC is considered a linear elastic material, homogeneous, isotropic, and compliant with Hooke's Law. The maximum deflection always occurred at the free end, while the minimum deflection was at the fixed point. The deflection behavior of this cross-arm resembled that of a cantilever beam, involving a three-dimensional problem. The Poisson's ratio effect can be ignored due to the beam's length being larger than the thickness of the perpendicular cross-section and shorter than the beam's curvature radius (Feynman, 1964)

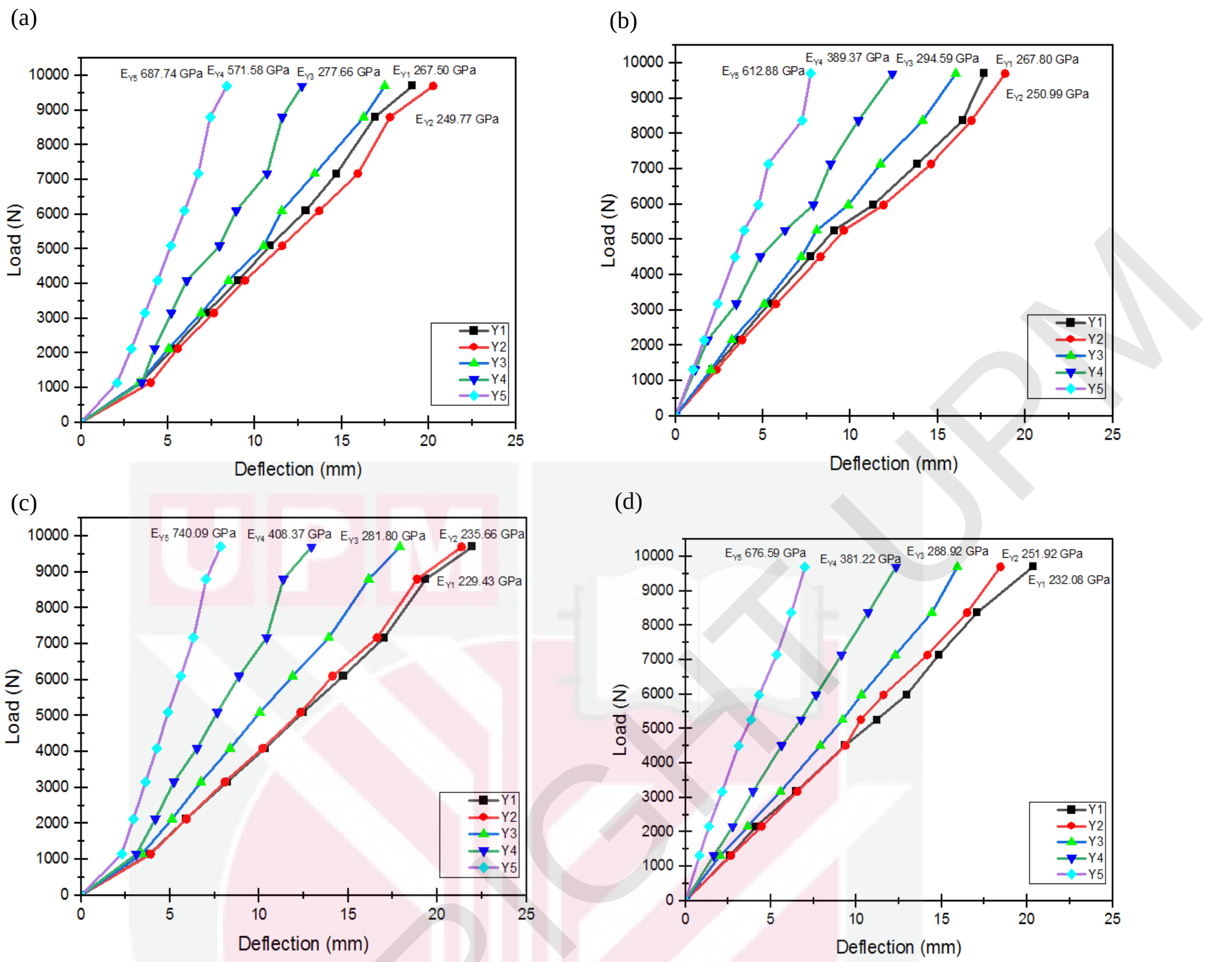

Figure 4.32: Load deflection for existing and enhanced PGFRPC cross-arm (a) existing right main member (b) enhanced right main member (c) existing left main member (d) enhanced left main member.

To assess the impact of honeycomb sandwich enhancement at the critical point (Point Y3), all cross-arm deflection values were used to analyze beam behavior during load application. Without enhancement, it was observed that the deflection of the right side of the cross-arm member was slightly smaller than the left side, likely due to assembly fitting and fixed-point arrangement. These factors also influenced deflection values, as seen in Figure 4.32, where the deflection values at Points Y1 were greater than at Points Y2, as discussed in Chapter 4.2.

Implementing the honeycomb sandwich composite structure at the critical point of the PGFRPC cross-arm resulted in a slight reduction in deflection values compared to the existing cross-arm. This is due to the incorporation of high-quality bending behavior, such as that found in a honeycomb sandwich composite structure, into the existing cross-arm. The combination of this structure with the pultruded cross-arm enhances the structure's resistance to bending forces (Bai et al., 2021). Consequently, this helps delay the breaking of glass fibers when subjected to external forces, thereby preserving the integrity of the composite laminate.

The use of honeycomb sandwich composites to enhance the critical point of the PGFRPC cross-arm was validated by the deflection values of the enhanced cross-arm at Point Y3. The deflection values decreased from 17.89 mm to 15.91 mm for the left main members and from 17.47 mm to 16.03 mm for the right main members, resulting in an almost 11% reduction for the left main member and an 8% reduction for the right main member. Furthermore, the addition of the honeycomb sandwich composite structure, which has lower stiffness and higher flexibility, delayed glass fiber rupture in the enhanced cross-arm, increasing their toughness and rigidity.

Using Equation 3.25, the elastic modulus of the cross-arm at each point was determined. The elastic modulus of the enhanced cross-arm was slightly higher compared to the existing cross-arm at Points Y1, Y2, and Y3 for both sides of the main cross-arm, indicating that the flexural strength of the existing cross-arm is lower than that of the enhanced cross-arm, consistent with the literature (Asyraf et al., 2021b). However, the elastic modulus at Points Y4 and Y5 of the enhanced cross-arm was slightly lower than that of the existing cross-arm. This unexpected situation is suspected to be due to the point location and the load being absorbed more at the enhanced point, resulting in a lower elastic modulus value at points after the enhanced structure (Gan et al., 2018; H. Zhang et al., 2018).

Despite this, the elastic modulus at Point Y3 for both existing and enhanced cross-arms increased slightly, with values of 277.66 GPa and 294.59 GPa for the right main members, and 281.80 GPa and 288.92 GPa respectively. As expected, both strength and elastic modulus increased with the implementation of the honeycomb sandwich composite structure (M. K. Lee & Barr, 2004). Additionally, the elastic modulus for the cross-arm in the assembled condition aligns well with the full-scale individual beam cross-arm during the 3PB test mentioned in subsection 4.5. It is believed that the different load applications for different structural conditions during the 3PB test and cantilever beam test were the major reasons for the differences in the calculation of strength and elastic modulus, despite the possible influence of different boundary conditions.

4.6.2 Flexural creep test for assembly cross-arm

The properties of the assembled PGFRPC cross-arm were examined using a two-point bending test, simulating the cantilever beam application. The testing procedures followed those established by Asyraf et al. (2021) and Sharaf et al. (2020). Deflection values were measured using dial gauges positioned at five points (Y1 to Y5) on each cross-arm member, with Y1 closest to the free end. The gauges were spaced 0.61 m apart. The applied load at the free end of the cross-arm was measured with a 3-ton crane scale. A static load of 6467 N, representing the vertical force on the assembled cross-arm during working load application according to TNB standards, was used (Sharaf et al., 2020). The test duration was approximately 1,000 hours, conducted in an open area with an ambient temperature of 31.1°C and relative humidity of 66.14%, as shown in Figure 4.33.

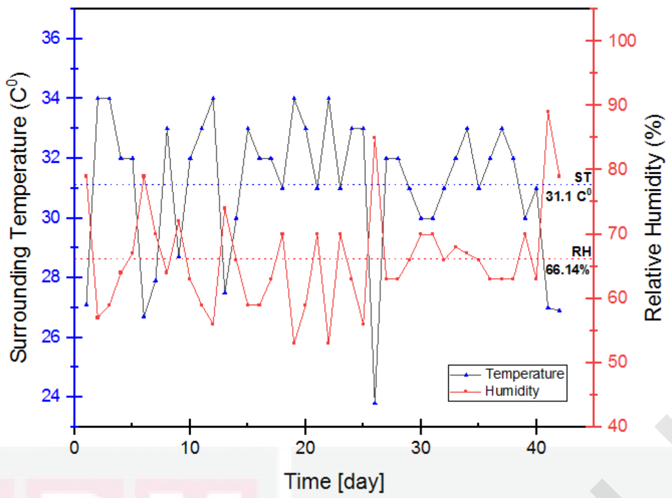

Figure 4.33: Records of ambient temperature and relative humidity during the creep test of the assembled cross-arm.

Figure 4.34 displays the creep strain-time curves for both the existing and honeycomb sandwich-enhanced cross-arms under actual operating loads at Points Y1 to Y5. Each strain gauge indicated varying creep strain values due to the tension and compression along the main member beams during loading (Hunt et al., 2015). The elastic strain values changed along the beam length from the loading end to the fixed point as stress increased (Sezgin et al., 2010). The study showed that the maximum creep strain was concentrated at Point Y3, consistent with previous findings (Asyraf et al., 2021b), as this point serves as the center of the main members in both the current and reinforced cross-arm designs. This result was attributed to beam buckling, with the working load applied at the free end of the main member beams (Bozkurt et al., 2019; Sayyad & Ghugal, 2017).

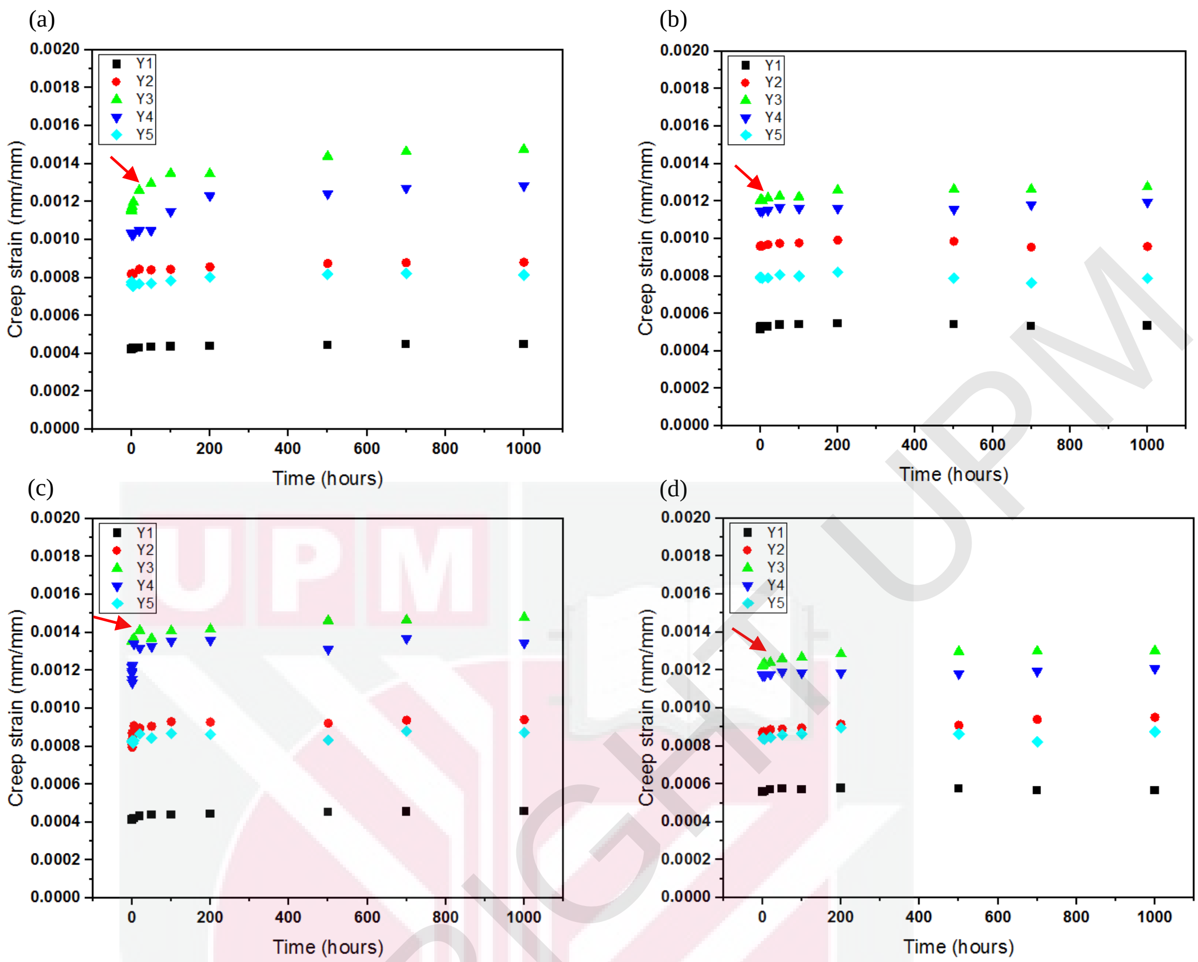

Figure 4.34: Creep strain for existing and enhanced PGFRPC cross-arm from experimental results (a) existing right main member (b) enhanced right main member (c) existing left main member (d) enhanced left main member.

When comparing the existing and enhanced PGFRPC cross-arms, it was observed that the creep strain in the right and left main members differed due to asymmetrical jig and fixing installation. However, the creep strain curve pattern was similar, following standard creep strain curves (ASTM-D2990, 2017). This result indicates that the cross-arm can withstand and sustain loading conditions. Despite some misalignment issues in the experimental setup designed to mimic real-world applications, it was demonstrated that reinforcing the cross-arms with a honeycomb sandwich composite structure improved their creep resistance. The enhanced cross-arm exhibited lower creep strain than the existing one, due to the fabric interlayer contact mechanism, where the last cross-arm layer overlapped the upper layer of the honeycomb sandwich composite structure with epoxy resin, enhancing the beam's strength (Z. Xiang et al., 2020). Overall, the honeycomb sandwich composite reduced buckling reactions and improved structural integrity.

Figure 4.34 also showed the creep strain patterns transitioning from an elastic to a viscoelastic stage. The red arrows highlight how the existing composite cross-arm exhibited an extended transition period from the elastic to the viscoelastic phase. The honeycomb sandwich composite structure stabilized this transition, reducing the likelihood of structural failure. The strain value at Point Y3, the highest value obtained in both the existing and enhanced cross-arm compared to other points (Y1, Y2, Y4, and Y5), confirmed that Point Y3 is the critical point. This study aimed to enhance the cross-arm's performance by strengthening Point Y3 with the honeycomb sandwich structure.

According to Figure 4.34, the creep strain in the existing right and left main members of the cross-arm exceeded 0.0014 mm/mm, while the enhanced cross-arm's creep strain did not reach 0.0014 mm/mm. Additionally, the creep strain in the enhanced cross-arm was reduced by almost 20% compared to the existing cross-arm, especially at the critical point (Point Y3). Using the creep deflection results and applied load, the initial elastic modulus ($E_{e,0}$) and initial creep strain (ε_0) were calculated using Equations 3.25 and 3.27. The initial elastic modulus results showed an inverse relationship with the measured points on the cross-arm members, with the highest modulus at the fixed point (Y5) and the lowest at the free end (Y1), as shown in Table 4.18. However, the enhanced cross-arm had a slightly higher initial creep strain at all points compared to the existing cross-arm but decreased slowly over time. This stability was due to the honeycomb sandwich structure increasing material strength. Overall, adding a composite structure enhances the creep resistance of the cross-arm assembly, countering the lateral force from dead weight and reducing structural buckling (Anand et al., 2018; Supian et al., 2023).

Table 4.18: Results obtained from experimental for existing and enhanced cross-arm member.

Cross arm	Location	Stress, (MPa)	ε_0, (10^{-4})	$E_{e,0}$ (GPa)
Existing (Right)	Y1	97.292	4.2080	231.21
	Y2	196.04	8.1784	239.71
	Y3	294.79	11.516	255.97
	Y4	393.54	10.333	380.85
	Y5	492.29	7.7840	632.44
Enhanced (Right)	Y1	97.292	5.2491	185.35
	Y2	196.04	9.5999	204.21
	Y3	294.79	12.063	244.38
	Y4	393.54	11.490	342.51
	Y5	492.29	7.9412	619.92
Existing (Left)	Y1	97.292	4.1054	236.98
	Y2	196.04	8.1032	241.93
	Y3	294.79	11.516	255.98
	Y4	393.54	11.867	331.63
	Y5	492.29	8.2715	595.17
Enhanced (Left)	Y1	97.292	5.5599	174.99
	Y2	196.04	8.6793	225.87
	Y3	294.79	12.232	241.00
	Y4	393.54	11.741	335.18
	Y5	492.29	8.3973	586.25

Stress at different points on the cross-arm was calculated using Equation 3.26, considering the distance from the fixed point. As mentioned in section 3.7, the dial gauges were arranged to maintain a 0.61 m distance from the fixed point and between each gauge. Therefore, the effective lengths at Points Y1, Y2, Y3, Y4, and Y5 were 3.05 m, 2.44 m, 1.83 m, 1.22 m, and 0.61 m, respectively. Table 4.18 shows that stress on the cross-arm member increased linearly from the free end to the fixed point, consistent with previous studies (Riezzo et al., 2019).

4.6.3 Empirical creep model for PGFRPC cross-arm

The creep properties of the PGFRPC cross-arm were analyzed using the Findley Power Law Model, as previously discussed for replicating creep characteristics (Du et al., 2013). This model was applied to fit the creep strain curve and estimate strain over time using data from Figure 4.34. Material-specific parameters (*m* and *n*) were derived through curve fitting, as expressed in Equations 3.33 and 3.34.

Table 4.19: Summary of variable obtained from Findley Power Law Model for existing and enhanced cross-arm member.

Cross arm	Location	ε_0, (10^{-4})	m, (10^{-6})	n	$E_{e,0} = \sigma/\varepsilon_0$ (GPa)	E_t=σ/m (GPa)	R^2
Existing (Right)	Y1	4.1931	5.2515	0.2588	232.03	18527	0.9895
	Y2	8.1479	7.0621	0.3329	240.60	27760	0.9691
	Y3	11.300	50.479	0.2864	260.88	5839.9	0.9831
	Y4	10.200	16.427	0.4176	385.82	23957	0.9322
	Y5	7.6134	2.2890	0.4866	646.61	215070	0.8782
	Average		16.302	0.3565	353.19	58230	0.9504
Enhanced (Right)	Y1	5.2068	7.4449	0.1584	186.86	13068	0.8658
	Y2	9.5757	7.6785	0.1060	204.73	25531	0.8552
	Y3	12.000	5.2135	0.3874	245.66	56544	0.9479
	Y4	11.500	0.1581	0.8030	342.21	2489210	0.8058
	Y5	7.8932	5.9679	0.4670	623.68	82489	0.8309
	Average		5.2926	0.3844	320.63	533360	0.8611
Existing (Left)	Y1	4.0699	10.967	0.2292	239.05	8871.0	0.9791
	Y2	7.9939	54.121	0.1493	245.24	3622.3	0.8821
	Y3	13.500	10.082	0.3741	255.36	29239	0.9365
	Y4	11.600	74.788	0.1583	339.26	5262.1	0.8541
	Y5	8.2078	10.696	0.2288	599.78	46025	0.8012
	Average		32.131	0.2280	328.34	18604	0.8906
Enhanced (Left)	Y1	5.5392	8.7106	0.1166	175.64	11169	0.9879
	Y2	8.6914	3.3689	0.4552	225.56	58192	0.9527
	Y3	12.200	12.729	0.2879	241.63	23159	0.9762
	Y4	11.700	1.9019	0.3896	336.36	206920	0.8609
	Y5	8.3441	9.5628	0.1724	589.99	51479	0.8525
	Average		7.2546	0.2843	313.84	70184	0.9260

Table 4.19 demonstrates the use of Findley's power law model equation to replicate the creep characteristics of a PGFRPC cross-arm. The equation closely matches the observed data, confirming Findley's model's effectiveness in simulating PGFRPC cross-arm creep behavior. The R^2 values for all graphs were near 1, indicating a good fit with Findley's model. The initial elastic modulus over time was determined by dividing the cross-arm stress by the initial strain at selected points. The stresses for the PGFRPC cross-arm at Points Y1, Y2, Y3, Y4, and Y5 were 97.292 MPa, 196.04 MPa, 294.79 MPa, 393.54 MPa, and 492.29 MPa, respectively.

The transient creep (*m*) values for existing and enhanced cross-arms in Table 4.19 were compared. The reinforced cross-arm showed lower transient creep than the original composite cross-arm, indicating a superior steady-state creep response. This suggests that adding a honeycomb sandwich composite during retrofitting does not affect the secondary stage of creep, as the PGFRPC already has excellent creep resistance (Cardoso & Harries, 2019; Loni et al., 2013). The average transient creep for the existing and enhanced right cross-arm members were 16.302 x 10^{-6} and 5.2926 x 10^{-6} , respectively. For the left cross-arm members, the averages were 32.131 x 10^{-6} and 7.2546 x 10^{-6}. Transient creep strain, the initial inelastic flow creep, decreases until the steady-state period is reached (C. Yang et al., 1999).

The existing composite cross-arm has a lower material stress-independent exponent (*n*) than the enhanced composite cross-arm, with differences of approximately 7.8% and 24.7% for right and left main members, respectively. The n values for both cross-arms were within the standard range for stress-independent material exponents (Anand et al., 2018; D'Antino & Pisani, 2019; Sá et al., 2011a). The n parameter appears temperature-dependent, likely due to test temperatures being close to the glass transition temperature (Loni et al., 2013). While load deflection and transient creep improved in the enhanced cross-arm, further enhancement using the honeycomb sandwich composite method is necessary, and compatibility needs further study.

The initial creep strains (ε_0), for both existing and enhanced cross-arms were proportional to the applied stress according to Hooke's law. Table 4.18 shows that initial creep strain in the enhanced right cross-arm members was slightly higher than in the existing cross-arm, while in the left cross-arm members, the difference was due to assembly conditions as seen in the experiment (refer to Figure 4.34). The instantaneous strain in this assembly cross-arm aligns with individual full-scale cross-arm studies using the 3PB test. Reinforcing the existing cross-arm with a honeycomb sandwich structure increases the beam's bending strength. This improvement results from the load distribution between the flexible matrix and the rigid fiber bundles in both the beam and the honeycomb sandwich structure (Koohbor et al., 2015). The facesheet of the honeycomb sandwich composite incorporates woven E-glass fibers, creating a continuous fiber-reinforced composite with solvent-free epoxy resin for high-strength applications. The results indicate that Point Y3 exhibited the highest creep strain, focusing enhancement efforts on that point.

4.6.4 Creep model accuracy and verification

To verify the creep behavior in this study, a comparison was made between the initial elastic modulus derived from experimental data and the empirical Findley's model. The initial elastic modulus, $E_{e,0}$, was inversely related to the measured point across the cross-arm members, with the highest elastic modulus at the fixed point (Point Y5) and the lowest at the free end point (Point Y1). This comparison, detailed in Table 4.20, includes initial elastic modulus values for both the existing and enhanced PGFRPC cross-arm, juxtaposing experimental data with the empirical Findley's model.

Table 4.20: Summary of initial elastic modulus obtained from experimental and empirical model for existing and enhanced cross-arm member.

Cross arm		Initial Elastic Modulus, $E_{e,0}$ (GPa)				
		Location				
		Y1	Y2	Y3	Y4	Y5
Existing	Right	231.21	239.71	255.97	380.85	632.44
Findley Model		232.03	240.60	260.88	385.82	646.61
Error (%)		0.35	0.37	1.91	1.31	2.24
Enhanced		185.35	204.21	244.38	342.51	619.92
Findley Model		186.86	204.73	245.66	342.21	623.68
Error (%)		0.81	0.25	0.52	0.09	0.61
Existing	Left	236.98	241.93	255.98	331.63	595.17
Findley Model		239.05	245.24	255.36	339.26	599.78
Error (%)		0.87	1.37	0.24	2.30	0.78
Enhanced		174.99	225.87	241.00	335.18	586.25
Findley Model		174.59	225.85	240.98	335.28	586.35
Error (%)		0.23	0.01	0.01	0.03	0.02

Table 4.20 shows the initial elastic modulus obtained from experimental and empirical models. The close alignment of these values confirms that Findley's Power Law model

effectively fits the creep behavior of PGFRPC cross-arm studies, as supported by previous research (Alhayek et al., 2022). Although the elastic modulus values for both the assembled and individual cross-arms followed the same trend, the values were higher for the assembled cross-arm condition.

The primary reason for this difference is the condition of the cross-arm: in the assembled state, all cross-arm members are affected by the applied load through tension and compression (Alhayek et al., 2022), unlike the individual cross-arm member tests. Additionally, the load application method varies, with a 3-PB test for individual cross-arms and a cantilever beam concept for the assembled cross-arm. The fitting and fixed point arrangement of the assembly also impact the results, particularly between the right and left cross-arm members.

As shown in Table 4.20, all recorded percentage errors were below 5%, indicating that the numerical models, including Findley's Power Law models, aligned accurately with the experimental data. According to Kim et al. (2017), Sayahi et al. (2013), and Zhang et al. (2007), the acceptable threshold for percentage error when comparing experimental results to numerical values should be under 20%. Table 4.21 presents the accuracy classifications for comparing experimental data and numerical analysis. When the percentage error is below 20%, it signifies that the experimental data is consistent with the numerical model. This study successfully validated the creep properties of both existing and enhanced PGFRPC cross-arms using precise and consistent experimental data.

Table 4.21: Accuracy classification according to percentage error intervals.

Accuracy classification	Percentage error range (%)
High acceptable	0.1-9.9
Good	10-14.9
Satisfactory	15-19.9
Fair	20-24.9
Unsatisfactory	More than 25

(Source: Kim et al., 2017; Sayahi et al., 2013; Z. Zhang et al., 2007).

4.6.5 Prediction of time-dependent full-scale assembly cross-arm

To predict the full-scale flexural modulus over time, $E_{e,\mathrm{exist}}(t)$ and $E_{e,\mathrm{enhanced}}(t)$ for the composite cross-arm, Findley's equation from the fitting curve in Table 4.19 was used, as shown in Table 4.22. Since Point Y3 was identified as the critical point in the previous chapter, this prediction focused only on this point. The elastic moduli reduction factors over time ($\chi_{e,\mathrm{existing}}(t)$ and $\chi_{e,\mathrm{enhanced}}(t)$) for existing and enhanced PGFRPC cross-arms were determined, with the highest stiffness reduction during the test period corresponding to the elastic modulus.

Table 4.22: Equation of elastic moduli at given time for assembly cross-arm.

Cross arm		Equation to predict elastic modulus at given time for assembly cross-arm
Existing	Right	$E_{e,existing\ (Right)}(t) = 260.88 \times \left[\frac{1}{1 + \left(\frac{t^{0.2864}}{22.39}\right)}\right]$
	Left	$E_{e,existing\ (Left)}(t) = 255.36 \times \left[\frac{1}{1 + \left(\frac{t^{0.3741}}{114.50}\right)}\right]$
Enhanced	Right	$E_{e,enhanced\ (Right)}(t) = 245.66 \times \left[\frac{1}{1 + \left(\frac{t^{0.3874}}{230.17}\right)}\right]$
	Left	$E_{e,enhanced\ (Left)}(t) = 241.63 \times \left[\frac{1}{1 + \left(\frac{t^{0.2879}}{95.85}\right)}\right]$

Using the equations in Table 4.22, the predicted elastic modulus values for the cross-arm over time were calculated. Since the assembly cross-arm had nearly identical elastic modulus values for the right and left cross-arm members, the average values were used for both existing and enhanced cross-arm curves. Figure 4.35 indicates that the highest stiffness reduction occurred in the early stage, around 24 hours into the initial test period. However, the reduction rate slowed due to bending after the early stage. The curve also shows that the reduction factor decreased consistently for both existing and enhanced cross-arms. The fitted line closely matches the experimental values, enabling the prediction of the reduction factor and effective moduli up to 50 years.

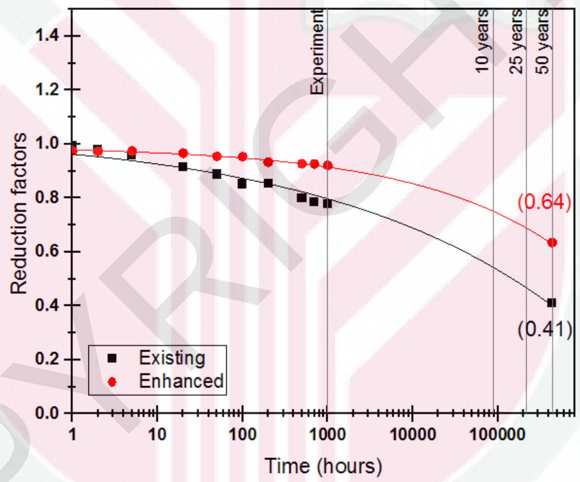

Figure 4.35: Predicted curves of the existing and enhanced assembly cross-arm till 50 years.

At the end of the testing period (1,000 hours), the average elastic moduli for the existing cross-arm decreased by approximately 22% from the initial effective moduli, reaching 200.30 GPa. For the enhanced cross-arm, the average elastic moduli decreased by approximately 11% from the initial effective moduli, reaching 228.70 GPa. The average elastic modulus for the existing and enhanced cross-arms at 50 years is predicted to decrease by approximately 59% and 39%, respectively. This demonstrates that using a honeycomb sandwich structure enhances the existing assembly PGFRPC cross-arm by nearly 20%. The differences in individual conditions are due to different load application methods and assembly conditions, but the overall trend is consistent.

Figure 4.35 shows that, compared to the initial value, the flexural moduli reductions for the enhanced cross-arm slowly decreased over the entire five-decade prediction period compared to the existing cross-arm. Generally, materials maintain their initial stiffness when the reduction factor is close to 1, but a reduction factor near 0 indicates a significant loss of structural stiffness. The predicted elastic moduli for the enhanced cross-arm, with the addition of the honeycomb sandwich structure, remained higher than the existing cross-arm at 10, 25, and 50 years, as shown in Table 4.23. The regression analysis, based on curve fitting for both existing and enhanced cross-arms, shows a good fit with experimental and predicted data points, with R^2 values ranging from 0.98 to 0.99 (E. Barbero et al., 2000; Bhattacharya et al., 2021).

Table 4.23: Summary of predicted life-span of assembly PGFRPC existing and enhanced cross-arm.

Cross arm	$E_{e@10\ years}$ (GPa)	$E_{e@25\ years}$ (GPa)	$E_{e@50\ years}$ (GPa)	Reduction factor $_{@\ 50\ years}$	R^2
Existing	139.28	120.25	105.92	0.41	0.9896
Enhanced	185.18	170.25	157.68	0.64	0.9984

This study proves that the use of honeycomb sandwich composite structure in order to enhance the existing assembly PGFRPC cross-arm can increase the strength of the cross-arm and extend the life span of the assembly cross-arm. Using this comprehensive knowledge for the full-scale assembly cross-arm member can reduce the maintenance cost of the cross-arm.

CHAPTER 5

CONCLUSIONS AND RECOMMENDATIONS

5.1 Conclusions

Transmission tower cross-arms are critical components that endure significant bending and creep loads throughout their lifespan, exacerbated by environmental factors that can lead to sudden failure. This study addresses these challenges by exploring the use of a commercial pultruded composite material, PGFRPC (Pultruded Glass Fiber Reinforced Polymer Composite), which is reinforced with E-glass fibers and unsaturated polyester, known for its enhanced resistance to bending and creep loads, and improved long-term mechanical properties. To further optimize the cross-arm design, a honeycomb sandwich composite structure was incorporated due to its superior structural characteristics and lightweight nature.

The analysis of deformation behavior under actual working load conditions revealed that the PGFRPC cross-arm exhibited significantly less deflection compared to the Balau wood cross-arm. This was evident in both normal and broken wire conditions, with deflection values approximately 30% lower under normal conditions and 22% lower under broken wire conditions. The PGFRPC cross-arm demonstrated superior bending stress resistance, toughness, and stiffness, making it a promising alternative to traditional wooden cross-arms. Additionally, the characterization of fiber angle orientation showed that a woven glass-fiber honeycomb sandwich panel with a 0° facesheet orientation is optimal for bending applications, offering the highest load-bearing capacity before failure.

Design optimization using the TRIZ-morphological chart-ANP method resulted in the selection of Concept Design 2 (SOS2) as the optimal design for the honeycomb sandwich composite structure. This systematic approach facilitated the development of a design that promises improved structural performance. Subsequent evaluations of load deflection and creep performance demonstrated that the enhanced cross-arm with the honeycomb structure reduced deflection by approximately 36.7% and exhibited superior creep resistance over 50 years. This significant improvement in mechanical properties suggests potential maintenance cost savings and extended lifespan for transmission tower cross-arms.

The comprehensive evaluation of the flexural properties of a full-scale assembled PGFRPC cross-arm in a 132 kV 13L transmission tower confirmed the benefits of the honeycomb sandwich composite structure. The enhanced cross-arm showed a linear load-deflection relationship and reduced deflection by approximately 10% compared to the existing design. Creep tests highlighted superior creep resistance and stability at critical points, with the enhanced cross-arm demonstrating a 20% improvement in elastic modulus retention over 50 years. Overall, this study successfully validated the superior performance of the enhanced PGFRPC cross-arm, proving that incorporating a honeycomb sandwich composite structure can significantly improve the strength and extend the lifespan of transmission tower cross-arms.

5.2 Recommendations for future research

Based on the results obtained in this study, several recommendations for future study as outlined below:

1. The load-deflection behaviour results for assembly conditions was slightly unstable because the load was manually applied to the beam, which may cause inconsistency. It is proposed for future study to consider an automated mechanism for load application to improve the angle of the cross-arm, reduce the difference in

deflection value between cross-arms member and obtain consistent and stable results.

2. Currently, this study was conducted based on conventional load based method for full-scale individual and assemble cross-arms condition. Therefore, it is proposed for future study to study on the dynamic results, flexibility reaction, failure mood, and creep analysis of the cross-arm structure during normal and broken wire conditions. Besides that, the safety factor for both normal and broken wire condition could be varied to comprehend the effects of greater load on the composites structure.
3. For honeycomb sandwich composite structure used in cross-arm application, several limitations in this study should be studied in the future are the type of woven prepreg used for the facesheet, the effect of honeycomb core thickness, the effect of facesheet ply lay-up, and the effect of span length, along with a better study of the failure mode for the large-scale panel. Additionally, scanning electron microscopy (SEM) measurement should be carried out to show the dispersion and morphology of the glass fibre in the composite. Moreover, the behaviour based on sandwich panels needs to be studied under long-term loading to consider the creep effect of the woven prepreg honeycomb sandwich base.
4. In this study, the enhanced cross-arm using honeycomb sandwich composite structure at the center of the existing cross-arm is one of the ways to improve the bending behaviour, creep resistant performance and service life of the structure. Study needs should also compare the application of different parameter of the honeycomb sandwich location, type of epoxy used and incorporation sleeve or bracing in the beam profile on bending and creep properties of the cross-arm.
5. In this study, a dial gauge was utilized as the measurement tool for assessing creep strain in the creep study. Therefore, it is advisable to perform creep and mechanical

tests using a strain gauge along with a data logger in extreme tropical conditions to verify the measurement accuracy of the dial gauge.

REFERENCES

Abedzade Atar, H., Zarrebini, M., Hasani, H., & Rezaeepazhand, J. (2020). The effect of core geometry on flexural stiffness and transverse shear rigidity of weight-wise identical corrugated core sandwich panels reinforced with 3D flat spacer knitted fabric. *Polymer Composites*, *41*(9), 3638–3648.

Abu Bakar, M. S., Salit, M. S., Mohamad Yusoff, M. Z., Zainudin, E. S., & Ya, H. H. (2020). The crashworthiness performance of stacking sequence on filament wound hybrid composite energy absorption tube subjected to quasi-static compression load. *Journal of Materials Research and Technology*, *9*(1), 654–666.

ACMA. (2012). Pre-standard for load & resistance factor design (LRFD) of pultruded fiber reinforced polymer (FRP) structures. *Arlington, VA: ACMA*, 14.

Adekomaya, O., & Adama, K. (2017). Glass-Fibre Reinforced Composites: the Effect of Fibre Loading and Orientation on Tensile and Impact Strength. *Nigerian Journal of Technology*, *36*(3), 782–787.

Ahsan, M., Baharom, M. N. R. Bin, Zainal, Z., Mahmod, L. H., Ullah, I., Yousof, M. F. M., Mohd Jamail, N. A., Kamarudin, M. S., & Rahman, R. A. (2022). Historical Review of Advancements in Insulated Cross-Arm Technology. *Energies*, *15*(21).

Albayrak, U., & Morshid, L. (2020). Evaluation of seismic performance of steel lattice transmission towers. *Civil Engineering Journal (Iran)*, *6*(10), 2024–2044.

Albermani, F. G. A., & Kitipornchai, S. (2003). Numerical simulation of structural behaviour of transmission towers. *Thin-Walled Structures*, *41*(2–3), 167–177.

Albizu, I., Mazón, A. J., & Zamora, I. (2005). Methods for increasing the rating of overhead lines. *2005 IEEE Russia Power Tech, PowerTech*.

Alhassan, A. B., Zhang, X., Shen, H., & Xu, H. (2020). Power transmission line inspection robots: A review, trends and challenges for future research. *International Journal of Electrical Power and Energy Systems*, *118*.

Alhayek, A., Syamsir, A., Anggraini, V., Muda, Z. C., & Nor, N. M. (2019). Numerical Modelling of Glass Fiber Reinforced Polymer (GFRP) Cross Arm. *International Journal of Recent Technology and Engineering*, *8*(4), 6484–6489.

Alhayek, A., Syamsir, A., Supian, A. B. M., Usman, F., Asyraf, M. R. M., & Atiqah, M. A. (2022). Flexural Creep Behaviour of Pultruded GFRP Composites Cross-Arm: A Comparative Study on the Effects of Stacking Sequence. *Polymers*, *14*(7).

Alhayek, A., Syamsir, A., Supian, A. B. M., Usman, F., Najeeb, M. I., & Asyraf, M. R. M. (2023). A Mathematical Model of Flexural-Creep Behaviour for Future Service Expectancy of a GFRP Composite Cross-Arm with the Influence of Outdoor Temperature. *Fibers and Polymers*.

Allen, H. G. (2013). *Analysis and Design of Structural Sandwich Panels: The Commonwealth and International Library: Structures and Solid Body Mechanics*

Division.

Alsubari, S., Zuhri, M. Y. M., Sapuan, S. M., Ishak, M. R., Ilyas, R. A., & Asyraf, M. R. M. (2021). Potential of Natural Fiber Reinforced Polymer Composites in Sandwich Structures: A Review on Its Mechanical Properties. *Polymers*, *13*(3), 423.

Amaro, A. M., Reis, P. N. B., de Moura, M., & Santos, J. B. (2012). Influence of the specimen thickness on low velocity impact behavior of composites. *Journal of Polymer Engineering*, *32*(1).

An, L., Wang, Z., Wang, G. G., & Li, Z. (2010). Design optimization of base widths of transmission tower using mode-pursuing sampling global optimization method. *ICCASM 2010 - 2010 International Conference on Computer Application and System Modeling, Proceedings*, *8*.

Anand, A., Banerjee, P., Prusty, R. K., & Chandra Ray, B. (2018). Lifetime Prediction of Nano-Silica based Glass Fibre/Epoxy composite by Time Temperature Superposition Principle. *IOP Conference Series: Materials Science and Engineering*, *338*(1).

Andreotti, A., Araneo, R., Mahmood, F., & Pierno, A. (2020). An accurate approach for the evaluation of the performance of overhead distribution lines due to indirect lightning. *Electric Power Systems Research*, *186*.

Ang, M. H., Wang Wei, & Low Teck-Seng. (2002). *On the estimation of the large deflection of a cantilever beam*. 1604–1609.

Antonucci, V., Caputo, F., Ferraro, P., Langella, A., Lopresto, V., Pagliarulo, V., Ricciardi, M. R., Riccio, A., & Toscano, C. (2016). Low velocity impact response of carbon fiber laminates fabricated by pulsed infusion: A review of damage investigation and semi-empirical models validation. *Progress in Aerospace Sciences*, *81*, 26–40.

Arnandha, Y., Satyarno, I., Awaludin, A., Irawati, I. S., Prasetya, Y., Prayitno, D. A., Winata, D. C., Satrio, M. H., & Amalia, A. (2017). Physical and Mechanical Properties of WPC Board from Sengon Sawdust and Recycled HDPE Plastic. *Procedia Engineering*, *171*, 695–704.

Ashraf, W., Ishak, M. R., Zuhri, M. Y. M., Yidris, N., Yaacob, A. M. B., & Asyraf, M. R. M. (2019). Investigation of different facesheet materials on compression properties of honeycomb sandwich composite. *Seminar Enau Kebangsaan*, *March*, 129–132.

Ashraf, W., Nawab, Y., Umair, M., Shaker, K., & Karahan, M. (2017). Investigation of mechanical behavior of woven/knitted hybrid composites. *Journal of the Textile Institute*, *108*(9), 1510–1517.

Asi, O. (2009). Effect of different woven linear densities on the bearing strength behaviour of glass fiber reinforced epoxy composites pinned joints. *Composite Structures*, *90*(1), 43–52.

ASTM-D2990. (2017). Standard Test Methods for Tensile, Compressive, and Flexural Creep and Creep- Rupture of Plastics. *Annual Book of ASTM Standards*, *i*, 1–20.

ASTM C393/C393M. (2020). Standard Test Method for Core Shear Properties of

Sandwich Constructions by Beam Flexure. In *ASTM Volume 15.03: Space Simulation; Aerospace And Aircraft; Composite Materials* (p. 8).

ASTM International. (2009). ASTM D 7250/D 7250M Standard Practice for Determining Sandwich Beam Flexural and Shear Stiffness. *Annual Book of ASTM Standards*.

Asyraf, M. R. M., Ishak, M. ., Sapuan, S. M., & Yidris, N. (2021a). Utilization of Bracing Arms as Additional Reinforcement in Pultruded Glass Fiber-Reinforced Polymer Composite Cross-Arms: Creep Experimental and Numerical Analyses. *Polymers*, *13*(4), 620.

Asyraf, M. R. M., Ishak, M. R., Norrrahim, M. N. F., Nurazzi, N. M., Shazleen, S. S., Ilyas, R. A., Rafidah, M., & Razman, M. R. (2021). Recent advances of thermal properties of sugar palm lignocellulosic fibre reinforced polymer composites. *International Journal of Biological Macromolecules*, *193*, 1587–1599.

Asyraf, M. R. M., Ishak, M. R., Sapuan, S. M., & Yidris, N. (2021b). Comparison of Static and Long-term Creep Behaviors between Balau Wood and Glass Fiber Reinforced Polymer Composite for Cross-arm Application. *Fibers and Polymers*, *22*(3), 793–803.

Asyraf, M. R. M., Ishak, M. R., Sapuan, S. M., & Yidris, N. (2021c). Influence of additional bracing arms as reinforcement members inwooden timber cross-arms on their long-term creep responses and properties. *Applied Sciences (Switzerland), 11*(5), 1–16.

Asyraf, M. R. M., Ishak, M. R., Sapuan, S. M., & Yidris, N. (2021d). Utilization of Bracing Arms as Additional Reinforcement in Pultruded Glass Fiber-Reinforced Polymer Composite Cross-Arms: Creep Experimental and Numerical Analyses. *Polymers*.

Asyraf, M. R. M., Ishak, M. R., Sapuan, S. M., Yidris, N., & Ilyas, R. A. (2020). Woods and composites cantilever beam: A comprehensive review of experimental and numerical creep methodologies. In *Journal of Materials Research and Technology* (Vol. 9, Issue 3, pp. 6759–6776).

Asyraf, M. R. M., Ishak, M. R., Sapuan, S. M., Yidris, N., Rafidah, M., Ilyas, R. A., & Razman, M. R. (2020). Potential application of green composites for cross arm component in transmission tower: A brief review. *International Journal of Polymer Science*.

Asyraf, M. R. M., Ishak, M. R., Syamsir, A., Amir, A. L., Nurazzi, N. M., Norrrahim, M. N. F., Asrofi, M., Rafidah, M., Ilyas, R. A., Rashid, M. Z. A., & Razman, M. R. (2023). Filament-wound glass-fibre reinforced polymer composites: Potential applications for cross arm structure in transmission towers. *Polymer Bulletin*, *80*(2), 1059–1084.

Asyraf, M. R. M., Rafidah, M., Madenci, E., Özkılıç, Y. O., Aksoylu, C., Razman, M. R., Ramli, Z., Zakaria, S. Z. S., & Khan, T. (2023). Creep Properties and Analysis of Cross Arms' Materials and Structures in Latticed Transmission Towers: Current Progress and Future Perspectives. *Materials*, *16*(4).

Azammi, A. M. N., Sapuan, S. M., Ishak, M. R., & Sultan, M. T. H. (2018). Conceptual design of automobile engine rubber mounting composite using TRIZ-Morphological chart-analytic network process technique. *Defence Technology*, *14*(4), 268–277.

Azwa, Z. N., Yousif, B. F., Manalo, A. C., & Karunasena, W. (2013). A review on the degradability of polymeric composites based on natural fibres. *Materials and Design*, *47*, 424–442.

B. Burkhardt, G. Baettig, G.P. Terrasi, K. O. Papailiou, & F. Schmuck. (2003). New Solutions With Composite Insulators And Composite Structures For Compact Lines. *C I R E D*, *17th Inter*(54), 12–15.

Bai, R., Ou, H., Peng, K., Wu, W., Lei, Z., Liu, T., Chen, M., Song, L., & Lin, R. (2020). Failure study of honeycomb sandwich structure with embedded part under axial pullout loading. *Thin-Walled Structures*, *146*, 106489.

Bai, Y., Zhang, J., & Shen, H. (2021). Residual compressive load-carrying capacity of cross-laminated timber walls after exposed to one-side fire. *Journal of Building Engineering*, *34*.

Bakar, M. S. A., Mohamad, D., Ishak, Z. A. M., Yusof, Z. M., & Salwi, N. (2018). Durability control of moisture degradation in GFRP cross arm transmission line towers. *AIP Conference Proceedings*, *2031*.

Bakis, C. E., Bank, L. C., Brown, V. L., Cosenza, E., Davalos, J. F., Lesko, J. J., Machida, A., Rizkalla, S. H., & Triantafillou, T. C. (2003). Fiber-Reinforced Polymer Composites for Construction - State-of-the-Art Review. *Perspectives in Civil Engineering: Commemorating the 150th Anniversary of the American Society of Civil Engineers*, 369–383.

Bandaru, A. K., Vetiyatil, L., & Ahmad, S. (2015). The effect of hybridization on the ballistic impact behavior of hybrid composite armors. *Composites Part B: Engineering*, *76*, 300–319.

Bank, L. C. (1989a). Flexural and shear moduli of full-section fiber reinforced plastic (FRP) pultruded beams. *Journal of Testing and Evaluation*, *17*(1), 40–45.

Bank, L. C. (1989b). Properties of pultruded fiber reinforced plastic structural members. *Transportation Research Record*, *1223*, 117–124.

Bank, L. C. (2006). Composite for construction: Structural design with FRP materials. In *Technology & Engineering* (Illustrate, p. 560). John Wiley & Sons, 2006.

Bank, L. C. (2007). Composites for Construction: Structural Design with FRP Materials. In *Composites for Construction: Structural Design with FRP Materials*.

Bank, L. C., & Mosallam, A. S. (1992). Creep and failure of a full-size fiber-reinforced plastic pultruded frame. *Composites Engineering*, *2*(3).

Barbero, E., Fernández-Sáez, J., & Navarro, C. (2000). Statistical analysis of the mechanical properties of composite materials. *Composites Part B: Engineering*, *31*(5), 375–381.

Barbero, E. J., Fu, S., & Raftoyiannis, I. (1991). Ultimate Bending Strength of Composite Beams. *Journal of Materials in Civil Engineering*, *3*(4), 292–306.

Barretta, R., & Luciano, R. (2014). Exact solutions of isotropic viscoelastic functionally graded Kirchhoff plates. *Composite Structures*, *118*(1), 448–454.

Barretta, R., Luciano, R., & Willis, J. R. (2015). On torsion of random composite beams. *Composite Structures*, *132*, 915–922.

Barten, H. J. (1944). On the deflection of a cantilever beam. *Quarterly of Applied Mathematics*, *2*(2), 168–171.

Beddu, S., Syamsir, A., Arifin, Z., & Ishak, M. (2018). Creep behavior of glass fibre reinforced polymer structures in crossarms transmission line towers. *AIP Conference Proceedings*, *020039*(November).

Beléndez, T., Neipp, C., & Beléndez, A. (2002). Large and small deflections of a cantilever beam. *European Journal of Physics*, *23*(3), 371–379.

Beléndez, T., Neipp, C., & Beléndez, A. (2003). Numerical and Experimental Analysis of a Cantilever Beam: A Laboratory Project to Introduce Geometric Nonlinearity in Mechanics of Materials. *International Journal of Engineering Education*, *19*(6), 885–892.

Betts, D., Sadeghian, P., & Fam, A. (2017). Tensile properties of flax FRP composites. *Proceedings of the 6th Asia-Pacific Conference on FRP in Structures, APFIS 2017*.

Betts, D., Sadeghian, P., & Fam, A. (2021). Experimental and analytical investigations of the flexural behavior of hollow ±55° filament wound GFRP tubes. *Thin-Walled Structures*, *159*.

Bhattacharya, S., Kalita, K., Čep, R., & Chakraborty, S. (2021). A comparative analysis on prediction performance of regression models during machining of composite materials. *Materials*, *14*(21).

Bhowmik, C., & Chakraborti, P. (2019). Study of Dynamics Characteristics of Composite Transmission Tower Using Carbon Fiber Epoxy (Thermoset) as Structural Material. *Advances in Modelling and Analysis C*, *74*(1), 22–26.

Bhudolia, S. K., Kam, K. K. C., & Joshi, S. C. (2018). Mechanical and vibration response of insulated hybrid composites. *Journal of Industrial Textiles*, *47*(8), 1887–1907.

Birman, V., & Kardomateas, G. A. (2018). Review of current trends in research and applications of sandwich structures. *Composites Part B: Engineering*, *142*, 221–240.

Bisshopp, K. E., & Drucker, D. C. (1945). Large deflection of cantilever beams. *Quarterly of Applied Mathematics*, *3*(3), 272–275.

Bozkurt, Ö. Y., Bulut, M., Erkliğ, A., & Faydh, W. A. (2019). Axial and lateral buckling analysis of fiber reinforced S-glass/epoxy composites containing nano-clay particles. *Composites Part B: Engineering*, *158*, 82–91.

Bulut, M., Erkliğ, A., Alsaadi, M., & Kchany, S. (2017). Effects of stacking sequence on mechanical properties of hybrid composites reinforced with carbon, Kevlar and S-glass fibers. *Materialpruefung/Materials Testing*, *59*(5), 472–479.

Burnley, L., & Correia, G. (2019). Manipulating Fiber Orientation for the Reduction of Warpage in Carbon Fiber Composite Sandwich Panels. *California Polytechnic State University, San Luis Obispo*, 10-undefined.

Campbell, D. B. (1970). Unbalanced Tensions in Transmission Lines. *Journal of the Structural Division*, *96*(10), 2189–2207.

Cantwell, W. J., Scudamore, R., Ratcliffe, J., & Davies, P. (1999). Interfacial fracture in sandwich laminates. *Composites Science and Technology*, *59*(14), 2079–2085.

Cao, L., Guo, L., & Dhanasekar, M. (2020). Development of a new outer sleeve assembly for beam-column connections. *Journal of Constructional Steel Research*, *164*, 105769.

Cardoso, D. C. T., & Harries, K. A. (2019). A viscoelastic model for time-dependent behavior of pultruded GFRP. *Construction and Building Materials*, *208*, 63–74.

Cascini, G., Rissone, P., Rotini, F., & Russo, D. (2011). Systematic design through the integration of TRIZ and optimization tools. *Procedia Engineering*, *9*, 674–679.

Chang, B., Wang, Z., & Bi, G. (2024). Study on the Energy Absorption Characteristics of Different Composite Honeycomb Sandwich Structures under Impact Energy. *Applied Sciences (Switzerland)*, *14*(7).

Chen, A., Zang, W., & Li, L. (2023). Shear Strength of Honeycomb Sandwich Panel with Impact Damage. *Journal of Physics: Conference Series*, *2541*(1).

Chen, L. (2010). An integral approach for large deflection cantilever beams. *International Journal of Non-Linear Mechanics*, *45*(3), 301–305.

Chengal wood technical informations. (2019). Malaysian Timber Council.

Composite Materials Handbook, Volume 6. Structural Sandwich Composites. (2013). SAE International.

Cordin, M., Bechtold, T., & Pham, T. (2018). Effect of fibre orientation on the mechanical properties of polypropylene–lyocell composites. *Cellulose*, *25*(12), 7197–7210.

Corradi, M., Vo, T. P., Poologanathan, K., & Osofero, A. I. (2018). Flexural behaviour of hardwood and softwood beams with mechanically connected GFRP plates. *Composite Structures*, *206*, 610–620.

Correia, J. R., Branco, F. A., & Ferreira, J. G. (2007). Flexural behaviour of GFRP-concrete hybrid beams with interconnection slip. *Composite Structures*, *77*(1), 66–78.

Cowin, S. C. (2001). Mechanics of materials. In *Bone Mechanics Handbook, Second Edition*.

D'Alessandro, V., Petrone, G., Franco, F., & De Rosa, S. (2013). A review of the vibroacoustics of sandwich panels: Models and experiments. *Journal of Sandwich Structures and Materials*, *15*(5), 541–582.

D'Antino, T., & Pisani, M. A. (2019). Long-term behavior of GFRP reinforcing bars. *Composite Structures*, *227*.

Daconti, J. R., & Lawry, D. C. (2003). Increasing Power Transfer Capability of Existing Transmission Lines. *Proceedings of the IEEE Power Engineering Society Transmission and Distribution Conference*, *3*, 1004–1009.

Davalos, J. F., Qiao, P., Frank Xu, X., Robinson, J., & Barth, K. E. (2001). Modeling and characterization of fiber-reinforced plastic honeycomb sandwich panels for highway bridge applications. *Composite Structures*, *52*(3–4), 441–452.

Dawood, M., Taylor, E., Ballew, W., & Rizkalla, S. (2010). Static and fatigue bending behavior of pultruded GFRP sandwich panels with through-Thickness fiber insertions. *Composites Part B: Engineering*, *41*(5), 363–374.

De Bona, F., & Zelenika, S. (1997). A generalized elastica-type approach to the analysis of large displacements of spring-strips. *Proceedings of the Institution of Mechanical Engineers, Part C: Journal of Mechanical Engineering Science*, *211*(7), 509–517.

Demirci, M. (2020). Investigation of the usability of MWCNTs Filled GFR/aluminum honeycomb sandwich composites for automotive vehicles. *International Journal of Automotive Engineering and Technologies*, *9*(3), 138–153.

Deogonda, P., & Chalwa, V. N. (2013). Mechanical Property of Glass Fiber Reinforcement Epoxy Composites. *International Journal of Scientific Engineering and Research (IJSER)*, *1*(4), 6–9.

Du, Y., Yan, N., & Kortschot, M. T. (2012). Light-weight honeycomb core sandwich panels containing biofiber-reinforced thermoset polymer composite skins: Fabrication and evaluation. *Composites Part B: Engineering*, *43*(7), 2875–2882.

Du, Y., Yan, N., & Kortschot, M. T. (2013). An experimental study of creep behavior of lightweight natural fiber-reinforced polymer composite/honeycomb core sandwich panels. *Composite Structures*, *106*, 160–166.

Dunlop, R. D., Gutman, R., & Marchenko, P. P. (1978). *Analytical Development of Loadability Characteristics for Ehv and Uhv Transmission Lines.*

Engineering Department of TNB Transmission Division. (2013). *Investigation report on wooden crossarm failure at 132kV KKSR-PPAN L2*.

Estep, D. D., GangaRao, H. V. S., Dittenber, D. B., & Qureshi, M. A. (2016). Response of pultruded glass composite box beams under bending and shear. *Composites Part B: Engineering*, *88*, 150–161.

Fagerberg, L., & Zenkert, D. (2005). Imperfection-induced wrinkling material failure in sandwich panels. *Journal of Sandwich Structures and Materials*, *7*(3), 195–219.

Fam, A., Sharaf, T., & Sadeghian, P. (2016). Fiber Element Model of Sandwich Panels with Soft Cores and Composite Skins in Bending Considering Large Shear Deformations and Localized Skin Wrinkling. *Journal of Engineering Mechanics*, *142*(5).

Farooq, U., Ahmad, M. S., Rakha, S. A., Ali, N., Khurram, A. A., & Subhani, T. (2017). Interfacial Mechanical Performance of Composite Honeycomb Sandwich Panels for Aerospace Applications. *Arabian Journal for Science and Engineering*, *42*(5), 1775–1782.

Ferdous, W., Manalo, A., & Aravinthan, T. (2017). Effect of beam orientation on the static behaviour of phenolic core sandwich composites with different shear span-to-depth ratios. *Composite Structures*, *168*, 292–304.

Feynman, R. P. (1964). Feynman lectures on physics. Volume 2: Mainly electromagnetism and matter. In *American Journal of Physics* (2nd Printi, Vol. 33, p. 750). Addison-Wesley Pub (Sd).

Findley, W. N. (1944). Creep characteristics of plastics. *In Symposium on Plastics, ASTM*, 118–134.

Findley, W. N., Lai, J. S., Onaran, K., & Christensen, R. M. (1977). Creep and Relaxation of Nonlinear Viscoelastic Materials With an Introduction to Linear Viscoelasticity. In *Journal of Applied Mechanics* (Vol. 44, Issue 2).

Fiorineschi, L., Frillici, F. S., & Rotini, F. (2018). Enhancing functional decomposition and morphology with TRIZ: Literature review. *Computers in Industry*, *94*, 1–15.

Fleming, J. F., & Pohlman, J. C. (1977). Longitudinal load analysis of transmission line systems. *IEEE Transactions on Power Apparatus and Systems*, *96*(5), 1657–1665.

Fotouhi, M., Jalalvand, M., & Wisnom, M. R. (2017). High performance quasi-isotropic thin-ply carbon/glass hybrid composites with pseudo-ductile behaviour in all fibre orientations. *Composites Science and Technology*, *152*, 101–110.

François-Heude, A., Richaud, E., Desnoux, E., & Colin, X. (2014). Influence of temperature, UV-light wavelength and intensity on polypropylene photothermal oxidation. *Polymer Degradation and Stability*, *100*(1), 10–20.

Fu, H., Dun, M., Wang, H., Wang, W., Ou, R., Wang, Y., Liu, T., & Wang, Q. (2020). Creep response of wood flour-high-density polyethylene/laminated veneer lumber coextruded composites. *Construction and Building Materials*, *237*.

Fu, Y., & Sadeghian, P. (2020). Flexural and shear characteristics of bio-based sandwich beams made of hollow and foam-filled paper honeycomb cores and flax fiber composite skins. *Thin-Walled Structures*, *153*.

G. Navas, H. V. (2013). TRIZ: Design Problem Solving with Systematic Innovation. In *Advances in Industrial Design Engineering*. InTech.

Gan, Y., Zhang, H., Šavija, B., Schlangen, E., & van Breugel, K. (2018). Static and fatigue tests on cementitious cantilever beams using nanoindenter. *Micromachines*, *9*(12).

Garrido, M., Correia, J. R., & Keller, T. (2016). Effect of service temperature on the shear creep response of rigid polyurethane foam used in composite sandwich floor panels. *Construction and Building Materials*, *118*, 235–244.

Genedy, M., Daghash, S., Soliman, E., & Reda Taha, M. M. (2015). Improving fatigue performance of GFRP composite using Carbon Nanotubes. *Fibers*, *3*(1), 13–29.

Ghani, J. A., Natasha, A. R., Hassan, C. H. C., & Syarif, J. (2016). TRIZ approach for machining process innovation in cryogenic environment. *International Journal of Materials and Product Technology*, *53*(3/4), 286.

Godara, A., & Raabe, D. (2007). Influence of fiber orientation on global mechanical behavior and mesoscale strain localization in a short glass-fiber-reinforced epoxy polymer composite during tensile deformation investigated using digital image correlation. *Composites Science and Technology*, *67*(11–12), 2417–2427.

Grove, S. M., Popham, E., & Miles, M. E. (2006). An investigation of the skin/core bond in honeycomb sandwich structures using statistical experimentation techniques. *Composites Part A: Applied Science and Manufacturing*, *37*(5), 804–812.

Grzybowski, S., Talabathula, S., & Ward, R. (2012). Added critical flashover voltage by fiberglass crossarm to 15 kV polymer suspension insulator. *Conference Record of IEEE International Symposium on Electrical Insulation*, 404–408.

Güden, M., & Kavi, H. (2006). Quasi-static axial compression behavior of constraint hexagonal and square-packed empty and aluminum foam-filled aluminum multi-tubes. *Thin-Walled Structures*, *44*(7), 739–750.

Hashim, M. K. R., Majid, M. S. A., Jamir, M. R. M., Kasim, F. H., & Sultan, M. T. H. (2021). The effect of stacking sequence and ply orientation on the mechanical properties of pineapple leaf fibre (Palf)/carbon hybrid laminate composites. *Polymers*, *13*(3), 1–24.

He, P., Dong, Y., Yan, Y., Li, J., & Lu, Z. (2021). Research on Monitoring System of Transmission Tower Operation State Based on Multi-Sensor Data Fusion. *Journal of Physics: Conference Series*, *2143*(1).

Hegde, S. R., & Hojjati, M. (2019). Effect of core and facesheet thickness on mechanical property of composite sandwich structures subjected to thermal fatigue. *International Journal of Fatigue*, *127*, 16–24.

Ho, W. (2008). Integrated analytic hierarchy process and its applications - A literature review. *European Journal of Operational Research*, *186*(1), 211–228.

Hu, Y., Li, X., Lang, A. W., Zhang, Y., & Nutt, S. R. (2016). Water immersion aging of polydicyclopentadiene resin and glass fiber composites. *Polymer Degradation and Stability*, *124*, 35–42.

Huang, X., Zhao, Y., Zhao, L., & Yang, L. (2018). A method for settlement detection of the transmission line tower under wind force. *Sensors (Switzerland)*, *18*(12).

Hunt, J. F., Zhang, H., & Huang, Y. (2015). Analysis of cantilever-beam bending stress relaxation properties of thin wood composites. *BioResources*, *10*(2), 3131–3145.

Hussein, R. D., Ruan, D., Lu, G., Guillow, S., & Yoon, J. W. (2017). Crushing response of square aluminium tubes filled with polyurethane foam and aluminium honeycomb. *Thin-Walled Structures*, *110*, 140–154.

Hussein, R. D., Ruan, D., Lu, G., & Sbarski, I. (2016). Axial crushing behaviour of honeycomb-filled square carbon fibre reinforced plastic (CFRP) tubes. *Composite Structures*, *140*, 166–179.

Ilyas, R. A., Aisyah, H. A., Nordin, A. H., Ngadi, N., Zuhri, M. Y. M., Asyraf, M. R. M., Sapuan, S. M., Zainudin, E. S., Sharma, S., Abral, H., Asrofi, M., Syafri, E., Sari, N. H., Rafidah, M., Zakaria, S. Z. S., Razman, M. R., Majid, N. A., Ramli, Z., Azmi, A., … Ibrahim, R. (2022). Natural-Fiber-Reinforced Chitosan, Chitosan Blends and Their Nanocomposites for Various Advanced Applications. *Polymers*, *14*(5), 874.

Ilyas, R. A., Sapuan, S. M., Norrrahim, M. N. F., Yasim-Anuar, T. A. T., Kadier, A., Kalil, M. S., Atikah, M. S. N., Ibrahim, R., Asrofi, M., Abral, H., Nazrin, A., Syafiq, R., Aisyah, H. A., & Asyraf, M. R. M. (2021). Nanocellulose/starch biopolymer nanocomposites: Processing, manufacturing, and applications. In F. M. Al-Oqla (Ed.), *Advanced Processing, Properties, and Application of Strach and Other Bio-based Polymer* (1st ed.). Elsevier Inc.

Ishak, M. R., Sapuan, S. M., Leman, Z., Rahman, M. Z. A., & Anwar, U. M. K. (2012). Characterization of sugar palm (Arenga pinnata) fibres Tensile and thermal properties. *Journal of Thermal Analysis and Calorimetry*, *109*(2), 981–989.

Izumi, K., Takahashi, T., Homma, H., & Kuroyagi, T. (2000). Development of line post type polymer insulation arm for 154 kV. *IEEE Transactions on Power Delivery*, *15*(4), 1304–1310.

Jaafar, C. N. A., Rizal, M. A. M., & Zainol, I. (2018). Effect of kenaf alkalization treatment on morphological and mechanical properties of epoxy/silica/kenaf composite. *International Journal of Engineering and Technology(UAE)*, *7*(4), 258–263.

Jama-Rodzeńska, A., Białowiec, A., Koziel, J. A., & Sowiński, J. (2021). Waste to phosphorus: A transdisciplinary solution to P recovery from wastewater based on the TRIZ approach. *Journal of Environmental Management*, *287*.

Jannat Alipour, H., Aminnejad, S., & Jazaeri, M. (2007). Decreasing the right of way of transmission lines by using towers with polymer insulation arms. *POWERENG 2007 - International Conference on Power Engineering - Energy and Electrical Drives Proceedings*, 571–576.

Ji, M., Guo, Y., Han, X., Fu, Y., Kang, J., & Wei, Q. (2022). Dynamic cushioning energy absorption of paper composite sandwich structures with corrugation and honeycomb cores under drop impact. *Journal of Sandwich Structures and Materials*, *24*(2), 1270–1286.

Jiang, M., Cong, X., Yi, X., Liu, X., & Rudd, C. (2022). A stochastic overlap network model of electrical properties for conductive weft yarn composites and their experimental study. *Composites Science and Technology*, *217*.

Jiang, M., Hu, Y., Rudd, C., Cao, Z., Liu, X., & Yi, X. (2023). Simultaneously improving electrical properties and interlaminar fracture toughness: A novel multifunctional composite based on Inter-Woven Wire Fabric. *Composites Communications*, 101563.

Johari, A. N., Ishak, M. R., Leman, Z., Yusoff, M. Z. M., & Asyraf, M. R. M. (2020a). Creep Behaviour Monitoring of Short-term Duration for Fiber-glass Reinforced

Composite Cross-arms with Unsaturated Polyester Resin Samples Using Conventional Analysis. *Journal of Mechanical Engineering and Sciences*, *14*(3).

Johari, A. N., Ishak, M. R., Leman, Z., Yusoff, M. Z. M., & Asyraf, M. R. M. (2020b). Influence of CaCO3 in pultruded glass fiber/unsaturated polyester resin composite on flexural creep behavior using conventional and time-temperature superposition principle methods. *Polimery/Polymers*, *65*(11–12), 792–800.

Joseph, C., Muthukumar, C., Ng, L. F., Subramanian, J., Ramesh, C., Krishnasamy, S., & Thiagamani, S. M. K. (2023). The effect of nanoclay on the performance of basalt-epoxy facesheet and foam core sandwich panels. *Journal of Sandwich Structures and Materials*, *25*(7), 730–746.

Kamarudin, S. A., Usman, F., Omar, R. C., & Yatim, M. Y. M. (2018). Analysis and optimization of 275 kV transmission tower by using linear static analysis and P-delta analysis. *International Journal of Engineering and Technology(UAE)*, *7*(4), 734–738.

Kang, W., Albermani, F., Kitipornchai, S., & Lam, H. F. (2007). Modeling and analysis of lattice towers with more accurate models. *Advanced Steel Construction*, *3*(2), 565–582.

Karahan, M. (2008). Comparison of Ballistic Performance and Energy Absorption Capabilities of Woven and Unidirectional Aramid Fabrics. *Textile Research Journal*, *78*(8), 718–730.

Kasiviswanathan, S., Santhanam, K., & Kumaravel, A. (2015). Evaluation of mechanical properties of natural hybrid fibers, reinforced polyester composite materials. *Carbon - Science and Technology*, *7*(4), 43–49.

Kelkar, A. D., Tate, J. S., & Chaphalkar, P. (2006). Performance evaluation of VARTM manufactured textile composites for the aerospace and defense applications. *Materials Science and Engineering B: Solid-State Materials for Advanced Technology*, *132*(1–2), 126–128.

Khalili, S., Khalili, S. M. R., Farsani, R. E., & Mahajan, P. (2020). Flexural properties of sandwich composite panels with glass laminate aluminum reinforced epoxy facesheets strengthened by SMA wires. *Polymer Testing*, *89*.

Kharratzadeh, M., Shokrieh, M. M., & Salamat-talab, M. (2018). Effect of interface fiber angle on the mode I delamination growth of plain woven glass fiber-reinforced composites. *Theoretical and Applied Fracture Mechanics*, *98*, 1–12.

Kim, K. Y., Park, J., & Sohmshetty, R. (2017). Prediction measurement with mean acceptable error for proper inconsistency in noisy weldability prediction data. *Robotics and Computer-Integrated Manufacturing*, *43*, 18–29.

Kishore, T. S., & Singal, S. K. (2014). Optimal economic planning of power transmission lines: A review. *Renewable and Sustainable Energy Reviews*, *39*, 949–974.

Klasson, A., Crocetti, R., Björnsson, I., & Frühwald Hansson, E. (2018). Design for lateral stability of slender timber beams considering slip in the lateral bracing system. *Structures*, *16*, 157–163.

Koehler, F., & Swingler, J. (2018). Practical model for tower earthing systems in lightning simulations. *Electric Power Systems Research*, *158*, 306–314.

Koohbor, B., Mallon, S., Kidane, A., & Sutton, M. A. (2014). A DIC-based study of in-plane mechanical response and fracture of orthotropic carbon fiber reinforced composite. *Composites Part B: Engineering*, *66*, 388–399.

Koohbor, B., Ravindran, S., & Kidane, A. (2015). Meso-scale strain localization and failure response of an orthotropic woven glass-fiber reinforced composite. *Composites Part B: Engineering*, *78*, 308–318.

Kremer, G. O., Chiu, M.-C., Lin, C.-Y., Gupta, S., Claudio, D., & Thevenot, H. (2012). Application of axiomatic design, TRIZ, and mixed integer programming to develop innovative designs: a locomotive ballast arrangement case study. *The International Journal of Advanced Manufacturing Technology*, *61*(5–8), 827–842.

Labuda, I. (2015). Possibilities of applying TRIZ methodology elements (the 40 Inventive Principles) in the process of architectural design. *Procedia Engineering*, *131*, 476–499.

Lala, S. Das, Deoghare, A. B., & Chatterjee, S. (2018). Effect of reinforcements on polymer matrix bio-composites - An overview. *IEEE Journal of Selected Topics in Quantum Electronics*, *25*(6), 1039–1058.

Lee, M. K., & Barr, B. I. G. (2004). An overview of the fatigue behaviour of plain and fibre reinforced concrete. *Cement and Concrete Composites*, *26*(4), 299–305.

Lee, S. M., & Tsotsis, T. K. (2000). Indentation failure behavior of honeycomb sandwich panels. *Composites Science and Technology*, *60*(8), 1147–1159.

Ley, R. P., Lin, W., & Mbanefo, U. (1999). *NASA/CR-1999-208994 Facesheet Wrinkling In Sandwich Structures*.

Li, G., Liu, W., Joseph, T., Liang, J., & Song, Z. (2020). Double-Thyristor-Based Protection for Valve-Side Single-Phase-to-Ground Faults in HB-MMC-Based Bipolar HVDC Systems. *IEEE Transactions on Industrial Electronics*, *67*(7), 5810–5815.

Li, M., Liu, R. Q., Luo, C. J., Guo, H. W., & Ding, B. C. (2013). Numerical and experimental analyses on series aluminum honeycomb structures under quasi-static load. *Zhendong Yu Chongji/Journal of Vibration and Shock*, *32*(9), 50–56.

Li, P. Y., Chen, B., Xie, W. P., & Xiao, X. (2015). A comparative study on frequency sensitivity of a transmission tower. *Journal of Sensors*, *2015*.

Li, X., Liu, W., Fang, H., Huo, R., & Wu, P. (2019). Flexural creep behavior and life prediction of GFRP-balsa sandwich beams. *Composite Structures*, *224*.

Liang, H., Yan, X., & Liu, C. (2023). Optimization of Local Joint Design for Cup-Type Angle Steel Transmission Tower. *Advances in Transdisciplinary Engineering*, *43*, 1350–1357.

Liang, Z., Yake, T., Chen, C., Kai, N., & Haowei, P. (2023). Capacity Assessment of a

Transmission Tower Considering the Wind-Ice Probability Distributions. *Journal of Physics: Conference Series*, *2445*(1).

Lindsey, K. E. (1978). Mathematical theory of longitudinally loaded elastic-plastic transmission lines — statics. *IEEE Transactions on Power Apparatus and Systems*, *PAS-97*(2), 574–582.

Liu, G., & Li, H. (2009). A new framework for evaluating along-wind responses of a transmission tower. *Earthquake Engineering and Engineering Vibration*, *8*(1), 87–93.

Liu, Q., & Hughes, M. (2008). The fracture behaviour and toughness of woven flax fibre reinforced epoxy composites. *Composites Part A: Applied Science and Manufacturing*, *39*(10), 1644–1652.

Liu, Q., Xu, X., Ma, J., Wang, J., Shi, Y., & Hui, D. (2017). Lateral crushing and bending responses of CFRP square tube filled with aluminum honeycomb. *Composites Part B: Engineering*, *118*, 104–115.

Liu, T. Q., Liu, X., & Feng, P. (2020). A comprehensive review on mechanical properties of pultruded FRP composites subjected to long-term environmental effects. *Composites Part B: Engineering*, *191*.

Liu, T., Vieira, J. D., & Harries, K. A. (2020). Predicting Flange Local Buckling Capacity of Pultruded GFRP I-Sections Subject to Flexure. *Journal of Composites for Construction*, *24*(4), 04020025.

Liu, W., Feng, P., & Huang, J. (2017). Bilinear softening model and double K fracture criterion for quasi-brittle fracture of pultruded FRP composites. *Composite Structures*, *160*, 1119–1125.

Liu, Y., Li, X., Zheng, X., & Song, Z. (2020). Experimental study on seismic response of precast bridge piers with double-grouted sleeve connections. *Engineering Structures*, *221*, 111023.

Liu, Y., You, J., Du, H., Chang, S., & Xu, S. (2022). A New Positioning Method for Climbing Robots Based on 3D Model of Transmission Tower and Visual Sensor. *Sensors*, *22*(19).

Lomov, S. V., Boisse, P., Deluycker, E., Morestin, F., Vanclooster, K., Vandepitte, D., Verpoest, I., & Willems, A. (2008). Full-field strain measurements in textile deformability studies. *Composites Part A: Applied Science and Manufacturing*, *39*(8), 1232–1244.

Loni, S., Stefanou, I., & Valvo, P. S. (2013). Experimental study on the creep behavior of GFRP pultruded beams. *XXI Congressi AIMETA (Associazione Italiana Di Meccanica Teorica e Applicata)*, 1–10.

Lu, T., Solis-Ramos, E., Yi, Y. B., & Kumosa, M. (2016). Synergistic environmental degradation of glass reinforced polymer composites. *Polymer Degradation and Stability*, *131*, 1–8.

Luo, H., Chen, F., Wang, X., Dai, W., Xiong, Y., Yang, J., & Gong, R. (2019). A novel two-layer honeycomb sandwich structure absorber with high-performance microwave absorption. *Composites Part A: Applied Science and Manufacturing*, *119*, 1–7.

Ma, P., Jin, L., & Wu, L. (2019). Experimental and numerical comparisons of ballistic impact behaviors between 3D angle-interlock woven fabric and its reinforced composite. *Journal of Industrial Textiles*, *48*(6), 1044–1058.

Mak, K., Fam, A., & MacDougall, C. (2015). Flexural Behavior of Sandwich Panels with Bio-FRP Skins Made of Flax Fibers and Epoxidized Pine-Oil Resin. *Journal of Composites for Construction*, *19*(6).

Mallon, S., Koohbor, B., Kidane, A., & Sutton, M. A. (2015). Fracture Behavior of Prestressed Composites Subjected to Shock Loading: A DIC-Based Study. *Experimental Mechanics*, *55*(1), 211–225.

Mansor, M. R. R., Sapuan, S. M. M., Zainudin, E. S. S., Nuraini, A. A. A., & Hambali, A. (2014). Conceptual design of kenaf fiber polymer composite automotive parking brake lever using integrated TRIZ-Morphological Chart-Analytic Hierarchy Process method. *Materials and Design*, *54*, 473–482.

Marzuki, H. F. A., & Jaafar, M. (2016). Laminate Design of Lightweight Glass Fiber Reinforced Epoxy Composite for Electrical Transmission Structure. *Procedia Chemistry*, *19*, 871–878.

Mazani, N., Sapuan, S. M. M., Sanyang, M. L. L., Atiqah, A., & Ilyas, R. A. A. (2019). Design and Fabrication of a Shoe Shelf From Kenaf Fiber Reinforced Unsaturated Polyester Composites. In H. Ariffin, S. M. Sapuan, & M. A. Hassan (Eds.), *Lignocellulose for Future Bioeconomy* (1st ed., Issue 2000, pp. 315–332). Elsevier.

Mittelstedt, C. (2020). Buckling and post-buckling of thin-walled composite laminated beams-a review of engineering analysis methods. *Applied Mechanics Reviews*, *72*(2).

Mohamad, D., Beddu, S., Syamsir, A., Zahari, N. M., Abu Seman, S. A. H., Razali, M. F., Abas, A., & Ng, F. C. (2020). Performance Evaluation of Composite Cross-Arm Structure under Different Magnitude of Loading. *IOP Conference Series: Materials Science and Engineering*, *920*(1).

Mohamad, D., Beddu, S., Syamsir, A., Zahari, N. M., Razali, M. F., Abu Seman, S. A. H., Abas, A., & Ng, F. C. (2020). Failure analysis of various fiberglass cross-arm designs under multi-axial loading. *IOP Conference Series: Materials Science and Engineering*, *920*(1).

Mohamad, D., Syamsir, A., Beddu, S., Abas, A., Ng, F. C., Razali, M. F., & Seman, S. A. H. A. (2019). Numerical Study of Composite Fiberglass Cross Arms under Statics Loading and Improvement with Sleeve Installation. *IOP Conference Series: Materials Science and Engineering*, *530*(1).

Mohamad, D., Syamsir, A., Beddu, S., Kamal, N. L. M., Zainoodin, M. M., Razali, M. F., Abas, A., Seman, S. A. H. A., & Ng, F. C. (2019). Effect of Laminate Properties on the Failure of Cross Arm Structure under Multi-Axial Load. *IOP Conference Series: Materials Science and Engineering*, *530*(1).

Mohamad, D., Syamsir, A., Itam, Z., Bakar, H. A., Abas, A., Ng, F. C., Razali, M. F., & Seman, S. A. H. A. (2019). Numerical Simulation on the Statics Deformation Study of Composite Cross Arms of Different Materials and Configurations. *IOP Conference Series: Materials Science and Engineering*, *530*(1).

Mohamad, D., Syamsir, A., Sa'Don, S. N., Zahari, N. M., Seman, S. A. H. A., Razali, M. F., Abas, A., & Ng, F. C. (2019). Stacking Sequence Effects on Performance of Composite Laminate Structure Subjected to Multi-Axial Quasi-Static Loading. *IOP Conference Series: Materials Science and Engineering*, *530*(1).

Mohammadi, E., Hosseini, S. S., & AsgariMarnani, J. (2018). An Interactive Solution for Lateral-Torsional Buckling of the Mono-Symmetric Beam-Columns with Discrete Lateral Bracings. *Structures*, *14*, 164–177.

Mohammadi, E., Hosseini, S. S., & Rohanimanesh, M. S. (2016). Elastic lateral-torsional buckling strength and torsional bracing stiffness requirement for monosymmetric I-beams. *Thin-Walled Structures*, *104*, 116–125.

Mohd Nurazzi, N., Khalina, A., Sapuan, S. M., Dayang Laila, A. H. A. M., Rahmah, M., & Hanafee, Z. (2017). A review: Fibres, polymer matrices and composites. *Pertanika Journal of Science and Technology*, *25*(4), 1085–1102.

Mohebkhah, A., & Showkati, H. (2005). Bracing requirements for inelastic castellated beams. *Journal of Constructional Steel Research*, *61*(10), 1373–1386.

Mosallam, A. S., & Bank, L. C. (1992). Short-Term Behavior of Pultruded Fiber-Reinforced Plastic Frame. *Journal of Structural Engineering*, *118*(7), 1937–1954.

Mozer, J. D., Wood, W. A., & Hribar, J. A. (1981). Broken wire tests on a model transmission line system. *IEEE Transactions on Power Apparatus and Systems*, *PAS-100*(3), 938–947.

Nadhirah, A., Beddu, S., Mohamad, D., Zainoodin, M., Nabihah, S., Mubin, N., Agusril, Itam, Z., Mansor, H., Kamal, N. M., Alam, M. A., Muda, Z. C., Yusof, Z. M., Nasional, U. T., Yusof, Z. M., Berhad, T. N., & Sentral, B. D. (2017). Properties of fiberglass crossarm in transmission tower - a review. *International Journal of Applied Engineering Research*, *12*(24), 15228–15233.

Nallathambi, A. K., Lakshmana Rao, C., & Srinivasan, S. M. (2010). Large deflection of constant curvature cantilever beam under follower load. *International Journal of Mechanical Sciences*, *52*(3), 440–445.

Naresh, K., Cantwell, W. J., Khan, K. A., & Umer, R. (2021). Single and multi-layer core designs for Pseudo-Ductile failure in honeycomb sandwich structures. *Composite Structures*, *256*, 113059.

Niknejad, A., Abedi, M. M., Liaghat, G. H., & Zamani Nejad, M. (2012). Prediction of the mean folding force during the axial compression in foam-filled grooved tubes by theoretical analysis. *Materials and Design*, *37*, 144–151.

Ntuli, M., Xezile, R., Mbuli, N., Pretorius, J. H. C., & Motsoeneng, L. (2016). Increasing the capacity of transmission lines via current uprating: An updated review of benefits, considerations and developments. *Proceedings of the 2016 Australasian Universities*

Power Engineering Conference, AUPEC 2016.

Nurazzi, N. M., Khalina, A., Sapuan, S. M., Ilyas, R. A., Rafiqah, S. A., & Hanafee, Z. M. (2019). Thermal properties of treated sugar palm yarn/glass fiber reinforced unsaturated polyester hybrid composites. *Journal of Materials Research and Technology*, *December*.

Omrani, E., Menezes, P. L., & Rohatgi, P. K. (2016). State of the art on tribological behavior of polymer matrix composites reinforced with natural fibers in the green materials world. *Engineering Science and Technology, an International Journal*, *19*(2), 717–736.

Önder, A., & Robinson, M. (2020). Investigating the feasibility of a new testing method for GFRP/polymer foam sandwich composites used in railway passenger vehicles. *Composite Structures*, *233*.

P.K. Mallick. (2007). Fiber-reinforced composites. In *Materials, Manufacturing and Design* (Third Edit). Taylor & Francis.

Pai, Y., Pai K, D., & Kini, M. V. (2021). Effect of Aramid Fabric Orientation Angle on the Mechanical Characteristics of Basalt-Aramid/Epoxy Hybrid Interply Composites. *Materials Research*, *24*(5).

Pandita, S. D., Yuan, X., Manan, M. A., Lau, C. H., Subramanian, A. S., & Wei, J. (2014). Evaluation of jute/glass hybrid composite sandwich: Water resistance, impact properties and life cycle assessment. *Journal of Reinforced Plastics and Composites*, *33*(1), 14–25.

Papailiou, K. O. (1999). Composite insulators are gaining ground-25 years of Swiss experience. *1999 IEEE Transmission and Distribution Conference (Cat. No. 99CH36333)*, 827–833 vol.2.

Park, J. S., Stallings, J. M., & Kang, Y. J. (2004). Lateral-torsional buckling of prismatic beams with continuous top-flange bracing. *Journal of Constructional Steel Research*, *60*(2), 147–160.

Patel, P., & Chokshi, S. (2018). A Review of Fabrication Methods and Stacking Sequence Arrangements of Fiber for Composite. *International Journal of Current Engineering and Scientific Research (Ijcesr)*, *4*, 13–20.

Patil, H., & Jeyakarthikeyan, P. V. (2018). Mesh convergence study and estimation of discretization error of hub in clutch disc with integration of ANSYS. *IOP Conference Series: Materials Science and Engineering*, *402*(1).

Paul, S. K., & Sahu, P. (2020). Finite Element Analysis of Retrofitting of Rc Beam With CFRP Using Abaqus. *International Research Journal of Engineering and Technology (IRJET)*, *07*(02), 1268–1273.

Peesapati, V., Zachariades, C., Li, Q., Rowland, S. M., Cotton, I., Allison, F., & Chambers, D. (2012). 3D electric field computation of a composite cross-arm. *Conference Record of IEEE International Symposium on Electrical Insulation*, 464–468.

Pérez, C. J., Alvarez, V. A., & Vázquez, A. (2008). Creep behaviour of layered silicate/starch-polycaprolactone blends nanocomposites. *Materials Science and Engineering: A*, *480*(1–2), 259–265.

Petras, A., & Sutcliffe, M. P. F. (1999). Failure mode maps for honeycomb sandwich panels. *Composite Structures*, *44*(4), 237–252.

Petrone, G., Rao, S., De Rosa, S., Mace, B. R., Franco, F., & Bhattacharyya, D. (2013). Behaviour of fibre-reinforced honeycomb core under low velocity impact loading. *Composite Structures*, *100*, 356–362.

Plevris, N., & Triantafillou, T. C. (1995). Creep Behavior of FRP-Reinforced Wood Members. *Journal of Structural Engineering*, *121*(2), 174–186.

POSKITT, T. J. (1964). Abstract. Some Problems in the Structural Analysis of Overhead Electric Lines. *Proceedings of the Institution of Civil Engineers*, *28*(3), 397–404.

Prasad Rao, N., Samuel Knight, G. M., Mohan, S. J., & Lakshmanan, N. (2012). Studies on failure of transmission line towers in testing. *Engineering Structures*, *35*, 55–70.

Qi, Y., Fang, H., Shi, H., Liu, W., Qi, Y., & Bai, Y. (2017). Bending performance of GFRP-wood sandwich beams with lattice-web reinforcement in flatwise and sidewise directions. *Construction and Building Materials*, *156*, 532–545.

Qin, Q., & Wang, T. J. (2013). Low-velocity impact response of fully clamped metal foam core sandwich beam incorporating local denting effect. *Composite Structures*, *96*, 346–356.

Rao, N. P., Mohan, S. J., & Lakshmanan, N. (2005). A study on failure of cross arms in transmission line towers during prototype testing. *International Journal of Structural Stability and Dynamics*, *5*(3), 435–455.

Rawi, I. M., & Ab Kadir, M. Z. A. (2015). Investigation on the 132kV overhead lines lightning-related flashovers in Malaysia. *International Symposium on Lightning Protection, XIII SIPDA*, 239–243.

Rawi, I. M., Rahman, M. S. A., Kadir, M. Z. A. A., & Izadi, M. (2017). Wood and fiberglass crossarm performance against lightning strikes on transmission towers. *International Conference on Power Systems Transient (IPST)*.

Reis, P. N. B., Neto, M. A., & Amaro, A. M. (2018). Effect of the extreme conditions on the tensile impact strength of GFRP composites. *Composite Structures*, *188*, 48–54.

Riccio, A., Di Felice, G., Saputo, S., & Scaramuzzino, F. (2014). Stacking sequence effects on damage onset in composite laminate subjected to low velocity impact. *Procedia Engineering*, *88*, 222–229.

Richardson Jr, A. S. (1977). *Dynamic load model study for overhead transmission lines. Final report, January 1977--September 1977*.

Riezzo, M. A., Simmons, M., Russell, B., Sket, F., Martínez, V., & González, C. (2019). Dynamic characterisation of interlaminar fracture toughness in carbon fibre epoxy composite laminates. *Composites Part A: Applied Science and Manufacturing*, *126*.

Robert, V., & Lemelin, D. R. (2002). Flexural considerations in steel transmission tower design. *Proceedings of the Conference: Electrical Transmission in a New Age*, 148–155.

Roberts, T. M., & Al-Ubaidi, H. (2002). Flexural and Torsional Properties of Pultruded Fiber Reinforced Plastic I-Profiles. *Journal of Composites for Construction*, *6*(1), 28–34.

Rosato, D., & Rosato, D. (2003). Product Design. *Plastics Engineered Product Design*, 198–343.

Rosli, M. U., Ariffin, M. K. A., Sapuan, S. M., & Sulaiman, S. (2013). Integrated AHP-TRIZ innovation method for automotive door panel design. *International Journal of Engineering and Technology*, *5*(3), 3158–3167.

Roy, R., Park, S. J., Kweon, J. H., & Choi, J. H. (2014). Characterization of Nomex honeycomb core constituent material mechanical properties. *Composite Structures*, *117*(1), 255–266.

Rudo, D. N., & Karbhari, V. M. (1999). Physical behaviors of fiber reinforcement as applied to tooth stabilization. *Dental Clinics of North America*, *43*(1), 7–35, v.

S., A., & S., A. (2011). Modeling and Analysis of the Crankshaft using ANSYS Software. *International Journal of Computational Engineering Research*, *3*(5), 265–269.

Sá, M. F., Gomes, A. M., Correia, J. R., & Silvestre, N. (2011a). Creep behavior of pultruded GFRP elements - Part 1: Literature review and experimental study. *Composite Structures*, *93*(10), 2450–2459.

Sá, M. F., Gomes, A. M., Correia, J. R., & Silvestre, N. (2011b). Creep behavior of pultruded GFRP elements - Part 2: Analytical study. *Composite Structures*, *93*(9), 2409–2418.

Sá, M. F., Gomes, A. M., Correia, J. R., & Silvestre, N. (2016). Flexural creep response of pultruded GFRP deck panels: Proposal for obtaining full-section viscoelastic moduli and creep coefficients. *Composites Part B: Engineering*, *98*, 213–224.

San YT, Jin YT, L. S. (2011). *Systematic innovation inmanufacturing. Selangor*.

Santulli, C., Sarasini, F., Tirillò, J., Valente, T., Valente, M., Caruso, A. P., Infantino, M., Nisini, E., & Minak, G. (2013). Mechanical behaviour of jute cloth/wool felts hybrid laminates. *Materials and Design*, *50*, 309–321.

Sanyang, M. L., Sapuan, S. M., Jawaid, M., Ishak, M. R., & Sahari, J. (2016). Effect of sugar palm-derived cellulose reinforcement on the mechanical and water barrier properties of sugar palm starch biocomposite films. *BioResources*, *11*(2), 4134–4145.

Sapuan, S. M., Lok, H. Y., Ishak, M. R., & Misri, S. (2013). Mechanical properties of hybrid glass/sugar palm fibre reinforced unsaturated polyester composites. *Chinese Journal of Polymer Science (English Edition)*, *31*(10), 1394–1403.

Sarah Sulaiman, S., Md Khali, R., & Hamizah Aminudin, N. (2018). Legal Issues and Challenges in Regulating the Rights to Wayleave in Malaysia. *International Journal* *of Engineering & Technology*, *7*(3.30), 174.

Sathishkumar, T. P., Satheeshkumar, S., & Naveen, J. (2014). Glass fiber-reinforced polymer composites - A review. *Journal of Reinforced Plastics and Composites*, *33*(13), 1258–1275.

Sayahi, M., Sghaier, S., & Belhadjsalah, H. (2013). Finite element analysis of ball burnishing process: Comparisons between numerical results and experiments. *International Journal of Advanced Manufacturing Technology*, *67*(5–8), 1665–1673.

Sayyad, A. S., & Ghugal, Y. M. (2017). Bending, buckling and free vibration of laminated composite and sandwich beams: A critical review of literature. *Composite Structures*, *171*, 486–504.

Scott, D. W., & Zureick, A. H. (1998). Compression creep of a pultruded e-glass/vinylester composite. *Composites Science and Technology*, *58*(8), 1361–1369.

Segovia, F., Blanchet, P., Laghdir, A., & Cloutier, A. (2013). Mechanical behaviour of sugar maple in cantilever bending under constant and variable relative humidity conditions. *International Wood Products Journal*, *4*(4), 225–231.

Selvaraj. (2012). Structural evaluation of FRP Pultruded Sections in overhead transmission line Towers. *International Journal of Civil and Structural Engineering*, *2*(3).

Selvaraj, M. (2015). Structural Assessment of a 66 kV Overhead Power Transmission line tower built with Polymer Composite Material. *World Congress on Advances in Structural Engineering and Mechanics (ASEM15), Central Po*, 9.

Selvaraj, M., Kulkarni, S., & Babu, R. R. (2013). Analysis and experimental testing of a built-up composite cross arm in a transmission line tower for mechanical performance. *Composite Structures*, *96*, 1–7.

Selvaraj, M., Kulkarni, S. M., & Babu, R. R. (2012). Behavioral Analysis of built up transmission line tower from FRP pultruded sections. *International Journal of Emerging Technology and Advanced Engineering*, *2*(9).

Sezgin, F. E., Tanoğlu, M., Eğilmez, O. Ö., & Dönmez, C. (2010). Mechanical behavior of polypropylene-based honeycomb-core composite sandwich structures. *Journal of Reinforced Plastics and Composites*, *29*(10), 1569–1579.

Shao, Y., & Shanmugam, J. (2004). Deflection Creep of Pultruded Composite Sheet Piling. *Journal of Composites for Construction*, *8*(5), 471–479.

Sharaf, H. K., Ishak, M. R., Sapuan, S. M., & Yidris, N. (2020). Conceptual design of the cross-arm for the application in the transmission towers by using TRIZ–morphological chart–ANP methods. *Journal of Materials Research and Technology*, *9*(4), 9182–9188.

Sharaf, H. K., Ishak, M. R., Sapuan, S. M., Yidris, N., & Fattahi, A. (2020). Experimental and numerical investigation of the mechanical behavior of full-scale wooden cross arm in the transmission towers in terms of load-deflection test. *Journal of Materials Research and Technology*, *9*(4), 7937–7946.

Shariatinasab, R., Gholinezhad, J., Sheshyekani, K., & Alemi, M. R. (2016). The effect of wide band modeling of tower-footing grounding system on the lightning performance of transmission lines: A probabilistic evaluation. *Electric Power Systems Research*, *141*, 1–10.

Sheu, D. D., & Lee, H.-K. (2011). A proposed process for systematic innovation. *International Journal of Production Research*, *49*(3), 847–868.

Shi, S., Sun, Z., Hu, X., & Chen, H. (2014). Flexural strength and energy absorption of carbon-fiber-aluminum-honeycomb composite sandwich reinforced by aluminum grid. *Thin-Walled Structures*, *84*, 416–422.

Shibata, S., Cao, Y., & Fukumoto, I. (2005). Press forming of short natural fiber-reinforced biodegradable resin: Effects of fiber volume and length on flexural properties. *Polymer Testing*, *24*(8), 1005–1011.

Shifa, M., Tariq, F., & Baloch, R. A. (2017). *Effect of Carbon Nanotubes on Mechanical Properties of Honeycomb Sandwich Panels*. *1*(1), 1–6.

Shindo, Y., Takeda, T., Narita, F., Saito, N., Watanabe, S., & Sanada, K. (2009). Delamination growth mechanisms in woven glass fiber reinforced polymer composites under Mode II fatigue loading at cryogenic temperatures. *Composites Science and Technology*, *69*(11–12), 1904–1911.

Singh, S., Khairandish, M. I., Razahi, M. M., Kumar, R., Chohan, J. S., Tiwary, A., Sharma, S., Li, C., Ilyas, R. A., Asyraf, M. R. M., & Zakaria, S. Z. S. (2022). Preference Index of Sustainable Natural Fibers in Stone Matrix Asphalt Mixture Using Waste Marble. *Materials*, *15*(8), 2729.

Song, S., Yin, J., Liu, L., Yang, Z., Han, C., & Xiong, C. (2024). Low-velocity impact responses of polymethacrylimide foam–reinforced all-composite Kagome honeycomb sandwich structures. *Polymer Composites*, *45*(7), 6155–6168.

Sousa, J. M., Correia, J. R., Firmo, J. P., Cabral-Fonseca, S., & Gonilha, J. (2018). Effects of thermal cycles on adhesively bonded joints between pultruded GFRP adherends. *Composite Structures*, *202*, 518–529.

Sun, G., Wang, E., Zhang, J., Li, S., Zhang, Y., & Li, Q. (2020). Experimental study on the dynamic responses of foam sandwich panels with different facesheets and core gradients subjected to blast impulse. *International Journal of Impact Engineering*, *135*.

Sun, Z., Xiao, J., Tao, L., Wei, Y., Wang, S., Zhang, H., Zhu, S., & Yu, M. (2018). Preparation of high-performance carbon fiber-reinforced epoxy composites by compression resin transfer molding. *Materials*, *12*(1).

Supian, M., Bakar, A., Syamsir, A., Alhayek, A., Rizal, M., Asyraf, M. R., Itam, Z., Muhammad, S., Shaik, M., Aziz, N. A., Jamal, T., Aminah, S., Mansor, M., Abu Bakar, M. S., Syamsir, A., Alhayek, A., Asyraf, M. R., Itam, Z., Shaik, S. M., … Mohd Mansor, S. A. (2023). The Reduction Factor of Pultrude Glass Fibre-Reinforced Polyester Composite Cross-Arm: A Comparative Study on Mathematical Modelling for Life-Span Prediction. *Materials*, *16*(15).

Syamsir, A., Ean, L. W., Asyraf, M. R. M., Supian, A. B. M., Madenci, E., Özkılıç, Y. O., & Aksoylu, C. (2023). Recent Advances of GFRP Composite Cross Arms in Energy Transmission Tower: A Short Review on Design Improvements and Mechanical Properties. *Materials*, *16*(7).

Syamsir, A., Mohamad, D., Beddu, S., Itam, Z., & Sadon, S. N. (2019). An examination on durability and degradation of glass fiber reinforced polymer structures. *Test Engineering and Management*, *81*(11–12), 3379–3388.

Syamsir, A., Nadhirah, A., Mohamad, D., Beddu, S., Muhammad Asyraf, M. A. R., Itam, Z., & Anggraini, V. (2022). Performance Analysis of Full Assembly Glass Fiber-Reinforced Polymer Composite Cross-Arm in Transmission Tower. *Polymers*, *14*(8).

Tari, H. (2013). On the parametric large deflection study of Euler-Bernoulli cantilever beams subjected to combined tip point loading. *International Journal of Non-Linear Mechanics*, *49*, 90–99.

The National Electricity Board. (1988). *People behind the lights*.

Thiruganasambanthan, T., Ilyas, R. A., Norrahim, M. N. F., Kumar, T. S. M., Siengchin, S., Misenan, M. S. M., Farid, M. A. A., Nurazzi, N. M., Asyraf, M. R. M., Zakaria, S. Z. S., & Razman, M. R. (2022). Emerging Developments on Nanocellulose as Liquid Crystals: A Biomimetic Approach. *Polymers*, *14*(8), 1546.

Tungjitpornkull, S., & Sombatsompop, N. (2009). Processing technique and fiber orientation angle affecting the mechanical properties of E-glass fiber reinforced wood/PVC composites. *Journal of Materials Processing Technology*, *209*(6), 3079–3088.

Turvey, G. J. (2016). Testing and analysis of pultruded GFRP continuous beams for the deflection serviceability limit state. *Composite Structures*, *141*, 213–220.

Turvey, G. J., & Zhang, Y. (2018a). Mechanical properties of pultruded GFRP WF, channel and angle profiles for limit state/permissible stress design. *Composites Part B: Engineering*, *148*, 260–271.

Turvey, G. J., & Zhang, Y. S. (2018b). Flexural moduli and end connection stiffnesses of symmetrically loaded GFRP beams for limit state serviceability design analysis. *Composite Structures*, *202*, 1164–1175.

Vieira, P. R., Carvalho, E. M. L., Vieira, J. D., & Toledo Filho, R. D. (2018). Experimental fatigue behavior of pultruded glass fibre reinforced polymer composite materials. *Composites Part B: Engineering*, *146*, 69–75.

Wang, C. M., Lam, K. Y., He, X. Q., & Chucheepsakul, S. (1997). Large deflections of an end supported beam subjected to a point load. *International Journal of Non-Linear Mechanics*, *32*(1), 63–72.

Wang, F., Du, K., Sun, J., Huang, F., & Xiong, Z. (2019). Shaking table array tests of an ultra-high-voltage cup-Type transmission tower-line system. *Shock and Vibration*, *2019*.

Wang, F. Y., Xu, Y. L., & Zhan, S. (2017). Concurrent multi-scale modeling of a transmission tower structure and its experimental verification. *Advanced Steel Construction*, *13*(3), 258–272.

Wang, I. T. (2014). Numerical and experimental verification of finite element mesh convergence under explosion loading. *Journal of Vibroengineering*, *16*(4), 1786–1798.

Wang, T. M. (1968). Nonlinear bending of beams with concentrated loads. *Journal of the Franklin Institute*, *285*(5), 386–390.

Wang, Y. G., Lin, W. H., & Liu, N. (2012). A homotopy perturbation-based method for large deflection of a cantilever beam under a terminal follower force. *International Journal for Computational Methods in Engineering Science and Mechanics*, *13*(3), 197–201.

Wang, Z. (2019). Recent advances in novel metallic honeycomb structure. In *Composites Part B: Engineering* (Vol. 166, pp. 731–741). Elsevier Ltd.

Wang, Z., & Liu, J. (2019). Numerical and theoretical analysis of honeycomb structure filled with circular aluminum tubes subjected to axial compression. *Composites Part B: Engineering*, *165*, 626–635.

Wang, Z., Liu, J., Lu, Z., & Hui, D. (2017). Mechanical behavior of composited structure filled with tandem honeycombs. *Composites Part B: Engineering*, *114*, 128–138.

Wei, X., Wu, Q., Gao, Y., & Xiong, J. (2020). Bending characteristics of all-composite hexagon honeycomb sandwich beams: experimental tests and a three-dimensional failure mechanism map. *Mechanics of Materials*, *148*.

Wen, H. M., Reddy, T. Y., Reid, S. R., & Soden, P. D. (1998). Indentation, penetration and perforation of composite laminates and sandwich panels under quasi-static and projectile loading. *Key Engineering Materials*, *143 PART II*, 501–552.

Wg, C. E. N. T. C. (2018). *Prospect for New Guidance in the Design of Frp*.

Wroblewski, L., Hristozov, D., & Sadeghian, P. (2016). Durability of bond between concrete beams and FRP composites made of flax and glass fibers. *Construction and Building Materials*, *126*, 800–811.

Wu, X., Yu, H., Guo, L., Zhang, L., Sun, X., & Chai, Z. (2019). Experimental and numerical investigation of static and fatigue behaviors of composites honeycomb sandwich structure. *Composite Structures*, *213*, 165–172.

Xiang, J., & Du, J. (2017). Energy absorption characteristics of bio-inspired honeycomb structure under axial impact loading. *Materials Science and Engineering A*, *696*, 283–289.

Xiang, Z., Liu, Y., Zhou, X., Wu, Z., & Hu, X. (2020). Interlayer contact mechanism of the frictional behavior of glass-fiber woven fabrics and improvements of winding characteristics. *Composite Structures*, *233*.

Xin, H., Liu, Y., Mosallam, A. S., He, J., & Du, A. (2017). Evaluation on material behaviors of pultruded glass fiber reinforced polymer (GFRP) laminates. *Composite*

Structures, *182*, 283–300.

Xin, H., Liu, Y., Mosallam, A., & Zhang, Y. (2016). Moisture diffusion and hygrothermal aging of pultruded glass fiber reinforced polymer laminates in bridge application. *Composites Part B: Engineering*, *100*, 197–207.

Xin, H., Liu, Y., Mosallam, A., Zhang, Y., & Wang, C. (2016). Hygrothermal aging effects on flexural behavior of pultruded glass fiber reinforced polymer laminates in bridge applications. *Construction and Building Materials*, *127*, 237–247.

Xiong, J., Ma, L., Stocchi, A., Yang, J., Wu, L., & Pan, S. (2014). Bending response of carbon fiber composite sandwich beams with three dimensional honeycomb cores. *Composite Structures*, *108*(1), 234–242.

Xue, D., He, L., Tan, S., Li, Y., Xue, P., & Yang, X. (2022). Study on compression characteristics of honeycomb sandwich structure with multistage carbon fiber reinforced composites. *Polymer Composites*.

Yaakob, M. Y., Husin, M. A., Tan, R. J., Tan, T. T., Mohamed, K. A., Noh, M. S. A. M., & Pieter, H. H. I. (2020). Shear tensile and flexural performance of sandwich composite with hexagonal cell wood core variation. *International Journal of Emerging Trends in Engineering Research*, *8*(1 Special Issue 2), 195–200.

Yan, L., Chouw, N., & Jayaraman, K. (2014). Flax fibre and its composites - A review. *Composites Part B: Engineering*, *56*, 296–317.

Yan, Q., Chen, T., & Xie, Z. (2018). Seismic experimental study on a precast concrete beam-column connection with grout sleeves. *Engineering Structures*, *155*, 330–344.

Yang, C., Daemen, J. J. K., & Yin, J. H. (1999). Experimental investigation of creep behavior of salt rock. *International Journal of Rock Mechanics and Mining Sciences*, *36*(2), 233–242.

Yang, J. Q., & Feng, P. (2020). Analysis-oriented models for FRP-confined concrete: 3D interpretation and general methodology. *Engineering Structures*, *216*.

Yang, M. C. (2009). Observations on concept generation and sketching in engineering design. *Research in Engineering Design*, *20*(1), 1–11.

Yang, X., Li, N., Peng, Z., Liao, J., & Wang, Q. (2014). Potential distribution computation and structure optimization for composite cross-arms in 750 kV AC transmission line. *IEEE Transactions on Dielectrics and Electrical Insulation*, *21*(4), 1660–1669.

Yang, Z., Wang, H., Ma, X., Shang, F., Ma, Y., Shao, Z., & Hou, D. (2018). Flexural creep tests and long-term mechanical behavior of fiber-reinforced polymeric composite tubes. *Composite Structures*, *193*, 154–164.

Yeh, H. Y., & Yang, S. C. (1997). Building of a composite transmission tower. *Journal of Reinforced Plastics and Composites*, *16*(5), 414–424.

Yeh, H. Y., & Yeh, H. L. (2001). A simple failure analysis of the composite transmission tower. *Journal of Reinforced Plastics and Composites*, *20*(12), 1054–1065.

Yin, H., Wen, G., Hou, S., & Chen, K. (2011). Crushing analysis and multiobjective crashworthiness optimization of honeycomb-filled single and bitubular polygonal tubes. *Materials and Design*, *32*(8–9), 4449–4460.

Yuan, Z., Kardomateas, G. A., & Frostig, Y. (2016). Geometric Nonlinearity Effects in the Response of Sandwich Wide Panels. *Journal of Applied Mechanics, Transactions ASME*, *83*(9).

Zainuddin, S., Hosur, M. V., Zhou, Y., Kumar, A., & Jeelani, S. (2010). Durability study of neat/nanophased GFRP composites subjected to different environmental conditioning. *Materials Science and Engineering A*, *527*(13–14), 3091–3099.

Zarei Mahmoudabadi, M., & Sadighi, M. (2011). A study on the static and dynamic loading of the foam filled metal hexagonal honeycomb - Theoretical and experimental. *Materials Science and Engineering A*, *530*(1), 333–343.

Zeng, W., Yan, J., Hong, Y., & Cheng, S. S. (2021). Numerical analysis of large deflection of the cantilever beam subjected to a force pointing at a fixed point. *Applied Mathematical Modelling*, *92*, 719–730.

Zhang, H., Šavija, B., Xu, Y., & Schlangen, E. (2018). Size effect on splitting strength of hardened cement paste: Experimental and numerical study. *Cement and Concrete Composites*, *94*, 264–276.

Zhang, J., Yang, H., Li, X., & Ye, W. (2020). A method of reducing motor vibration: Natural frequency, damping ratio, and vibration analysis of CFRP motor frame. *Shock and Vibration*, *2020*.

Zhang, J., Zhu, Y., Yuan, H., & Huang, W. (2022). Failure behavior of sandwich beams with glass fiber-reinforced epoxy/aluminum laminates face-sheets and aluminum honeycomb core under three-point bending. *Thin-Walled Structures*, *177*.

Zhang, L., Liu, W., Wang, L., & Ling, Z. (2019). Mechanical behavior and damage monitoring of pultruded wood-cored GFRP sandwich components. *Composite Structures*, *215*, 502–520.

Zhang, M., & Matinlinna, J. P. (2012). E-Glass Fiber Reinforced Composites in Dental Applications. *Silicon*, *4*(1), 73–78.

Zhang, X., Ju, Y., & Wang, F. (2018). Statistical Analysis of Wind-Induced Dynamic Response of Power Towers and Four-Circuit Transmission Tower-Line System. *Shock and Vibration*, *2018*.

Zhang, Y., Li, Y., Ma, H., & Yu, T. (2013). Tensile and interfacial properties of unidirectional flax/glass fiber reinforced hybrid composites. *Composites Science and Technology*, *88*, 172–177.

Zhang, Z., Wu, C., Nie, X., Bai, Y., & Zhu, L. (2016). Bonded sleeve connections for joining tubular GFRP beam to steel member: Numerical investigation with experimental validation. *Composite Structures*, *157*, 51–61.

Zhang, Z., Zhang, W., Zhai, Z. J., & Chen, Q. Y. (2007). Evaluation of various turbulence models in predicting airflow and turbulence in enclosed environments by CFD: Part

2—comparison with experimental data from literature. *HVAC and R Research*, *13*(6), 871–886.

Zhao, D., Liu, T. Q., Lu, X., & Meng, X. (2022). Experimental and numerical analysis of a novel curved sandwich panel with pultruded GFRP strip core. *Composite Structures*, *288*.

Zhao, W., Liu, Z., Yu, G., & Wu, L. (2021). A new multifunctional carbon fiber honeycomb sandwich structure with excellent mechanical and thermal performances. *Composite Structures*, *274*.

Zhou, G., Hill, M., & Hookham, N. (2007). Investigation of parameters governing the damage and energy absorption characteristics of honeycomb Sandwich panels. *Journal of Sandwich Structures and Materials*, *9*(4), 309–342.

Zhou, G., Hill, M., Loughlan, J., & Hookham, N. (2006). Damage characteristics of composite honeycomb sandwich panels in bending under quasi-static loading. *Journal of Sandwich Structures and Materials*, *8*(1), 55–90.

Zhu, S., & Chai, G. B. (2011). Effect of adhesive in sandwich panels subjected to low-velocity impact. *Proceedings of the Institution of Mechanical Engineers, Part L: Journal of Materials: Design and Applications*, *225*(3), 171–181.

Zou, X., Feng, P., Bao, Y., Wang, J., & Xin, H. (2020). Experimental and analytical studies on shear behaviors of FRP-concrete composite sections. *Engineering Structures*, *215*.

Zou, X., Feng, P., & Wang, J. (2018). Bolted Shear Connection of FRP-Concrete Hybrid Beams. *Journal of Composites for Construction*, *22*(3).

Zou, X. X., Feng, P., & Wang, J. Q. (2016). Perforated FRP ribs for shear connecting of FRP-concrete hybrid beams/decks. *Composite Structures*, *152*, 267–276.

APPENDICES

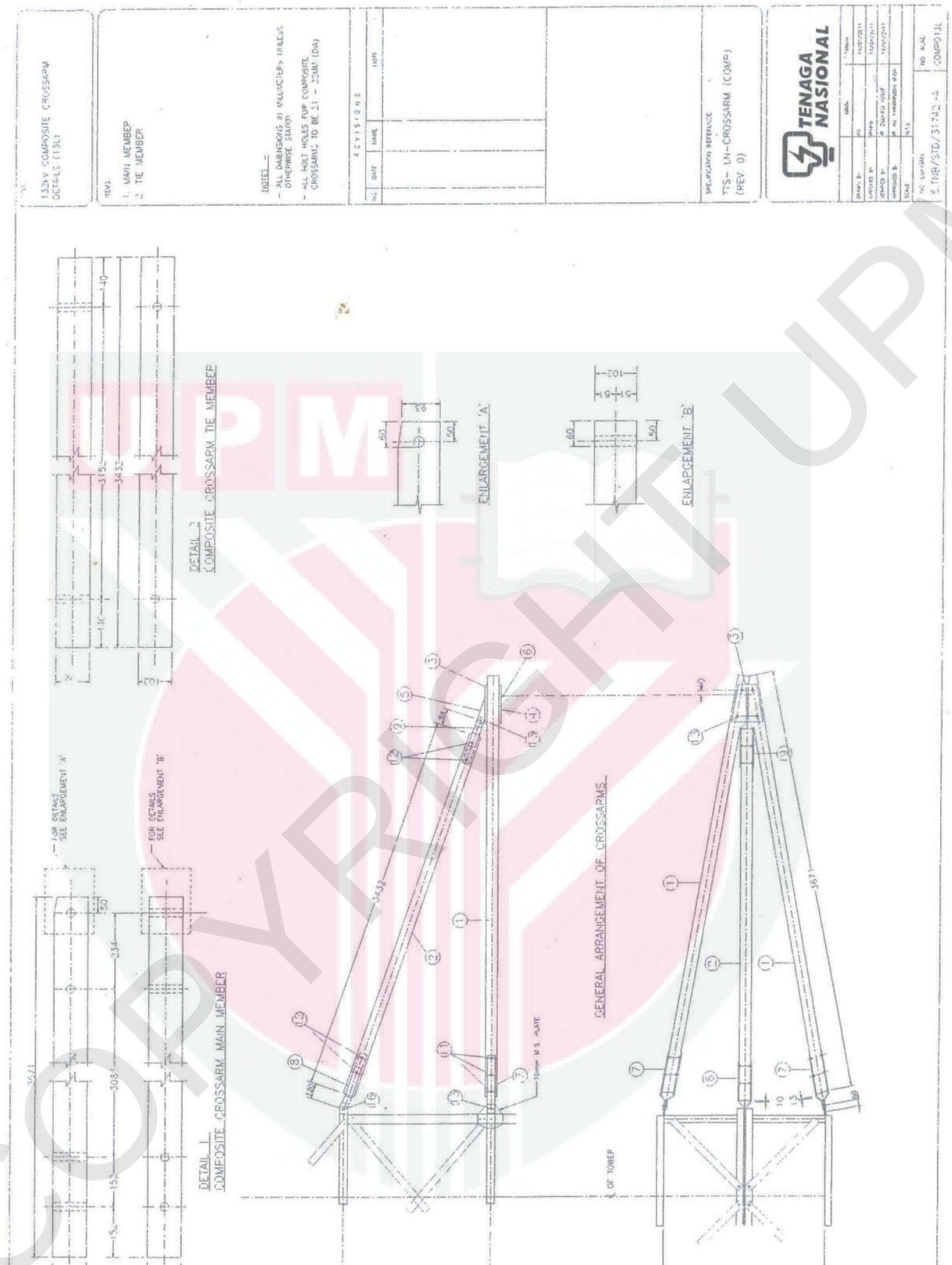

132kV COMPOSITE CROSSARM DETAILS (13L)
1. MAIN MEMBER
2. TIE MEMBER
TENAGA NASIONAL
DETAIL 1 COMPOSITE CROSSARM MAIN MEMBER
DETAIL 2 COMPOSITE CROSSARM TIE MEMBER
ENLARGEMENT 'A'
ENLARGEMENT 'B'
GENERAL ARRANGEMENT OF CROSSARMS

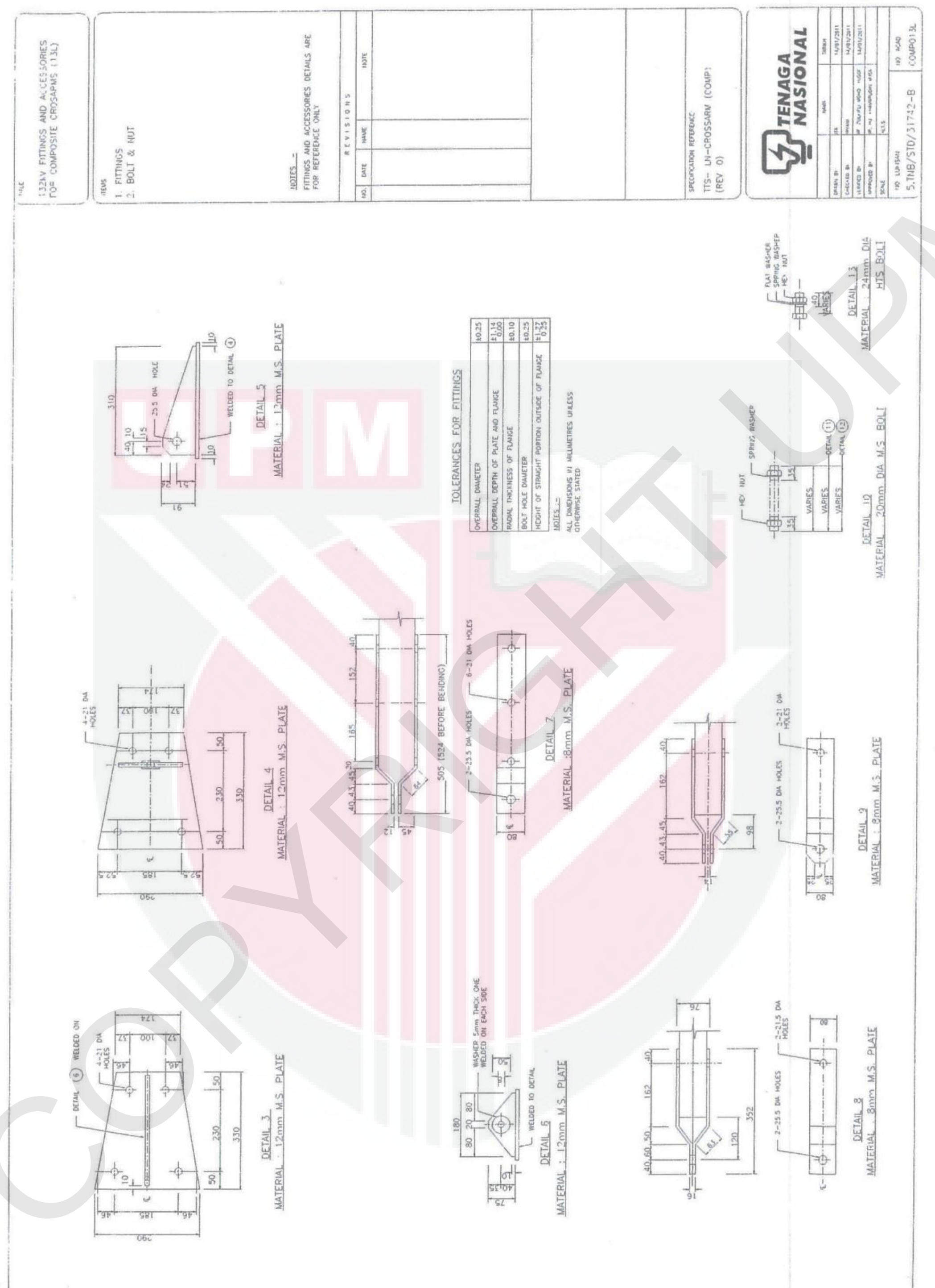
132kV FITTINGS AND ACCESSORIES FOR COMPOSITE CROSARMS (13L)
ITEMS
1. FITTINGS
2. BOLT & NUT
NOTES :-
FITTINGS AND ACCESSORIES DETAILS ARE FOR REFERENCE ONLY
REVISIONS
NO. DATE NAME NOTE
SPECIFICATION REFERENCE
TTS- LN-CROSSARM (COMP) (REV 0)
TENAGA NASIONAL
S.TNB/STD/31742-B
COMP013L
DETAIL 3
MATERIAL : 12mm M.S. PLATE
DETAIL 4
MATERIAL : 12mm M.S. PLATE
DETAIL 5
MATERIAL : 12mm M.S. PLATE
DETAIL 6
MATERIAL : 12mm M.S. PLATE
DETAIL 7
MATERIAL : 8mm M.S. PLATE
505 (524 BEFORE BENDING)
TOLERANCES FOR FITTINGS
OVERALL DIAMETER ±0.25
OVERALL DEPTH OF PLATE AND FLANGE
RADIAL THICKNESS OF FLANGE ±0.10
BOLT HOLE DIAMETER ±0.25
HEIGHT OF STRAIGHT PORTION OUTSIDE OF FLANGE
NOTES :-
ALL DIMENSIONS IN MILLIMETRES UNLESS OTHERWISE STATED
DETAIL 8
MATERIAL : 8mm M.S. PLATE
DETAIL 9
MATERIAL : 8mm M.S. PLATE
DETAIL 10
MATERIAL : 20mm DIA M.S. BOLT
DETAIL 13
MATERIAL : 24mm DIA HTS BOLT

JURUTERA PROFESIONAL
CIVIL
IR. CHOO LAY BENG
12779
MALAYSIA

ELECTRIUS

SUMMARY OF RESULTANT FORCES

No	Description	Resultant Forces (kN)	Resultant Forces with Safety Factor (kN)	Angles (°)
1	13 L Crossarms Assembly Under Normal Condition	7.98	15.96 (F.S: 2.0)	54.2
2	13 L Crossarms Assembly Under Broken Wire Condition	16.5	20.63 (F.S: 1.25)	•12.6 at Horizontal Plane •17.57 at Vertical Plane •55.4 at YZ Plane from Y Axis (Projected Angle)
3	23 L Crossarms Assembly Under Normal Condition	15.89	31.78 (F.S: 2.0)	54.5
4	23 L Crossarms Assembly Under Broken Wire Condition	19.54	24.43 (F.S:1.25)	•24.1 at Horizontal Plane •30.6 at Vertical Plane •55.4 at YZ Plane from Y Axis (Projected Angle)
5	24 L Crossarms Assembly Under Normal Condition	24.27	48.54 (F.S: 2.0)	61.1
6	24 L Crossarms Assembly Under Broken Wire Condition	31.79	39.74 (F.S: 1.25)	•18.59 at Horizontal Plane •31.14 at Vertical Plane •62.2 at YZ Plane from Y Axis (Projected Angle)

Prepared by:
Nickson Tan
Design Engineer
B. (Hons) Civil Eng, UNITEN

Prepared by:
25/3/19.
Ian Lee
General Manager
B. (Hons) Mech Eng, UNITEN

Checked by:
30/3/19
TNB TRANSMISSION DIVISION
Zulkifli Mohd Yusof
Ketua Jurutera (Talian & Kabel)
Jabatan Kejuruteraan

RESEARCH & DEVELOPMENT . ENGINEERING DESIGN . TYPE TEST . MANUFACTURING

ELECTRIUS SDN BHD (941833-D)
Office: No. 10, Jalan BK 1/15, Kinrara Industrial Park, Bandar Kinrara, Off 6½ Miles Jalan Puchong, 47100 Selangor DE
E: info@electrius.com.my T: +603.8076.2254 F: +603.8075.1827

LIST OF PUBLICATIONS

Journal articles

Amir, A. L., Ishak, M. R., Yidris, N., Zuhri, M. Y. M., & Asyraf, M. R. M. (2021a). Advances of composite cross arms with incorporation of material core structures: Manufacturability, recent progress and views. Journal of Materials Research and Technology, 13, 1115–1131. [Q1, Impact factor: 6.4]

Amir, A. L., Ishak, M. R., Yidris, N., Zuhri, M. Y. M., & Asyraf, M. R. M. (2021b). Potential of honeycomb-filled composite structure in composite cross-arm component: A review on recent progress and its mechanical properties. Polymers, 13(8). [Q1, Impact factor: 5.0]

Amir, A. L., Ishak, M. R., Yidris, N., Zuhri, M. Y. M., Asyraf, M. R. M., & Zakaria, S. Z. S. (2023). Influence of Woven Glass-Fibre Prepreg Orientation on the Flexural Properties of a Sustainable Composite Honeycomb Sandwich Panel for Structural Applications. Materials, 16(14). [Q3, Impact factor: 3.4]

Amir, A. L., Ishak, M. R., Yidris, N., & Mohd Zuhri, M. Y. (2024). Flexural creep response of honeycomb sandwich pultruded GFRP composite cross-arm: Obtaining full-scale viscoelastic moduli and creep coefficients. Journal of Materials Research and Technology, 29, 225–241. [Q1, Impact factor: 6.4]

Amir, A. L., Ishak, M. R., Yidris, N., Mohd Zuhri, M. Y., Asyraf, M. R. M., Razman, M. R., & Ramli, Z. (2024). Full-scale evaluation of creep coefficients and viscoelastic moduli in honeycomb sandwich pultruded GFRP composite cross-arms: Experimental and numerical study. Results in Engineering, 101850. [Q1, Impact factor: 6.0]

Asyraf, M. R. M., Ishak, M. R., Sheng, D. D. C. V., Hasni, A. H. M., **Amir, A. L.**, Rased, M. F. A., Rafidah, M., Norrrahim, M. N. F., Razman, M. R., & Iskandar, Z. (2023). Conceptual Design of a Sustainable Bionanocomposite Bracket for a Transmission Tower's Cross Arm Using a Hybrid Concurrent Engineering Approach. Sustainability, 15(14). [Q3, Impact factor: 3.3]

Asyraf, M. R. M., Ishak, M. R., Norrrahim, M. N. F., **Amir, A. L.**, Nurazzi, N. M., Ilyas, R. A., Asrofi, M., Rafidah, M., & Razman, M. R. (2022). Potential of Flax Fiber Reinforced Biopolymer Composites for Cross-Arm Application in Transmission Tower: A Review. Fibers and Polymers, 23(4), 853–877. [Q1, Impact factor: 2.2]

Asyraf, M. R. M., Ishak, M. R., Syamsir, A., **Amir, A. L.**, Nurazzi, N. M., Norrrahim, M. N. F., Asrofi, M., Rafidah, M., Ilyas, R. A., Rashid, M. Z. A., & Razman, M. R. (2022). Filament-wound glass-fibre reinforced polymer composites: Potential applications for cross arm structure in transmission towers. Polymer Bulletin. [Q2, Impact factor: 3.1]

Ishak, M. R., Asyraf, M. R. M., **Amir, A. L.,** Sapuan, S. M., & Yidris, N. **(2020)**. Potential health risks and precautions during biocomposites product preparations. In INTROPica (Issue 19, pp. 22–24).

Conferences Proceeding

Amir, A. L., Yamunan, S., Ishak, M. R., Yidris, N., & Zuhri, M. Y. M. (2024). Flexural Creep Behavior in Utilization of Woven Glass-Fibre as Reinforcement in Pultruded Glass Fibre-Reinforced Polymer Composite Cross-Arms: Experimental and Numerical Analysis. In *Aerotech VIII Conference 2022*. E3S Web of Conferences, 477, 00007. (SCOPUS)